

UC Berkeley

UC Berkeley Electronic Theses and Dissertations

Title

Probabilistic Methods to Identify Seismically Hazardous Older- Type Concrete Frame Buildings

Permalink

<https://escholarship.org/uc/item/0g37n2qh>

Author

Galanis, Panagiotis

Publication Date

2014

Peer reviewed|Thesis/dissertation

Probabilistic Methods to Identify Seismically Hazardous Older-Type Concrete Frame Buildings

By

Panagiotis Galanis

A dissertation submitted in partial satisfaction of the

requirements for the degree of

Doctor of Philosophy

in

Engineering – Civil and Environmental Engineering

in the

Graduate Division

of the University of California, Berkeley

Committee in charge

Professor Jack P. Moehle, Chair

Professor Khalid M. Mosalam

Professor David R. Brillinger

Fall 2014

ABSTRACT

Probabilistic Methods to Identify Seismically Hazardous Older-Type Concrete Frame Buildings

By

Panagiotis Galanis

Doctor of Philosophy in Engineering – Civil and Environmental Engineering

University of California, Berkeley

Professor Jack P. Moehle, Chair

Earthquakes that have occurred recently across the globe in various countries including United States, Japan, New Zealand, Haiti, Turkey and Italy have brought into light the poor seismic performance of older-type, non-ductile concrete buildings. These buildings, mainly designed and constructed prior to 1980s, lack proper seismic detailing and may pose an unacceptably high seismic risk.

Non-ductile concrete buildings pose one of the greatest seismic safety problems in the world due to the large amount of old buildings constructed in earthquake prone regions. It is indicative that according to the Concrete Coalition and the California inventory project there are 16,000-17,000 of these buildings in high earthquake risk counties of California. Many of these buildings have high occupancies, including residential, commercial and critical services. In case of a severe earthquake, the severe damage or even collapse that could occur in these buildings could result in large number of casualties.

While engineers generally recognize that proactive steps are required to address the risk posed by these buildings, mitigation efforts are largely stymied by insufficient knowledge about the scale of the problem, insufficient tools to identify the truly dangerous buildings, high costs of strengthening, and owner resistance to pay for the strengthening with uncertain benefits. This study constitutes an effort to identify seismically hazardous concrete frame buildings through simplified methods that do not require complicated analysis.

Three idealized concrete frame buildings with different heights are used as archetypes. The study attempts to link the collapse performance of these buildings with various structural deficiencies that appear commonly in older construction practice. To evaluate the performance of these buildings non-linear dynamic analysis for several far-fault ground motions is performed. The analysis considers nonlinearities associated with flexural yielding, shear and axial failure. The main deficiencies explored are development of weak story mechanisms due to strong column-

weak beam designs, brittle shear or axial failure modes associated with inadequate column shear reinforcement detailing, and splicing and connectivity weaknesses between structural members.

The results indicate that the suggested methods can be used to assess the collapse risk of older-type concrete buildings. The methods developed in the current study use simple engineering parameters such as column-to-beam strength ratio and column flexural to shear strength ratio to estimate the collapse risk of older type concrete buildings. A probabilistic approach is suggested that takes into account record-to-record variability and could accommodate as well uncertainty associated with structural properties and collapse modeling.

In Chapter 7 the proposed methodology is evaluated by applying it to the three idealized buildings developed. The estimated probabilities of collapse calculated for each of the buildings according to the proposed methodology are compared with the values provided by sophisticated non-linear dynamic analyses. The results suggest that the proposed methodology successfully identifies deficiencies that are leading to high collapse potential and provides an effective tool in classifying collapse prone concrete frame buildings.

In memory of my grandfather, Andreas Mykoniatis

ACKNOWLEDGMENTS

This work was supported mainly by the Fulbright Foundation through the International Fulbright Science and Technology Award that the author received in 2009 to pursue doctoral studies in the United States. Additional funding was provided by the U.S. National Science Foundation under Award 0618804 and the Applied Technology Council, through the ATC-78 project.

While the writing of a dissertation may be a solitary experience, many people deserve my thanks for the contributions they have provided along the way.

First of all, I would like to express my sincerest gratitude to my advisor Professor Jack Moehle. His patient guidance, keen insights and persistence in finding practical solutions to challenging problems have shaped not only this doctoral dissertation but also my entire approach to research.

I would like to thank particularly Professors Filip Filippou, Khalid Mosalam, Stephen Mahin and David Brillinger for serving as members in my qualifying exam and dissertation committees and for providing me with stimulating comments related to my research work.

I would also like to thank the committee members of the ATC-78 project including Ken Elwood, Robert Hanson, Cody Harrington, John Heintz, William T. Holmes, Abbie Liel, Mike Mehrain, Chris Rojahn, Siamak Sattar, and Peter Somers for their invaluable contributions and inputs. The contribution of Francesca Renouard in the development of Appendix F is also acknowledged.

My friends and colleagues in the Department of Civil and Environmental Engineering at U.C. Berkeley, namely, Grigoris Antonellis, Marco Broccardo, Veronique Le Corveque, Mayssa Dabaghi, Pardeep Kumar, Simon Kwong, Mohamed Moustafa, Eleni Stavropoulou, Ahmet Can Tanyeri, and Tea Visnija, provided support and assistance for which I am grateful.

I am also grateful to Professor George Gazetas, Professor Elisavet Vintzileou, and Mr. Alkimos Papathanasiou for being great mentors and for encouraging me to pursue doctoral studies.

I would like to express my deepest gratitude to my friends in Greece Giorgos Alexandrou, Vassilis Dimoudis, Giorgos Karounos, Maria Tzoumanika, and Pantelis Vrachnelis for their continuous support all these years.

Finally I am eternally grateful to my parents Iraklis and Ino. Their sacrifices and encouragements made this degree and all my achievements in life a reality for me.

TABLE OF CONTENTS

1	INTRODUCTION.....	1
1.1	Motivation.....	1
1.2	Brief History of Seismic Codes in California.....	2
1.2.1	Non-Ductile Concrete Buildings.....	3
1.2.2	Buildings Designed after 1980s.....	3
1.3	Scope of the Study.....	3
1.4	Manuscript Organization.....	4
2	SEISMIC RISK EVALUATION OF OLDER-TYPE CONCRETE BUILDINGS: THEORETICAL ASPECTS.....	5
2.1	Collapse Simulation of Concrete Buildings.....	5
2.1.1	Column Models for Collapse Simulation.....	6
2.1.2	Haselton et al. (2008).....	7
2.1.3	Elwood and Moehle (2002).....	9
2.1.4	Modeling Inadequate Lap-Splicing Conditions for the Column Longitudinal Steel Reinforcement.....	12
2.1.5	Beam Column Joints for Collapse Simulation.....	14
2.2	Seismic Risk Assessment.....	18
2.2.1	Regress Using Unscaled Ground Motions (Cloud Analysis).....	19
2.2.2	Scaling Records to the Target IM Level - IDA.....	20
2.3	Identifying Parameters Influencing the Collapse Performance.....	26
2.4	Estimating Story Drift Demand.....	28
2.5	Estimating Column Drift Capacity.....	31
3	EVALUATION OF COLLAPSE SIMULATION OF CONCRETE FRAME STRUCTURES.....	36
3.1	Experimental Investigation.....	36
3.2	Input Ground Motions.....	39
3.3	Material Properties.....	41
3.4	Comparison of Analytical Models with Test Results.....	42
3.5	Summary of the Experimental Evaluation.....	61

4	DEVELOPMENT OF ARCHETYPE BUILDINGS – COLLAPSE SIMULATION MODELS	62
4.1	Development of the Archetype Buildings.....	62
4.2	Analytical Modeling - Collapse Simulation Models	66
4.2.1	Linear Elastic Stiffness Properties	66
4.2.2	Nonlinear Modeling for Flexure-Controlled Members.....	67
4.2.3	Nonlinear Modeling for Shear-Controlled Members.....	68
4.2.4	Dynamic Simulation	68
5	A STRENGTH-BASED APPROACH TO EVALUATE THE COLLAPSE POTENTIAL OF OLDER-TYPE CONCRETE FRAME BUILDINGS	71
5.1	Pushover Analysis to Evaluate the Seismic Performance of Existing Concrete Buildings.....	71
5.2	Assessment of Seismic Behavior	75
5.3	Using Collapse Indicators to Perform Earthquake Risk Assessment for Existing Buildings.....	78
5.4	Earthquake Risk Assessment for Buildings with Non-Uniform Structural Parameters.....	87
5.5	Limitations of the Strength-Based Approach in Collapse Evaluation	90
6	A DISPLACEMENT-BASED METHODOLOGY TO EVALUATE THE COLLAPSE POTENTIAL OF OLDER-TYPE CONCRETE FRAME BUILDINGS	91
6.1	Determination of Story Drift Ratio Demand	91
6.1.1	Estimating Maximum Displacement at the Effective Height of the Building.....	92
6.1.2	Estimating Maximum Story Drift	96
6.2	Determination of Column Drift Capacity	110
6.3	A Methodology to Estimate the Column Failure Potential.....	111
6.3.1	Estimating Column Drift Demand using only Hand Calculations.....	111
6.3.2	Estimating Column Drift Capacity	113
6.3.3	Estimating Column Failure Potential.....	115
6.4	Evaluation of the Story Collapse Potential	116
6.5	Evaluation of the Building Collapse Potential.....	117

7	EVALUATION OF THE DISPLACEMENT-BASED METHOD FOR THE IDEALIZED BUILDINGS.....	118
7.1	Evaluation of the Collapse Potential for the Idealized buildings.....	118
7.1.1	Evaluation of Collapse Potential for the 4-Story Idealized Building	120
7.1.2	Evaluation of Collapse Potential for the 8-Story Idealized Building	122
7.1.3	Evaluation of Collapse Potential for the 12-Story Idealized Building.....	126
8	SUMMARY AND CONCLUSIONS	129
8.1	Collapse Simulation	130
8.2	Collapse Indicators – a Strength-Based Approach for Collapse Evaluation	131
8.3	A Displacement-Based Approach for Collapse Evaluation.....	132
8.4	Recommendations for Future Study	133
	REFERENCES.....	135
A.	DESIGN PARAMETERS OF THE IDEALIZED BUILDINGS	141
B.	RECALIBRATION OF HASELTON ET AL. FLEXURE- CONTROLLED MODEL PARAMETERS	163
C.	EIGENVALUE ANALYSIS OF THE STUDIED BUILDINGS	165
D.	AN APPROXIMATE PROCEDURE TO ESTIMATE THE BASE SHEAR CAPACITY OF CONCRETE FRAME BUILDINGS	168
E.	COLLAPSE PERFORMANCE TABLES FOR THE IDEALIZED BUILDINGS	173
F.	APPROXIMATE RELATIONSHIPS TO ESTIMATE THE FUNDAMENTAL BUILDING PERIOD	184
G.	STORY DRIFT PROFILES	198

LIST OF FIGURES

Figure 2.1	Simulated collapse modes for concrete frames:.....	6
Figure 2.2	Backbone curve of the component model suggested by Ibarra	7
Figure 2.3	Illustration of the components utilized by the model suggested by Haselton et al.	8
Figure 2.4	Illustration of the components utilized in the limit-state model using a lumped plasticity approach	10
Figure 2.5	Shear and axial response according to the limit state material	11
Figure 2.6	Normalized moment – lateral drift ratio for columns with inadequate lap splicing conditions for far fault displacement histories.....	13
Figure 2.7	Assumed zero-length plastic hinge rotational behavior for inadequate lap-splicing conditions.....	14
Figure 2.8	Proposed scissors model (Hassan and Moehle, 2012)	15
Figure 2.9	Proposed backbone curve of joint shear stress strain (Hassan and Moehle, 2012) ..	16
Figure 2.10	Axial load-drift ratio relationship at axial failure for exterior and corner joints (Hassan 2013)	17
Figure 2.11	Estimating the conditional distribution of EDP IM at Sa(T ₁) using “cloud analysis” (a) conditional mean value from linear regression (b) comparison of strip of EDP data Gaussian CCDF based on linear regression	19
Figure 2.12	Multiple stripes of data for different IM Levels (Baker 2007)	21
Figure 2.13	Development of fragility curves	26
Figure 2.14	Approach for establishing collapse indicator limits. Example collapse fragilities for different collapse indicator values.....	28
Figure 2.15	5-story SMRF (Shome, 1999).....	29
Figure 2.16	20-story SMRF (Gupta, 1999)	29
Figure 2.17	Backbone curve of component force-deformation response in ASCE-41	32
Figure 2.18	Comparison of column deformation capacity values provided by different models	34
Figure 3.1	Reinforced concrete column specimen details:.....	38
Figure 3.2	Experimental setup.....	38
Figure 3.3	Filtered Llolejo input ground motion (Chile 1985) ;	40
Figure 3.4	Filtered Kobe Input Ground Motion (Japan 1995):	40
Figure 3.5	Comparison of Test 1 results with the Haselton model	46
Figure 3.6	Comparison of Test 2 results with the Haselton model	46
Figure 3.7	Comparison of Test 3 results with the Haselton model	47
Figure 3.8	Comparison of Test 4 results with the Haselton model	47
Figure 3.9	Comparison of Test 5 results with the Haselton model	48
Figure 3.10	Comparison of Test 6 results with the Haselton model	48
Figure 3.11	Comparison of Test 7 results with the Haselton model	49
Figure 3.12	Comparison of Test 8 results with the Haselton model	49
Figure 3.13	Comparison of Test 9 results with the Haselton model	50
Figure 3.14	Comparison of Test 10 results with the Haselton model	50
Figure 3.15	Comparison of Test 11 results with the Haselton model	51
Figure 3.16	Comparison of Test 4 Results with the Elwood model.....	51

Figure 3.17	Comparison of Test 6 results with the Elwood model.....	52
Figure 3.18	Comparison of Test 10 results with the Elwood model.....	52
Figure 3.19	Comparison of Test 3 results with the Haselton model with $\lambda=\lambda_{\text{mean}}+\lambda_{\text{std}}$	53
Figure 3.20	Comparison of Test 9 results with the Haselton model with $\lambda=\lambda_{\text{mean}}+\lambda_{\text{std}}$	54
Figure 3.21	Comparison of Test 1 results with the Haselton - Elwood model	55
Figure 3.22	Comparison of Test 2 results with the Haselton - Elwood model	55
Figure 3.23	Comparison of Test 7 results with the Haselton - Elwood model	56
Figure 3.24	Comparison of Test 8 results with the Haselton - Elwood model	56
Figure 4.1	Three- dimensional view of the studied buildings.....	63
Figure 4.2	Schematic elevation view of the simulated frames.....	64
Figure 4.3	Lumped plasticity model.....	67
Figure 4.4	Empirical and fitted log-normal cumulative distribution function of probability of collapse	69
Figure 5.1	Pushover analysis of the three “modern code design” building models.....	72
Figure 5.2	Failure mechanisms of the three “modern code design” building models.....	73
Figure 5.3	Pushover analysis of the 8-Story building models for different $\Sigma M_{nc}/\Sigma M_{nb}$ ratios ..	74
Figure 5.4	Failure mechanisms of the 8-Story building models for different $\Sigma M_{nc}/\Sigma M_{nb}$ ratios.....	75
Figure 5.5	Incremental Dynamic Analysis (IDA) curves for the 8-story “modern code design” building model.....	76
Figure 5.6	Collapse fragility functions of the “modern code design” building models.....	77
Figure 5.7	Comparison of collapse performance of the studied building models for $R_e=3$ and $V_p/V_n=0.6$	79
Figure 5.8	Collapse Performance of (a) 4-Story (b) 8-Story (c) 12-Story building models with $V_p/V_n=0.6$	80
Figure 5.9	Comparison of the fragility curves of the 8-Story Building having $\Sigma M_{nc}/\Sigma M_{nb}=1.2$	81
Figure 5.10	Comparison of the collapse performance of the three Idealized Buildings for $\Sigma M_{nc}/\Sigma M_{nb}=1.2$ and $R_e=3$	82
Figure 5.11	Comparison of the collapse performance of the 4-Story Building for (a) $V_p/V_n=0.6$, (b) $V_p/V_n=0.8$, (c) $V_p/V_n=1.0$ and (d) $V_p/V_n=1.2$	83
Figure 5.12	Comparison of the collapse performance of the 8-Story Building for (a) $V_p/V_n=0.6$, (b) $V_p/V_n=0.8$, (c) $V_p/V_n=1.0$ and (d) $V_p/V_n=1.2$	84
Figure 5.13	Comparison of the collapse performance of the 12-Story Building for (a) $V_p/V_n=0.6$, (b) $V_p/V_n=0.8$, (c) $V_p/V_n=1.0$ and (d) $V_p/V_n=1.2$	85
Figure 5.14	Comparison of the collapse performance of the three Idealized Buildings with $R_e=3$ for (a) $V_p/V_n=0.6$, (b) $V_p/V_n=0.8$, (c) $V_p/V_n=1.0$ and (d) $V_p/V_n=1.2$	86
Figure 5.15	Illustration of joins A,B,C,D,E, and F of the 8-story idealized building.....	87
Figure 5.16	Comparison of the collapse performance of the idealized 8-story building with: a) uniform $\Sigma M_{nc}/\Sigma M_{nb}$ values, and b) non-uniform $\Sigma M_{nc}/\Sigma M_{nb}$ values.....	89
Figure 6.1	Ratio of (maximum displacement at effective modal height of non-linear analysis (IDA)) / (estimated displacement at effective modal height of equation 6.1) for different R indices of the 8-Story building ($V_p/V_n=0.6$).....	96
Figure 6.2	Two idealized story drift patterns for an example building frame.....	97

Figure 6.3-a	Alpha coefficient story profiles for different variations of the 4-story idealized buildings.....	99
Figure 6.3-b	Alpha coefficient value at the 1 st story for different variations of the 4-story idealized building.....	100
Figure 6.4-a	Alpha coefficient story profiles for different variations of the 8-story idealized buildings.....	101
Figure 6.4-b	Alpha factor coefficient at the 1 st story for different variations of the 8-story idealized building.....	102
Figure 6.5-a	Alpha coefficient story profiles for different variations of the 12-story idealized buildings.....	103
Figure 6.5-b	Alpha factor coefficient at the 1 st story for different variations of the 12-story idealized building.....	104
Figure 6.6-a	Comparison of the alpha coefficient story profiles for the 8-story with uniform DCRs (idealized building) and with critical story at the mid-height ($V_p/V_n=0.8$ for both cases) (for the critical 4 th story case $DCR_{4th}=1.30DCR_{1st}$).....	105
Figure 6.6-b	Comparison of the alpha coefficient values at the critical story for the 8-story with uniform DCRs (idealized building) and with critical story at the mid-height ($V_p/V_n=0.8$ for both cases) (for the critical 4 th story case $DCR_{4th}=1.30DCR_{1st}$).....	106
Figure 6.7	Assumed zero-length plastic hinge rotational behavior for inadequate lap-splicing conditions.....	107
Figure 6.8-a	Comparison of the alpha coefficient story profiles for different variation of the 8-story idealized building with adequate and inadequate lap splicing conditions at the base of the 1 st story ($V_p/V_n=0.8$ for both cases).....	108
Figure 6.8-b	Comparison of the alpha coefficient value at the critical 1 st story for different variations of the 8-story idealized building with adequate and inadequate lap splicing conditions at the base of the 1 st story ($V_p/V_n=0.8$ for both cases).....	109
Figure 6.9	Illustration of the calculation of axial load for the critical 1 st story of the 4-story idealized building.....	114
Figure 7.1	Uniform Hazard Spectra (UHS) for the idealized buildings located at Berkeley, CA (Site Class D).....	119
Figure A.1	Three- dimensional view of the studied buildings.....	142
Figure A.2	Plan view of the archetype idealized buildings.....	143
Figure A.3	Schematic elevation view of the 4-story archetype building.....	145
Figure A.4	Schematic elevation view of the 8-story archetype building.....	147
Figure A.5	Schematic elevation view of the 12-story archetype building.....	149
Figure C.1	Eigenvectors of 1 st and 2 nd modes, 4-story building.....	165
Figure C.2	Eigenvectors of 1 st and 2 nd modes, 8-story building.....	166
Figure C.3	Eigenvectors of 1 st and 2 nd modes, 12-story building.....	167
Figure D.1	Schematic Drawing for the calculation of story plastic shear capacity.....	169
Figure F.1	Schematic illustration of the generic frame model used to represent the idealized 8-story building.....	186
Figure F.2	Effect of building height (H) on the fundamental period T_1 of the building.....	190
Figure F.3	Effect of normalized base shear strength (V/W) on the fundamental period T_1 of the building.....	190
Figure F.4	Effect of longitudinal reinforcement ratio (ρ_{long}) on the fundamental period T_1 of the building.....	191

Figure F.5	Comparison of relationships for estimation of the fundamental building period	193
Figure F.6	Comparison of relationships for estimation of the fundamental building period with analytical data (Effect of V/W on T_1).....	195
Figure F.7	Comparison of relationships for estimation of the fundamental building period with analytical data (Effect of H on T_1).....	196
Figure G.1	Observed story drift ratio demand (δ_1/h_1) at the 1 st story over estimated average drift (δ_{eff}/h_{eff})	200

LIST OF TABLES

Table 2.1	Far-field record set used in the current study.....	23
Table 2.2	Far-field ground motion parameter information	24
Table 2.3	Critical seismic deficiencies found in pre-1980 concrete buildings	27
Table 2.4	Regression relationships of maximum story drift and different intensity measures	30
Table 2.5	Classification of column condition	32
Table 2.6	Column deformation capacities according to column condition	33
Table 2.7	Column deformation capacities for condition iii columns.....	34
Table 3.1	Test matrix	39
Table 3.2	Concrete mean strength properties.....	41
Table 3.3	Steel reinforcement mean strength properties.....	41
Table 3.4	Column modeling properties.....	43
Table 3.5	Modeling parameters (Haselton model).....	43
Table 3.6	Modeling parameters (Elwood model)	44
Table 3.7	Fundamental Period and damping ratio	45
Table 3.8	Actual test results	57
Table 3.9	Haselton analytical model results	58
Table 3.10	Elwood analytical model results	59
Table 3.11	Haselton-Elwood analytical model results.....	60
Table 3.12	Haselton analytical model results with $\lambda = \lambda_{\text{mean}} + \lambda_{\text{std}}$	61
Table 4.1	Combinations of V_p/V_n and $\Sigma M_{nc}/\Sigma M_{nb}$ considered in the current study.....	65
Table 4.2	Modification factor values for the cracked stiffness properties of the structural members	66
Table 5.1	Combination of non-uniform joint $\Sigma M_{nc}/\Sigma M_{nb}$ values.....	88
Table 6.1	Coefficients of the studied buildings utilized in equation 6.1	93
Table 6.2	Mean ratio of (maximum displacement at effective modal height floor level of non-linear analysis) / (estimated displacement at effective modal height floor level of equation 6.1) for different V_p/V_n and $\Sigma M_{nc}/\Sigma M_{nb}$ ratios of the 4-Story Idealized Building.....	94
Table 6.3	Mean ratio of (maximum displacement at effective modal height floor level of non-linear analysis) / (estimated displacement at effective modal height floor level of equation 6.1) for different V_p/V_n and $\Sigma M_{nc}/\Sigma M_{nb}$ ratios of the 8-Story Idealized Building.....	94
Table 6.4	Mean ratio of (maximum displacement at effective modal height floor level of non-linear analysis) / (estimated displacement at effective modal height floor level of equation 6.1) for different V_p/V_n and $\Sigma M_{nc}/\Sigma M_{nb}$ ratios of the 12-Story Idealized Building.....	95
Table 6.5	Values of α_x for buildings with 1 st Story Critical.....	112
Table 6.6	Uncertainty in predictions of drift demand	113
Table 7.1	Spectral acceleration values used for the collapse evaluation	120
Table 7.2	Comparison of collapse evaluation using the displacement-based methodology and IDA for the 4-story idealized building	121

Table 7.3	Comparison of collapse evaluation using the displacement-based methodology and IDA for the 8-story idealized building	123
Table 7.4	Comparison of collapse evaluation using the displacement-based methodology and IDA for the 8-story idealized building with inadequate lap splicing conditions at the base of the 1 st story.....	125
Table 7.5	Comparison of collapse evaluation using the displacement-based methodology and IDA for the 8-story idealized building with weak story at the mid-height ..	126
Table 7.6	Comparison of collapse evaluation using the displacement-based methodology and IDA for the 12-story idealized building	127
Table A.1	Interior column reinforcement schedule of the 4-story archetype building.....	145
Table A.2	Corner column reinforcement schedule of the 4-story archetype building.....	146
Table A.3	Beam reinforcement schedule of the 4-story archetype building	146
Table A.4	Interior column reinforcement schedule of the 8-story archetype building.....	147
Table A.5	Corner column reinforcement schedule of the 8-story archetype building.....	148
Table A.6	Beam reinforcement schedule of the 8-story archetype building	148
Table A.7	Interior column reinforcement schedule of the 12-story archetype building.....	150
Table A.8	Corner column reinforcement schedule of the 12-story archetype building.....	151
Table A.9	Beam reinforcement schedule of the 12-story archetype building	152
Table A.10	Reinforcement and modeling parameter details of the 4-story building for the case of $V_p/V_n=0.6$ (Archetype 4-story building)	153
Table A.11	Reinforcement and modeling parameter details of the 4-story building for the case of $V_p/V_n=0.8$	153
Table A.12	Reinforcement and modeling parameter details of the 4-story building for the case of $V_p/V_n=1.0$	154
Table A.13	Reinforcement and modeling parameter details of the 4-story building for the case of $V_p/V_n=1.2$	154
Table A.14	Reinforcement and modeling parameter details of the 8-story building for the case of $V_p/V_n=0.6$ (Archetype 8-story building)	155
Table A.15	Reinforcement and modeling parameter details of the 8-story building for the case of $V_p/V_n=0.8$	156
Table A.16	Reinforcement and modeling parameter details of the 8-story building for the case of $V_p/V_n=1.0$	157
Table A.17	Reinforcement and modeling parameter details of the 8-story building for the case of $V_p/V_n=1.2$	158
Table A.18	Reinforcement and modeling parameter details of the 12-story building for the case of $V_p/V_n=0.6$ (Archetype 12-story building)	159
Table A.19	Reinforcement and modeling parameter details of the 12-story building for the case of $V_p/V_n=0.8$	160
Table A.20	Reinforcement and modeling parameter details of the 12-story building for the case of $V_p/V_n=1.0$	161
Table A.21	Reinforcement and modeling parameter details of the 12-story building for the case of $V_p/V_n=1.2$	162
Table D.1	Comparison of pushover and estimated maximum base shear capacity of the 4-story building.....	171
Table D.2	Comparison of pushover and estimated maximum base shear capacity of the 8-story Building	171

Table D.3	Comparison of pushover and estimated maximum base shear capacity of the 12-story building.....	172
Table E.1	Probability of collapse matrix for the 4-story building with $V_p/V_n = 0.6$ (R_e normalization factor).....	173
Table E.2	Probability of collapse matrix for the 4-story building with $V_p/V_n = 0.8$ (R_e normalization factor).....	174
Table E.3	Probability of collapse matrix for the 4-story building with $V_p/V_n = 1.0$ (R_e normalization factor).....	174
Table E.4	Probability of collapse matrix for the 4-story building with $V_p/V_n = 1.2$ (R_e normalization factor).....	174
Table E.5	Probability of collapse matrix for the 8-story building with $V_p/V_n = 0.6$ (R_e normalization factor).....	175
Table E.6	Probability of collapse matrix for the 8-story building with $V_p/V_n = 0.8$ (R_e normalization factor).....	175
Table E.7	Probability of collapse matrix for the 8-story building with $V_p/V_n = 1.0$ (R_e normalization factor).....	176
Table E.8	Probability of collapse matrix for the 8-story building with $V_p/V_n = 1.2$ (R_e normalization factor).....	176
Table E.9	Probability of collapse matrix for the 12-story building with $V_p/V_n = 0.6$ (R_e normalization factor).....	177
Table E.10	Probability of collapse matrix for the 12-story building with $V_p/V_n = 0.8$ (R_e normalization factor).....	177
Table E.11	Probability of collapse matrix for the 12-story building with $V_p/V_n = 1.0$ (R_e normalization factor).....	177
Table E.12	Probability of collapse matrix for the 12-story building with $V_p/V_n = 1.2$ (R_e normalization factor).....	178
Table E.13	Probability of collapse matrix for the 4-story building with $V_p/V_n=0.6$ (M normalization factor).....	179
Table E.14	Probability of collapse matrix for the 4-story building with $V_p/V_n=0.8$ (M normalization factor).....	179
Table E.15	Probability of collapse matrix for the 4-story building with $V_p/V_n=1.0$ (M normalization factor).....	180
Table E.16	Probability of collapse matrix for the 4-story building with $V_p/V_n=1.2$ (M normalization factor).....	180
Table E.17	Probability of collapse matrix for the 8-story building with $V_p/V_n=0.6$ (M normalization factor).....	180
Table E.18	Probability of collapse matrix for the 8-story building with $V_p/V_n=0.8$ (M normalization factor).....	181
Table E.19	Probability of collapse matrix for the 8-story building with $V_p/V_n=1.0$ (M normalization factor).....	181
Table E.20	Probability of collapse matrix for the 8-story building with $V_p/V_n=1.2$ (M normalization factor).....	181
Table E.21	Probability of collapse matrix for the 12-story building with $V_p/V_n=0.6$ (M normalization factor).....	182
Table E.22	Probability of collapse matrix for the 12-story building with $V_p/V_n=0.8$ (M normalization factor).....	182

Table E.23	Probability of collapse matrix for the 12-story building with $Vp/Vn=1.0$ (M normalization factor)	182
Table E.24	Probability of collapse matrix for the 12-story building with $Vp/Vn=1.2$ (M normalization factor)	183
Table F.1	Comparison of eigenvalue analysis of the idealized building models and the equivalent generic frame model.....	189
Table F.2	Regression parameters for model $T_{G.F.,1}$	192
Table F.3	Regression parameters for model $T_{G.F.,2}$	192
Table F.4	Comparison of eigenvalue analysis of the idealized building models and the estimated building period values	196
Table G.1.a	Least squares estimation results of $\alpha_x = \exp(\hat{\beta}_0)$ for the idealized 4- story building	201
Table G.1.b	Least squares estimation results of $\hat{\sigma}_{m, \frac{\delta_x}{h_x}}$ for the idealized 4- story building.....	202
Table G.2.a	Least squares estimation results of $\alpha_x = \exp(\hat{\beta}_0)$ for the idealized 8- story building	203
Table G.2.b	Least squares estimation results of $\hat{\sigma}_{m, \frac{\delta_x}{h_x}}$ for the idealized 8- story building.....	204
Table G.3.a	Least squares estimation results of $\alpha_x = \exp(\hat{\beta}_0)$ for the idealized 12- story building	205
Table G.3.b	Least squares estimation results of $\hat{\sigma}_{m, \frac{\delta_x}{h_x}}$ for the idealized 12- story building....	207
Table G.4.a	Least squares estimation results of $\alpha_x = \exp(\hat{\beta}_0)$ for the idealized 8- story building with critical story at the mid-height ($DCR_{4th}=1.30DCR_{1st}$)	209
Table G.4.b	Least squares estimation results of $\hat{\sigma}_{m, \frac{\delta_x}{h_x}}$ for the idealized 8- story building with critical story at the mid-height ($DCR_{4th}=1.30DCR_{1st}$).....	210
Table G.5.a	Least squares estimation results of $\alpha_x = \exp(\hat{\beta}_0)$ for the idealized 8- story building with inadequate lap splicing conditions at the base of the 1 st story	211
Table G.5.b	Least squares estimation results of $\hat{\sigma}_{m, \frac{\delta_x}{h_x}}$ for the idealized 8- story building inadequate lap splicing conditions at the base of the 1 st story	212

1 Introduction

1.1 MOTIVATION

Strong earthquakes are not very frequent phenomena. When they occur, however they can have destructive consequences. In recent years, earthquakes in Haiti, Chile, New Zealand and Japan demonstrated the potentially large impact in the economies of those countries. This has raised a new challenge for the 21st century regarding the appropriate earthquake design of structures so that the casualties occurring due to such phenomena can be limited. It has also raised the challenge of identifying potentially hazardous existing buildings.

The United States and especially the earthquake prone state of California have suffered several times in the past by strong earthquakes. The impact of a major earthquake striking the City of Los Angeles nowadays would be substantial. Sophisticated models estimate that property damages would be greater than \$20 billion, in addition to a large number of fatalities. Thus, many federal agencies and private institutions, recognizing the need and the challenge of mitigating the high seismic risk posed by collapse of specific structures, have devoted a significant portion of their research activity towards mitigation of that problem.

Concrete is a popular building material in regions with high seismicity. In most instances, concrete performs well. However, in order to do so, it needs to be properly proportioned and detailed. This was proved by various past earthquakes, including the 1971 San Fernando earthquake, the 1989 Loma Prieta earthquake, and the 1994 Northridge earthquake, where many concrete buildings were seriously damaged or even collapsed with fatal consequences for their occupants. These events have triggered discussions among the engineering community concerning the largest magnitude earthquake that could be generated by known faults as well as how buildings should be detailed to minimize earthquake loss. Recognizing the potential losses, U.S. seismic codes have been improved significantly starting in the mid-1970s, especially as regards the proportioning and detailing of reinforced concrete construction.

The lack of proper seismic detailing of older buildings renders them seismically vulnerable in case of a strong earthquake. Contrary to new construction that follows seismic proportioning and detailing to enable ductile response, older buildings commonly have non-ductile seismic performance with low strength and deformation capacity. These buildings constitute a significant safety concern in United States and around the world and are commonly referred to as non-ductile concrete buildings.

The seismic risk posed by older concrete buildings was demonstrated in the 1971 San Fernando earthquake. In that event the Olive View Hospital, a recently constructed building, almost

collapsed and an older concrete Veteran Administration Hospital building collapsed and killed over 40 occupants. Since that time, the overall life-safety risk from older concrete buildings often has been compared to unreinforced masonry buildings (URM).

Although various programs to mitigate the risk of URM buildings are common in zones of high seismicity in the United States, no such programs have been implemented for older concrete buildings. Some reasons that explain the lack of seismic risk programs for concrete buildings include:

- It is often difficult to visually determine seismic deficiencies in concrete buildings. Careful studying of drawings, on-site inspection of the considered building and supplemental sophisticated linear or non-linear analysis might be required to identify seismically hazardous buildings
- While various studies have suggested that older concrete buildings are very hazardous, exposing their occupants to unacceptably high life-safety risk, past experience following major earthquakes indicates that these buildings, while vulnerable to structural damage, do not have high collapse rates in most parts of the world.
- Concrete buildings are often large, the occupancy is high and ownership groups are often politically powerful and resistant to seismic retrofitting because of its high costs and extensive service disruption.
- Current evaluation and retrofit code standards (ASCE/SEI 31, “Seismic Evaluation of Existing Buildings” and ASCE/SEI 41, “Seismic Rehabilitation of Existing Buildings”) are considered by many engineers in practice to be overly conservative and expensive to implement.

A premise of the present study is that, if a reliable and inexpensive evaluation technique was available, both authorities and building owners/tenants would act proactively to quantify the collapse risk of older buildings and take action to mitigate the risk accordingly.

1.2 BRIEF HISTORY OF SEISMIC CODES IN CALIFORNIA

Building codes have seen major developments over the past century. The highest risk from existing concrete buildings occurs because a significant number of them constructed in the 20th century in the United States were designed prior to important developments in the building code seismic requirements.

The earliest seismic design provisions in the United States were introduced in the Appendix of the 1927 Uniform Building Code (UBC) after the 1925 Santa Barbara earthquake. After the damages observed in the 1933 Long Beach Earthquake, the state of California, introduced the Field Act and Riley Act that endorsed early design requirements for public buildings.

In 1957 the Structural Engineers Association of California published the first edition of “Recommended Lateral Force Requirements and Commentary.” However the seismic design provisions remained in the Appendix of the UBC until the International Conference of Building Officials adopted seismic design provisions into the main code in 1961.

1.2.1 Non-Ductile Concrete Buildings

“Design of Multistory Reinforced Concrete Buildings for Earthquake Motions (Blume et al., 1961) introduced modern concepts for earthquake-resistant reinforced concrete buildings. The recommendations of this book influenced many engineers, but its recommendations were not required by the building codes until after the 1971 San Fernando earthquake. The 1976 Uniform Building Code introduced the requirement for special detailing of concrete frames in addition to incorporation of larger seismic design loads than were required in previous code provisions. Most engineers consider 1976 a critical date before which concrete frames equivalent to the present day ductile moment resisting frames were not fully implemented in the design of buildings. Buildings designed prior to 1976 correspond to the older-type construction that this study is mainly attempting to evaluate. Due to the lack of adequate detailing in most of the cases, these buildings are susceptible to brittle failure modes and thus are termed as non-ductile concrete buildings to distinguish them from buildings constructed after this date.

1.2.2 Buildings Designed after 1980s

A common practice for buildings has been to have portions of the structure that are designed to carry seismic forces while having others designed to carry only gravity loads. Some frames designed as gravity-only frames experienced extensive damages in the 1994 Northridge earthquake leading to strict requirements for proportioning and detailing of those frames in ACI 318-95. Buildings designed in the State of California after 1995, if proportioned appropriately according to the prevailing design provisions, are considered to have adequate collapse resistance for earthquake loading equal to what is assumed in today’s design practice (probability of collapse for the Maximum Considered Earthquake shaking intensity approximately equal to 10%).

1.3 SCOPE OF THE STUDY

The current study presents evaluation methodologies to determine the collapse risk of older concrete buildings designed prior to 1980s. The intent is to enable identification of relatively few buildings in this class that have high collapse propensity without the need for extensive testing or sophisticated nonlinear dynamic analysis. It is expected that evaluation of entire inventories of this structural class would thus be affordable and feasible and the concrete buildings posing the greatest threat of life loss could be potentially mitigated.

The evaluation methods described in the current study are limited to reinforced concrete frame type structures with rigid diaphragms. However the method could be expanded in the future to cover other concrete building systems, particularly those with walls or masonry infill walls.

1.4 MANUSCRIPT ORGANIZATION

This dissertation is organized in eight chapters, with specific content identified below.

Chapter 2 provides literature review corresponding to collapse modeling, seismic risk evaluation methodologies and other theoretical aspects corresponding to identifying seismically hazardous older-type concrete buildings.

Chapter 3 presents an analytical and experimental study of eleven scaled concrete frames with different reinforcement details. The chapter includes descriptions of the tests performed as well as analytical modeling techniques. The results provide insight into the effectiveness of the modeling tools used in subsequent chapters.

Chapter 4 provides information on the development of the archetype buildings that were utilized for the calibration of the methodology. The chapter also describes state of the art simulation tools that were used to model the non-linear dynamic response and assess the collapse performance of the considered buildings.

Chapter 5 presents a strength-based approach that could be used to evaluate the seismic performance of buildings. The method explores the use of collapse indicators, that is, easy-to-calculate engineering parameters, to estimate the collapse risk.

Chapter 6 presents a displacement-based approach to evaluate the seismic performance of buildings. Calibration of the methodology is presented and consequently tested for the considered buildings.

Chapter 7 evaluates the displacement based approach presented in Chapter 6. The methodology proposed in Chapter 6 is applied for the three idealized buildings developed in Chapter 4 and the results are compared with those derived from sophisticated non-linear dynamic analyses for the studied buildings.

Chapter 8 presents a summary of research findings and conclusions as well as a list of topics for future research.

2 Seismic Risk Evaluation of Older-Type Concrete Buildings: Theoretical Aspects

The current chapter provides background information regarding basic aspects of the methodology. The Chapter begins with a review of the modeling techniques used in the current study to simulate collapse. Considerations regarding the applicability and the assumptions involved are also discussed. Consequently the definition of seismic risk analysis is provided along with two methods to perform structural vulnerability analysis and derive fragility curves. The chapter concludes with a discussion of how collapse can be identified by using simple engineering parameters and how story drift demand and column drift capacity can be defined in a probabilistic framework.

2.1 COLLAPSE SIMULATION OF CONCRETE BUILDINGS

The last years there has been a great interest related to building code performance objectives (performance-based design). One very important issue that has arisen lately has been life-safety performance, which is primarily governed by structural collapse. Advances in computational power and state of the art simulation tools have enabled development of non-linear seismic analysis numerical models that allow simulation of structural collapse.

Two main failure modes for building collapse are considered in the current study:

- a) Side-sway collapse is caused due to excessive story drifts in one story. The combination of the earthquake lateral forces and the P-Delta effects result in large story drifts that cause the structure to collapse in a sideways manner.
- b) Vertical collapse is one of the most common collapse modes for older-type concrete buildings. It is mainly caused by column members that are lightly confined. Such members are susceptible to shear failures, which after a certain story drift level lead to inability of the damaged members to support the axial loads due to gravity.

Figure 2.1 provides an illustration of the collapse modes considered in the current study.

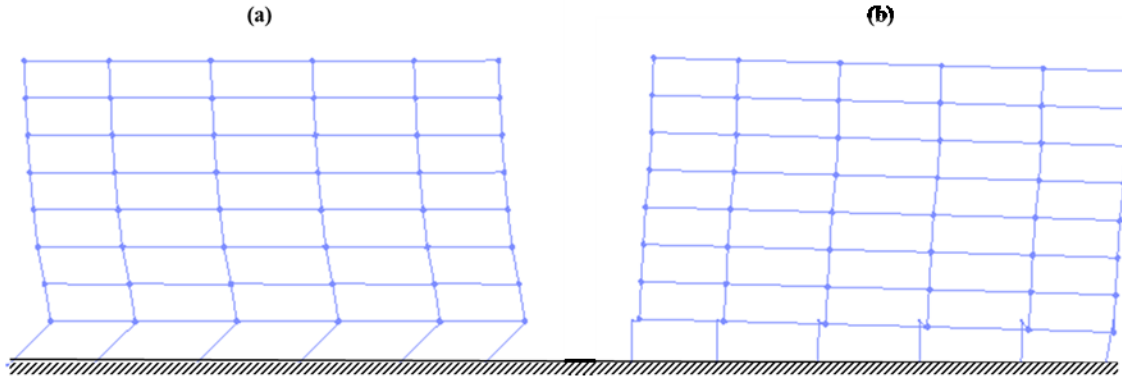


Figure 2.1 Simulated collapse modes for concrete frames:
(a) Side-sway collapse, (b) Vertical collapse

Although in the literature there are a variety of sophisticated simulation tools to evaluate the non-linear flexural response of structural components and collapse due to the side-sway mechanism, only recently there have been efforts to develop analytical models for shear-critical columns, with the ultimate goal of understanding the vertical collapse risk of existing buildings.

2.1.1 Column Models for Collapse Simulation

Columns are one of the most important structural components in the building since they are transferring both the lateral and gravity loads to the foundation soil. Thus, the dynamic performance of column members is a main emphasis of many collapse studies.

Several models exist in the literature for simulating the inelastic dynamic response of column members at collapse. Important model characteristics include the following (Ghannoum, 2013):

- **Computational Efficiency.** Collapse simulation studies require a large number of simulations up to structural collapse. Therefore, models with high computational efficiency may be preferred to more accurate modeling techniques. The main models that satisfy this requirement correspond to center-line elements with lumped-plasticity or fiber-section implementations.
- **Calibration to a wide range of column failure modes.** The considered models should be calibrated using laboratory data that account for different failure models.
- **Ability to simulate shear and axial degrading behavior, including both in-cycle and cyclic degradation.** In-cycle degradation is directly related with the incorporation of the post-peak negative stiffness branch in the backbone curve of models simulating flexural, shear or axial degradation. It has been observed that members subjected to long duration motions with large number of cycles experience strength degradation due to cyclic loading.

Available models in the current literature that satisfy most of the characteristics listed above include those of Elwood and Moehle (2002) , Haselton et al. (2008), and Leborgne and

Ghannoum (2012). The first two of these are used in the present study. These are described below.

2.1.2 Haselton et al. (2008)

In 2005 Ibarra et al. developed a model that was capable of modeling strength deterioration that precipitates side-sway collapse. The model was implemented in OpenSees based on the Clough hysteretic model. This model consists of a tri-linear monotonic backbone curve and includes aspects of hysteretic model response related to cyclic strength and stiffness deterioration.

The developed model requires the specification of seven parameters to control the monotonic and cyclic response. The parameters are: M_y ; M_c/M_y ; K_e ; $\theta_{cap,pl}$; θ_{pc} ; λ ; and c , each shown schematically in Figure 2.2.

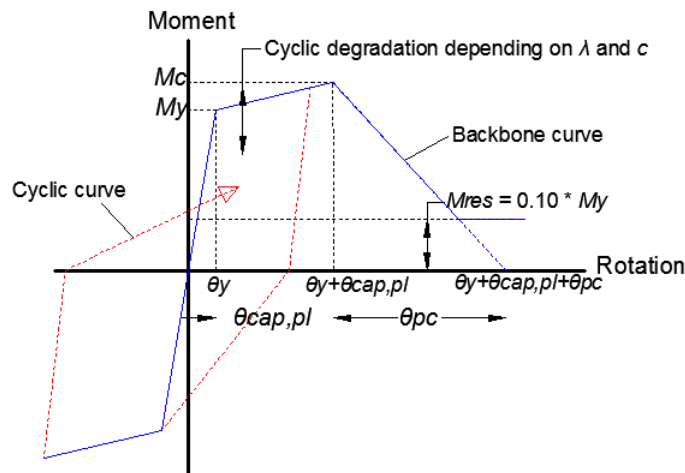


Figure 2.2 Backbone curve of the component model suggested by Ibarra

In 2008, Haselton et al. (PEER 2007/03), used a database of 255 rectangular columns provided by Berry et al. (2004) to calibrate the parameters utilized by the element model developed by Ibarra et al.

The proposed model by Haselton follows a lumped-plasticity approach with zero-length rotational springs placed at the ends of the elastic line elements. The zero-length springs are assumed to account for non-linear material response. Figure 2.3 shows the arrangement of the components according to the lumped plasticity approach suggested by Haselton et al.

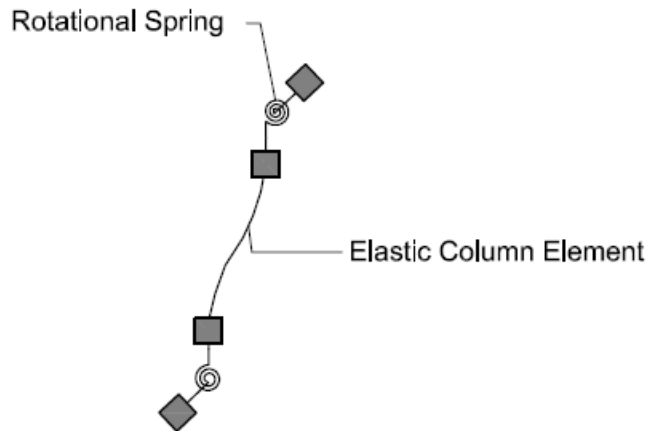


Figure 2.3 Illustration of the components utilized by the model suggested by Haselton et al.

The zero-length parameters were calibrated by Haselton et al. using regression estimates that matched the responses observed in laboratory tests and the lumped plasticity model. The calibrations were based on mean values and are supposed to be less conservative than the values provided by ASCE-41.

The column database used for calibration consists of 220 column tests of column members that failed in flexure and 35 (255 columns in total) that failed in a flexure-shear failure mode. The model was not calibrated for columns that sustain shear failure prior to flexural yielding. The interested reader can find the calibrated model parameters for each of the 255 laboratory tests as well as the suggested parameter relationships in Haselton et al. (2008).

In the original formulation the regression estimates were not distinguished between flexure and flexure-shear failure. Dr. Liel and her colleagues re-calibrated the regression relationships such that only columns that were reported to fail in flexure were included (ATC-78,2013). The updated relationships suggested by this re-calibration are provided in Appendix B.

Although the model has the advantage of defining through regression the parameters that should define the column response, the model does not distinguish between flexure and flexure-shear failure. Thus this model cannot explicitly model shear-induced axial failure. This limitation renders the model more applicable for collapse simulations where the columns are flexure-controlled and the collapse failure is governed by a side-sway mechanism.

For the reasons suggested above and after the evaluation of the model suggested by Haselton using laboratory tests (Chapter 3) , in the current study it was decided to use this modeling technique for collapse simulation only for columns that are flexure-critical. This will be explained further in Chapter 4.

2.1.3 Elwood and Moehle (2002)

Elwood and Moehle (2002) used a set of 50 tests compiled by Sezen (2002) to develop an empirical model that relates the shear demand to the drift at shear failure. The relationship defines a failure surface based on the transverse reinforcement ratio and axial loading ratio of the member. If the shear demand exceeds a specified limit, shear failure is triggered. Similar to the limit surface defined for the shear failure an empirical relationship that relates the axial demand with the drift at axial failure was suggested. Equations 2.1 and 2.2 provide the proposed relationships that define the failure surfaces for the shear and axial failure correspondingly.

$$\frac{\Delta_s}{L} = \frac{3}{100} + 4\rho'' - \frac{1}{500} \frac{v}{\sqrt{f'_c}} - \frac{1}{40} \frac{P}{A_g * f'_c} \geq \frac{1}{100} \quad (\text{Eq. 2.1})$$

$$\frac{\Delta_a}{L} = \frac{4}{100} \frac{1 + (\tan \theta)^2}{\tan \theta + P \left(\frac{s}{A_{st} f_y d_c \tan \theta} \right)} \quad (\text{Eq. 2.2})$$

where ρ'' corresponds to the transverse reinforcement ratio, s is the spacing of transverse reinforcement (given in inches), f_y is the reinforcing steel yield strength (given in psi), d_c is the depth of the column core from center line to center line of the ties (given in inches), A_{st} is the transverse reinforcement area (given in inches²), v is the shear stress demand (given in psi), f'_c is the concrete strength (given in psi), P is the axial force (given in pounds), and A_g is the gross sectional area of the column (given in inches²).

The proposed model was implemented in OpenSees as the limit state material. The model was formulated such that it includes zero length shear and axial springs placed at the ends of column connected in series with the member center-line element. The model can be used in combination with either zero-length rotational springs or with force-based fiber elements. Figure 2.4 illustrates the arrangement of the various components of the limit state model for columns as it was implement in the current study.

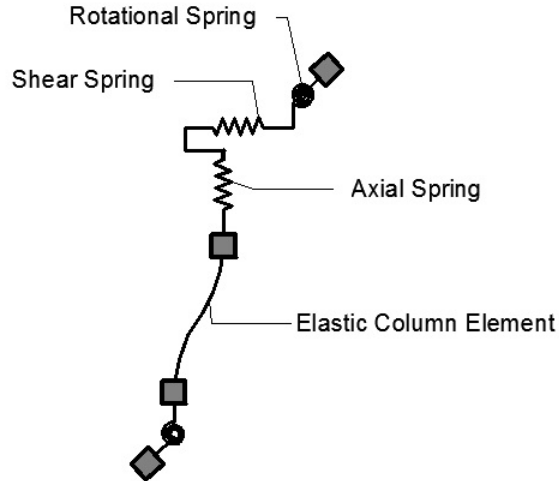


Figure 2.4 Illustration of the components utilized in the limit-state model using a lumped plasticity approach

The limit state material couples the response of the shear and axial springs with the elastic column element. At every converged time step, the drift observed and the shear and axial demand in the elastic column element are compared to the limit surfaces provided from Equations 2.1 and 2.2. If the demand is higher than the value proposed by each of the equations then shear or axial failure is triggered and the shear or axial spring starts deforming.

In the original formulation shear-induced axial failure could precede shear failure for certain cases if the limiting surface provided in Equation 2.2 is exceeded by Equation 2.1. In the current study, this error was fixed, such that axial failure according to Equation 2.2 can occur if only shear failure according to Equation 2.1 has occurred first. This modification was performed by the author of this study after suggestion provided by Dr. Elwood.

Both the shear and axial springs are defined as bi-linear curves with an elastic branch (prior to shear or axial failure) and a degrading branch (after shear or axial failure is triggered). The elastic branch of both the shear and axial springs should reflect the shear and axial elastic properties of the corresponding column. Regarding the degrading branch, Elwood and Moehle (2002) suggest that, according to experimental studies by Nakamura and Yoshimura (2002), axial failure occurs when the shear strength degrades to approximately zero, so $K_{deg,s}$ for the shear spring should be estimated as follows in Equation 2.3:

$$K_{deg,s} = \frac{V_u}{(\Delta_\alpha - \Delta s)} \quad (\text{Eq. 2.3})$$

, where V_u is the ultimate shear strength of the column and Δ_s and Δ_a should be calculated according to Equation 2.1 and 2.2 respectively.

Regarding the axial spring Elwood recommends to use degrading slope $K_{deg,a}$ according to Equation 2.4

$$K_{deg,a} = \frac{1}{100} K_{el,a} \quad (\text{Eq. 2.4})$$

, where $K_{el,a}$ is the elastic axial stiffness of the corresponding column member.

Figure 2.5 provides a schematic plot of the shear and axial response as modeled by the limit state material.

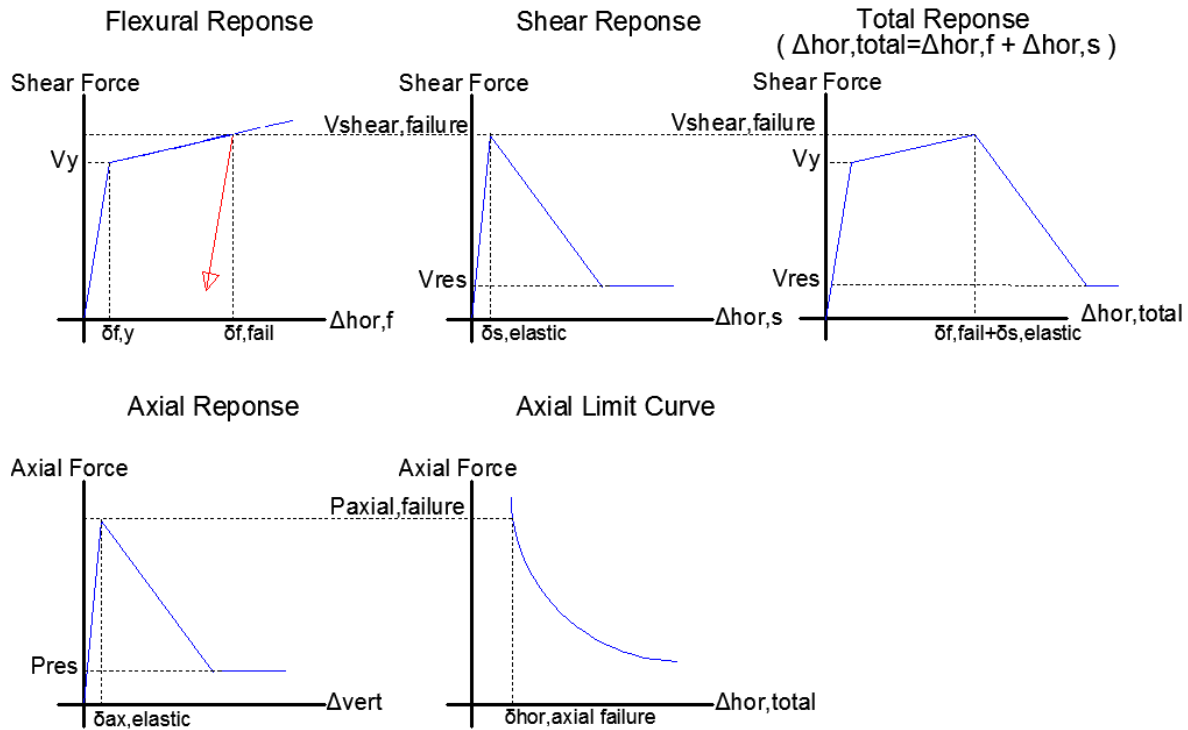


Figure 2.5 Shear and axial response according to the limit state material

As originally suggested, the limit state material was not intended to be utilized for cases where shear failure precedes flexural yielding. The material was modified by the author such that if the shear demand exceeds the shear strength as defined according to ASCE 41-06 (2006) then shear failure is triggered. The shear strength relationship is provided in Equation 2.5.

$$V_n = k \left[\frac{A_v f_{yt} d}{s} + \lambda \left(\frac{6\sqrt{f'_c}}{M/Vd} \right) \sqrt{\left(1 + \frac{N_u}{6\sqrt{f'_c} A_g} \right)} 0.8A_g \right], \quad (\text{Eq. 2.5})$$

2.1.4 Modeling Inadequate Lap-Splicing Conditions for the Column Longitudinal Steel Reinforcement

A common practice in older-type concrete buildings was to use lap-splices for the column longitudinal reinforcement designed for compression forces. This typically resulted in splice lengths equal to 20-24 bar diameters (d_b) long. The lap splices would be located in the column just above the floor slab and would be enclosed by light transverse reinforcement. Observations from past earthquakes as well as laboratory tests have revealed that such splices may be prone to failure under earthquake loading.

Under significant earthquake actions the splicing region is subjected to high tensile stress due to applied moments. The 20-24 d_b splice length without transverse reinforcement is unlikely to be capable of multiple yielding cycles in tension. Failure of the splice will lead to loss of tension capacity and loss of moment strength in the column at the base of the column.

Lynn et al. (1996) investigated the seismic performance of columns following 1970s construction detailing. Eight columns were tested, in which three were provided with inadequate splices at the base of the column. All the specimens failed in shear and although the stresses at the spliced bars did not reach yielding, extensive cracking occurred along the lap splicing region.

Melek and Wallace (2004) performed an experimental assessment of columns following the same cross-sectional geometry and reinforcement detailing used by Lynn (1996). The column height was changed such that the columns would develop their flexural strengths (assuming adequate lap splices) before failing in shear. The specimens were subjected to uni-directional cyclic loading consisting of different loading histories and axial load levels. Extensive damage in the splicing region occurred in all of the specimens.

The results of the experimental investigation by Melek and Wallace are summarized below.

- All the specimens reached maximum calculated yielding moments, indicating that actual bond strength is higher than the bond strength that can be inferred from the ACI 318-11 requirements.
- After the specimens reached lateral drifts ranging between 1.0 to 1.5%, lateral strength degradation was initiated and no hardening branch was observed.
- For near fault displacement history, 62% of the peak lateral force was maintained for lateral drift ratios up to 5%.
- For the far fault displacement history, 36% of the peak lateral force was maintained at 5% lateral drift ratio.

- Specimens subjected to low axial loading did not lose their axial load capacity until 10% drift ratio, while columns with medium and high axial loads lost their axial load capacity at approximately 5% lateral drift ratio.

Figure 2.6 plots the envelope relation between normalized moment and drift ratio for far fault displacement histories.

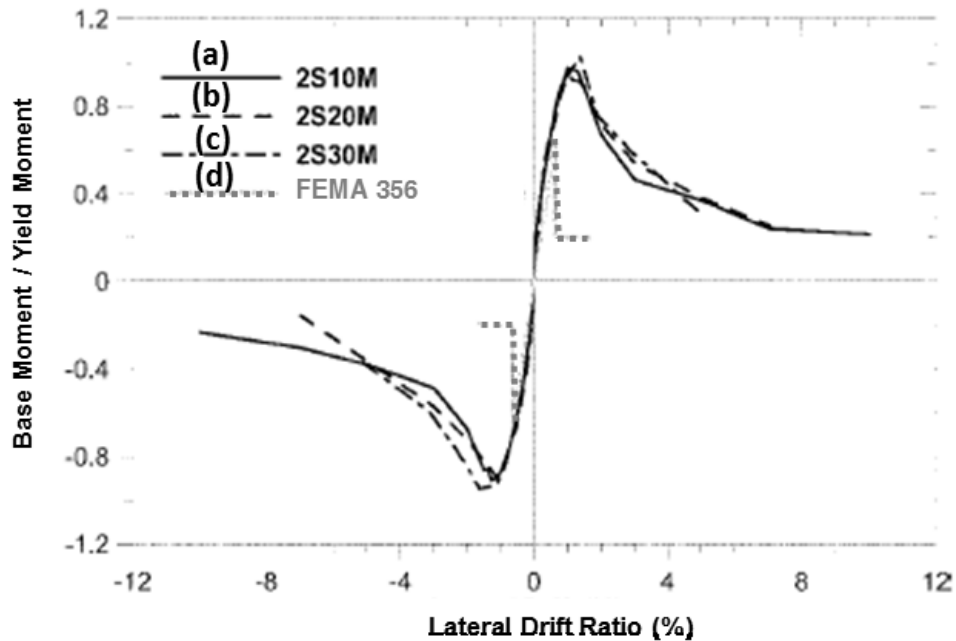


Figure 2.6 Normalized moment – lateral drift ratio for columns with inadequate lap splicing conditions for far fault displacement histories for (a) $P/(A_g * f'_c) = 0.10$ (b) $P/(A_g * f'_c) = 0.20$ (c) $P/(A_g * f'_c) = 0.30$ and (d) FEMA 356 suggested envelope

The FEMA 356 guidelines for modeling columns with inadequate splicing conditions provide conservative criteria in comparison with the data obtained by Melek and Wallace. Therefore, the data of Melek and Wallace for far-fault displacement histories were used to calibrate a simple model to simulate the effect of inadequate column lap splicing.

To model columns with inadequate lap splicing conditions, a lumped plasticity approach using zero-length plastic hinges at the column ends was employed. The backbone moment rotation curve of the plastic hinge where the inadequate lap-splicing connection occurs is shown in Figure 2.7. For the other end of the column, the backbone curve of the plastic hinge was modeled according to Haselton et al. (2008) as discussed in Section 2.1.2. The relatively small data set did not warrant development of an analytical model with cyclic strength deterioration, so only in-cycle deterioration was considered.

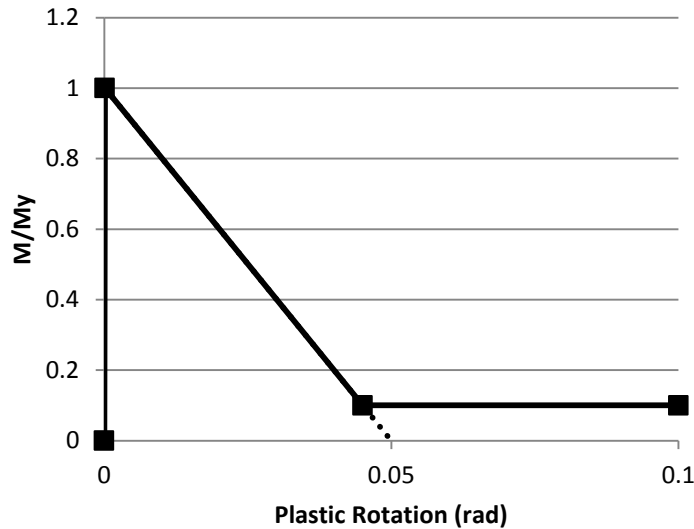


Figure 2.7 Assumed zero-length plastic hinge rotational behavior for inadequate lap-splicing conditions

2.1.5 Beam Column Joints for Collapse Simulation

In the current study the beam-column joints are assumed rigid and potential joint failure is not considered. However, for purpose of completeness, this section presents a brief review of available models for older-type beam-column joints.

The role of joint failure in the collapse of buildings is a subject of current debate. While it is less clear whether joints have contributed to vertical load collapse of existing buildings, it seems irrefutable that joint damage can occur, and this damage can negatively affect the dynamic response of the building. Most reinforced concrete buildings designed prior to 1970s do not have joint transverse reinforcement. In such buildings beam-column joint failure could potentially precede the column shear failure, thereby altering significantly the collapse performance.

Several researchers have proposed analytical models for the shear deformability of joints and for the slip of reinforcement from the joints. Park and Mosalam (2013) and Hassan and Moehle (2012) summarize available research and present new models. Both models use the scissors modeling approach, which consists of a rotational spring connected with rigid links to the beam and column elements. The rigid links have length equal to the joint dimensions. A schematic illustration of the joint sub-assembly is provided in Figure 2.8. The rotational spring located at the central node could represent either (a) only the shear deformation of the joint (in that case an extra spring located at the beam column interface could represent the bar slip) or (b) the sum of the shear deformation of the joint and the joint rotation resulting from bar slip.

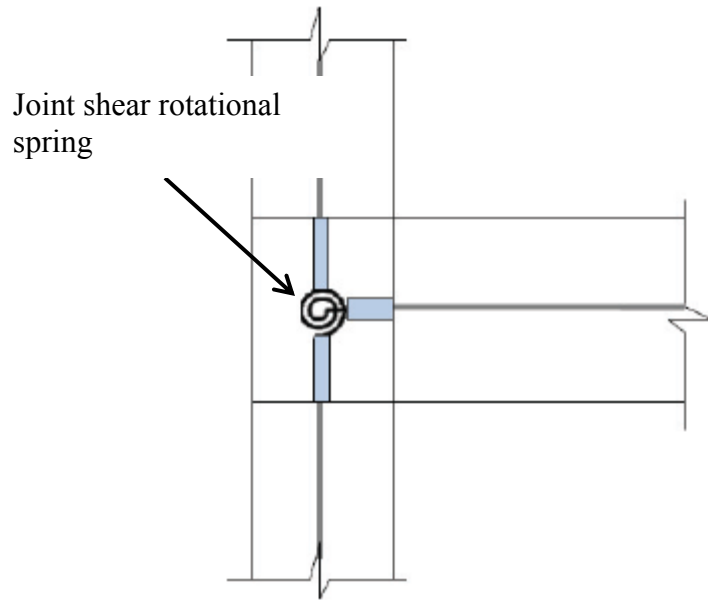


Figure 2.8 Proposed scissors model (Hassan and Moehle, 2012)

Both Park and Mosalam (2013) and Hassan and Moehle (2012) models use a relatively simple backbone curve to model the joint rotation spring for the corner joints. In Figure 2.9 the model suggested by Hassan is illustrated, where the corresponding values of shear stress at point 1, 2, 3, and 4 can be found in Hassan and Moehle (2012).

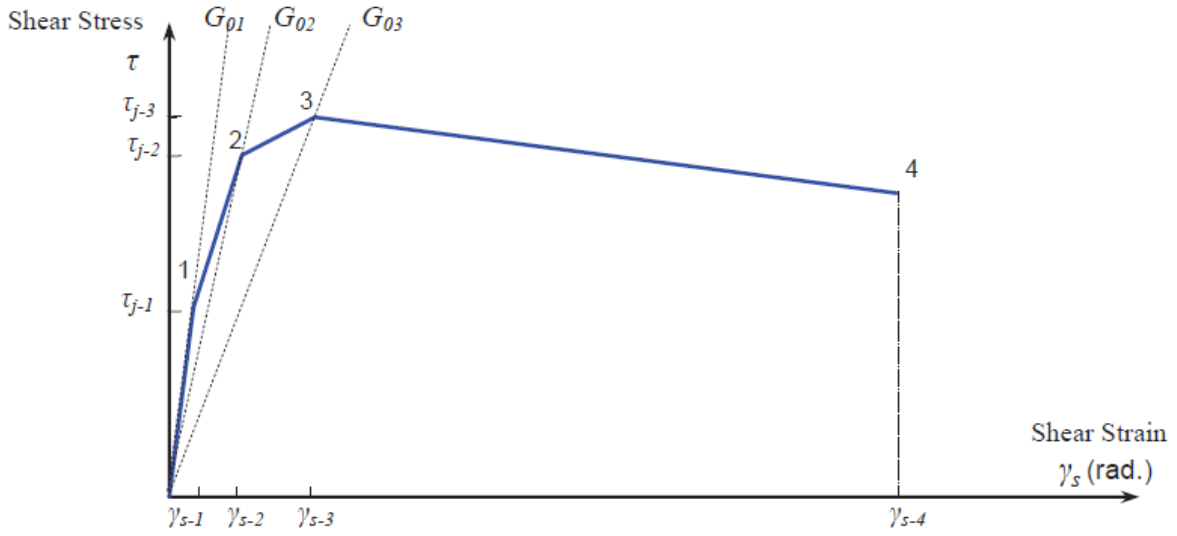


Figure 2.9 Proposed backbone curve of joint shear stress strain (Hassan and Moehle, 2012)

In Figure 2.9, point 1 corresponds to joint cracking, point 2 to pre-peak yielding strength, point 3 is the peak shear strength, and point 4 is the post-peak strength. Point 4 is the maximum drift that the joint can reach prior to axial failure in case of high axial load ($\frac{P}{A_g f'_c} > 0.3$) or severe joint distress for the case of low axial load ($\frac{P}{A_g f'_c} \leq 0.3$).

Hassan suggests the relationship provided in Equation 2.6 to calculate the drift where axial failure occurs in corner joints.

$$\left(\frac{\Delta}{L}\right)_{axial} = 0.057 * \left(\frac{P \tan \theta}{A_{sb} * f_{yb}}\right)^{-0.5} \quad (2.6)$$

where P is the axial load, A_{sb} is the bottom beam reinforcement, f_{yb} is the yield strength, and θ is the shear crack angle.

Based on tests of corner joints available in the literature, Hassan and Moehle (2013) define a line that discretizes the axial failure safe zone from the unsafe zone in Figure 2.10. Equation 2.7 describes the analytical expression of the inclined line in Figure 2.10.

$$\left(\frac{\Delta}{L}\right)_{axial} = \frac{1}{9} - \frac{P}{2.72 f'_c A_g} \quad (2.7)$$

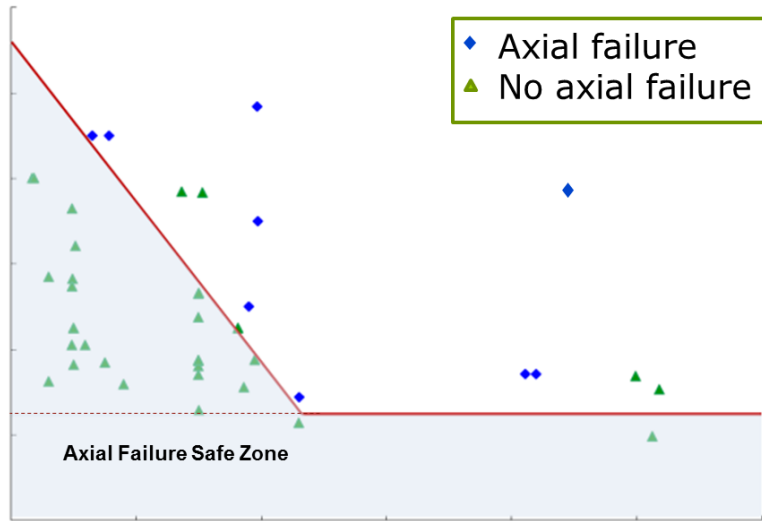


Figure 2.10 Axial load-drift ratio relationship at axial failure for exterior and corner joints (Hassan 2013)

2.2 SEISMIC RISK ASSESSMENT

“Risk assessment is all about risk management. The only reason you do an assessment is because somebody has to make a risk-management decision” (Smith, 2005).

Quantifying the seismic risk for existing buildings has the benefit of providing information to building owners or authorities such that informed decisions regarding seismic upgrading can be made.

Seismic risk has different meanings among different professions or stakeholders. From a seismological perspective, seismic risk is the probability of earthquakes with specific magnitude occurring at least once in a specific region during a specified period (Wang, 2006). From a structural engineering perspective, seismic risk is the probability that a structure will sustain certain damage at least once in a given period. In the current study we will focus on the latter definition of seismic risk.

Seismic risk assessment for structural engineering purposes consists of two main procedures:

- **Seismic Hazard Analysis.** This procedure is concerned with estimation of the probability of exceedance of a certain ground motion parameter or intensity measure during a certain period of time.
- **Assessment of Structural Vulnerability.** This procedure relates ground motion intensity with structural response, usually termed as Engineering Demand Parameter (EDP).

If we define risk as the annual rate of exceedance of a specified EDP level, then risk can be quantified by using Equation 2.8:

$$\lambda_{EDP}(edp) = \int_{IM} G_{EDP|IM}(edp | im) \left| \frac{d\lambda_{IM}(im)}{dim} \right| dim \quad (2.8)$$

,where EDP corresponds to the Engineering Demand Parameter, IM corresponds to the Intensity Measure, and $G_{EDP|IM}$ is the complementary cumulative distribution function (CCDF) of an EDP (e.g., collapse state or a certain story drift rate) given an earthquake Intensity Measure (IM). Estimating the parameters that define the $G_{EDP|IM}$ is the main objective of the current study.

The estimation of the annual probability of exceedance of a certain earthquake intensity level (in this study the earthquake intensity level will be defined as spectral acceleration at the fundamental period of the building) will be assumed to be provided by Probabilistic Seismic Hazard Analysis (PSHA), which can be performed relatively easily using software available online provided by USGS or by a specialist in engineering seismology.

In the following sections a review of two approaches commonly used by engineers to estimate $G_{EDP|IM}$ will be presented.

2.2.1 Regress using Unscaled Ground Motions (Cloud Analysis)

According to this method a set of ground motions is selected and then non-linear dynamic analysis is performed for each unscaled record. Consequently, the results of the analyses are plotted. Each earthquake corresponds to a dot in a graph that relates EDPs with IMs. The method is commonly termed as “cloud analysis” because the data as plotted in Figure 2.11a form an elliptical shape similar to that of a cloud (Baker 2007).

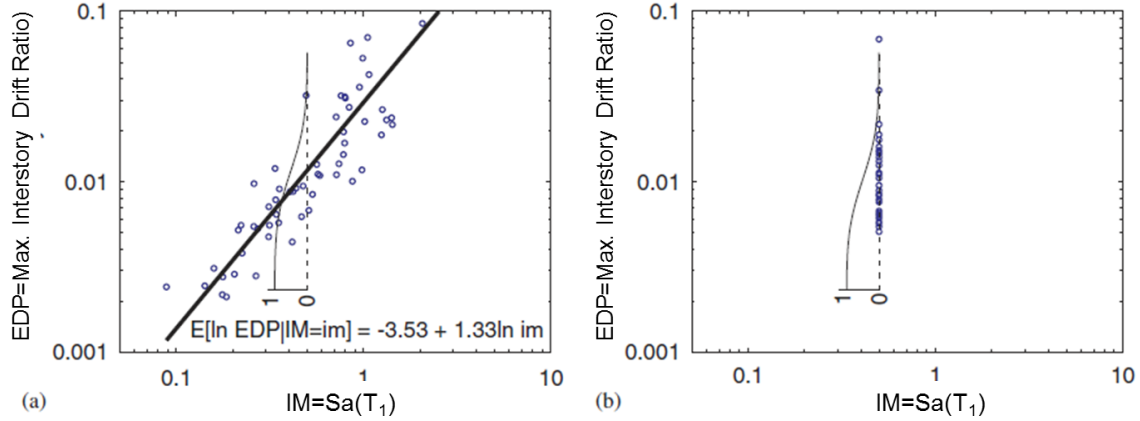


Figure 2.11 Estimating the conditional distribution of EDP | IM at Sa(T₁) using “cloud analysis” (a) conditional mean value from linear regression (b) comparison of strip of EDP data Gaussian CCDF based on linear regression (Baker 2007)

This method utilizes simple linear regression to relate IM and EDP through a model described in Equation 2.9:

$$\ln(EDP | IM) = \hat{\beta}_0 + \hat{\beta}_1 \ln(im) + \varepsilon \quad (2.9)$$

where $\hat{\beta}_0$ and $\hat{\beta}_1$ are the regression coefficients, IM is the predictor, and ε is the model error.

According to Equation 2.9, for a given IM the $\ln(\hat{EDP})$ prediction is provided. If it is assumed that variance is constant (homoscedasticity assumption) for all IMs, then the standard deviation can be estimated as shown in Equation 2.10

$$\hat{\sigma}_\varepsilon = \frac{1}{n-2} \sqrt{\sum_i^n (\ln(EDP_i) - \ln(\hat{EDP}_i))^2} \quad (2.10)$$

, where n is the number of simulated analyses. If $\ln(\text{EDP} | \text{IM})$ is assumed further to have normal distribution, then $G_{\text{EDP} | \text{IM}}$ is given by Equation 2.11:

$$G_{\text{EDP} | \text{IM}}(edp | im) = 1 - \Phi\left(\frac{\ln edp - \hat{\beta}_0 + \hat{\beta}_1 \ln(im)}{\hat{\sigma}_\varepsilon}\right) \quad (2.11)$$

, where Φ is the cumulative distribution function of the standard normal distribution.

The assumptions stated above impose restrictions on the applicability of the method. Specifically, since the variance of EDP is rarely constant at a wide range of IMs, the method should be applied only for a small range of IM levels.

However, this limitation can be overcome if we apply regression only for limited IM ranges (such that the regression is piecewise linear). This approach increases the computational effort and would remove the advantage of the method to provide a closed form solution for Equation 2.11.

2.2.2 Scaling Records to the Target IM Level - IDA

Instead of using unscaled motions having a wide range of IM levels as presented in the previous section, one can alternatively scale a set of motions so that each matches the IM of interest. At the IM of interest an empirical cumulative distribution function (ECDF) can be plotted and, assuming that the EDP follows a certain distribution (e.g., log-normal), we could estimate the distribution parameters required such that they fit the observed data of the ECDF. According to this method, $G_{\text{EDP} | \text{IM}}$ would be estimated according to Equation 2.12.

$$G_{\text{EDP} | \text{IM}}(edp | im) = 1 - \Phi\left(\frac{\ln(im) - \hat{\mu}}{\hat{\sigma}}\right) \quad (2.12)$$

where $\hat{\mu}$ and $\hat{\sigma}$ correspond to sample mean and standard deviation.

The procedure can be repeated several times for different IM levels such that multiple stripes of data are obtained, as shown in Figure 2.12. Interpolation can be used to estimate the probabilities of exceedance at intermediate IM levels.

This method has the drawback that a large number of dynamic analyses are required to obtain a large number of stripes. Furthermore, scaling of ground motions is required, which could

potentially lead to “artificial,” unrealistic, earthquake motions used in dynamic simulations, thereby creating a bias in the results. Although the drawbacks of this method seem to be rather important, the advantage to be able to cover a large range of IM levels makes it appealing. The latter advantage of the method has made it particularly popular at relatively high IM levels for which there are not enough available ground motions.

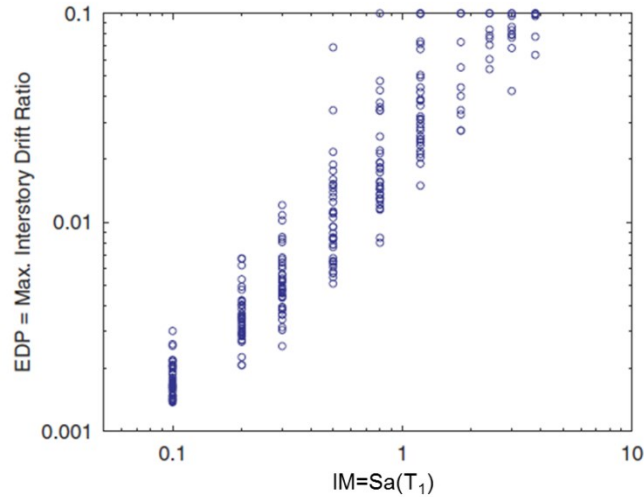


Figure 2.12 Multiple stripes of data for different IM Levels (Baker 2007)

2.2.2.1 Incremental Dynamic Analysis (IDA)

The method presented above can easily be formulated such that it can estimate the probability of exceedance of EDP at a wide range of IM levels until collapse of the structure. This extension of the method is called Incremental Dynamic Analysis (IDA) (Vamavatsikos and Cornell, 2002) (or alternatively dynamic pushover) and involves a series of dynamic non-linear analyses performed using scaled ground motions whose IM levels are selected and scaled to cover the whole structural response range from elastic behavior to dynamic instability (collapse).

In the current study, the IDA method was modified such that it focused on estimation of the probability of collapse, rather than examining the full range of response. The (modified) IDA procedure is described below.

1. The first step in performing collapse assessment through the IDA concept is selecting earthquake ground motion records. In the current study a set of 22 pairs of far-field records (recorded at sites less than 10 km from fault rupture) were selected. The record

set that was selected is the same as the set used for the ATC-63 project (FEMA,2009). The records were selected to meet a number of objectives listed below:

- **Source Magnitude:** Ground motions from large magnitude events ($M \geq 6.5$) are selected, as their longer durations and stronger shaking pose a greater risk for structures.
- **Source Type:** The record set includes ground motions from earthquakes generated from strike-slip and from thrust fault rupture types. These sources were selected since they were considered typical of shallow crustal earthquakes in California and other Western United States locations.
- **Site Conditions:** The records were selected such that they were recorded on different soil conditions ranging from class B to D (classes A, E, and F were not considered typical for buildings).
- **Number of Recordings for each Event:** To avoid event-bias, not more than two records for each event was considered in the record set.
- **Strong Recordings:** To avoid unrealistic scaling of ground motions to achieve structural collapse, the ground motions were selected such that they possess Peak Ground Acceleration (PGA) $> 0.2g$ and Peak Ground Velocity (PGV) $> 15\text{cm/sec}$. These values were considered the thresholds of earthquakes that could cause structural damage.
- **Recording Location:** To avoid soil-structure-foundation interaction, recordings from instruments located in free-field or ground floor of small buildings were used.

Tables 2.1 and 2.2 summarize the record set ground motion characteristics used in the current study.

Table 2.1 Far-field record set used in the current study

ID No.	Earthquake			Recording Station	
	M	Year	Name	Name	Owner
1	6.7	1994	Northridge	Beverly Hills- Mulljol	USC
2	6.7	1994	Northridge	Canyon Country- WLC	USC
3	7.1	1999	Duzce, Turkey	Bolu	ERD
4	7.1	1999	Hector Mine	Hector	SCSN
5	6.5	1979	Imperial Valley	Delta	UNAMUCSD
6	6.5	1979	Imperial Valley	El Centro Array #11	USGS
7	6.9	1995	Kobe, Japan	Nishi- Akashi	CUE
8	6.9	1995	Kobe, Japan	Shin-Osaka	CUE
9	7.5	1999	Kocaeli, Turkey	Duzce	ERD
10	7.5	1999	Kocaeli, Turkey	Arcelik	CDMG
11	7.3	1992	Landers	Yermo Fire Station	KOERI
12	7.3	1992	Landers	Coolwater	SCE
13	6.9	1989	Loma Prieta	Capitola	CDMG
14	6.9	1989	Loma Prieta	Gilroy Array #3	CDMG
15	7.4	1990	Manji, Iran	Abbar	BHRC
16	6.5	1987	Superstition Hills	El Centro Imp. Co	CDMG
17	6.5	1987	Superstition Hills	Poe Road (temp)	USGS
18	7.0	1992	Cape Mendocino	Rio Dell Overpass	CDMG
19	7.6	1999	Chi-Chi Taiwan	CHY101	CWB
20	7.6	1999	Chi-Chi Taiwan	TCU045LA	CWB
21	6.6	1971	San Fernando	LA - Hollywood Stor	CDMG
22	6.5	1976	Friuli, taly	Tolmezzo	..

Table 2.2 Far-field ground motion parameter information

ID No.	PEER-NGA Record Information		Recorded Motions	
	File Names - Horizontal Records		PGA _{max}	PGV _{max}
	Component 1	Component 2	(g)	(cm/s)
1	NORTHR/MUL009	NORTHR/MUL279	0.52	63
2	NORTR/LOS000	NORTR/LOS270	0.38	45
3	DUZCE/BOL000	DUZCE/BOL090	0.82	62
4	HECTOR/HEC000	HECTOR/HEC090	0.34	42
5	IMPVALL/H-DLT262	IMPVALL/H-DLT352	0.35	33
6	IMPVALL/H-E11140	IMPVALL/H-E11230	0.38	42
7	KOBE/NIS000	KOBE/NIS090	0.51	37
8	KOBE/SHI000	KOBE/SHI090	0.24	38
9	KOCAELI/DZC180	KOCAELI/DZC270	0.36	59
10	KOCAELI/ARC000	KOCAELI/ARC090	0.22	40
11	LANDERS/YER270	LANDERS/YER360	0.24	52
12	LANDERS/CLW-LN	LANDERS/CLW-TR	0.42	42
13	LOMAP/CAP000	LOMAP/CAP090	0.53	35
14	LOMAP/G03000	LOMAP/G03090	0.56	45
15	MANJIL/ABBAR-L	MANJIL/ABBAR-T	0.51	54
16	SUPERST/B-ICC000	SUPERST/B-ICC090	0.36	46
17	SUPERST/B-POE270	SUPERST/B-POE360	0.45	36
18	CAPEMEND/RIO270	CAPEMEND/RIO360	0.55	44
19	CHICHI/CHY101E	CHICHI/CHY101N	0.44	115
20	CHICHI/TCU045-E	CHICHI/TCU045-N	0.51	39
21	SFERN/PEL090	SFERN/PEL180	0.21	19
22	FRIULI/A-TMZ000	FRIULI/A-TMZ270	0.35	31

- The second step in the procedure corresponds to gradual scaling of each ground motion until the structure leads to collapse. For each ground motion analysis the maximum story drift ratio and corresponding $S_a(T_1)$ level are reported as a dot in Figure 2.13(a). Consequently the dots for each ground motion are connected by lines (assuming linear interpolation between $S_a(T_1)$ and maximum story drift ratio). These lines are termed as the IDA curves and correspond to a dynamic pushover for each record. In Figure 2.13(a), a total of 44 lines are shown (equal to the number of total records used).

3. The third step corresponds to defining collapse. As mentioned above, two collapse modes are considered in the current study. Side-sway collapse was defined when the story drift exceeds an unrealistically large value such that it is certain that collapse has occurred. However, from Figure 2.13(a) it becomes obvious that the structure in most cases is failing at drift equal to about 5-6 % where the slope of the IDA curves are approximately flat. This type of collapse was considered for models that possess column members expected to fail due to flexural degradation (and flexural induced axial failure). This issue will be discussed further in Chapter 4. In case the building possesses column members that experience shear and shear induced axial failure, collapse is defined to occur when more than 50% of the columns in a story fail in shear or shear-induced axial mode.

After a collapse point is identified, each ground motion is scaled in small increments equal to 0.03g downward such that the exact collapse point is tracked. In this methodology, this small increment of scaling after collapse has occurred corresponds to the accuracy by which the collapse point is defined. When the collapse point is identified between two collapse levels (e.g., collapse is not observed for $S_a = 0.81g$ but collapse is observed for $S_a = 0.84g$), the mean of these two values is reported as the collapse point (e.g. $S_a = \frac{0.81g + 0.84g}{2} = 0.825g$). The error tolerance in the current study is thus $0.03g/2 = 0.015g$.

4. After the collapse points for each considered record have been identified, an Empirical CDF is plotted as shown in Figure 2.13 (b). Following the suggestion by Shome and Cornell (1999), the parameters μ and σ as described in Equation 2.12 are estimated such that the assumed distribution fits the observed data. The fitted CDF is termed as fragility curve.
5. Using Equation 2.12 of the generic formulation of the method and substituting EDP with collapse, the Equation is defined as follows:

$$G_{\text{collapse}|\text{IM}}(\text{collapse} | \text{im}) = 1 - \Phi\left(\frac{\ln(\text{im}) - \hat{\mu}}{\hat{\sigma}}\right) \quad (2.13)$$

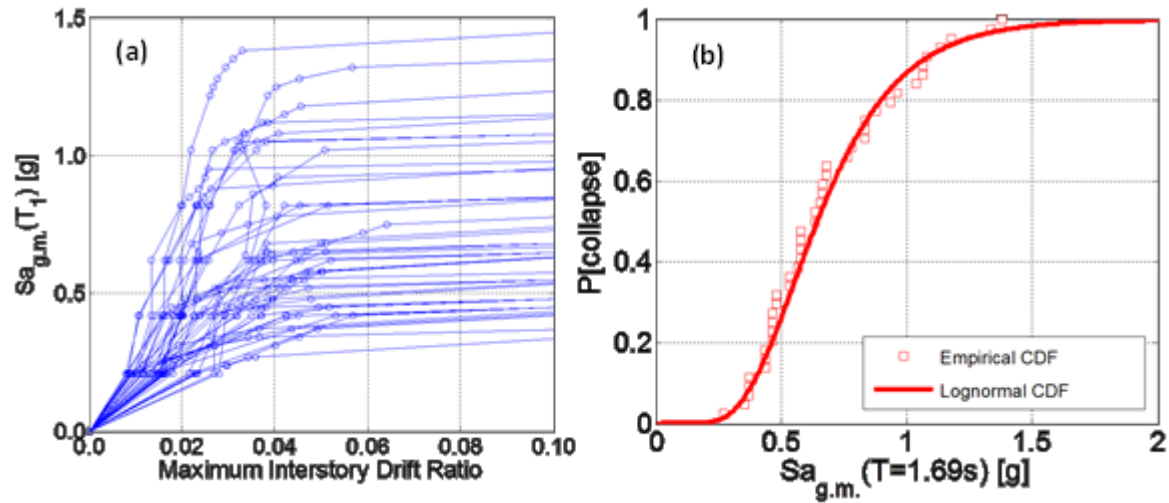


Figure 2.13 Development of fragility curves: (a) IDA curves for an 8-story building, (b) Derived fragility Curve for an 8-story building

2.3 IDENTIFYING PARAMETERS INFLUENCING THE COLLAPSE PERFORMANCE

As explained in Chapter 1, buildings designed prior to 1980s suffer from several structural deficiencies, mainly due to proportioning that creates a weak story or due to lack of appropriate seismic detailing. As part of the NEES Grand Challenge Program, in the NIST Program Plan, a list of critical deficiencies that according to engineers in practice have a significant influence to the collapse vulnerability of older-type concrete buildings was provided. The list is shown in Table 2.3

Table 2.3 Critical seismic deficiencies found in pre-1980 concrete buildings (NIST GCR 10-917-7)

<p>Type A: Shear-critical column</p>  <p>Shear and axial failure of columns in a moment frame or in gravity system.</p>	<p>Type F: Other Concrete Frames</p>  <p>Frames having typical era details with collapse mechanisms other than those resulting from deficiencies A through E (i.e. inadequate splices, frames with low lateral capacity, smooth reinforcement, etc.).</p>
<p>Type B: Captive Columns</p>  <p>Shear and axial failure of columns due to partial-height infills or other walls.</p>	<p>Type G: Discontinuous wall</p>  <p>Columns prone to crushing from overturning of discontinuous concrete or masonry infill wall, as distinct from Deficiency E where collapse is governed by large lateral deformation demands.</p>
<p>Type C: Beam-column Joints</p>  <p>Shear and axial failure of unconfined beam-column joints, particularly corner joints.</p>	<p>Type H: Severe plan irregularity</p>  <p>Conditions (including some corner buildings) leading to large torsional-induced demands.</p>
<p>Type D: Slab-column connections</p>  <p>Punching of slab-column connections under imposed lateral drifts.</p>	<p>Type I: Severe vertical irregularity</p>  <p>Setbacks causing concentration of damage and collapse at story where stiffness and strength changes. Can also be caused by change in materials and SFRS.</p>
<p>Type E: Weak column mechanism</p>  <p>Weak-column, strong-beam moment frame or similar system prone to story collapse from failure of weak columns.</p>	<p>Type J: Pounding</p>  <p>Collapse caused by pounding of adjacent buildings with non-coincident story heights.</p>

In the NIST program plan, it was suggested to link the deficiencies presented in Table 2.3 with simple engineering parameters. These parameters should not require any complicated analysis, but instead should be easy to calculate based on information obtained by reviewing the structural drawings. The program plan suggested that any of the parameters that according to analysis is

shown to be highly correlated with collapse performance of the structure could be termed a “collapse indicator.”

In Chapter 5, following directly the approach suggested by NIST, it was verified that certain parameters such as the column to beam bending moment strength ratio are highly correlated to collapse performance. The approach that was followed corresponds to varying the values of one parameter and accordingly obtaining the corresponding fragility curve of the building as depicted in Figure 2.14. It was shown that there is a critical point where further increase or decrease in the value of the parameter results in dramatic change of probability of collapse.

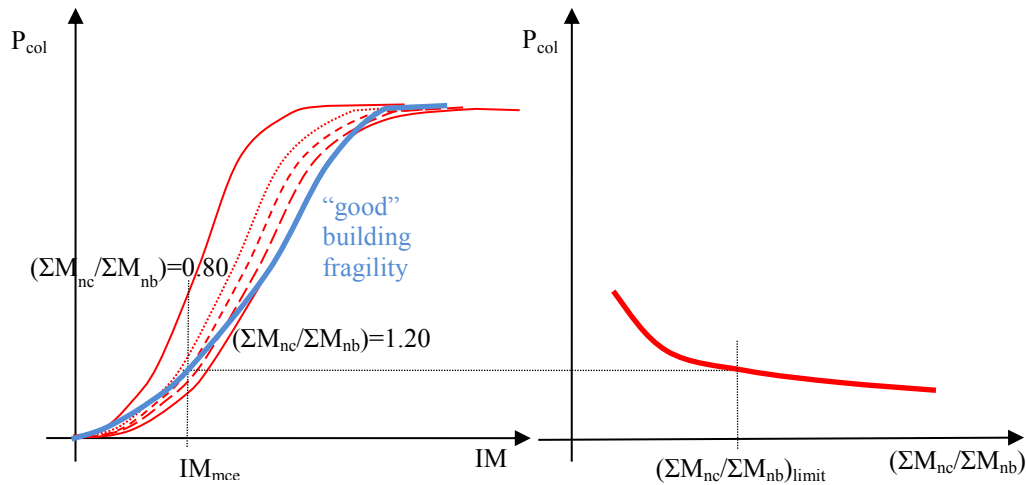


Figure 2.14 Approach for establishing collapse indicator limits. Example collapse fragilities for different collapse indicator values ($\Sigma M_{nc}/\Sigma M_{nb}$: column to beam bending moment strength ratio, IM: Earthquake Intensity Measure)

2.4 ESTIMATING STORY DRIFT DEMAND

The current study uses a large number of dynamic analyses performed through the IDA method to provide regression estimates regarding drift demands.

A similar approach was followed by Shome and Cornell (1999) to estimate maximum story drift ratio demands. In his study, Shome employed two structural steel, special moment resisting frames (SMRFs) designed according to the LRFD specifications (LRFD, 1994). To estimate story drift ratio demand Shome tried to perform statistical regression based on numerous non-linear dynamic analyses using scaled ground motions. Figures 2.15 and 2.16 depict the considered buildings:

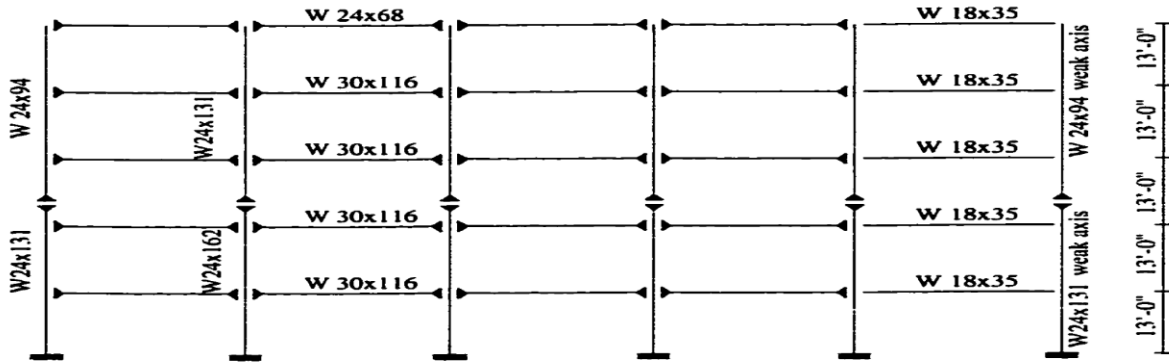


Figure 2.15 5-story SMRF (Shome, 1999)

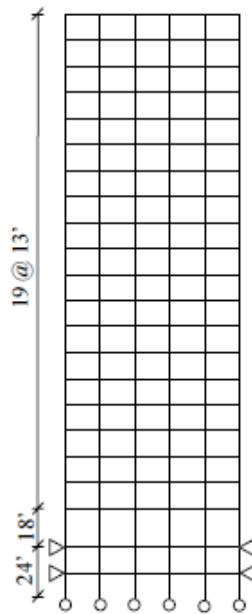


Figure 2.16 20-story SMRF (Gupta, 1999)

In his study Shome relates the maximum story drift with different intensity parameters using regression. The results of linear regression for both the 5 and 20 story building are cited below:

Table 2.4 Regression relationships of maximum story drift and different intensity measures (Shome, 1999)

Building	Predictor(s)	Regressions Fuction	R ²	σ _{ln,ε}
5-Story	Sa(T ₁)	DR=0.03*Sa(T ₁) ^{1.00}	0.76	0.38
	Sa(T ₂), Sa(T ₁)	DR=0.02*Sa(T ₁) ^{0.75} *Sa(T ₂) ^{0.25}	0.8	0.35
	Sa(T ₁) , M	DR=0.01(Sa(T ₁) ^{1.00} * e ^{0.13M}	0.77	0.37
	Sa(T ₁), R	DR=0.02*Sa(T ₁) ^{1.00} *R ^{0.11}	0.76	0.37
	Sa(T ₁) , D	DR=0.03*Sa(T ₁) ^{1.00} * e ^{0.003D}	0.76	0.38
20-Story	Sa(T ₁)	DR=0.16*Sa(T ₁) ^{0.95}	0.7	0.44
	Sa(T ₁), Sa(T ₂)	DR=0.09*Sa(T ₁) ^{0.56} *Sa(T ₂) ^{0.40}	0.8	0.36
	Sa(T ₁) , M	DR=0.01(Sa(T ₁)0.53* e ^{-0.08M}	0.71	0.44
	Sa(T ₁), R	DR=0.32*Sa(T ₁)0.95*R ^{-0.22}	0.72	0.43
	Sa(T ₁) , D	DR=0.19*Sa(T ₁)0.95* e ^{0.01D}	0.71	0.43

Where, Sa(T₁) (g) is the ground motion spectral acceleration at the 1st mode period, Sa(T₂) (g) is the ground motion spectral acceleration at the 2nd mode period, M corresponds to the earthquake magnitude, R is the epicentral distance, and D is the ground motion duration.

To derive the regression functions shown in Table 2.4 Shome assumed different linear regression models with the general formulation presented in Equation 2.14

$$\ln(IDR | IM_1, IM_2, \dots) = \hat{\beta}_0 + \hat{\beta}_1 \ln(im_1) + \hat{\beta}_2 \ln(im_2) + \dots + \varepsilon \quad (2.14)$$

The regression estimates demonstrated that for the 5-story building, Sa(T₁) is the most statistically significant parameter while Sa(T₂), M, R, and D did not seem to influence so much the results. In contrast, for the 20-story building both Sa(T₁) and Sa(T₂) are significant, which can be observed by the significant reduction in the error of the model that includes both Sa(T₁) and Sa(T₂). This observation is intuitive since for the taller building higher modes are expected to be more significant. The relatively high R² values demonstrate that the regression model largely explains the variability in the maximum story drift.

In Table 2.4, for the regression function with Sa(T₁) being the only predictor to estimate maximum story drift, $\hat{\beta}_1 \approx 1$ for both the 5 and 20-story buildings. This implies that the maximum story drift (DR) is an approximately linear function of Sa(T₁).

Based on the assumption that there is an approximately linear relationship between DR and $Sa(T_1)$ as demonstrated by Shome and Cornell (or in other words that $\beta_1=1.0$), Equation 2.14 can be simplified to Equation 2.15, which is more intuitive for engineers. The latter equation implies a linear relationship between the predicted maximum story drift demand Δ_D and the average drift ratio δ_{eff}/h_{eff} .

$$\ln(\Delta_D | IM_1) = \hat{\beta}_0 + \ln(\delta_{eff} / h_{eff}) + \varepsilon \quad (2.15)$$

, where Δ_D corresponds to the predicted story drift demand, δ_{eff} is the displacement at the effective height of the building (δ_{eff} is a function of $Sa(T_1)$), and h_{eff} is the effective height of the building assumed to be equal to 70% of the total building height.

Equation 2.15 was used in the current study to relate story drift demand and average drift ratio. The relationship 2.15 was calibrated using results from the non-linear dynamic analysis performed as part of the IDA. The calibration was performed such that the estimated coefficient $\hat{\beta}_0$ minimizes the sum of the square errors.

If we define $\alpha = \exp(\hat{\beta}_0)$ in Equation 2.15, then α links linearly the average drift ratio and the predicted maximum story drift ($\Delta_D = \alpha * \delta_{eff}/h_{eff}$). This procedure will be discussed further in Chapter 6 and Appendix G.

The regression results obtained in the current study using IDA agree with those estimated by Shome and Cornell. In the current study the goodness of fit of Equation 2.15 was checked visually. Further research is required to determine a model that would relate story drift ratio demand with intensity measures in an optimal way such that both simplicity and high accuracy are satisfied.

2.5 ESTIMATING COLUMN DRIFT CAPACITY

After the drift demand has been defined using the procedure described above, the current methodology requires estimation of the column drift capacity. In the current study, drift capacity is defined deterministically using the shear failure surface suggested by Elwood, as expressed by Equation 2.1 at the beginning of this chapter.

In the general formulation of the methodology, capacity can also be defined as random variable taking into account material and modeling uncertainties, but that approach was not pursued here.

Liel et al. (ATC-78, 2014) defined column deformation capacity in terms of column base rotation. The approach suggested by Liel attempts to follow the same procedure used by ASCE 41 to define component deformation capacities.

Following the ASCE 41 procedure, Liel suggests that columns should be classified according to their structural detailing using Table 2.5

Table 2.5 Classification of column condition (Li et al. 2013)

		Transverse Reinforcement Details		
		ACI conforming details with 135° hooks	Closed hoops with 90° hooks	Other (including lap spliced transverse reinforcement)
Ratio of flexural to shear strength	$(V_p/V_n) \leq 0.6$	<i>i</i>	<i>ii</i>	<i>ii</i>
	$1.1 \geq (V_p/V_n) \geq 0.6$	<i>ii</i>	<i>ii</i>	<i>iii</i>
	$(V_p/V_n) > 1.1$	<i>iii</i>	<i>iii</i>	<i>iii</i>

Based on linear regression of experimental results by Berry et al. (2004), Liel defines in Table 2.6 column deformation capacities that correspond to column axial failure level. The column deformation capacities defined by Liel could be compared with parameter *b* of the ASCE-41 backbone curve for column force-deformation response. The ASCE-41 backbone curve for component force-deformation response is presented in Figure 2.17. Table 2.7 presents a comparison between column deformation capacities as suggested by Liel et al. (2014) and ASCE-41

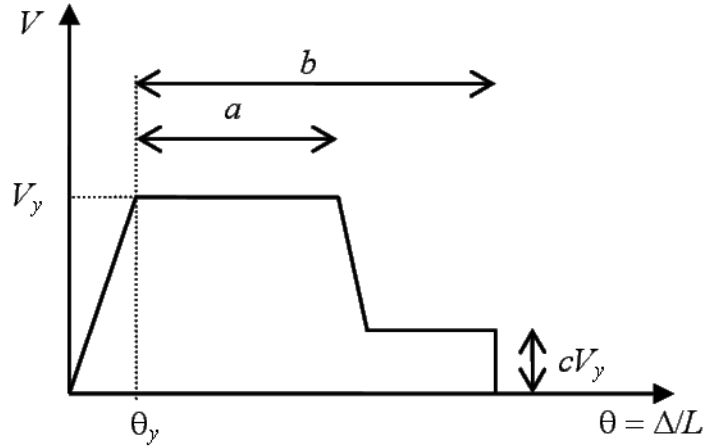


Figure 2.17 Backbone curve of component force-deformation response in ASCE-41 (Li et al. , 2013)

Table 2.6 Column deformation capacities according to column condition (Liel et al. 2014)

$P/A_g f'_c$	$\rho_v = A_w/b_w s$	Plastic Rotation Capacity θ_c
Condition <i>i</i>		
≤ 0.1	≥ 0.006	0.090
≥ 0.6	≥ 0.006	0.030
≤ 0.1	$= 0.002$	0.050
≥ 0.6	$= 0.002$	0.018
Condition <i>ii</i>		
≤ 0.1	≥ 0.006	0.082
≥ 0.6	≥ 0.006	0.023
≤ 0.1	≤ 0.0005	0.025
≥ 0.6	≤ 0.0005	0.011
Condition <i>iii</i>		
≤ 0.1	≥ 0.006	0.075
≥ 0.6	≥ 0.006	0.020
≤ 0.1	≤ 0.0005	0.016
≥ 0.6	≤ 0.0005	0.006

Table 2.7 Column deformation capacities for condition iii columns (Liel et al.,2014)

$P/A_g f'_c$	$\rho_v = A_v/b_w s$	ASCE 41 b	Liel et al. Plastic rotation capacity
≤ 0.1	≥ 0.006	0.060	0.075
≥ 0.6	≥ 0.006	0.008	0.020
≤ 0.1	≤ 0.0005	0.006	0.016
≥ 0.6	≤ 0.0005	0	0.006

A comparison of column deformation capacities provided by Liel et al., the ASCE 41 column deformation capacities, estimates of axial failure drift capacities based on the Equation 2.2, and experimental data is presented in Figure 2.18.

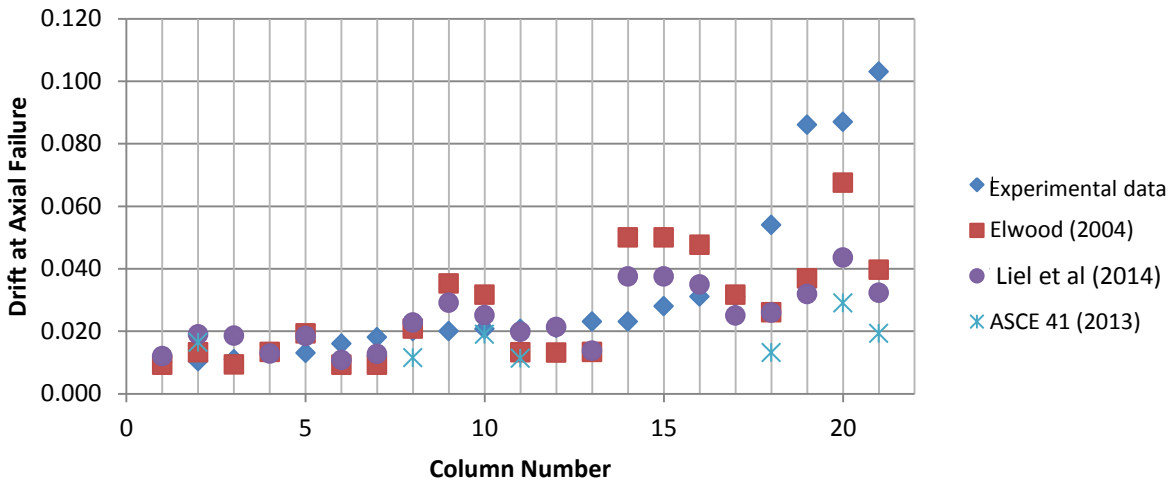


Figure 2.18 Comparison of column deformation capacity values provided by different models

Liel suggests that since linear regression was used to derive the estimated column rotation values in Table 2.6, it can be assumed that deformation capacities follow approximately a log-normal distribution. The standard deviation for the logarithm of the estimated quantities in Table 2.6 is provided equal to $\sigma_{\ln \Delta_c} = 0.60$.

Assuming a log-normal distribution for the column deformation capacity values provided above and a log-normal distribution for the story drift demand values as discussed in the previous section, the probability that demand will exceed capacity can be calculated by Equations 2.16 – 2.17:

$$\beta = \frac{\mu_{\ln, \Delta_C} - \mu_{\ln, \Delta_x}}{\sqrt{\sigma_{\ln, \Delta_C}^2 + \sigma_{\ln, \Delta_x}^2}} \quad (\text{Eq. 2.16})$$

$$P(\ln(\Delta_D) > \ln(\Delta_C)) = \Phi(-\beta) \quad (\text{Eq. 2.17})$$

3 Evaluation of Collapse Simulation of Concrete Frame Structures

Later chapters of this report will use non-linear dynamic analyses to evaluate the seismic performance of buildings. Modeling the non-linear response and more specifically brittle failure modes like shear and shear-induced axial failure that existing concrete buildings are susceptible to, is a particularly challenging task. Most of the models available in the literature have been calibrated by results of pseudo-static laboratory test, in which the tested column is subjected to displacement reversals of increasing amplitude until substantial loss of strength. As suggested in Haselton et al (2008), tests with a greater variety of loading histories are required to improve the accuracy of the current modeling techniques.

In this Chapter, the results of eleven one-story, one-bay reinforced concrete test structures subjected to base motions on a shaking table are presented. The columns in the test structures had either widely spaced transverse reinforcement or closely spaced transverse reinforcement resulting in relatively brittle or relatively ductile response. The base motions represented either a long-duration motion without significant long-period pulses or a shorter duration motion with a significant velocity pulse, imparted with an intensity that caused collapse of the test structures.

Analytical models of the test structures were developed for the purpose of exploring the simulation capabilities that have been used in this study to evaluate the performance of existing buildings.

In the sections below a brief overview of the experimental setup and material properties is provided. Consequently a comparison between results obtained by using collapse simulation analytical tools with those obtained from the actual laboratory tests is presented. The interested reader can find further details about the presented laboratory tests in Shin (2007).

3.1 EXPERIMENTAL INVESTIGATION

A laboratory test program was designed to test reinforced concrete columns subjected to dynamic lateral loading. The purpose of the test program was to investigate the dynamic response of column members with different ductility. Two different types of columns were tested. The first type had dense spacing of transverse reinforcement, similar to requirements of current code provisions for buildings in regions of high seismicity. This column type was intended to have a ductile load-displacement response. The second type had wide spacing of transverse reinforcement, characteristic of building practices prior to 1970s. This column type was intended to yield in flexure, followed by shear and axial failure. Fig. 3.1 illustrates the two

column types. Due to limitations of the shaking table, the scale of the test columns was approximately one-third of their full scale. Normal-weight concrete compressive strength ranged from 3 to 4 ksi. Longitudinal reinforcement was Grade 60.

For the shear-critical columns, the geometry by Lynn (1996) and Sezen (2002) was chosen as the prototype. The full-scale prototype column had a 18" square column with a net height equal to 9'-8". Eight #9 longitudinal bars were spaced evenly around the column perimeter with #3 ties with 12" spacing. The one-third scaled shear-critical columns consisted of a 6" square column with eight #3 longitudinal reinforcing bars spaced evenly around the column perimeter with a cover of equal to 2/3" (longitudinal reinforcement ratio equal to 2.44%). The longitudinal bars were embedded in a top and bottom beam stub. The bars were bent with 90-degree hooks of length $12d_b$ (where d_b is the longitudinal bar diameter) to prevent pullout failure. Plain 1/8" diameter wire was used for the transverse reinforcement. The transverse reinforcement consisted of a perimeter hoop plus two crossties (one in each direction). Hoops had 90-degree anchorage hook with length equal to $6d_b$. Crossties had 90-degree hook on one end and 135-degree hook on the other end. The transverse reinforcement was spaced at 4" center-to-center distance along the column height with the 90-degree hook crossties alternated along the height.

The ductile columns had the same gross dimensions with the same longitudinal reinforcement configuration as the shear-critical columns. The only difference between the two column types was the transverse reinforcement detailing. The transverse reinforcement details of the ductile columns were designed to comply with the ACI 318. For the ductile columns, (3/16)" diameter plain wire was used as transverse reinforcement with center-to-center spacing equal to 1-1/2" along the length of the column. The transverse reinforcement consisted of hoops with 135-degree hooks with anchorage length equal to $6d_b$ and of crossties with 135-degree hooks as well.

The single-bay frame that is shown in Fig. 3.2 was selected for the test series. Since the purpose of the test was to understand the non-linear dynamic behavior of columns, an idealized, reusable, nearly-rigid steel beam was used to connect and load the two concrete columns of a test frame. The base of the columns was supported by a nearly rigid load cell that connected to the stiff shaking table, creating a nearly-fixed base for the test frames. In the event of column axial failure, a pin-ended steel column was provided to catch the test structure and enable the test to proceed without total system vertical collapse. Axial load and inertial load were provided by lead ingots fixed to the steel beam. This resulted in at rest axial load of $0.1 \cdot A_g \cdot f'_c$. Additional axial load, producing a total axial force equal to $0.24 \cdot A_g \cdot f'_c$ was achieved in some of the tests by using a pneumatic jacking system, testing the sensitivity of dynamic response to axial loading.

At beam-column joints, the tie configurations had ductile details according to the ACI 318 code provisions (hoops with 38 mm spacing distance and 135 degree hooks for hoops and crossties alternated along the height of the joint) for both the ductile and the non-ductile specimens.

To achieve different frame response characteristics, the columns were combined in three different ways, that is, a combination of two ductile columns, two non-ductile columns, or one ductile column and one non-ductile column. Table 3.1 summarizes the combinations used for the test series.

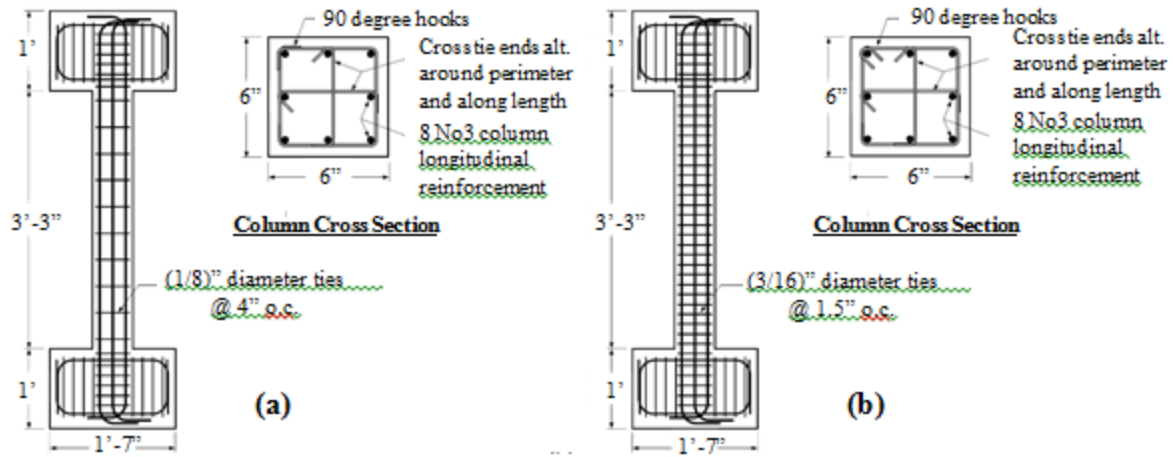


Figure 3.1 Reinforced concrete column specimen details:
(a) Non-ductile column (b) Ductile column

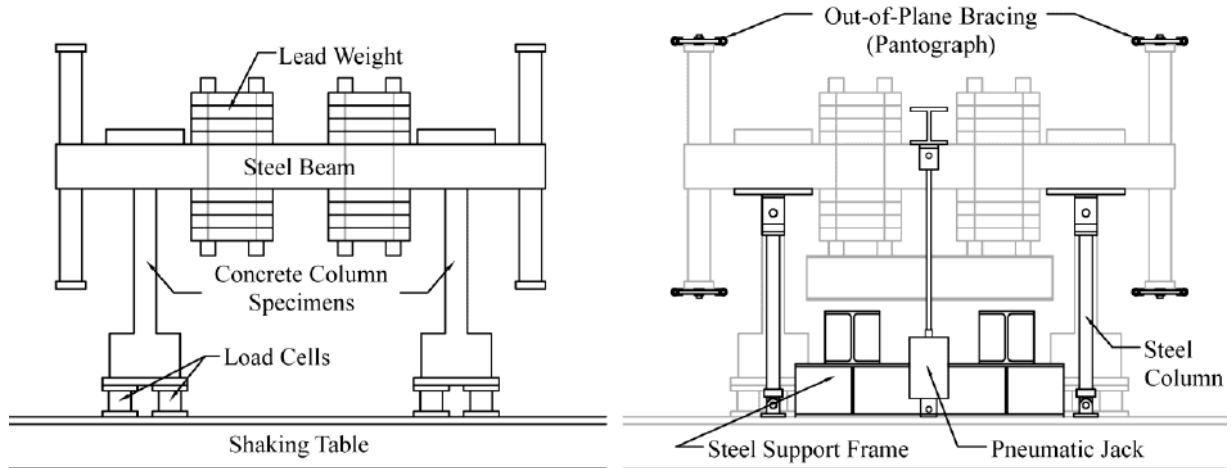


Figure 3.2 Experimental setup

Table 3.1 Test matrix

Test Number	Column Combination	Ground Motion	Axial Load Ratio ($P/A_g * \rho_c$)
1	Duct. - NonDuct.	Chile	0.10
2	Duct. - NonDuct.	Kobe	0.10
3	Duct. - Duct.	Chile	0.10
4	NonDuct. - NonDuct.	Chile	0.10
5	Duct. -Duct.	Kobe	0.10
6	NonDuct. - NonDuct.	Kobe	0.10
7	Duct. - NonDuct.	Chile	0.24
8	Duct. - NonDuct.	Kobe	0.24
9	Duct. - Duct.	Chile	0.24
10	NonDuct. - NonDuct.	Chile	0.24
11	Duct. -Duct.	Kobe	0.24
12¹	NonDuct. - NonDuct.	Kobe	0.24

3.2 INPUT GROUND MOTIONS

To understand how different types of ground motions can influence the dynamic response, two different unidirectional ground motion records were considered (out-of-plane motion was restrained by using a bracing mechanism). These were the ground motion recorded at Llolleo 100-degree component during the 1985 Chile earthquake (long-duration motion without significant long-period pulses) (Fig. 3.3); and the ground motion recorded at JMP station in the North-South direction during the 1995 Kobe Earthquake (shorter duration motion with a significant velocity pulse) (Fig. 3.4).

The ground motions were scaled so that they are consistent with the one-third scale similitude requirements by multiplying the duration of the ground motion by a factor of $1/\sqrt{3}$. The intensities of the ground motions were scaled to achieve the targeted responses; more specifically the amplitude of Llolleo input motion was scaled by a factor of 3.2 and the amplitude of Kobe input motion was scaled by a factor of 1.35. The ground motions were filtered by removing high and low frequencies to meet the shaking table limits.

¹ Data from this test were missing; the results from test 12 are not presented in the current study

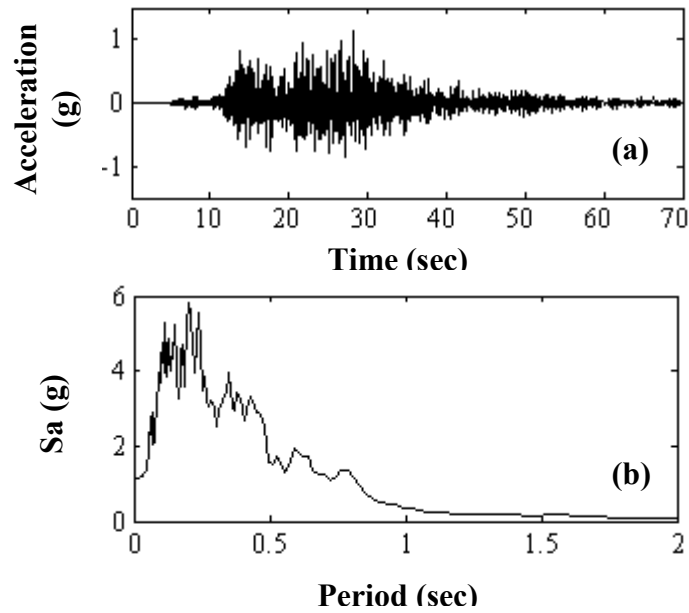


Figure 3.3 Filtered Lollo input ground motion (Chile 1985) ;
 (a) Ground motion , (b) Linear response spectrum (2% damping ratio)

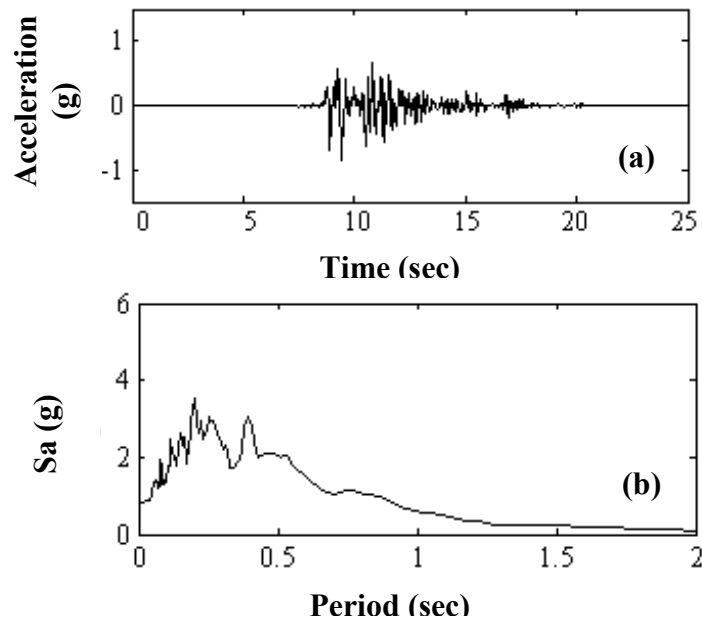


Figure 3.4 Filtered Kobe Input Ground Motion (Kobe 1995):
 (a) Ground motion, (b) Linear response spectrum (2% damping ratio)

3.3 MATERIAL PROPERTIES

Concrete had normal weight aggregates with specified nominal compressive strength equal to 3 ksi. The column specimens were cast in three groups. Concrete cylinders were cast and cured along with the specimens of each group. Table 3.2 lists the mean compressive and tensile strength values of the concrete specimens.

The longitudinal bars were specified as Grade 60 ASTM A706. Three samples of the #3 bars were tested to obtain the mean yield (f_y) and ultimate strength values (f_u). The wires were also tested to obtain mean strength properties. The results of the steel coupon tests are summarized in Table 3.3.

Table 3.2 Concrete mean strength properties

Batch	Mean Compressive Strength (ksi)	Mean Tensile Strength (ksi)
1	3.37	0.31
2	4.02	0.40
3	3.74	0.38

Table 3.3 Steel reinforcement mean strength properties

Steel Reinforcement	Yield Stress f_y (ksi)	Ultimate Stress f_u (ksi)
#3 (long. bars)	64.4	84.7
1/8" wire (transv. reinf.)	80.4	96.1
3/16" wire (transv. reinf.)	79.6	87.0

3.4 COMPARISON OF ANALYTICAL MODELS WITH TEST RESULTS

As mentioned at the beginning of this chapter, modeling the collapse behavior of non-ductile concrete specimens is a challenging task due to the brittle nature of their failure. In this section the results obtained from the laboratory tests are compared with those obtained from simulation of the frames using state-of-the-art collapse simulation tools. The results are discussed in term of lateral displacement at the top of the column and moment at the base of the column. Verification of the accuracy of different collapse simulation analytical tools used in the current study is essential for model calibration and for providing a measure of the accuracy of the collapse evaluation performed in Chapters 5 and 6.

A variety of different analytical models have been developed for dynamic simulation of the non-linear behavior of structural elements. The models used in the current study are proposed by Haselton et al. (2008)² and Elwood and Moehle (2002)³. Both of these models are implemented in OpenSees structural analysis software. The Elwood model was originally developed specifically for flexure-shear critical column members so it will be used to simulate only the response of non-ductile column members, while the Haselton model was developed to address a wider range of structural components, so it will be used to simulate the response of both ductile and non-ductile members.

As explained in Chapter 2 the Haselton model represents the column using a lumped plasticity approach comprising nonlinear springs at the column ends interconnected by a linear-elastic element. The nonlinear rotational spring behavior was based on the Clough model, using hysteresis implemented in OpenSees by Ibarra et al. (2005) with stiffness and strength degradation determined by parameters defined in Haselton et al. (2007). The Elwood model uses a similar approach, but adds a horizontal and axial spring to represent nonlinear shear and axial response.

The tested concrete frames were analyzed using the same procedure used in the following chapters to evaluate the collapse performance of buildings. The stiffness properties of the structural components were calculated according to ASCE 41-06, the strength values were calculated by moment-curvature analysis using software XTRACT, and the parameters related to non-linear deformation and strength degrading behavior were estimated according to the models proposed by Haselton and Elwood, respectively, with the following exceptions:

- As discussed in Chapter 2, the original Haselton model was calibrated using a database (Berry et al., 2004) including both ductile and non-ductile column members. For the purposes of the current study the relationships that define the modeling parameters for the ductile column members were re-calibrated by Dr. Liel and her colleagues such that columns sustaining apparent shear failures were excluded from the data (ATC-78, 2013). For the non-ductile column members the parameters were defined according to the original modeling parameters as suggested by Haselton et al. (2008). The interested reader can find both the original and the re-calibrated relationships that are used to calculate the column modeling parameters in Appendix B.
- As explained in Chapter 2, Elwood model was not intended originally to be capture shear failure when it preceded flexural yielding. Elwood model in this study was modified by

² For brevity this model will be referred as the Haselton model in the current study

³ For brevity this model will be referred as the Elwood model in the current study

the author such that if the shear demand exceeds the shear strength as defined according to ASCE-41-06 (2006) then shear failure is triggered. Also, in this Chapter the axial spring used to track shear-induced axial failure was not utilized, so the column axial response was not modeled explicitly.

The values of the modeling parameters used for all the frame combinations are provided in Tables 3.4 – 3.6 .

Table 3.4 Column modeling properties

Column	$v (P_{axial}/A_g * f'_c)$	Yield Strength M_y (kip-in)	Ultimate Strength M_u (kip-in)	Cracked Stiffness Factor (per ASCE-41)
Ductile	0.11	137.42	164.9	0.300
Ductile	0.24	150.00	180.0	0.440
Non-Ductile	0.11	137.42	164.9	0.300
Non-Ductile	0.24	150.00	180.0	0.440

Table 3.5 Modeling parameters (Haselton model)

Column	$v (P_{axial}/A_g * f'_c)$	Haselton			
		Plastic Rotation (θ_{pl})	Post Capping Rotation (θ_{pc})	Deterioration Rate Parameter λ	Residual Strength
Ductile	0.11	0.08	0.1000	87	0.1
Ductile	0.24	0.072	0.1000	74	0.1
Non-Ductile	0.11	0.029	0.0440	27	0.1
Non-Ductile	0.24	0.023	0.0300	23	0.1

Table 3.6 Modeling parameters (Elwood model)

Column	$v (P_{axial}/A_g * f'_c)$	Concrete Strength f'_c (ksi)	Transverse Reinf. Ratio $\rho_{transverse}$
Ductile	-	-	-
Ductile	-	-	-
Non-Ductile	0.11	3.7	0.0015
Non-Ductile	0.24	3.7	0.0015

Geometric nonlinearities were considered using the P-Delta formulation. Rayleigh damping was employed, with coefficients selected to achieve a damping ratio of 2% at the observed fundamental period of each test (approximately equal to 0.20 sec) and 0.02 sec (this value corresponds to the second mode period estimated from eigenvalue analysis of the concrete frames).

The actual period and damping ratio of the test frame were determined from free-vibration tests conducted prior to earthquake simulation. Table 3.7 summarizes the average period and damping ratios for the entire test series.

Table 3.7 **Fundamental Period and damping ratio**

Test	T (sec)	Damping Ratio ζ (%)
Analytical Model	0.18	2
1	0.22	2.9
2	0.22	2.6
3	0.22	2.8
4	0.23	2.9
5	0.23	2.7
6	0.21	2.5
7	0.18	1.4
8	0.18	1.5
9	0.2	1.6
10	0.2	1.6
11	0.19	1.5

Figures 3.5 to 3.15 compare measured and calculated responses using the Haselton model.

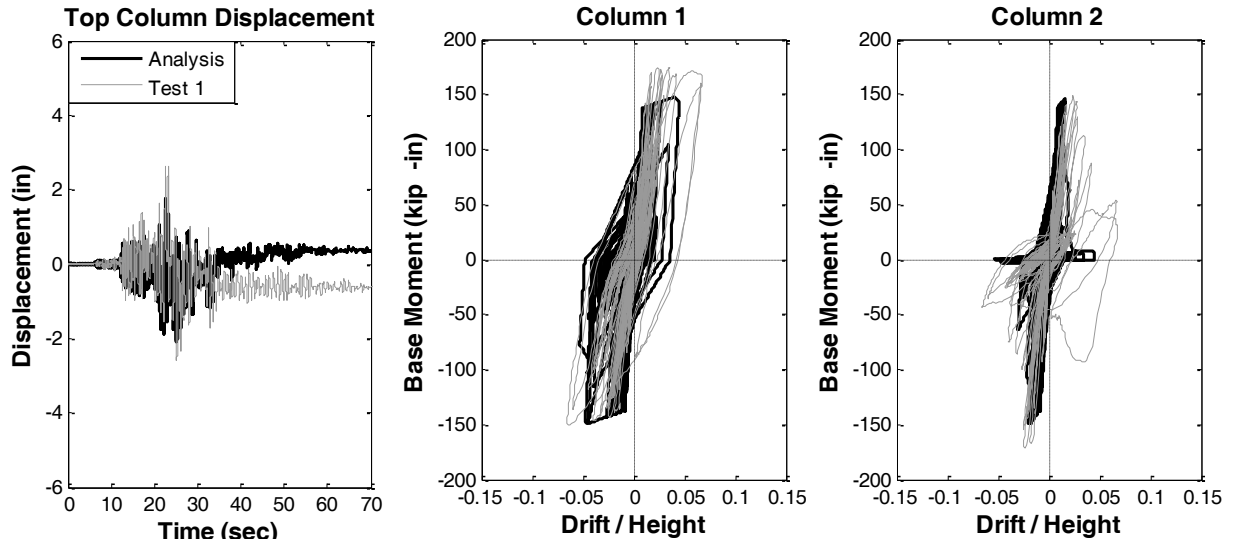


Figure 3.5 Comparison of test 1 results with the Haselton model

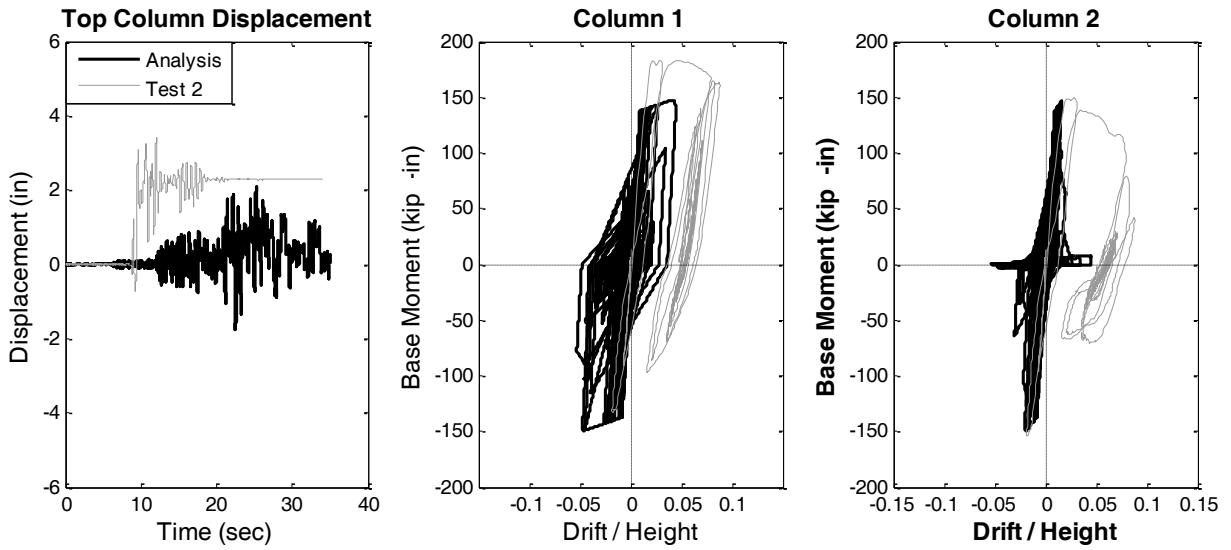


Figure 3.6 Comparison of Test 2 results with the Haselton model

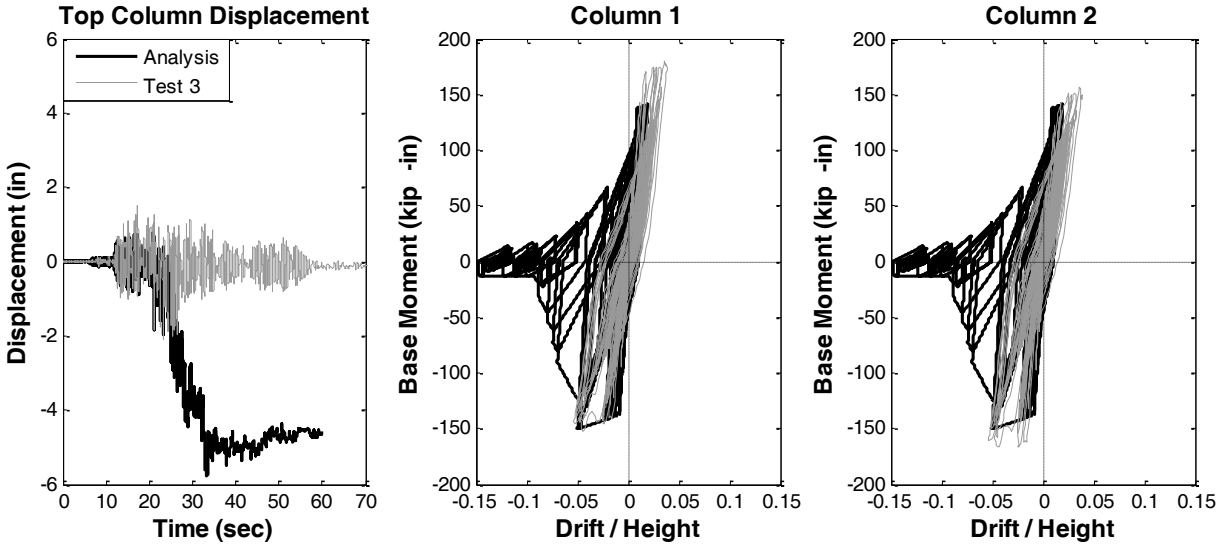


Figure 3.7 Comparison of Test 3 results with the Haselton model

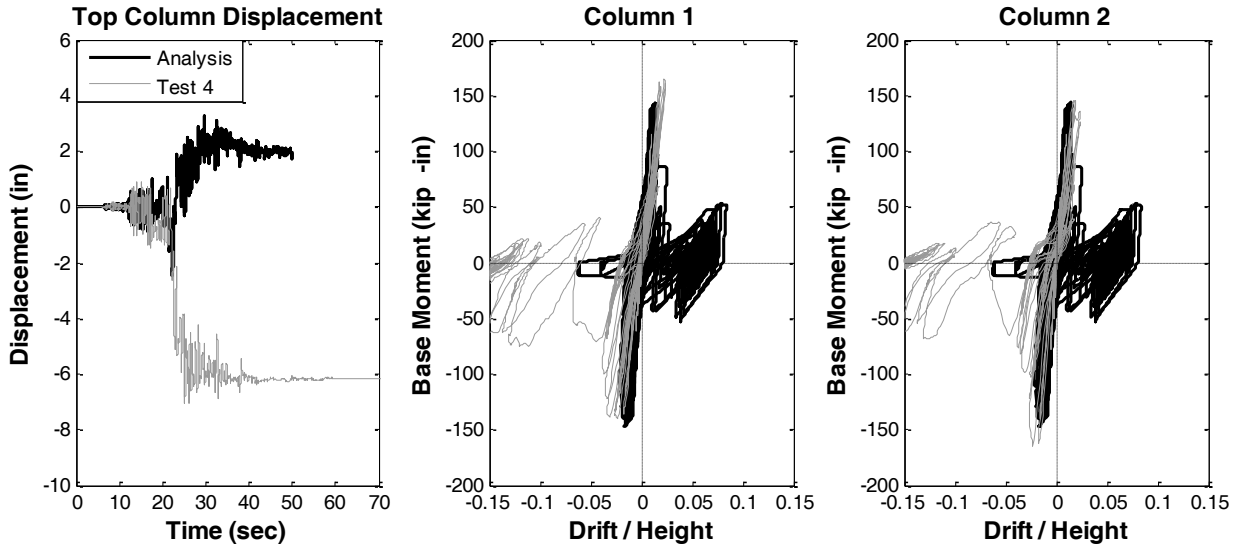


Figure 3.8 Comparison of Test 4 results with the Haselton model

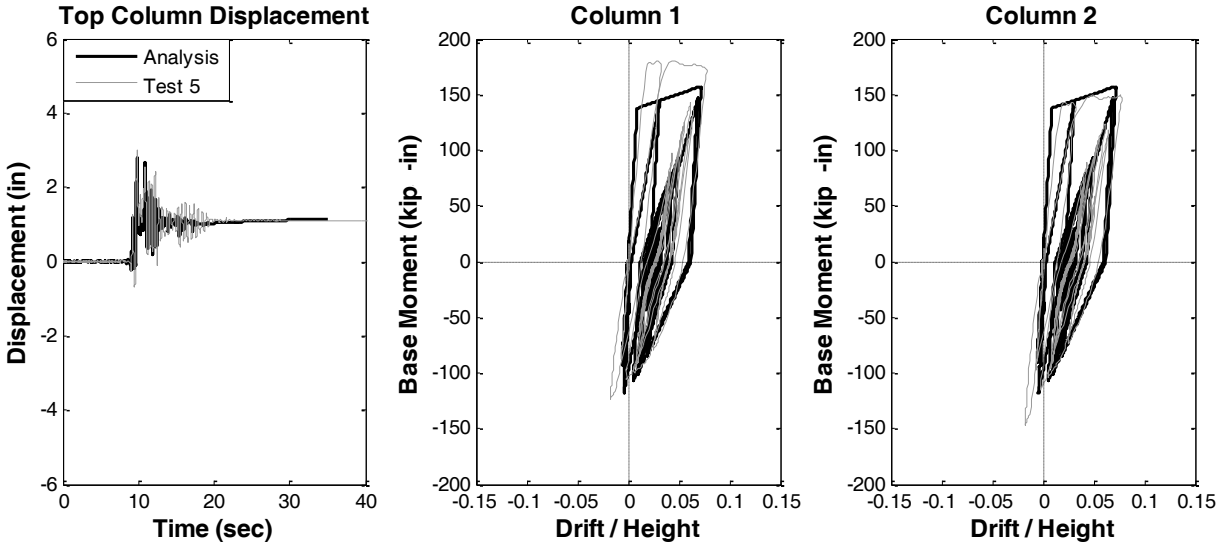


Figure 3.9 Comparison of Test 5 results with the Haselton model

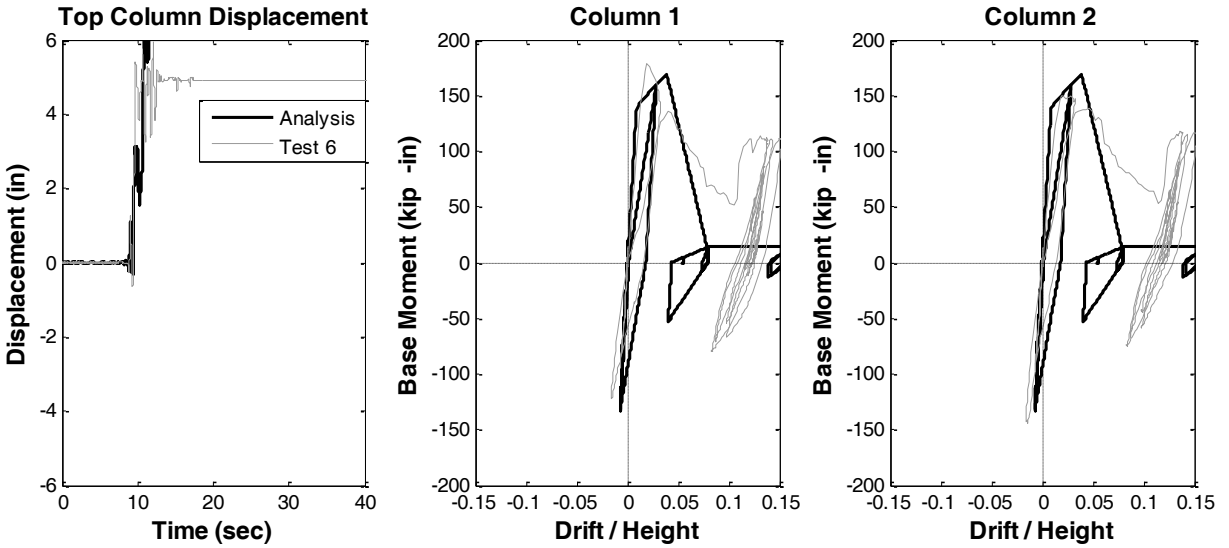


Figure 3.10 Comparison of Test 6 results with the Haselton model

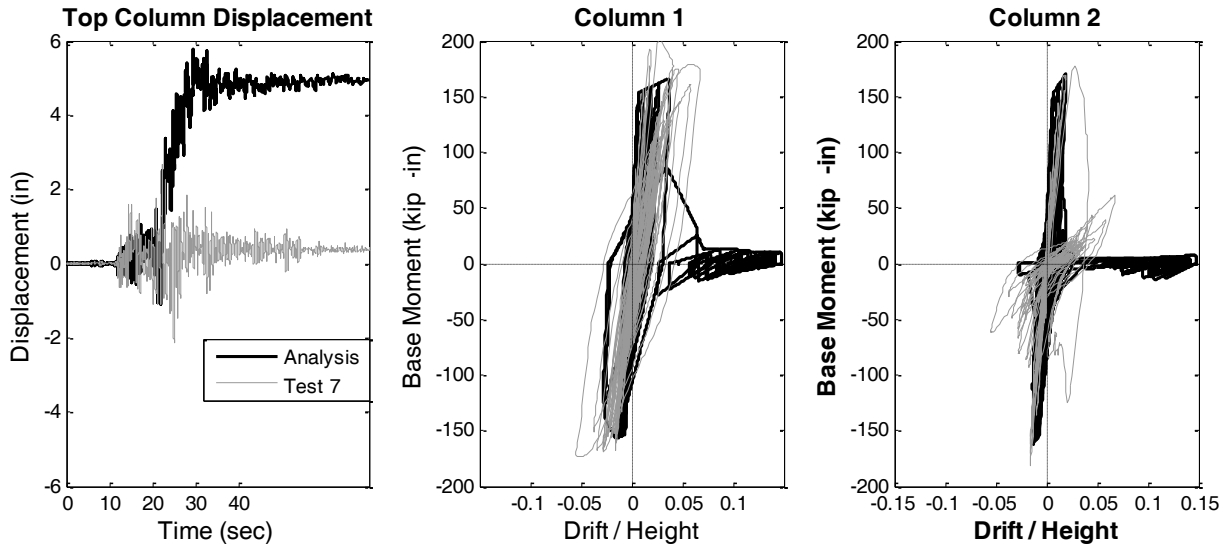


Figure 3.11 Comparison of Test 7 results with the Haselton model

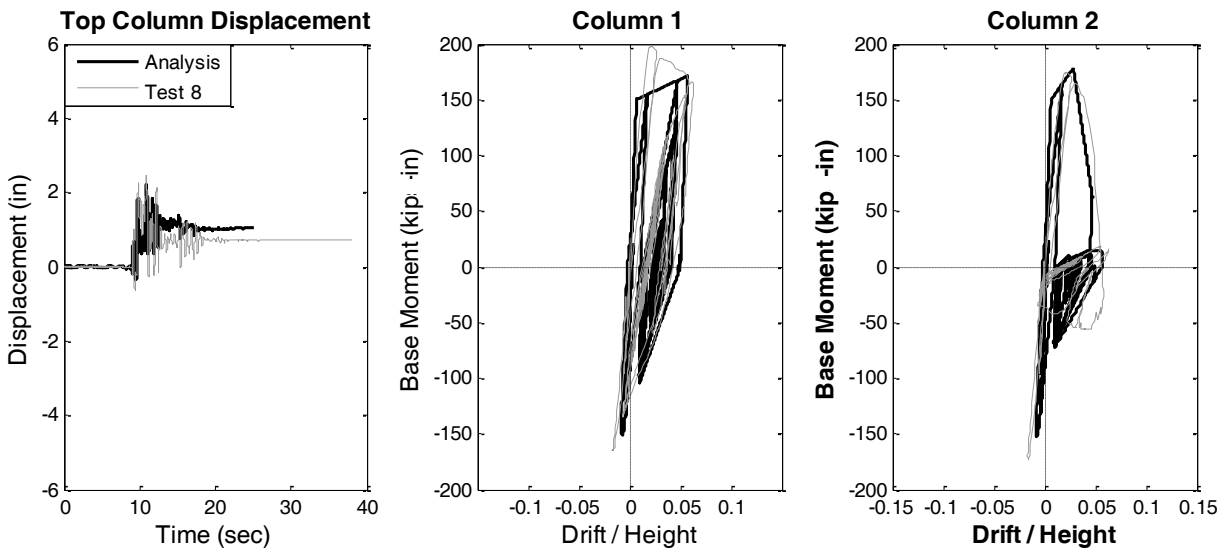


Figure 3.12 Comparison of Test 8 results with the Haselton model

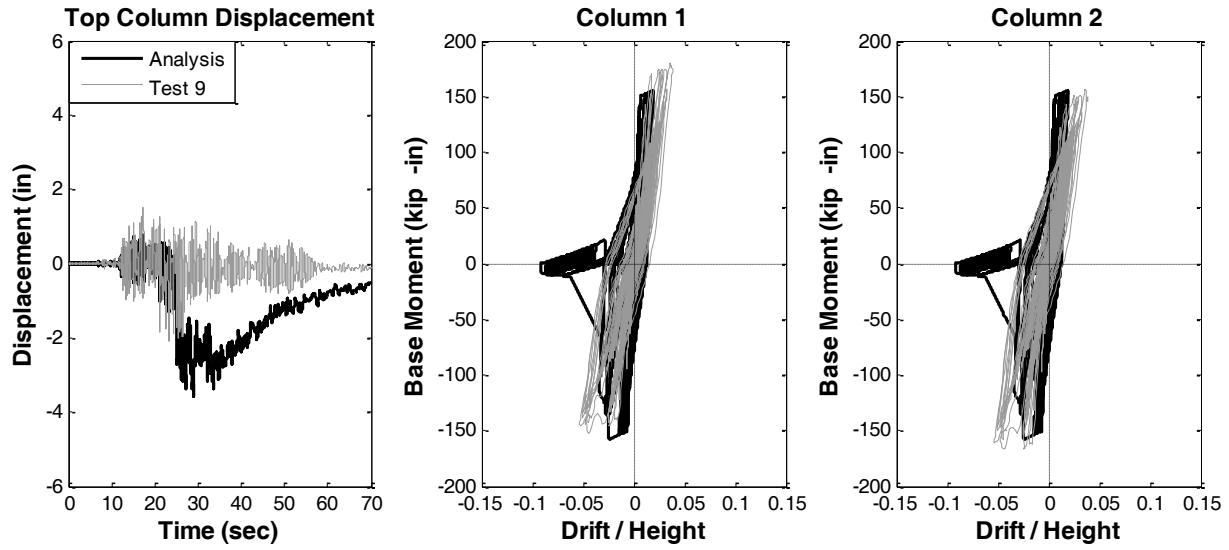


Figure 3.13 Comparison of Test 9 results with the Haselton model

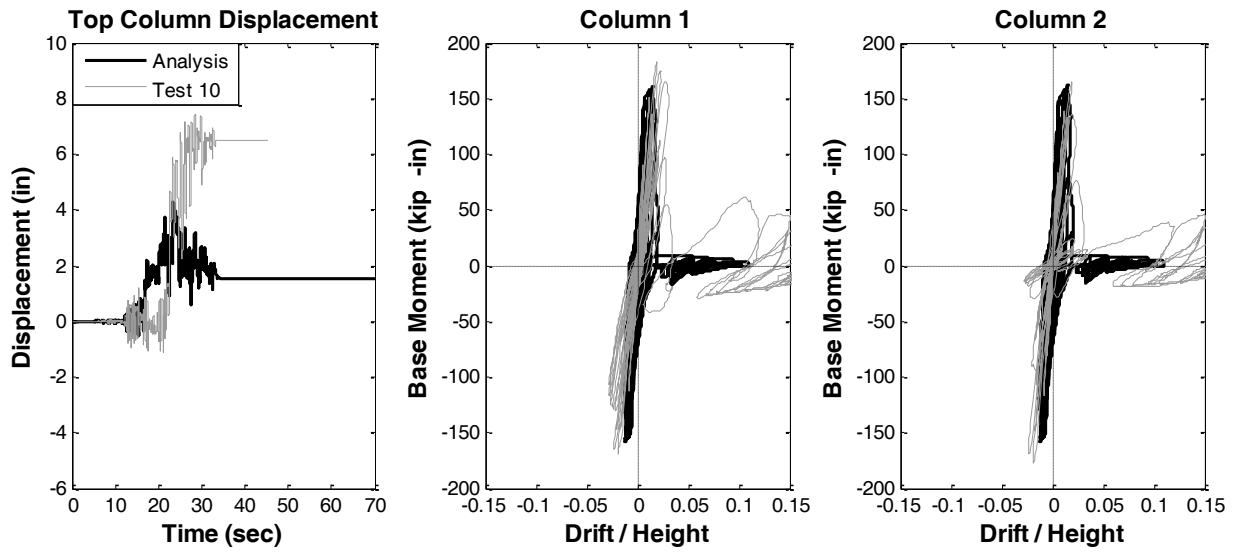


Figure 3.14 Comparison of Test 10 results with the Haselton model

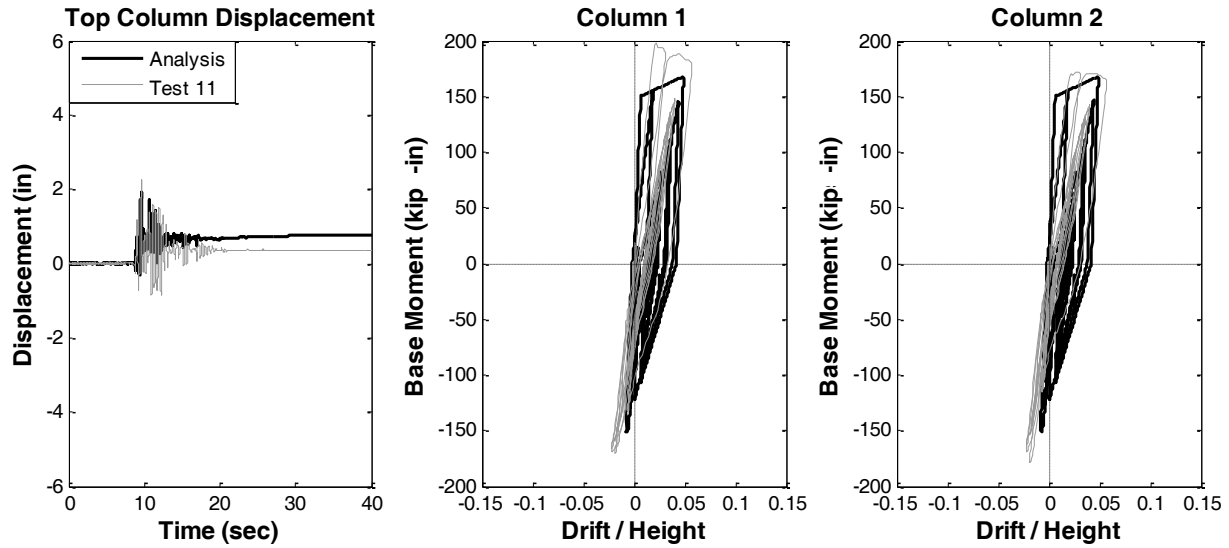


Figure 3.15 Comparison of Test 11 results with the Haselton model

For those frames that had non-ductile detailing in both column members, the Elwood model also was used to simulate their response. Figures 3.16-3.18 compare measured and calculated responses using the Elwood model.

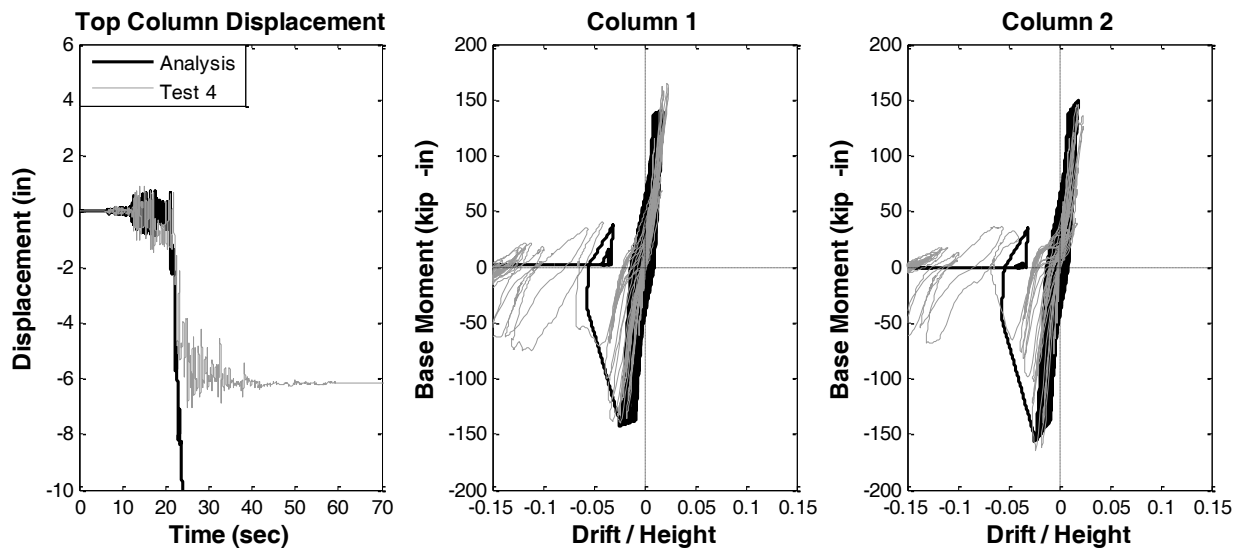


Figure 3.16 Comparison of Test 4 Results with the Elwood model

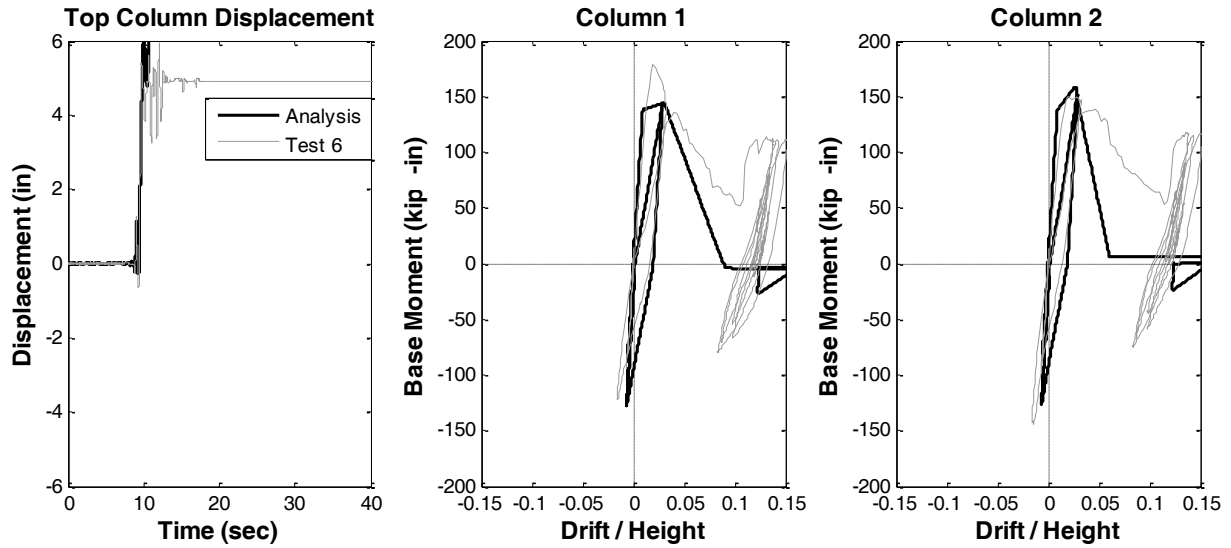


Figure 3.17 Comparison of Test 6 results with the Elwood model

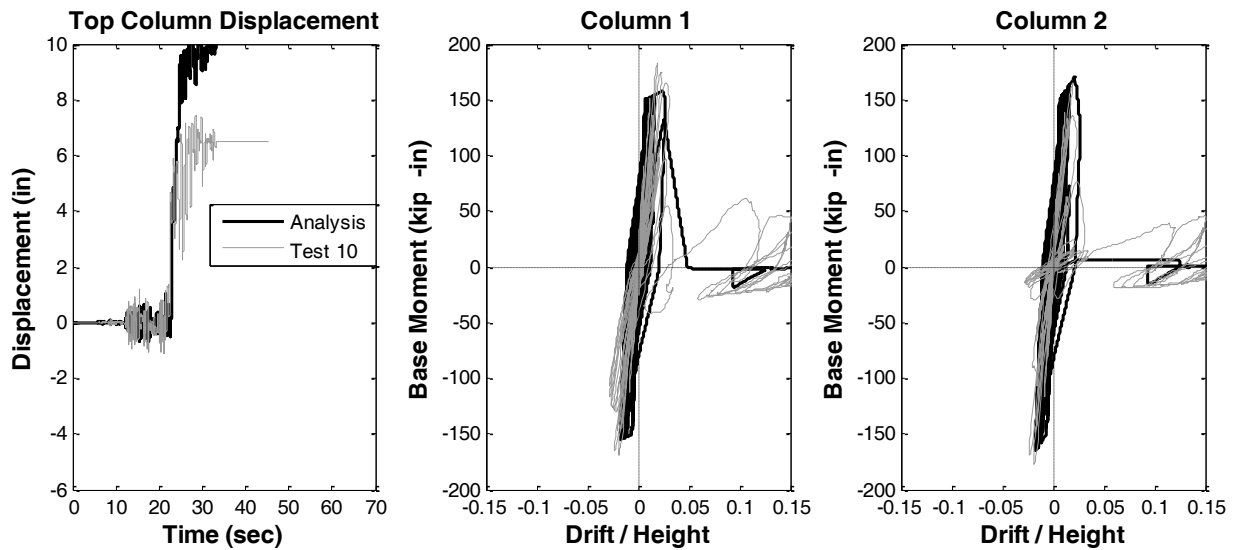


Figure 3.18 Comparison of Test 10 results with the Elwood model

For the case of frames consisting of two non-ductile columns (Tests 4, 6, and 10) the Elwood model simulates more accurately the onset of shear failure as well as the shear degradation compared to the Haselton model. As mentioned above, the improved simulation obtained with the Elwood model is understandable given that it was developed specifically to address non-ductile column members. For all the aforementioned cases it is observed that the Elwood model tracks accurately the onset of shear failure as well as the shear degradation for the case of the Chile motion (Tests 4 and 10), where there is high-cyclic strength degradation. For the case of

the Kobe motion (Test 6), where in-cycle strength degradation is predominant (monotonic shear failure), the Elwood model estimates relatively accurately the onset of shear failure. However, it overestimates the shear degradation by using a steeper shear degrading slope than was observed in the test (the same observation applies for the response of the non-ductile column in Test 2 as well). It should be noted, though, that the non-ductile columns experience shear-induced axial failure soon after the occurrence of shear failure. As explained above, to avoid axial collapse of the specimen pin-ended steel columns illustrated in Figure 2 were set such that they would be supporting the gravity load after any of the two columns failed axially. In this chapter the axial response of columns is not modeled explicitly (both axial failure and the steel column support were not modeled), so the combination of geometric nonlinearity and the almost zero-stiffness of the shear spring in the flat plateau branch of the backbone curve of the Elwood model are responsible for the increased displacements that are observed comparing to the test results.

As shown previously, the Haselton model was employed to simulate the dynamic response of frames consisting of two ductile columns (Tests 3, 5, 9, and 11). For the short-duration motion (Kobe – Tests 5 and 11), the Haselton model provides good agreement with the actual test results. For the long-duration motion (Chile – Test 3 and 9), excessive cyclic degradation appears to be responsible for the increased displacements of the analytical model. Increasing the value of the parameter related to the energy dissipation (λ) by one standard deviation above the mean value, (the mean values are used for the model parameters for all the other models) provides less degrading behavior for the column members and leads to more accurate simulation of the actual response of the frame. Figures 3.19 and 3.20 present the analytical results for the case of ductile frames subjected to the Kobe earthquake motion where λ is increased by one standard deviation. This suggests that the pseudo-static tests for which Haselton model was calibrated tend to overestimate the damage rates for earthquake loading, leading to a faster calculated degrading response than what was actually observed.

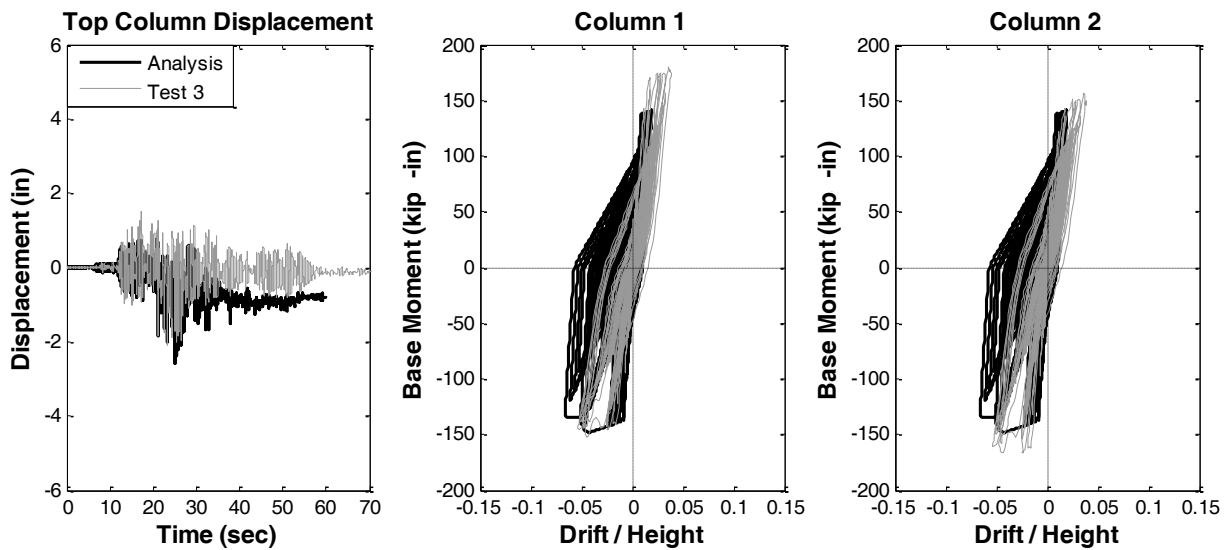


Figure 3.19 Comparison of Test 3 results with the Haselton model with $\lambda = \lambda_{\text{mean}} + \lambda_{\text{std}}$ (the other parameters were set equal to the mean values)

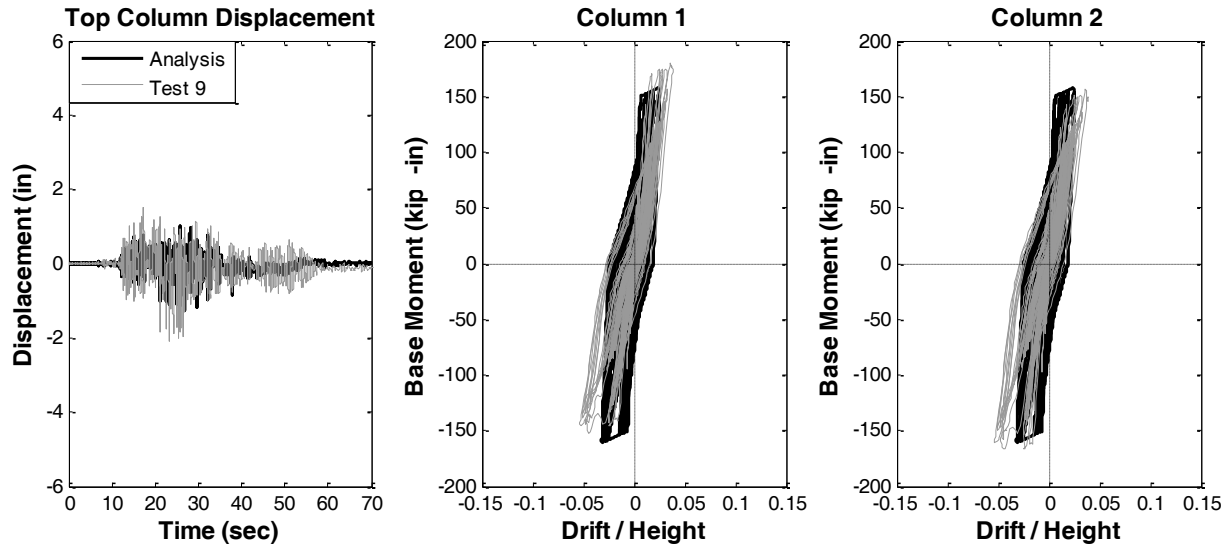


Figure 3.20 Comparison of Test 9 results with the Haselton model with $\lambda = \lambda_{\text{mean}} + \lambda_{\text{std}}$ (the other parameters were set equal to the mean values)

Also as reported above, the Haselton model was employed to simulate the response of both structural members in the case of frames consisting of ductile and non-ductile columns (Tests 1, 2, 7, and 8). For Test 8 the results are in relatively good agreement with the analysis. For Tests 1, 2, and 7 the Haselton model seems to be degrading faster than the actual test. The results cited above suggest that for the case of frames with a combination of a ductile and a non-ductile column member, a combination of the Elwood and Haselton model would provide a better estimate than using the Haselton model for both columns.

Figures 3.21-3.24 compare measured and calculated responses using a combination of the Haselton and Elwood models to simulate the response of the ductile and non-ductile column respectively.

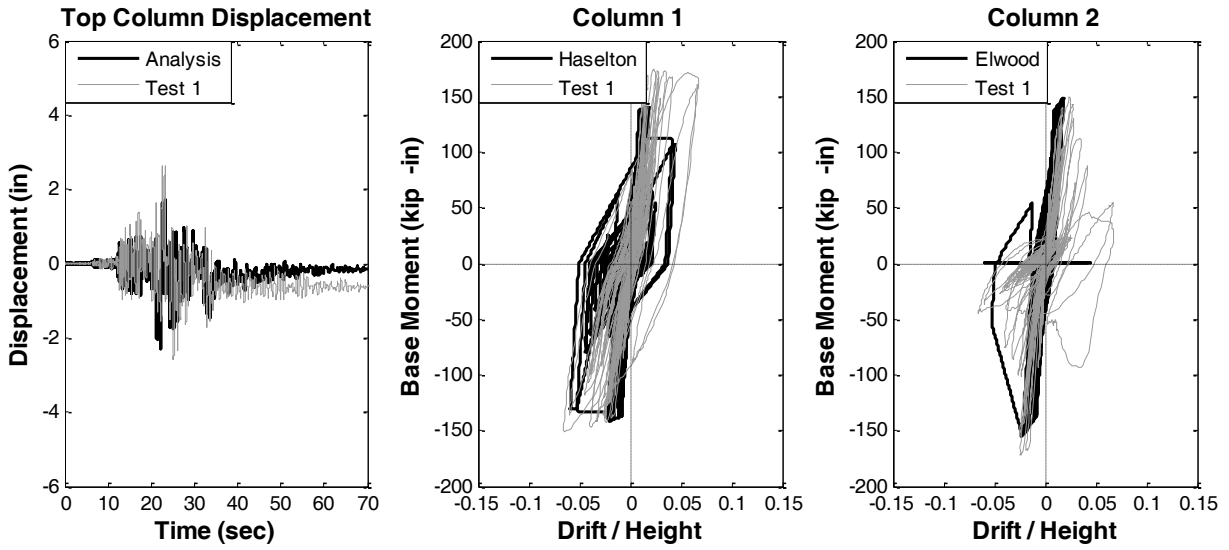


Figure 3.21 Comparison of Test 1 results with the Haselton - Elwood model

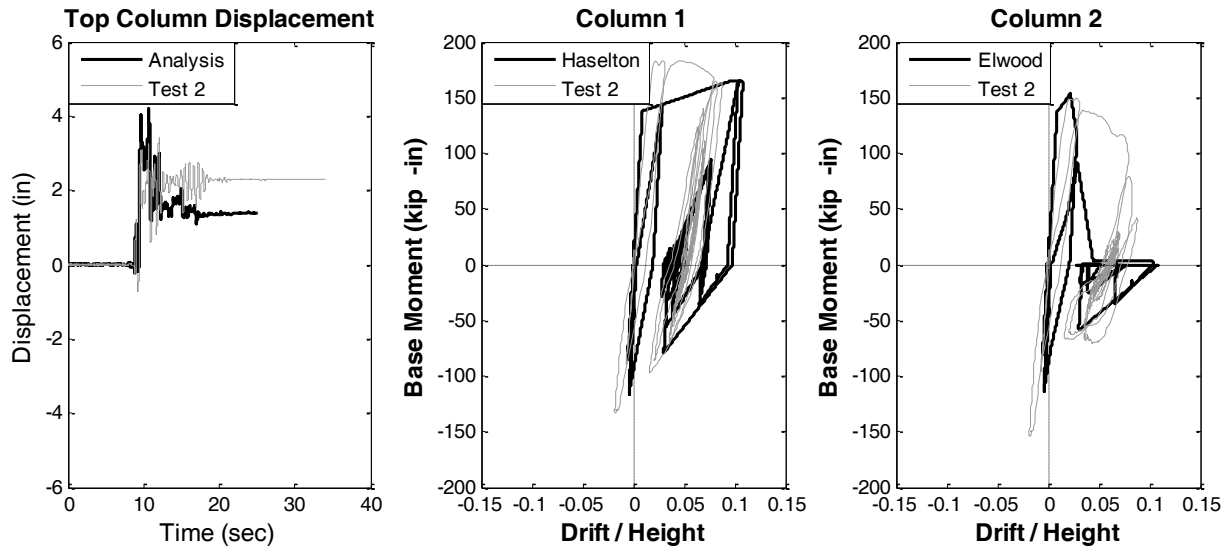


Figure 3.22 Comparison of Test 2 results with the Haselton - Elwood model

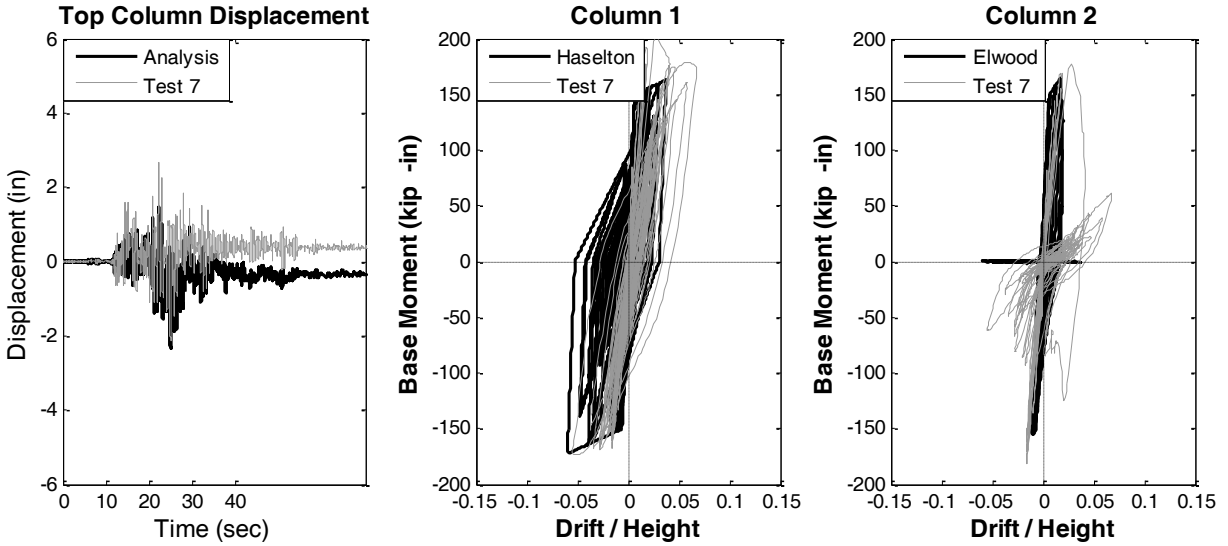


Figure 3.23 Comparison of Test 7 results with the Haselton - Elwood model

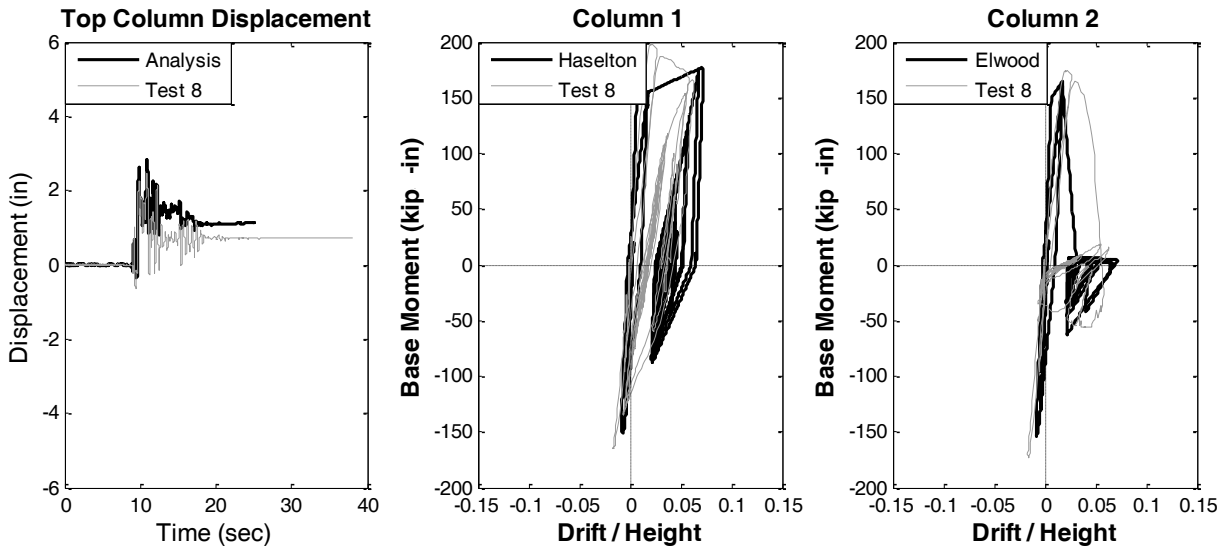


Figure 3.24 Comparison of Test 8 results with the Haselton - Elwood model

A comparison of the simulated response with the test results shows that, for the case of the frame consisting of ductile and non-ductile columns (Tests 1 and 2), the combination of the Haselton model with the Elwood model provides a relatively good agreement in terms of top column displacement (better than using the Haselton model).

Tables 3.8 – 3.12 compare maximum measured and calculated flexural strengths, transient displacements, and residual displacement. As indicated by the table values below, maximum base shear observed in the analytical models was very close to the test results. Regarding maximum horizontal displacement, for the case that both columns correspond to non-ductile detailing, Elwood model predicted accurately collapse for all the tests performed, while the combination of Haselton and Elwood model for a combination of ductile and non-ductile column members approximated with sufficient accuracy the maximum observed displacement (max. error=18%). The error between analytical and test results was higher for the case of residual offsets for most of the tests performed. However, for the cases of non-ductile columns and combination of ductile with non-ductile columns, with the exception of Test 7, both the analytical and test results have the same sign of residual displacements.

Table 3.8 Actual test results

Test	Max. Horizontal Displacement (in)	Residual Offset (in)	Max. Base Shear (kip)
1	2.82	-0.66	16.92
2	3.65	2.4	17.1
3	2.19	0.14	17.23
4	Collapsed	Collapsed	16.13
5	3.22	1.16	16.8
6	Collapsed	Collapsed	16.88
7	2.83	0.39	18.55
8	2.65	0.75	18.86
9	2.00	0.02	18.2
10	Collapsed	Collapsed	17.7
11	2.37	0.37	18.69

Table 3.9 Haselton analytical model results

Haselton			
Test	Max. Horizontal Displacement (in)	Residual Offset (in)	Max. Base Shear (kip)
1	2.08	0.37	16.7
2	1.96	-0.27	17.3
3	5.77	-4.61	17.09
4	3.26	2.02	16.12
5	2.81	1.14	16.96
6	7.71	7.22	17.09
7	5.76	4.94	18.83
8	2.23	1.04	19.02
9	3.57	-0.53	17.09
10	4.31	1.52	17.91
11	1.91	0.76	18.89

Table 3.10 Elwood analytical model results

Elwood			
Test	Max. Horizontal Displacement (in)	Residual Offset (in)	Max. Base Shear (kip)
1	-	-	-
2	-	-	-
3	-	-	-
4	Collapsed	Collapsed	16.13
5	-	-	-
6	Collapsed	Collapsed	17.09
7	-	-	-
8	-	-	-
9	-	-	-
10	Collapsed	Collapsed	17.7
11	-	-	-

Table 3.11 Haselton-Elwood analytical model results

Haselton+Elwood			
Test	Max. Horizontal Displacement (in)	Residual Offset (in)	Max. Base Shear (kip)
1	2.32	-0.15	16.7
2	4.21	1.4	17.1
3	-	-	-
4	-	-	-
5	-	-	-
6	-	-	-
7	2.34	-0.33	18.83
8	2.83	1.12	19.02
9	-	-	-
10	-	-	-
11	-	-	-

Table 3.12 Haselton analytical model results with $\lambda = \lambda_{\text{mean}} + \lambda_{\text{std}}$

Haselton ($\lambda = \lambda_{\text{mean}} + \lambda_{\text{std}}$)			
Test	Max. Horizontal Displacement (in)	Residual Offset (in)	Max. Base Shear (kip)
3	2.59	-0.83	17.09
9	1.25	0.01	17.09

3.5 SUMMARY OF THE EXPERIMENTAL EVALUATION

Based on the comparison between the experimental investigation and the analytical models employed in this study for collapse simulation, the following conclusions can be drawn:

- For the test structures studied here, the Elwood model was able to simulate the response of flexure-shear critical columns relatively well. For both ground motions, the Elwood model tracked the onset of shear failure relatively accurately. The Elwood model was able to track the post-failure response with acceptable accuracy for the long-duration motions (such as the Chile motion used in this study). However, for the case of short, pulse-like motions (such as the Kobe motion used in this study), the model tends to overestimate the degrading response by providing a more conservative (steeper) shear-degrading slope.
- The Haselton model provides a relatively accurate simulation of the dynamic response of ductile columns, especially for the short-duration Kobe motion. However, it tends to overestimate the damage rate for the case of the long-duration Chile motion. This shortcoming is probably because the Haselton model was calibrated to replicate results from pseudo-static tests with fewer cycles. This result suggests that additional studies are required in order to improve the accuracy in simulation of collapse for ductile columns.
- The combination of the Haselton and the Elwood models simulated successfully the dynamic response of structures with column members of different ductility.
- The results of this chapter suggest that, overall, the top column displacement can be reasonably represented using the Haselton (for ductile members) and the Elwood (for non-ductile members) models, including the time of large residual or collapse. One exception is Tests 3 and 9, for which excessive damage in the Haselton model results in overestimation of the lateral drifts.

4 Development of Archetype Buildings – Collapse Simulation Models

This section describes the configuration of the archetype buildings that served as the focus of the study. The chapter discusses also variations and analytical modeling of the archetype buildings with structural parameters representative to old construction so that different classes of older-type buildings can be evaluated. The seismic performance assessment procedure used in the current study (a modified version of IDA) is also presented in the current chapter.

4.1 DEVELOPMENT OF THE ARCHETYPE BUILDINGS

To study the relative vulnerability of older-type concrete buildings three idealized building prototypes were developed to calibrate the values of the suggested methodology. The considered buildings were designed for the purpose of the current study with varying building heights ranging from 4 to 12 stories. These archetype buildings were sequentially weakened by modifying transverse reinforcement and column to beam bending moment strength ratio to test the sensitivity to collapse from the introduction of various known seismic deficiencies, termed “collapse indicators.”

The studied buildings were modeled after an existing multi-story reinforced concrete building in the Seattle area, but none of the specific properties of the Seattle building were used. Instead, once the general configuration was established, the prototypes were designed so that they had performance characteristics desired for collapse indicator studies.

The studied buildings have 4, 8, and 12 stories. The idealized buildings consist of twelve earthquake-resisting space frames, six in each direction, that were designed to resist both gravity and earthquake forces. The studied buildings are shown in Figure 4.1 and 4.2.

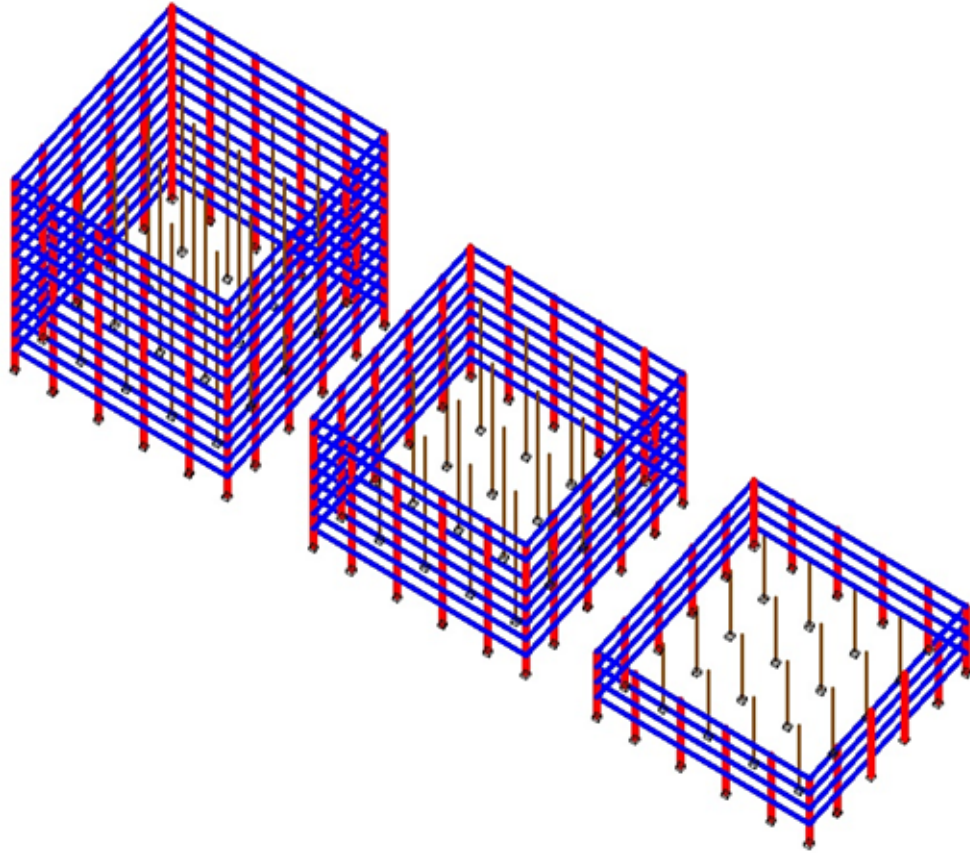
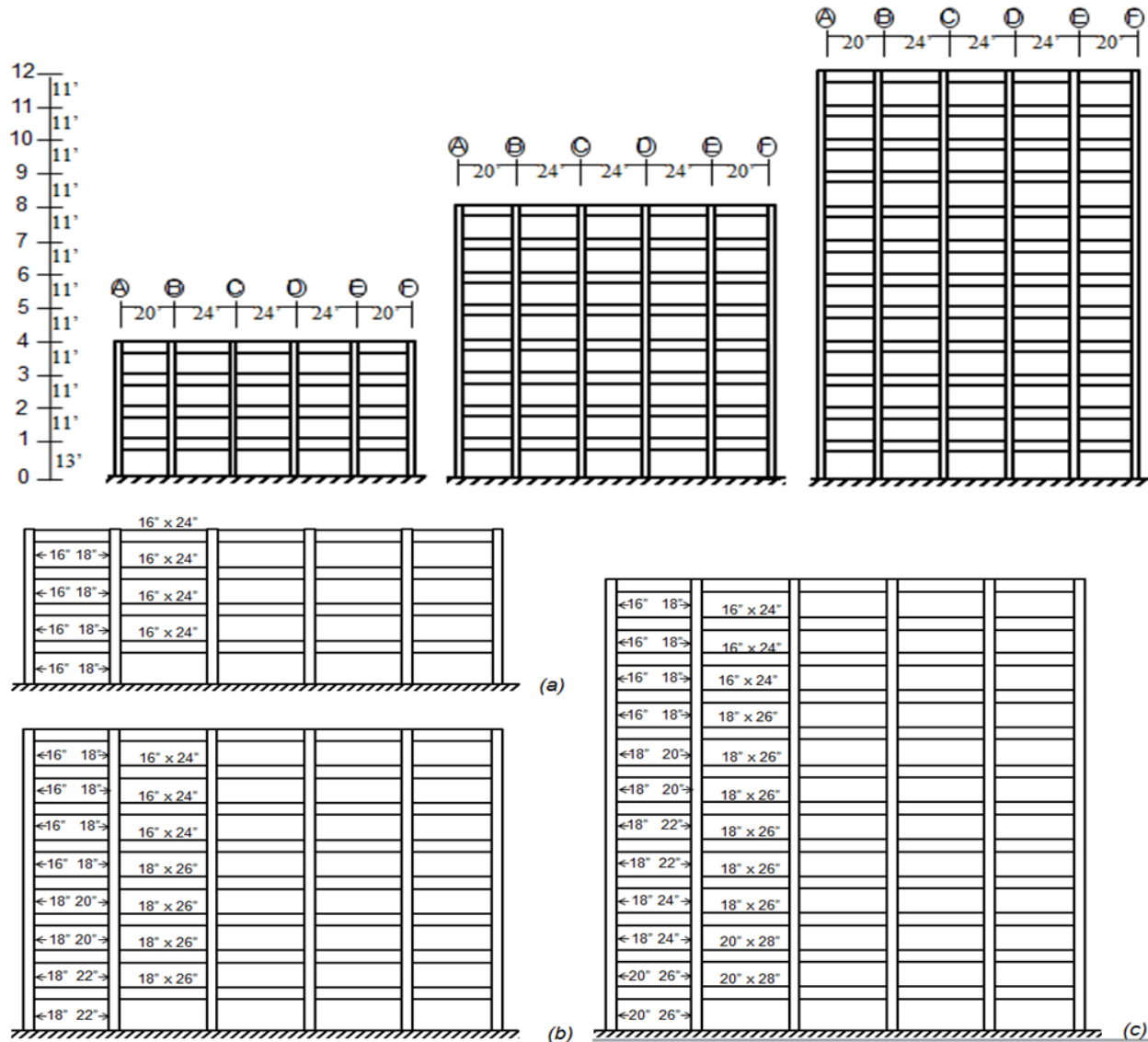


Figure 4.1 Three- dimensional view of the studied buildings (for clarity of presentation, only the perimeter frames are shown)



**Figure 4.2 Schematic elevation view of the simulated frames:
 (a) 4-story, (b) 8-story, and (c) 12-story buildings**

For each building configuration (4,8, and 12 stories) the structure initially was designed to carry 10% of its effective seismic weight and was detailed in accordance with the special moment frame requirement of ACI 318-11, except the column to beam bending moment strength ratio which was taken $\Sigma M_{nc}/\Sigma M_{nb} = 1.0$ at every joint except the roof level (ΣM_{nc} = sum of nominal moment strengths of columns at a beam-column joint and ΣM_{nb} = sum of nominal moment strengths of beams at the same joint). Variations on this design were introduced (a) by reducing or increasing the beam bending moment strengths to achieve different relative moment strengths of beams and columns at beam-column joints, and (b) by varying the spacing of column transverse reinforcement to achieve different relative shear demands and strengths of columns, with transverse reinforcement spacing representative of the range for modern designs and older designs. Sums of ratios of column nominal moment strengths to beam nominal moment strengths had values $0.6 \leq \Sigma M_{nc}/\Sigma M_{nb} \leq 1.8$. Shear strength demand corresponding to development of

column moment strength was calculated as $V_p = (M_{n,top} + M_{n,bot})/l$, (M_n corresponds to column moment strength and l to column height) and initial nominal shear strength V_n of a column was calculated in accordance to ASCE 41-06 (2006) as

$$V_n = k \left[\frac{A_v f_{yt} d}{s} + \lambda \left(\frac{6\sqrt{f'_c}}{M/Vd} \right) \sqrt{\left(1 + \frac{N_u}{6\sqrt{f'_c} A_g} \right)} 0.8A_g \right], \quad (\text{Eq. 4.1})$$

in which k and λ was assumed to be equal to 1.0, A_v = transverse reinforcement area, f_{yt} = transverse reinforcement yield strength, s = center-to-center spacing of transverse reinforcement, f'_c = concrete compressive strength, d = effective depth, N_u = applied axial compressive force, and A_g = gross cross-sectional area. The transverse reinforcement was varied to achieve $0.6 \leq V_p/V_n \leq 1.2$. The versions of the frames with $V_p/V_n = 0.6$ and $\Sigma M_{nc}/\Sigma M_{nb} = 1.2$ are referred to as the “modern code design” buildings.

Table 4.1 depicts all the various combinations that were considered in the current study. The individual building designs were set up such that a building had the same value of V_p/V_n in every story and the same value of $\Sigma M_{nc}/\Sigma M_{nb}$ at every joint (except the roof). Design requirements for beam-column joints and for other elements of the structural system were not considered.

Table 4.1 Combinations of V_p/V_n and $\Sigma M_{nc}/\Sigma M_{nb}$ considered in the current study (the shaded cell corresponds to modern building code design)

$V_p/V_n \backslash \Sigma M_{nc}/\Sigma M_{nb}$	0.6	0.8	1.0	1.2	1.4	1.6	1.8
0.6	✓	✓	✓	✓	✓	✓	✓
0.8	✓	✓	✓	✓	✓	✓	✓
1.0	✓	✓	✓	✓	✓	✓	✓
1.2	✓	✓	✓	✓	✓	✓	✓

Applying all the variations of Table 4.1 to 4, 8, and 12-story frames required 84 different designs. It was impractical to implement detailed designs for all the variations. Instead, the buildings with $\Sigma M_{nc}/\Sigma M_{nb} = 1.0$ were fully designed, and actual moment strengths were compared with required moment strengths. For typical members, the combination of resistance factors, code minimum reinforcement requirements, nominal member oversizing, and material over-strengths resulted in member expected strengths approximately 1.5 to 2.0 times required strengths, the factor depending on the number of stories in the frame. This factor was applied uniformly to all members in the frame to establish expected strengths, and then indicative longitudinal and transverse reinforcement was defined for each member. The indicative reinforcement was used to define force-deformation relations for nonlinear analyses that would be carried out as part of this study.

More details regarding the design parameters of the three idealized building are provided in Appendix A of the current study.

4.2 ANALYTICAL MODELING - COLLAPSE SIMULATION MODELS

Since the considered building configurations are symmetric, and it was the intent to simplify interpretation of results, only planar two dimensional (2D) models were used for nonlinear analyses. For the studied buildings each of the six frame lines were considered to resist earthquake lateral forces. The interior frames were considered to be more vulnerable than the perimeter frames because the interior columns resist higher tributary gravity forces and, therefore, would be more susceptible to axial collapse. Therefore, the planar 2D models considered resistance of a single interior frame only, with seismic mass equal to one-sixth of the building seismic mass (such that each frame was assumed to resist an equal portion of the building lateral force). The frame seismic mass was lumped at the ends of the structural members. Columns were fixed at the foundation. All beam-column joints at a given level were constrained to have equal horizontal displacements (that is, beams did not elongate and diaphragms were modeled as rigid). The structural analysis model was an assemblage of line elements representing the flexibilities of beams and columns rigidly connected at the beam-column joints and at the column-foundation joints. Joint flexibilities were set as rigid, without any flexibility. Rigid beam and column offsets extended from joint centerlines a distance of $h/4$, where h is the depth of either the column or the beam at a joint. The rigid offsets were assumed to be the same for all building variations independently of column-to-beam moment strength ratios. To incorporate non-linear geometry effects into the models, P-Delta formulation was applied directly to the column members of the 2D analysis frame.

4.2.1 Linear Elastic Stiffness Properties

Beams and columns were modeled with line elements to represent linear-elastic response and with concentrated end springs to represent inelastic response. The line elements have elastic flexural stiffness properties equal to gross section properties modified by stiffness reduction factors in accordance with ASCE/SEI 41 - 06. The stiffness reduction factors are listed in Table 4.2.

Table 4.2 Modification factor values for the cracked stiffness properties of the structural members

Structural Member	Modification Factor for Cracked Stiffness
beams	0.6*
columns	0.3-0.7**

* The tabulated value in ASCE/SEI-41 is 0.3. Here, flexural stiffness is calculated based on the gross section properties of the beam (depth and width). Thus, the beam stiffness factor is greater than ASCE/SEI 41 to account for additional stiffness provided by the floor slab acting as a top beam flange (or T beam).

** The stiffness modification factor applied to the columns varies from 0.3-0.7 according to the applied gravity load axial forces to which the columns are subjected.

Axial deformations of columns were based on gross-section stiffness where linear response was indicated. Axial deformations of beams were not permitted because the diaphragm was modeled as rigid.

Modeling of shear deformations for columns was dependent on the ratio V_p/V_n (V_p = shear corresponding to development of the probable moment strengths, at both ends of the column and V_n is the nominal shear strength in accordance with ASCE/SEI 41-06 for low ductility demand). When a V_p/V_n ratio equals 0.6, shear deformations were not taken into account. When V_p/V_n ratio equals 0.8, 1.0, or 1.2, shear deformations were taken into account using a shear spring at the top of each column element. The linear stiffness of the shear spring was set equal to:

$$K_v = \frac{0.4 * E_c * A_g}{l} \quad (\text{Eq. 4.2})$$

,where E_c corresponds to Young's Modulus of Elasticity for concrete, A_g is the gross cross-sectional area, and l is the height of the column element.

Modeling of shear deformations for beams was not performed in the current study.

4.2.2 Nonlinear Modeling for Flexure-Controlled Members

A lumped plasticity approach was used to model non-linear flexural behavior of beams and columns. This model consists of three parameters; the linear elastic line element and two plastic hinge (rotational) springs (one at each end, see Figure 4.3). Stiffness properties of the line elements are described in Section 4.2.1. Properties of the plastic hinge springs are described below.

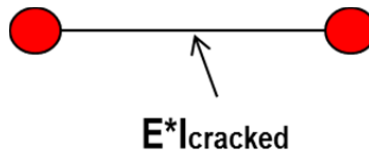


Figure 4.3 Lumped plasticity model (red circles represent the plastic hinges; the line between them represents a linear elastic element, E: Young's modulus of elasticity; I: second moment of inertia)

The rotational spring elements were implemented in OpenSees as zero-length rotational elements at the ends of beams and columns, as explained in Chapter 2, according to the model suggested by Haselton et al. (2008).

As discussed in Chapter 3, the Haselton et al. model demonstrated overall good agreement with experimental results for the case of ductile column members with detailing conforming to ACI 318-11 provisions. However, it was not accurate in simulating the response of members with non-ductile detailing whose failure is governed by shear and shear induced axial failure. Taking into account the experimental results presented in Chapter 3, it was decided that the Haselton et al. model would be used to model columns in buildings that were unlikely to have shear failure (that is, $V_p/V_n \leq 0.7$).

Furthermore, the relationships used for the parameter determination in the Haselton model were re-calibrated using the same column database used by Haselton et al. (2008) except those columns that were reported as failing in flexure-shear which were excluded from the calibration. This was done in order to make the regression relationships used to define the rotational springs more representative of column members with failure governed by flexure. The re-calibrated equations used to define the modeling parameters of the Haselton model are provided in Appendix B.

For analytical models of the considered buildings the values $\theta_{cap,pl}$, θ_{pc} , λ and c were calculated according to the re-calibrated relationships provided in Appendix B. The other parameters were calculated by moment-curvature analysis using software XTRACT (Imbsen Associates, 2004).

The modeling parameters of the considered buildings for the cases of flexure-controlled members are provided in Appendix A.

4.2.3 Nonlinear Modeling for Shear-Controlled Members

Shear-controlled members were defined as those having $V_p/V_n \geq 0.7$. Shear and axial failure of shear-controlled columns was modeled using the limit state material developed by Elwood and Moehle (2002) as described in Chapter 2.

To study the effect of V_p/V_n ratio in the dynamic response of a building frame, four different ratios were considered: $V_p/V_n=0.6, 0.8, 1.0$ and 1.2 . Consistent with the findings of Chapter 3 for models with $V_p/V_n > 0.7$ where the column members are susceptible to shear failure, the limit state material developed by Elwood was used to model the shear and axial failure.

The modeling parameters for variations of the considered buildings which have shear-controlled members are provided in Appendix A.

4.2.4 Dynamic Simulation

As discussed in Chapter 2, a modified version of Incremental Dynamic Analysis (IDA) was used to assess the collapse performance of the studied buildings. The nonlinear structural model was subjected to a recorded ground motion modified by a scaling factor and dynamically analyzed to determine the response. The response-history analysis was repeated, each time increasing the scale factor on the input ground motion until that record causes structural collapse, as identified by either story drifts that increase without bounds (maximum story drift ratio $\geq 10\%$) or excessive shear/axial deformation of columns ($\geq 50\%$ of column members in one story experiencing shear or axial failure).

After the IDA procedure was completed, post-processing of the results was required in order to develop the fragility curve of the specified model. First the Empirical Cumulative Distribution Function (ECDF) of collapse as a function of ground motion intensity was drawn as shown in Figure 4.4, using data points from the IDA. Then, a lognormal distribution was fit to the collapse data points (Figure 4.4). The lognormal collapse fragility is defined by two parameters, the logarithmic mean (μ_{ln}) and the logarithmic standard deviation (σ_{ln}).

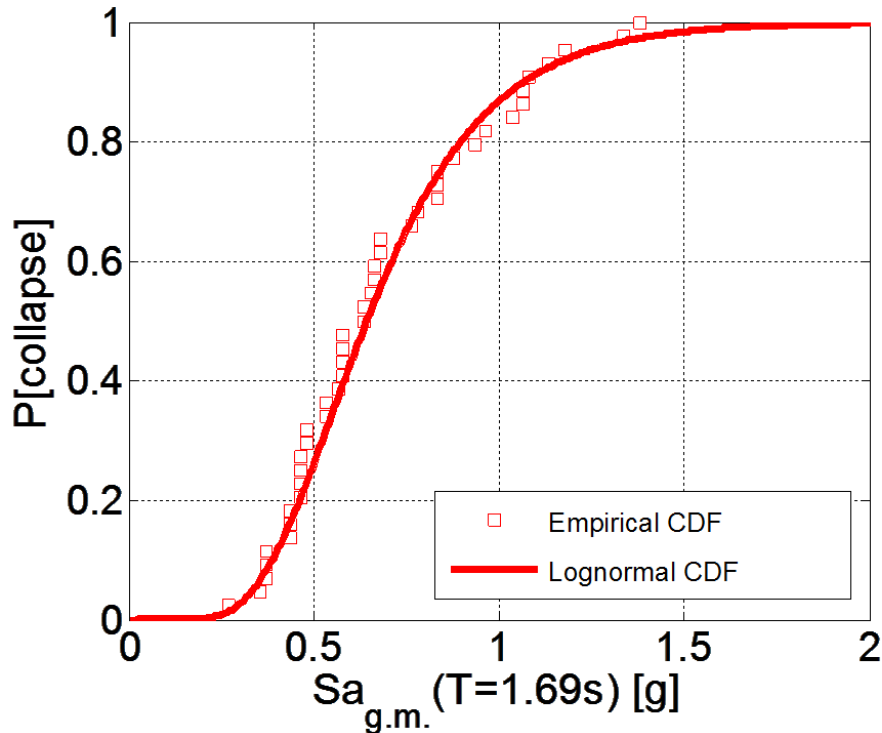


Figure 4.4 Empirical and fitted log-normal cumulative distribution function of probability of collapse (8-story building with $\Sigma M_{nc}/\Sigma M_{nb} = 1.2$ and $V_p/V_n=0.6$)

It should be noted that this study considered only the record-to-record collapse (aleatory) uncertainty. Modeling (epistemic) uncertainties were not considered. The effect of spectral shape of the ground motions in the estimation of the probability of collapse was also not considered. The current study used 44 recorded ground motions (22 pairs) selected to represent large earthquakes with moderate fault rupture distances (i.e., not near-fault conditions). More details regarding the considered ground motions are presented in Chapter 2 of the current study. Due to the large number of earthquake simulations, an optimized combination of solution algorithms was attempted to minimize the computational time. The starting value of the analysis time step corresponded to 0.01 seconds and varied down to 0.0001 seconds. For dynamic analyses, damping was assumed equal to 2% of critical damping. This effect was achieved in OpenSees by using Rayleigh damping with the following properties:

- Mass Proportional damping coefficient α_0 calculated according to the following equation:

$$a_0 = \zeta \frac{2 * \omega_1 * \omega_3}{\omega_1 + \omega_3} \quad (\text{Eq. 4.3})$$

- Stiffness Proportional damping coefficient α_1 calculated according to the following equation:

$$a_1 = \zeta \frac{2_3}{\omega_1 + \omega_3} \quad (\text{Eq. 4.4})$$

, where ζ is the damping ratio, and ω_1 and ω_3 are the natural frequencies determined by eigenvalue analysis of the first and third modes, respectively.

The results of the eigenvalue analysis for the idealized buildings are presented in Appendix C of the current study

5 A Strength-Based Approach to Evaluate the Collapse Potential of Older-Type Concrete Frame Buildings

In this chapter a method to identify high-risk older type concrete buildings is developed. The three idealized building configurations presented in Chapter 4 are used to perform assessment of the collapse performance of older-type concrete buildings. Variations of the archetype buildings with characteristics similar to those of older-type buildings are utilized for the collapse assessment. Incremental dynamic analysis is used to determine the probability of collapse for various combinations of the study variables.

The method presented in this chapter links the structural parameters column to beam moment strength ratio, and the flexural shear demand to shear strength ratio with the collapse performance of the archetype buildings and their variations. The results indicate that simple engineering parameters, the “collapse indicators,” could be used by engineers for a rapid seismic risk assessment of existing concrete buildings.

5.1 PUSHOVER ANALYSIS TO EVALUATE THE SEISMIC PERFORMANCE OF EXISTING CONCRETE BUILDINGS

Static pushover analysis has been traditionally a popular method to perform seismic evaluation of existing structures. To perform pushover analysis an engineer needs to model the strength and deformation characteristics of the components of the simulated structure. Pushover analysis can provide useful information regarding the seismic behavior of a structure, though since it is based on many assumptions the obtained results need to be viewed with caution as explained by Krawinkler (1996). Two of its basic assumptions are: a) the response of the structure is related to the response of an equivalent single-degree-of-freedom system b) the response of a building is controlled by a single mode and the shape of this mode remains constant throughout the dynamic response of the structure. Since both of these basic assumptions are incorrect, it is recognized that static analysis does not accurately represent behavior expected under dynamic loading.

To explore the characteristics of the archetype buildings and of their variations, nonlinear static (pushover) analysis using an inverted triangular load pattern was performed for the three studied buildings having $V_p/V_n = 0.6$ and $\Sigma M_{nc}/\Sigma M_{nb} = 1.2$, that is, flexure-controlled with code-required column to beam moment strength ratio. Pushover analysis is used here only to define an index strength and drift capacity. Figure 5.1 plots relations between roof drift ratio and base shear.

Base-shear strengths range from approximately $0.13W$ to $0.2W$. As demonstrated in Figure 5.1 drift ratio capacities are higher for the shorter buildings, apparently because of localized yielding and P-delta effects that are more dominant in the taller buildings.

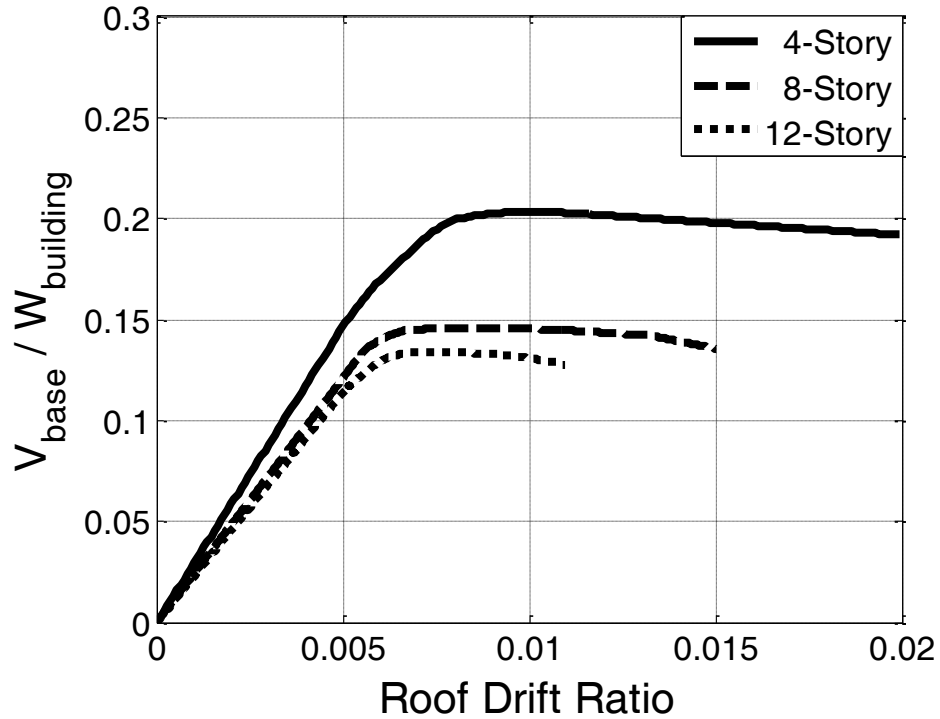


Figure 5.1 Pushover analysis of the three “modern code design” building models ($V_p/V_n=0.6$, $\Sigma M_{nc}/\Sigma M_{nb}=1.2$)

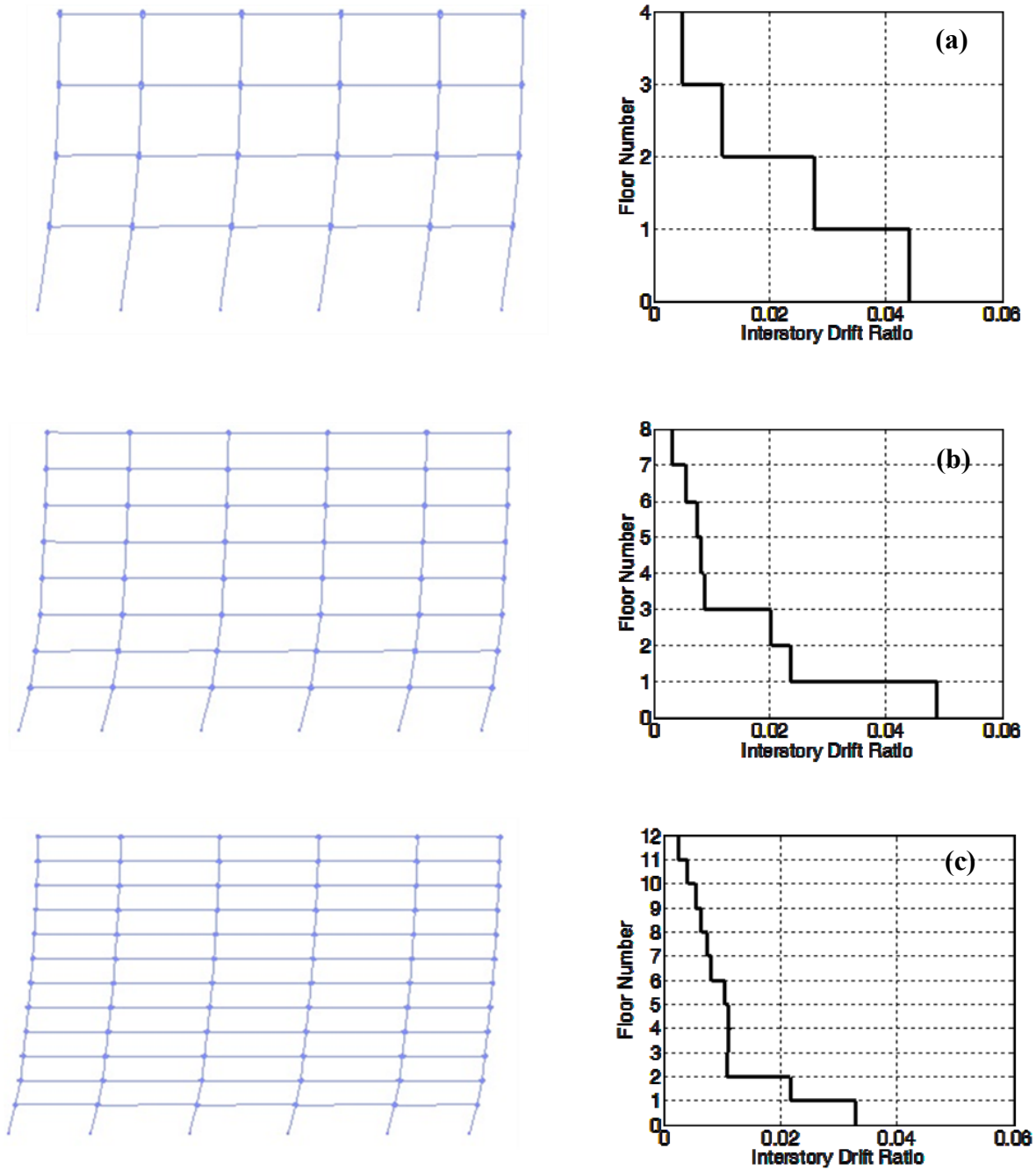


Figure 5.2 Failure mechanisms of the three “modern code design” building models ($V_p/V_n=0.6$, $\Sigma M_{nc}/\Sigma M_{nb}=1.2$): (a) 4-story building, (b) 8-story building, and (c) 12-story building

Figure 5.2 shows that the calculated yield mechanisms under static loading extended through the second, third, and fifth stories of the 4, 8, and 12-story buildings in this study.

As has been reported previously by Kuntz and Browning (2003) and others, the provision of $\Sigma M_{nc}/\Sigma M_{nb} = 1.2$ does not prevent formation of localized mechanisms that extend over only the lower stories. Figures 5.3 and 5.4 demonstrate how variation on the column-to-beam bending moment strength ratio changes the failure mechanism of the idealized 8-story building by distributing the damage imposed by the lateral loading over the height of the building. In Figure 5.3, pushover analysis demonstrates that as the $\Sigma M_{nc}/\Sigma M_{nb}$ ratio increases the building exhibits more ductile behavior. As illustrated in Figure 5.4, for the case of a low value of $\Sigma M_{nc}/\Sigma M_{nb} = 0.8$ all the damage is concentrated in the 1st story which in combination with the P-Delta effects leads to non-ductile lateral response. For the case of a high value of $\Sigma M_{nc}/\Sigma M_{nb} = 1.6$ the damage is more uniformly distributed through the 5th story affecting the lateral response of the structure which fails in a more ductile manner.

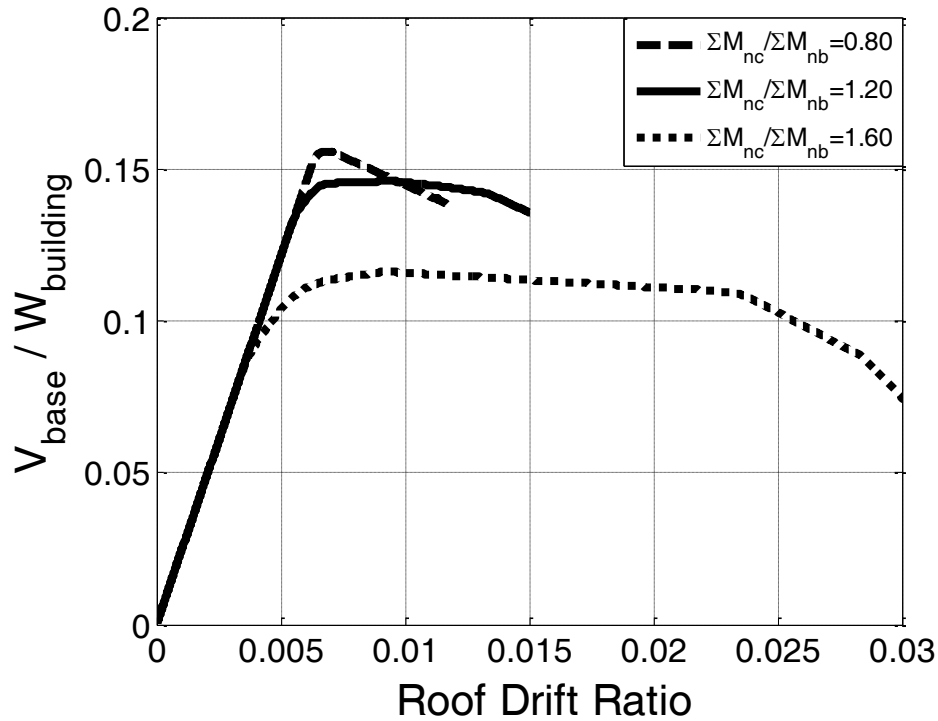


Figure 5.3 Pushover analysis of the 8-Story building models for different $\Sigma M_{nc}/\Sigma M_{nb}$ ratios ($V_p/V_n=0.6$)

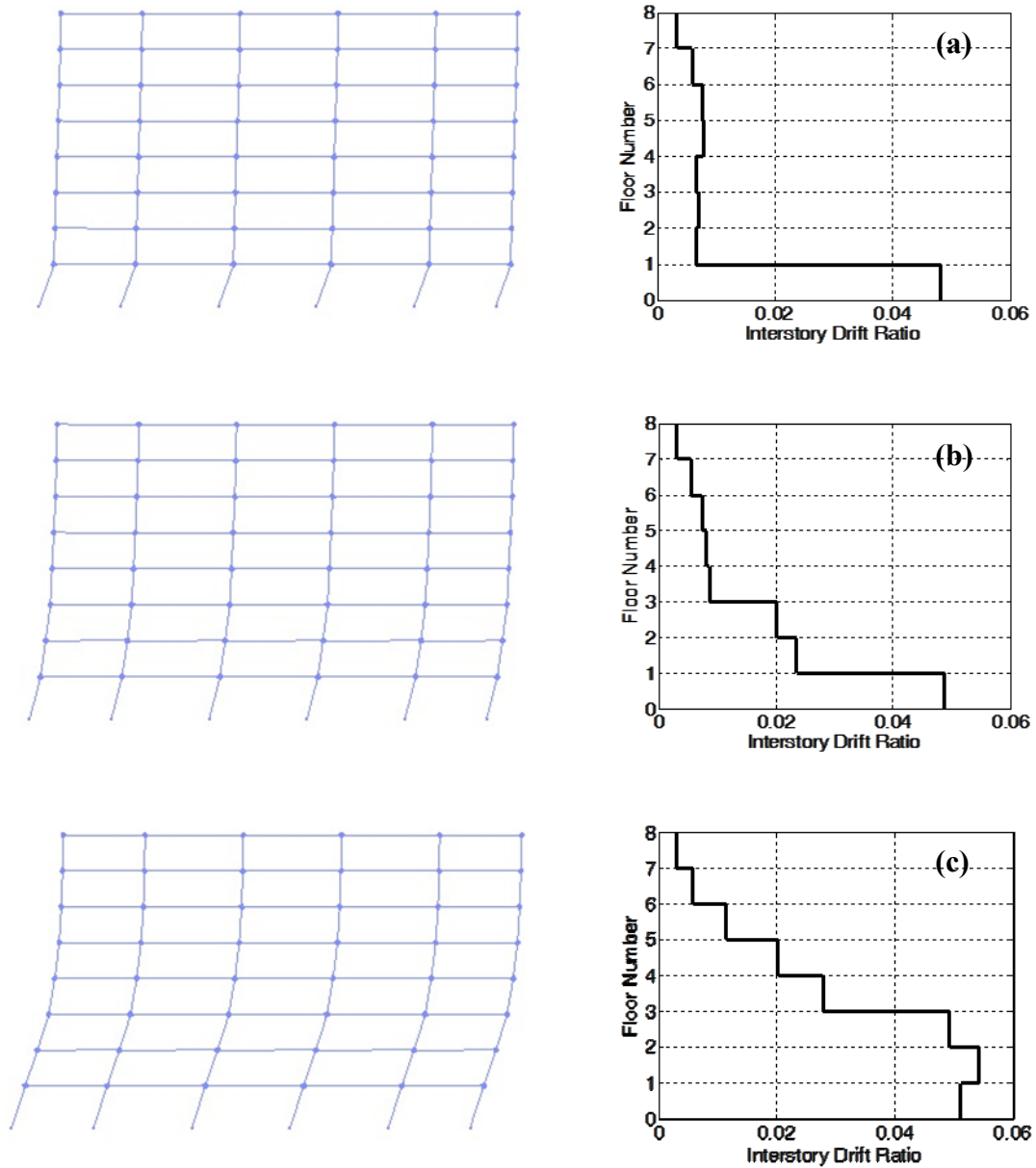


Figure 5.4 Failure mechanisms of the 8-Story building models for different $\Sigma M_{nc}/\Sigma M_{nb}$ ratios ($V_p/V_n=0.6$): (a) $\Sigma M_{nc}/\Sigma M_{nb}=0.80$, (b) $\Sigma M_{nc}/\Sigma M_{nb}=1.20$, and (c) $\Sigma M_{nc}/\Sigma M_{nb}=1.60$

5.2 ASSESSMENT OF SEISMIC BEHAVIOR

Seismic behavior of the studied building models was assessed using the incremental dynamic analysis (IDA) method. According to this method, an analytical model of a building was subjected to numerous dynamic analyses under multiple ground motions scaled gradually to increasing acceleration amplitude. Collapse was defined for the smallest input motion required to

achieve either one of the following two limit states: 1) Maximum story drift ratio exceeding 10% of story-height, or 2) Shear or axial failure in more than 50% of the columns in any story.

More details regarding the IDA procedure followed in this study can be found in Chapter 4.

Figure 5.5 shows a typical output from an IDA of a single building. Each line in the figure represents the response of the building to a single ground motion record scaled to increasing intensity. Note that the curves begin to flatten out at maximum story drift ratio of approximately 0.05, suggesting that the structure becomes unstable at around this story drift ratio. The latter value of story drift resulting in “dynamic” instability of the building is consistent with the results obtained from pushover analysis (Figure 5.4-b) where for story drift value of the 1st story slightly less than 0.05, the pushover curve starts having negative stiffness slope indicating “static” instability.

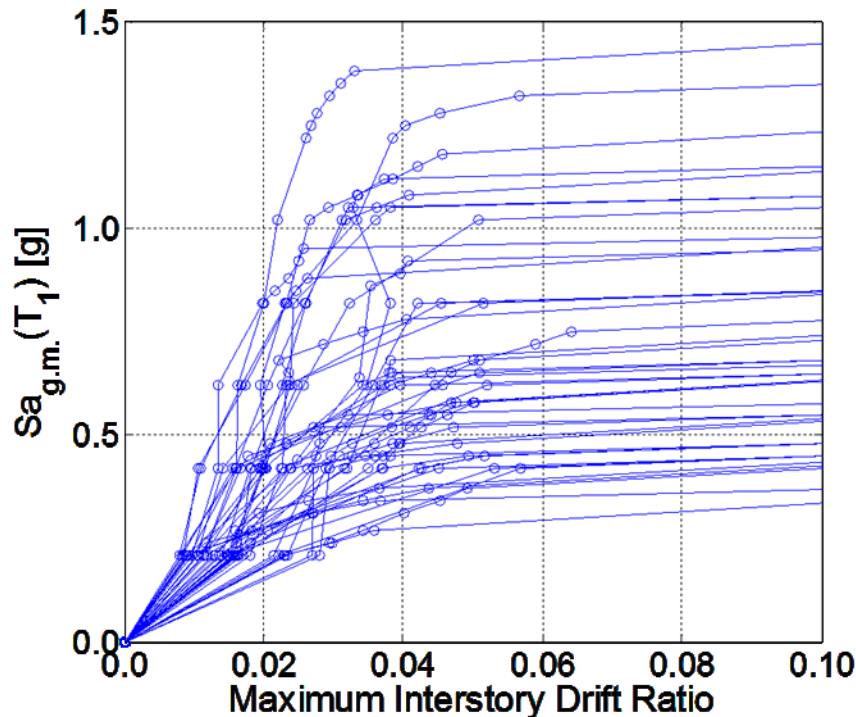


Figure 5.5 Incremental Dynamic Analysis (IDA) curves for the 8-story “modern code design” building model ($V_p/V_n=0.6$, $\Sigma M_{nc}/\Sigma M_{nb}=1.2$)

The collapse risk of each building model was obtained from statistics on the IDA results. In this study, collapse performance was evaluated using the probability of collapse as a function of the ground motion intensity level, defined in terms of $S_a(T_1)$. The collapse probabilities in terms of $S_a(T_1)$ were assumed to be log-normally distributed. Figure 5.6 shows the collapse fragility relations. The interested reader can find a more detailed description of the fragility curve development procedure in Chapter 4.

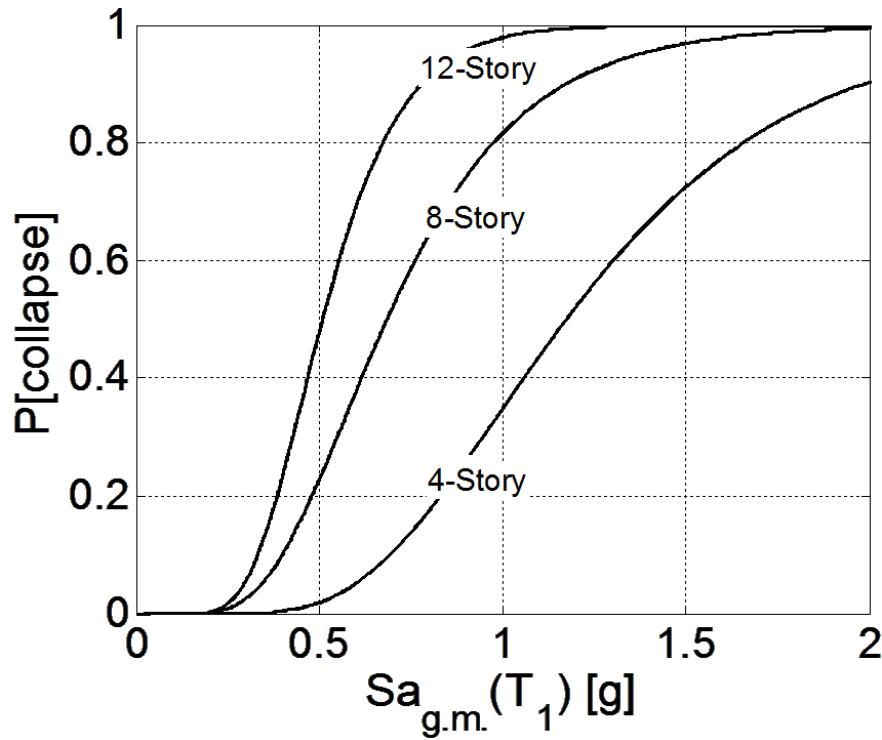


Figure 5.6 Collapse fragility functions of the “modern code design” building models ($V_p/V_n=0.6$, $\Sigma M_{nc}/\Sigma M_{nb}=1.2$)

The variation of structural parameters (beam moment strength and column transverse reinforcement) could lead to changes in the overall building strength. To avoid comparison bias that could occur due to differences in building strength, the results of the study were normalized with respect to the maximum base shear capacity of the frame V_{max} . The value of V_{max} was calculated from non-linear static analysis with inverted triangular load pattern. The normalized strength parameter R_e was defined as:

$$R_e = \frac{S_a(T_1) \times (W_{building} / g)}{V_{max}} \quad (\text{Eq. 5.1})$$

Note that R_e represents approximately the ratio of elastic demand to actual strength. It is not the same as the response modification coefficient R of ASCE 7-10, which is the ratio of the elastic demand for the design earthquake level to the required design strength.

Calculation of the R_e normalization factor requires the creation of a non-linear building model which could be a cumbersome procedure. Alternatively a simpler normalization factor could be used. The second normalization factor M uses an estimate of the maximum base shear capacity of the building $V_{max,estimated}$. The latter procedure requires only hand-calculations and it was developed by Mehrain (ATC-78, 2013). The procedure used to compute the $V_{max,estimated}$ is

described in Appendix D. It should be noted that the described procedure to estimate the base shear capacity of existing buildings includes numerous assumptions and, thus, it is just an approximation that could be used as an alternative to sophisticated non-linear analysis for rapid seismic risk evaluation. For clarity when this normalization method is used the normalized parameter would be referred to as M , where:

$$M = \frac{S_a(T_1) \times (W_{building} / g)}{V_{max,estimated}} \quad (\text{Eq. 5.2})$$

The normalization factor M is identical to the R_e factor except for the calculation of the base shear capacity that is computed as explained in Appendix D.

5.3 USING COLLAPSE INDICATORS TO PERFORM EARTHQUAKE RISK ASSESSEMENT FOR EXISTING BUILDINGS

For buildings assigned to the highest Seismic Risk categories and having moment frames as the seismic force-resisting system, ACI 318-11 requires that the moment frames be proportioned and detailed as special moment frames. For such frames, ACI 318-11 requires that the sum of column nominal moment strengths be at least 1.2 times the sum of beam nominal moment strengths at every beam-column joint. (Some localized exceptions to this requirement can be permitted.) This requirement is commonly referred to as the “strong-column, weak-beam” requirement. Its purpose is to promote beam yielding rather than column yielding, thereby spreading flexural yielding over multiple stories as the building responds to strong earthquake shaking. In buildings with relatively weak columns, column hinging may lead to deformations concentrated in one story, resulting in a so called weak-story mechanism. Older concrete buildings commonly do not satisfy the strong-column, weak-beam requirement, making them more vulnerable to damage and collapse because of the development of a weak story.

To study the effect of column-to-beam strength ratio on the collapse risk of buildings with otherwise good details, the beam moment strengths were scaled to achieve column-to-beam moment strength ratios $\Sigma M_{nc} / \Sigma M_{nb}$ varying from 0.6 to 1.8. Transverse reinforcement was sufficient to result in $V_p / V_n = 0.6$, such that shear failures were prevented in the study. Figure 5.7 presents partial results from the analyses, in this case plotting probability of collapse as a function of $\Sigma M_{nc} / \Sigma M_{nb}$ for $R_e = 3$. A notable observation is that there is rapid increase in collapse probability for values of $\Sigma M_{nc} / \Sigma M_{nb}$ less than approximately 1.2, the minimum value permitted by ACI 318-11 for special moment frames.

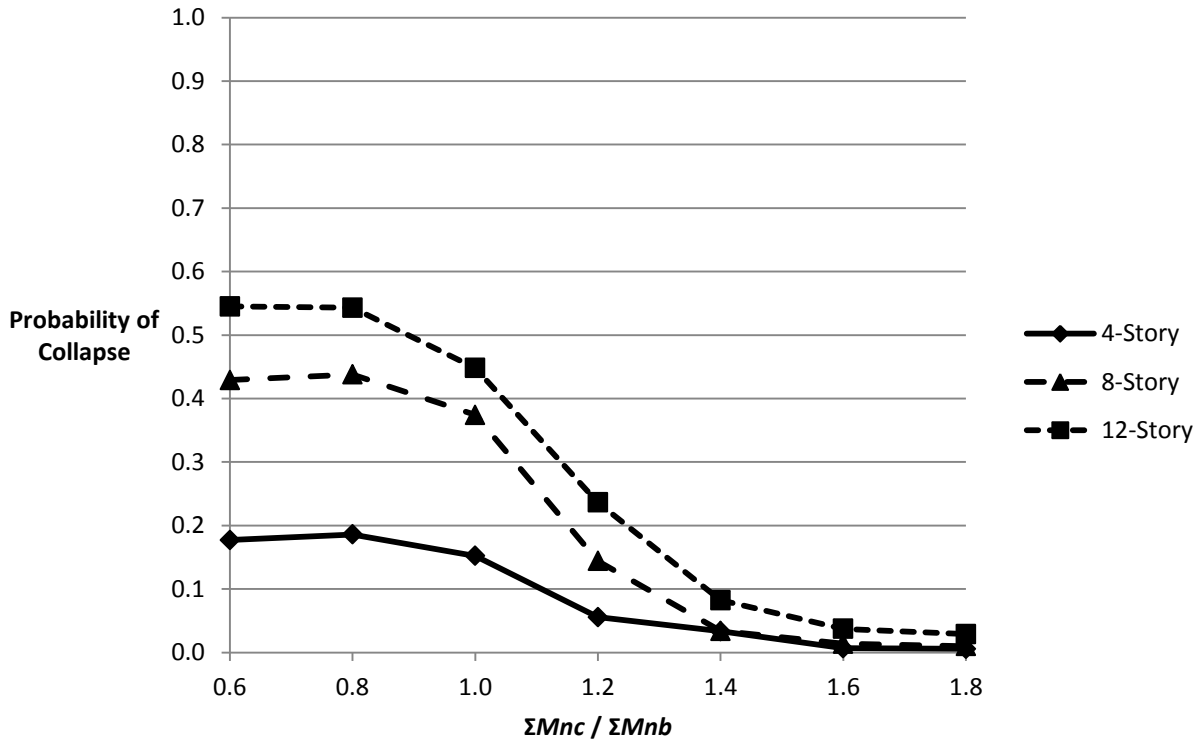


Figure 5.7 Comparison of collapse performance of the studied building models for $R_e=3$ and $V_p/V_n=0.6$

Figures 5.8 (a)-(c) depict the effect of $\Sigma M_{nc}/\Sigma M_{nb}$ for different values of the parameter R_e for the three building frames. Note that in this figure, all the buildings have closely spaced transverse reinforcement resulting in ductile flexural response without possibility of shear failure. From the figure, several observations can be made. In general, collapse probability increases as R_e increases. For values of $\Sigma M_{nc}/\Sigma M_{nb} = 1.2$ and $R_e = 3$, probability of collapse is approximately 10% for the four-story frame, increasing to approximately 20% for the 12-story frame. Thus, to achieve the same probability of collapse, a larger value of $\Sigma M_{nc}/\Sigma M_{nb}$ is required for taller buildings than for shorter buildings.

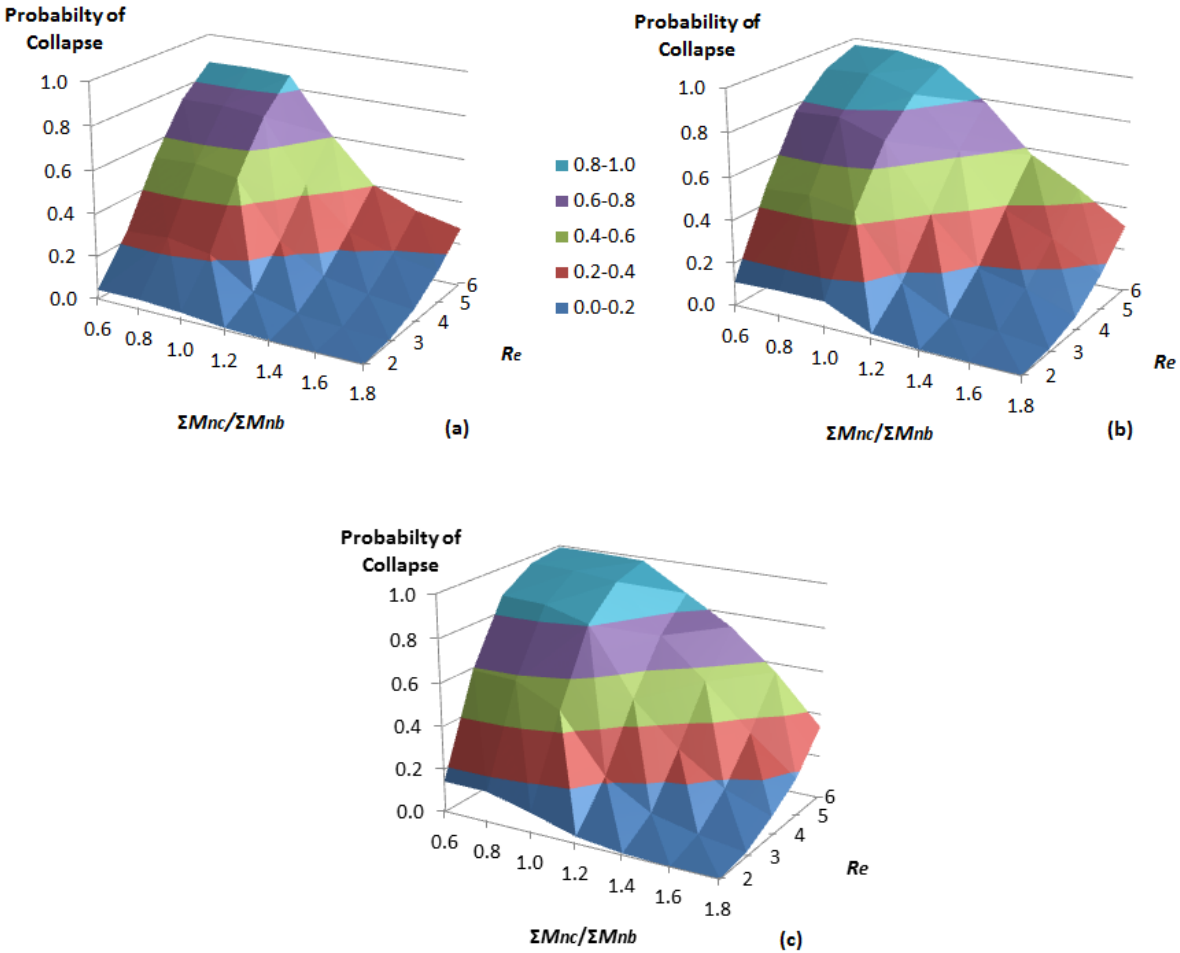


Figure 5.8 Collapse Performance of (a) 4-Story (b) 8-Story (c) 12-Story building models with $V_p/V_n=0.6$

Older-type concrete buildings commonly do not have closely spaced transverse reinforcement, making them more susceptible to shear and axial failures. To study this effect, the spacing of column transverse reinforcement was varied in each of the building models to achieve values of V_p/V_n ranging from 0.6 to 1.2. For each value of V_p/V_n , ratios of column-to-beam moment strengths $\Sigma M_{nc}/\Sigma M_{nb}$ were varied from 0.6 to 1.8, creating a full matrix of results for the range of V_p/V_n and $\Sigma M_{nc}/\Sigma M_{nb}$. For frames having $V_p/V_n > 0.7$, shear and axial failure was considered a possibility. Therefore, for these frames, the analytical model was modified to enable simulation of shear and axial failures.

Incremental dynamic analyses were conducted for each combination of the study variables. Figure 5.9 presents collapse fragility curves evaluated from the IDA results. The figure conveys information that can be interpreted in different ways. For example, for a given value of R_e , the collapse fragility is much higher for the frames with shear-critical columns than for frames with flexure-controlled columns. Alternatively, for a building with shear-critical columns to have the

same collapse fragility as a frame with flexure-controlled columns, it must have higher base-shear strength (that is, smaller R_e).

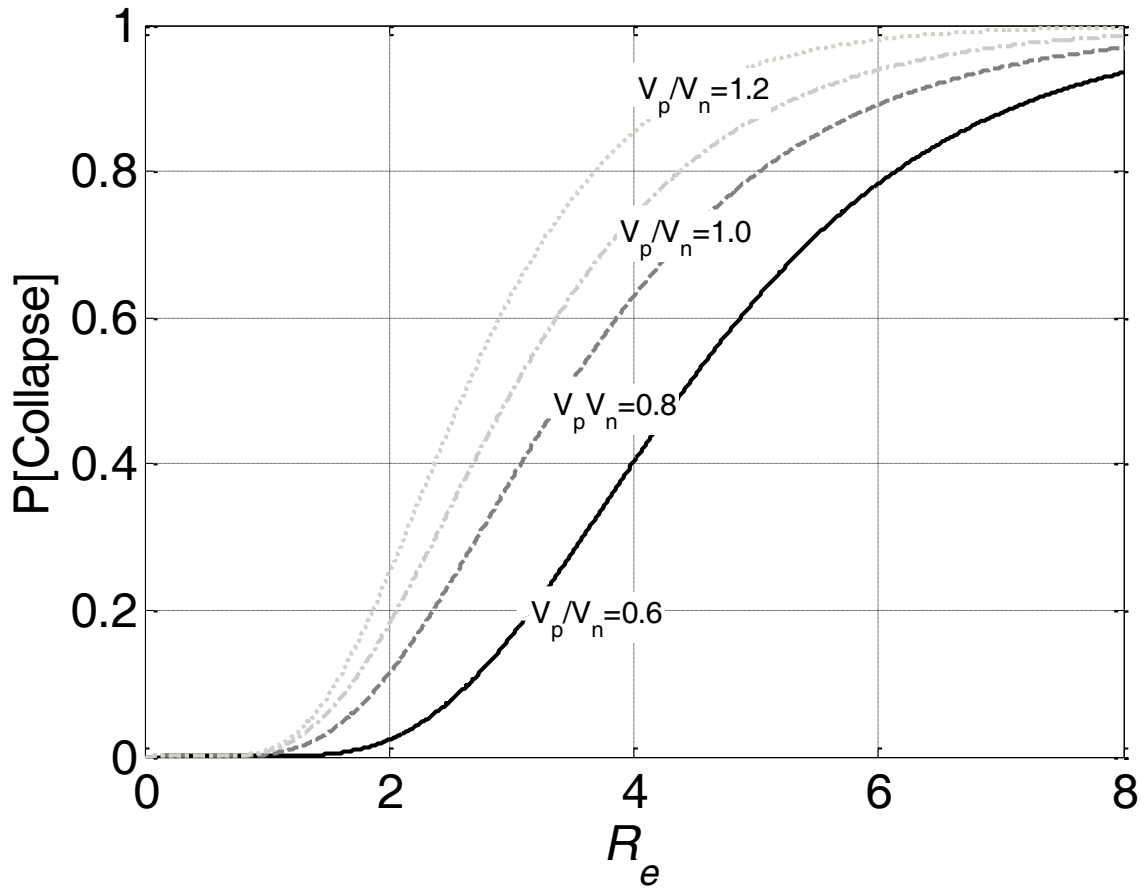


Figure 5.9 Comparison of the fragility curves of the 8-Story Building having $\Sigma M_{nc}/\Sigma M_{nb}=1.2$

Figure 5.10 compares the effect of V_p/V_n for the 4, 8, and 12-story frames, in each case for $\Sigma M_{nc}/\Sigma M_{nb} = 1.2$ and $R_e = 3$. For each configuration, the collapse probability increases as the transverse reinforcement spacing increases (that is, V_p/V_n increases). Also, for a given value of V_p/V_n , a taller building is always more vulnerable than a shorter one. This is because shear failure generally is restricted to a single story, such that most of the building lateral drift concentrates in that story. In a tall building, a single-story failure represents a more severe localization and therefore higher demand than occurs in an otherwise identical shorter building. P-delta effects also are greater for a taller building, exacerbating strength loss and thereby accelerating failure.

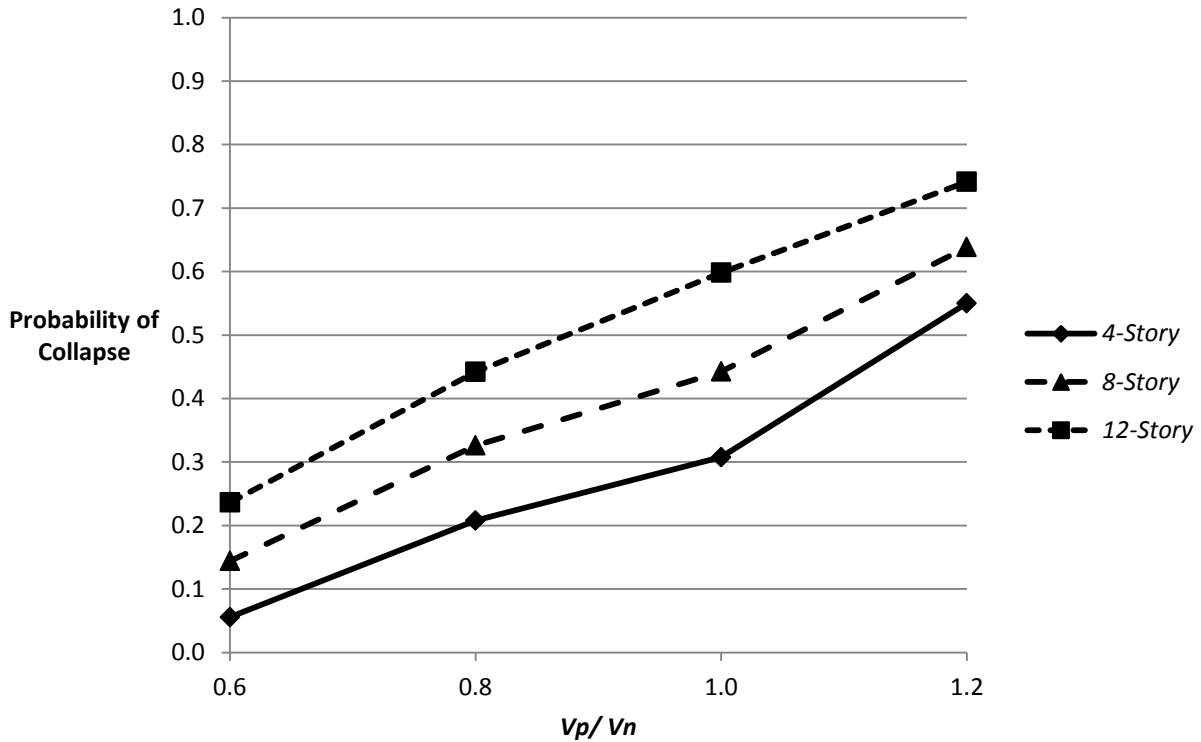


Figure 5.10 Comparison of the collapse performance of the three Idealized Buildings for $\Sigma M_{nc}/\Sigma M_{nb}=1.2$ and $R_e=3$

Figure 5.11-5.13 present collapse probability results for the complete matrix of V_p/V_n and $\Sigma M_{nc}/\Sigma M_{nb}$ values that were investigated for the 4,8 and 12-story buildings. Collapse probabilities increase with increasing R_e , increasing V_p/V_n , and decreasing $\Sigma M_{nc}/\Sigma M_{nb}$. The combination of low strength, high V_p/V_n , and low $\Sigma M_{nc}/\Sigma M_{nb}$ is especially critical.

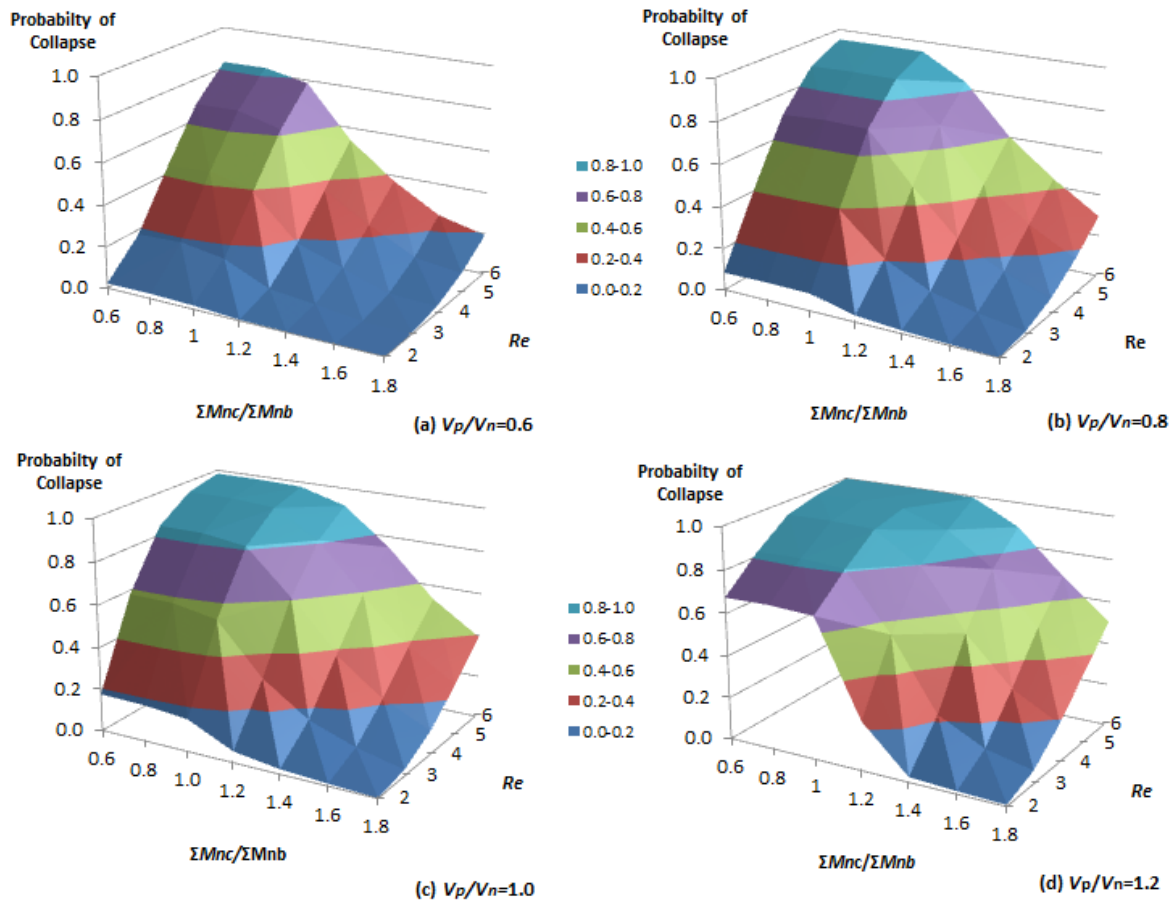


Figure 5.11 Comparison of the collapse performance of the 4-Story Building for (a) $V_p/V_n=0.6$, (b) $V_p/V_n=0.8$, (c) $V_p/V_n=1.0$ and (d) $V_p/V_n=1.2$

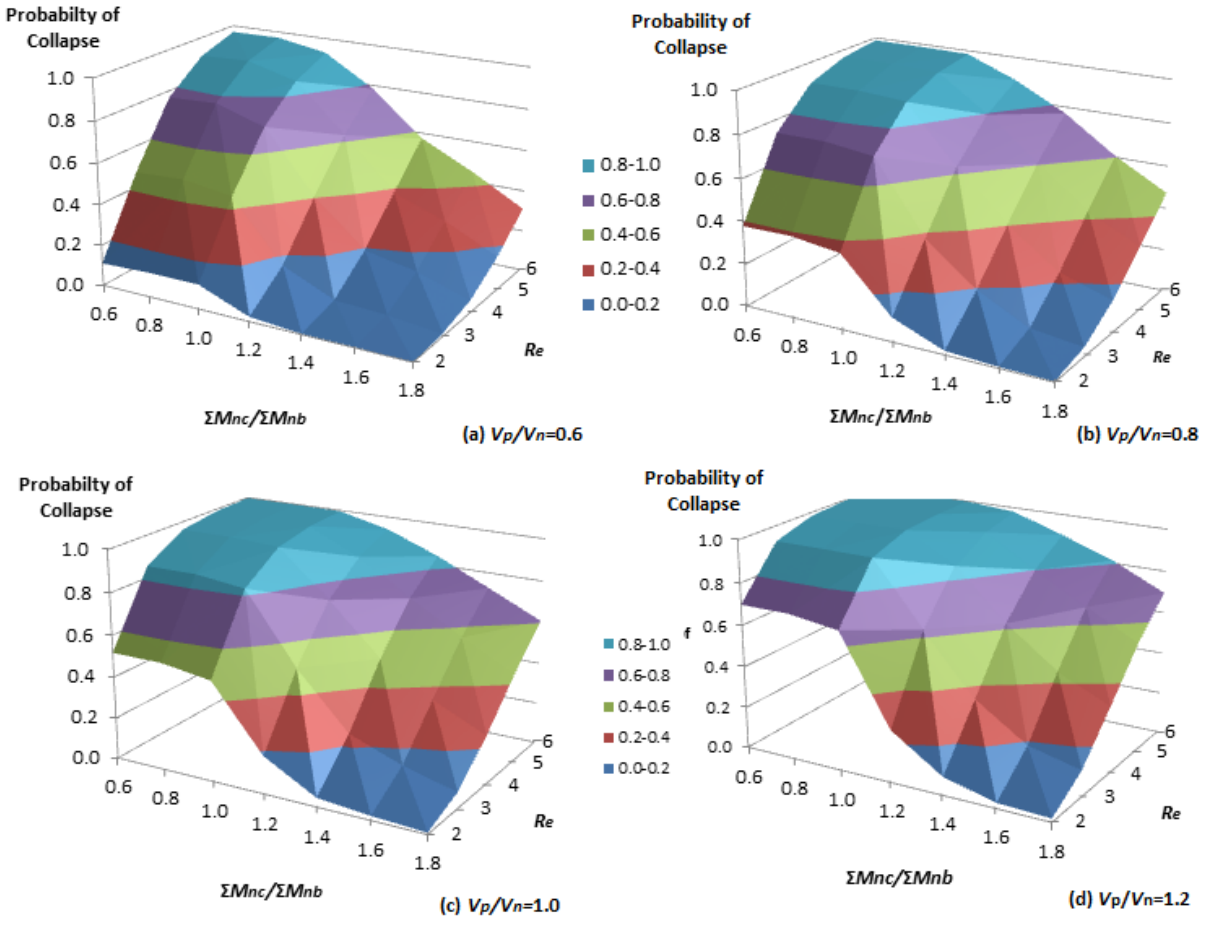


Figure 5.12 Comparison of the collapse performance of the 8-Story Building for (a) $V_p/V_n=0.6$, (b) $V_p/V_n=0.8$, (c) $V_p/V_n=1.0$ and (d) $V_p/V_n=1.2$

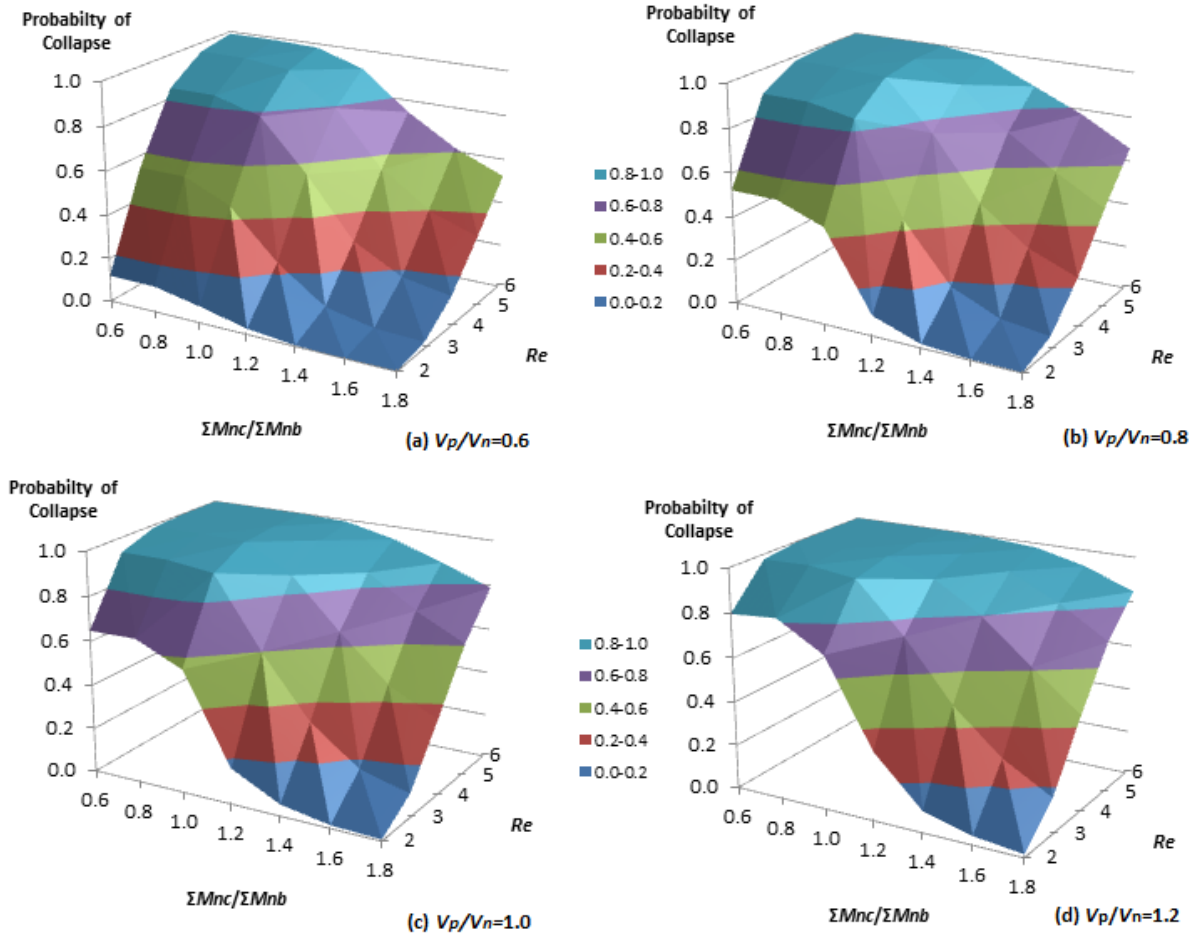


Figure 5.13 Comparison of the collapse performance of the 12-Story Building for (a) $V_p/V_n=0.6$, (b) $V_p/V_n=0.8$, (c) $V_p/V_n=1.0$ and (d) $V_p/V_n=1.2$

Figure 5.14 presents collapse probability results for the complete matrix of V_p/V_n and $\Sigma M_{nc}/\Sigma M_{nb}$ values for 4, 8, and 12-story frames. As previously noted, collapse probabilities increase with increasing V_p/V_n , and decreasing $\Sigma M_{nc}/\Sigma M_{nb}$. The combination of low strength, high V_p/V_n , and low $\Sigma M_{nc}/\Sigma M_{nb}$ is especially critical, and more-so for taller frames than for shorter frames. For the flexure-controlled frames (Figure 5.12a), collapse probabilities increase significantly for $\Sigma M_{nc}/\Sigma M_{nb}$ less than approximately 1.2 (the required value in ACI 318-11 for special moment frames). For frames with shear-critical columns (Figure 5.12 b, c, and d), the critical value of $\Sigma M_{nc}/\Sigma M_{nb}$ appears to shift to higher values. A list of the probability of collapse values for all the considered cases in a matrix format can be found in Appendix E.

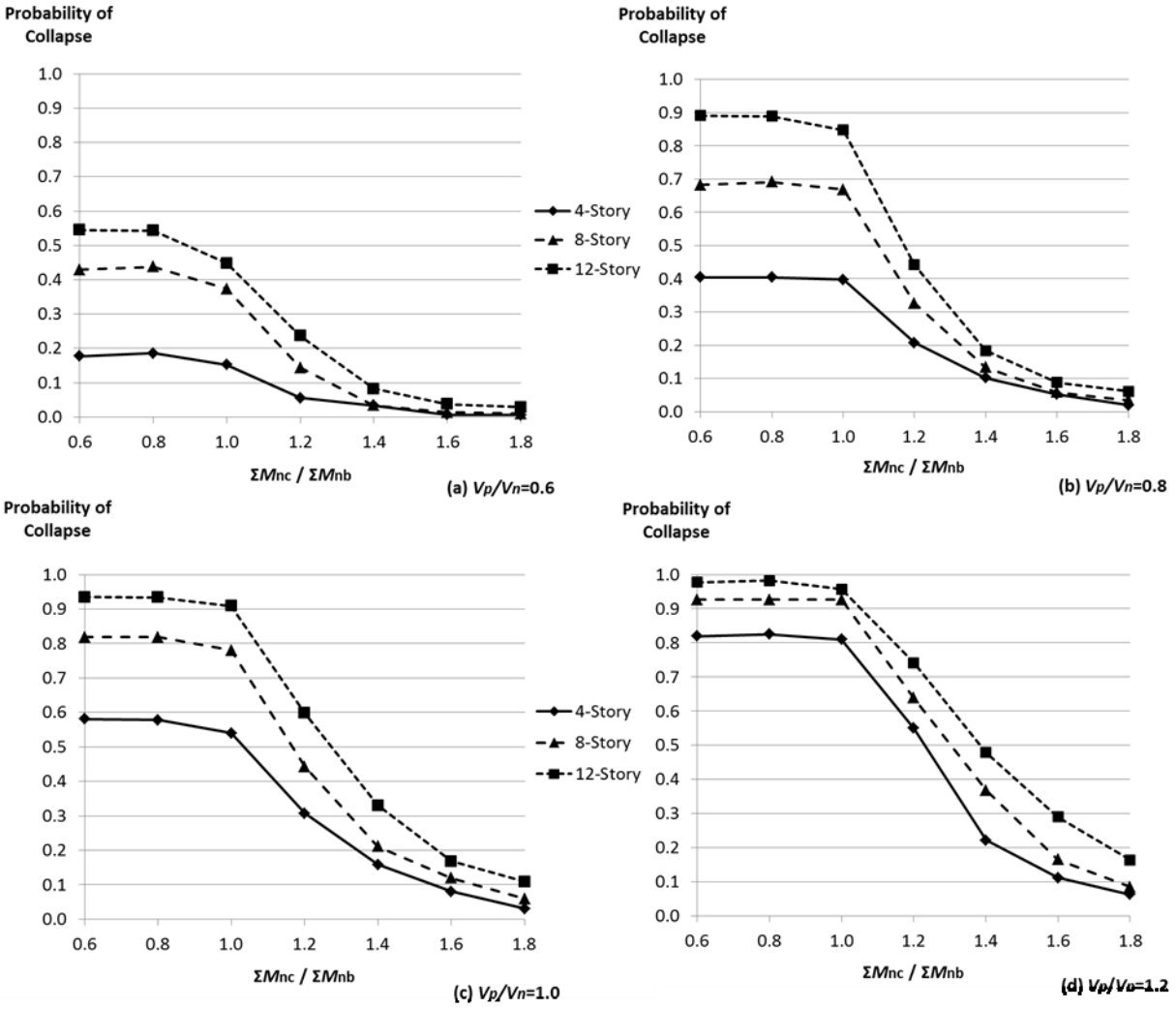


Figure 5.14 Comparison of the collapse performance of the three Idealized Buildings with $R_e=3$ for (a) $V_p/V_n=0.6$, (b) $V_p/V_n=0.8$, (c) $V_p/V_n=1.0$ and (d) $V_p/V_n=1.2$

5.4 EARTHQUAKE RISK ASSESSEMENT FOR BUILDINGS WITH NON-UNIFORM STRUCTURAL PARAMETERS

The results presented in the previous sections of this chapter correspond to the case of idealized buildings that possess uniform structural parameters for all the structural components. Although this presents a convenient simplification, since collapse potential is directly linked to a change in the value of one structural parameter, this is hardly the case for any existing building. In reality most of the buildings consist of components with varying structural parameter (collapse indicator) values, even within the same story.

In the current section the effect of varying $\Sigma M_{nc}/\Sigma M_{nb}$ values within a story of a building was explored. In the original idealized 8-story buildings, joints A,B,C,D,E, and F illustrated in Figure 5.15 possess uniform $\Sigma M_{nc}/\Sigma M_{nb}$ values for all the stories except the roof.

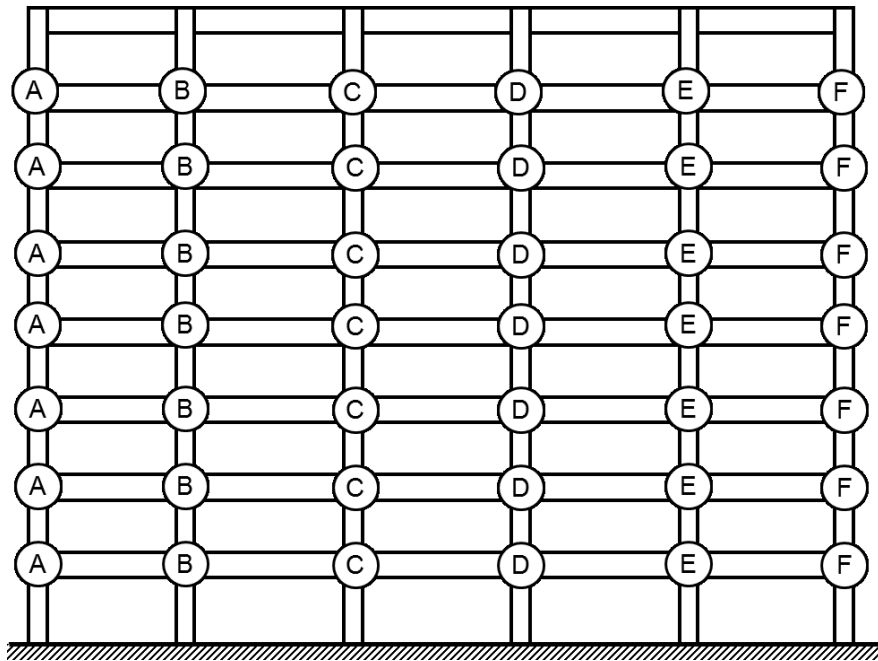


Figure 5.15 Illustration of joints A,B,C,D,E, and F of the 8-story idealized building

To study the effect of $\Sigma M_{nc}/\Sigma M_{nb}$ parameter variation, the beam moment strengths were modified such that different combinations of $\Sigma M_{nc}/\Sigma M_{nb}$ values for each joint in the same story are obtained. The effect was studied based on the 8-story idealized building.

The considered combinations are presented in Table 5.1. The modification of beam strength values was performed such that all the stories possess exactly the same joint $\Sigma M_{nc}/\Sigma M_{nb}$ combination values.

Table 5.1 Combination of non-uniform joint $\Sigma M_{nc}/\Sigma M_{nb}$ values

Non-Uniform $\Sigma M_{nc}/\Sigma M_{nb}$ Combination	Story Average ⁴ $\langle \Sigma M_{nc}/\Sigma M_{nb} \rangle$	Joint $\Sigma M_{nc}/\Sigma M_{nb}$ values					
		A	B	C	D	E	F
1	0.8	1.0	0.8	0.6	0.6	0.8	1.0
2	1.0	1.2	1.0	0.8	0.8	1.0	1.2
3	1.0	1.4	1.0	0.6	0.6	1.0	1.4
4	1.2	1.4	1.2	1.0	1.0	1.2	1.4
5	1.2	1.6	1.2	0.8	0.8	1.2	1.6
6	1.2	1.8	1.2	0.6	0.6	1.2	1.8
7	1.4	1.6	1.4	1.2	1.2	1.4	1.6
8	1.4	1.8	1.4	1.0	1.0	1.4	1.8
9	1.6	1.8	1.6	1.4	1.4	1.6	1.8

The collapse performance of each model with certain $\Sigma M_{nc}/\Sigma M_{nb}$ joint combinations was reported. Consequently the collapse performance of each considered model with non-uniform $\Sigma M_{nc}/\Sigma M_{nb}$ joint values was compared with the performance of an idealized frame with uniform $\Sigma M_{nc}/\Sigma M_{nb}$ joint values.

The collapse performance of the studied models with uniform (solid lines) and non-uniform (dashed lines) $\Sigma M_{nc}/\Sigma M_{nb}$ joint values is presented in Figure 5.16.

⁴ Story average is calculated as follows: $\langle \Sigma M_{nc} / \Sigma M_{nb} \rangle = \frac{\sum_{k=A}^F (\Sigma M_{nc} / \Sigma M_{nb})_k}{6}$

Probability of Collapse

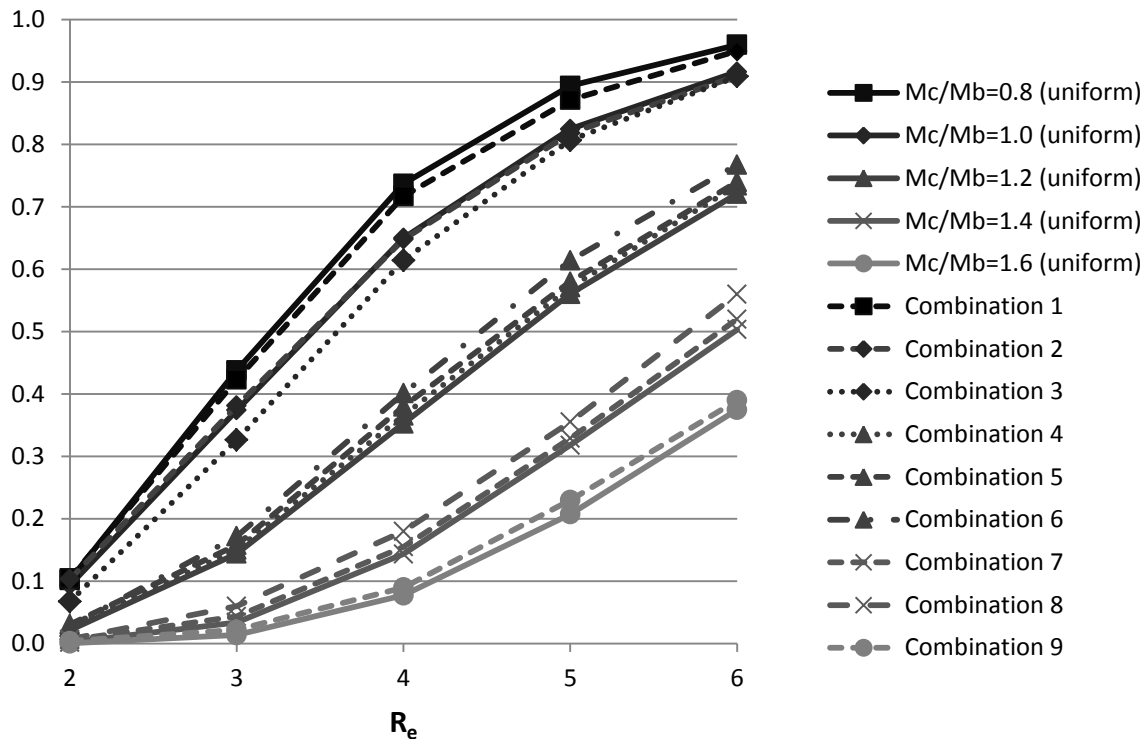


Figure 5.16 Comparison of the collapse performance of the idealized 8-story building with: a) uniform $\Sigma M_{nc}/\Sigma M_{nb}$ values, and b) non-uniform $\Sigma M_{nc}/\Sigma M_{nb}$ values

The results suggest that buildings with non-uniform $\Sigma M_{nc}/\Sigma M_{nb}$ joint values, and with story average $\langle \Sigma M_{nc}/\Sigma M_{nb} \rangle = B$ have similar collapse performance as the idealized buildings that possess uniform $\Sigma M_{nc}/\Sigma M_{nb} = B$ joint values. Therefore, story average $\langle \Sigma M_{nc}/\Sigma M_{nb} \rangle$ seems to be a relatively good indicator of the collapse performance of buildings that possess non-uniform joint $\Sigma M_{nc}/\Sigma M_{nb}$ values.

For the purposes of the ATC-78 project (ATC-78, 2013) Dr. Liel and her colleagues performed a similar study to explore the effect of varying V_p/V_n parameter for columns within the same story. The study was performed using a one story frame with multiple columns. Each column in that frame was assigned random transverse reinforcement ratio values such that it would correspond to a different V_p/V_n ratio values. Random realizations of each column transverse reinforcement characteristics were generated using Monte Carlo simulations. In the simulations the collapse performance of each one-story frame consisting of columns with different V_p/V_n ratios was evaluated using IDA. The results of Dr. Liel’s study demonstrated that story average of the column V_p/V_n ratio is a relatively good indicator of the response of frames.

5.5 LIMITATIONS OF THE STRENGTH-BASED APPROACH IN COLLAPSE EVALUATION

In the current chapter a methodology to evaluate the building collapse potential using simple engineering parameters was presented. The results of this study are limited to buildings possessing concrete moment frames to resist the earthquake loading. Buildings suffering from structural deficiencies other than those addressed in the current study (weak column mechanisms, shear critical columns) cannot be evaluated with the collapse evaluation approach presented in this Chapter. Although strength-based normalization parameters (R_e and M) were utilized to avoid comparison bias of buildings with different building strengths, the results of the current study should be applied with caution for buildings having very different strength and geometrical properties compared to the considered frames. Very tall buildings (taller than 12 stories) that are significantly influenced by higher mode effects or buildings suffering from severe vertical and plan irregularities were not considered in the current study.

6 A Displacement-Based Methodology to Evaluate the Collapse Potential of Older-Type Concrete Frame Buildings

In Chapter 5, a method to estimate the collapse potential of older-type concrete buildings was presented. Due to the inability to evaluate all possible building variations, the normalization factors R_e and M were utilized. Both normalization factors were defined such that seismic demand was normalized with respect to base shear strength. This normalization was employed such that it would reduce a potential comparison bias between buildings with similar geometry but different building strength. According to the methodology presented in Chapter 5 the probability of collapse of a certain building, possessing certain collapse indicator parameters is estimated based on its base shear strength and the earthquake intensity. In other words for the same building geometry, structural parameters ($\Sigma M_{nc}/\Sigma M_{nb}$ and V_p/V_n) and earthquake intensity, higher strength would lead to lower R_e (and M) and thus to lower probability of collapse. Although the approach presented in the previous Chapter seems to provide rational results, it suffers from one main disadvantage. According to the IDA procedure used to evaluate building collapse potential, the performance of a building is judged according to member deformations or story displacements. Thereby it is more intuitive to develop a methodology in which, for certain earthquake intensity, a parameter based on displacement rather than based on strength (like R_e or M) would influence the building collapse potential.

In the current Chapter an alternative approach using a displacement based method to evaluate building collapse is proposed. Initially, a procedure to estimate story drift ratio demand is presented given the dynamic properties of the considered building and the earthquake intensity level. The IDA results of the three idealized buildings presented in Chapter 4 are used to calibrate the parameters employed for calculation of story drift ratio demands. Consequently the estimated story drift ratio demand is shown that can be related to column drift capacity to estimate column failure potential. Finally, a simplified method that links column failure potential with building collapse performance, using only hand-calculations, is presented.

6.1 DETERMINATION OF STORY DRIFT RATIO DEMAND

A basic issue related with the collapse performance of structural systems is the determination of story drift ratio demand. In the current section the idealized buildings developed in Chapter 4 will be used to get insight on how story drift ratio demand can be estimated for variations of the idealized buildings considered in the current study using a simplified approach.

6.1.1 Estimating Maximum Displacement at the Effective Height of the Building

The first step in estimating the story drift ratio demand is estimating displacement at a certain height of the building for certain earthquake intensity.

To avoid suggesting a new relationship to estimate building displacement, the current study utilizes Equation 6.1 from ASCE-41 to determine the displacement at the roof building height. Since Equation 6.1 requires eigenvalue analysis in order to determine C_0 , it was considered more convenient to use Equation 6.1 to estimate the displacement at the floor level corresponding to the effective height of the equivalent single degree of freedom oscillator instead. For that floor level C_0 can be assumed to be approximately equal to 1.0 without significant error.

$$\delta_{eff} = C_0 * C_1 * C_2 * S_a * \frac{T_1^2}{4\pi^2} \quad (\text{Eq. 6.1})$$

, where, S_a is the spectral acceleration at the fundamental period of the building T_1 , and g is the gravitational acceleration.

Coefficients C_0 , C_1 , and C_2 modify the spectral displacement to estimate the displacement at effective building height considering various effects, as follows:

- Coefficient C_0 - Modification factor to relate spectral displacement of an equivalent SDOF system to the displacement at the effective height of the building MDOF system. To calculate the C_0 coefficient value the first mode mass participation factor should be multiplied by the ordinate of the first mode shape at the effective height. To avoid performing eigenvalue analysis the coefficient C_0 could be, approximately, assumed to be equal to unity.
- Coefficient C_1 – Modification factor to relate expected maximum inelastic displacements to displacements calculated for linear elastic response

$$C_1 = 1 + \frac{\mu_{strength} - 1}{aT_e^2} \quad (\text{Eq. 6.2})$$

Where, the parameter a is the site class factor and $\mu_{strength}$ is the ratio of elastic strength demand to yield strength coefficient.

For periods less than 0.2 sec, C_1 need not be taken greater than the value at $T=0.2$ seconds. For periods greater than 1.0 second, $C_1=1.0$

- Coefficient C_2 – modification factor to represent the effect of pinched hysteresis shape, cyclic stiffness degradation, and strength deterioration on maximum displacement response

$$C_2 = 1 + \frac{1}{800} \left(\frac{\mu_{strength} - 1}{T_{G.F.}} \right)^2 \quad (\text{Eq. 6.3})$$

For periods greater than 0.7 sec, $C_2=1.0$

(The interested reader can find further information regarding the procedure followed in section 6.3.2 in Chapter 7 of ASCE-41)

The coefficients C_0 , C_1 and C_2 employed in Equation 6.1 for the idealized buildings considered in the current study are presented in the Table 6.1 cited below:

Table 6.1 Coefficients of the studied buildings utilized in equation 6.1

	Building		
	4-Story	8-Story	12-Story
T1 (sec)	1.14	1.62	1.95
C0	1.05	1.09	1.08
C1	1.00	1.00	1.00
C2	1.00	1.00	1.00

6.1.1.1 Comparison of Estimated Floor Displacements and Non-Linear Response History Analysis

Equation 6.1 provides an estimate of maximum displacement at the effective modal height floor level for a given spectral acceleration value. In order to verify the validity of the provided equation, statistical processing of the results obtained through IDA was performed for variations of the idealized buildings.

The studied cases included buildings with components whose failure was flexural, shear or axially dominated.

The results of the comparison are presented in the tables below:

Table 6.2 Mean ratio of (maximum displacement at effective modal height floor level of non-linear analysis) / (estimated displacement at effective modal height floor level of equation 6.1) for different V_p/V_n and $\Sigma M_{nc}/\Sigma M_{nb}$ ratios of the 4-Story Idealized Building

$\Sigma M_{nc}/\Sigma M_{nb}$	V_p/V_n			
	0.6	0.8	1.0	1.2
0.6	0.88	0.80	0.82	0.91
0.8	0.88	0.80	0.82	0.91
1.0	0.87	0.81	0.81	0.90
1.2	0.92	0.82	0.83	0.85
1.4	0.99	0.85	0.85	0.84
1.6	1.12	0.91	0.86	0.85
1.8	1.17	0.94	0.91	0.87

Table 6.3 Mean ratio of (maximum displacement at effective modal height floor level of non-linear analysis) / (estimated displacement at effective modal height floor level of equation 6.1) for different V_p/V_n and $\Sigma M_{nc}/\Sigma M_{nb}$ ratios of the 8-Story Idealized Building

$\Sigma M_{nc}/\Sigma M_{nb}$	V_p/V_n			
	0.6	0.8	1.0	1.2
0.6	0.84	0.84	0.85	0.94
0.8	0.84	0.83	0.85	0.92
1.0	0.84	0.83	0.84	0.91
1.2	0.87	0.82	0.81	0.83
1.4	1.01	0.90	0.87	0.86
1.6	1.12	0.97	0.93	0.91
1.8	1.23	1.01	0.98	0.96

Table 6.4 Mean ratio of (maximum displacement at effective modal height floor level of non-linear analysis) / (estimated displacement at effective modal height floor level of equation 6.1) for different V_p/V_n and $\Sigma M_{nc}/\Sigma M_{nb}$ ratios of the 12-Story Idealized Building

$\Sigma M_{nc}/\Sigma M_{nb}$	V_p/V_n			
	0.6	0.8	1.0	1.2
0.6	0.95	0.96	0.97	0.99
0.8	0.94	0.96	0.97	1.00
1.0	0.94	0.94	0.96	0.96
1.2	0.99	0.96	0.93	0.90
1.4	1.25	1.10	1.02	0.96
1.6	1.42	1.18	1.10	1.05
1.8	1.46	1.24	1.16	1.12

Tables 6.2-6.4 demonstrate that for most of the cases equation 6.1 provides a conservative estimate of the maximum displacement at the effective modal height. The accuracy of the displacement estimation at the effective modal height floor level improves as the ratio of column to beam moment strength increases.

Since the modal period of the studied buildings is relatively high, the equal displacement rule (Chopra 2011) should hold approximately. In Equation 6.1 factors C_1 and C_2 are assumed to be equal to unity, in accordance with the fact that maximum floor displacements are expected to be overall independent of the base shear strength of the building.

In order to verify the assumption that the estimated displacement provided by Equation 6.1 is not influenced by the building strength, the displacements at the effective building height obtained from IDA for different values of $R_e = S_a * W_{building} / V_{max}$ were compared with those estimated by Equation 6.1. In Figure 6.1 the aforementioned comparison is performed for the 8-story idealized building. In Figure 6.1 each point corresponds to a scaled ground motion non-linear analysis result which was used for IDA.

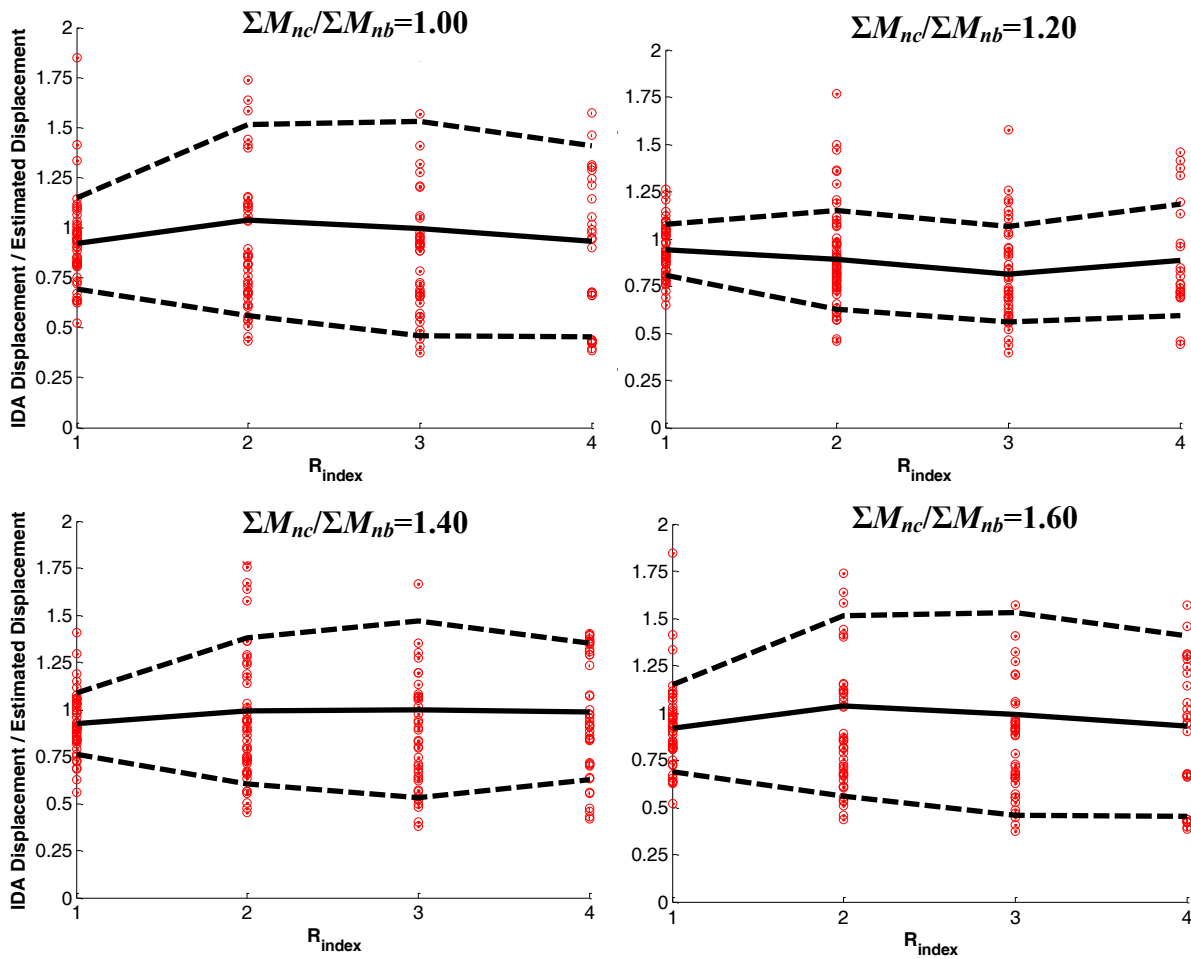


Figure 6.1 Ratio of (maximum displacement at effective modal height of non-linear analysis (IDA)) / (estimated displacement at effective modal height of equation 6.1) for different R indices of the 8-Story building ($V_p/V_n=0.6$)

Figure 6.1 confirms that variation in building strength does not influence significantly the accuracy of Equation 6.1. The mean value of the ratio between the displacements obtained from non-linear dynamic analyses to the displacements estimated by Equation 6.1 seems to form approximately a flat line in the figure above. This means that the estimated displacement is independent of R_e and thus of the building strength, so C_1 and C_2 were correctly assumed to be equal to unity in Equation 6.1.

6.1.2 Estimating Maximum Story Drift

After having estimated the maximum displacement at the floor corresponding to the effective height of the building according to the procedure explained in Section 6.1.1, story drift ratio

demand needs to be estimated for each story. Figure 6.2 illustrates the general concept. That figure demonstrates the drift profile of two extreme cases:

- Uniform story drift pattern which would ideally apply for a building with very high column-to-beam moment strength ratio, and
- Weak story drift pattern which would ideally apply for the case of building in which the first story has very low column-to-beam moment strength ratios.

(It is recognized that both these patterns correspond to extreme cases that would rarely appear in an existing building but are provided for the purpose of illustrating the presented concept.)

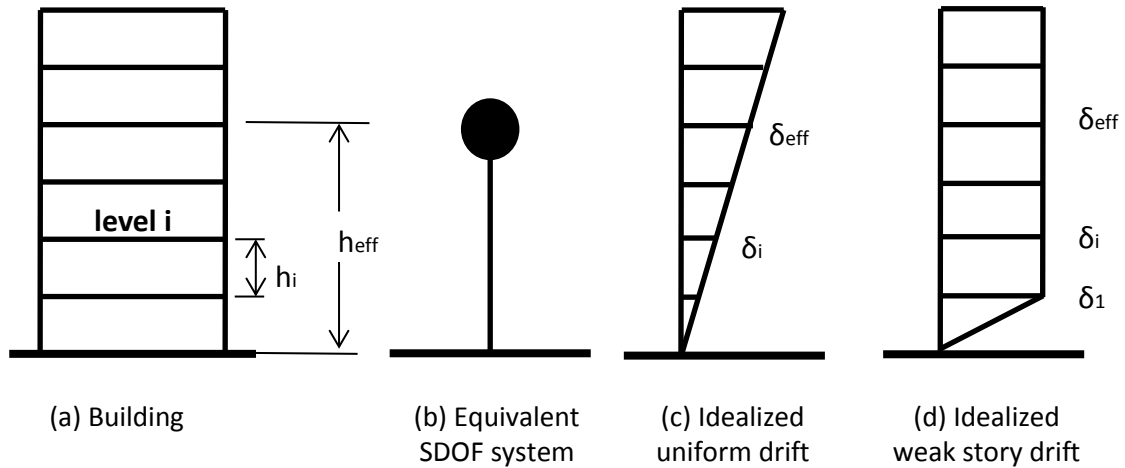


Figure 6.2 Two idealized story drift patterns for an example building frame

From the example of the two idealized story drift patterns presented above, it becomes obvious that the story drift profile depends largely on the column-to-beam bending moment ratio. In the current study the variable “alpha” (α), is used to estimate the maximum story drift demand as shown in Equation 6.4.

$$\overline{\Delta_{Dx}} = \frac{\delta_x}{h_x} = \alpha_x * \frac{\delta_{eff}}{h_{eff}} \quad (\text{Eq. 6.4})$$

where, δ_x is the story drift demand, h_x is the story height, α_x is the coefficient for story x used to approximate the expected story drift pattern, δ_{eff} is the estimated displacement at the effective height according to Equation 6.1, h_{eff} is the effective building height (it can be assumed that $h_{eff} \approx 0.7 * h_{building}$, where $h_{building}$ is the total building height). In Equation 6.4, α_x is used as an amplification factor of the estimated average drift ratio (δ_{eff}/h_{eff}) at the effective height of the building to the maximum story drift ratio demand ($\overline{\Delta_{Dx}} = \delta_x/h_x$) at story x . For the idealized uniform story drift pattern $\alpha_x=1.0$ for all stories while for the idealized weak story drift pattern $\alpha_1=h_{eff}/h_1$ and $\alpha_{x \neq 1}=0.0$.

6.1.2.1 Determination of Coefficient α

The coefficient α , was calibrated to match approximately the dynamic response of the idealized buildings considered in this study. It should be noted that these buildings were designed such that they possess uniform structural parameters V_p/V_n and $\Sigma M_{nc}/\Sigma M_{nb}$. Using results obtained from numerous non-linear dynamic analysis performed as part of the IDA procedure discussed in Chapter 4, the values of coefficient α were recorded for ground motion scaling factors slightly less than the factor required to achieve collapse. Statistical regression was performed between the estimated average drift ratio at the effective building height $\delta_{\text{eff}}/h_{\text{eff}}$ (predictor) and the maximum story drift ratio demand δ_x/h_x (response variable). The procedure was repeated for each story according to Equation 6.4. The coefficient α_x was chosen such that the sum of the square errors of Equation 6.4 to the data is minimized. Further information regarding the statistical procedure performed to estimate coefficient α_x is provided in Appendix G.

- ***Buildings with Uniform DCRs***

As discussed in Chapter 4 the idealized buildings developed for the purpose of this study have approximately uniform Demand over Capacity Ratio (DCR) (see Appendix D).

Figures 6.3-6.5 show the least square estimates of the coefficient α_x values for different variations of the idealized buildings which are representative of buildings that tend to have uniform strength characteristics and do not possess any significant strength deficiencies along the height.

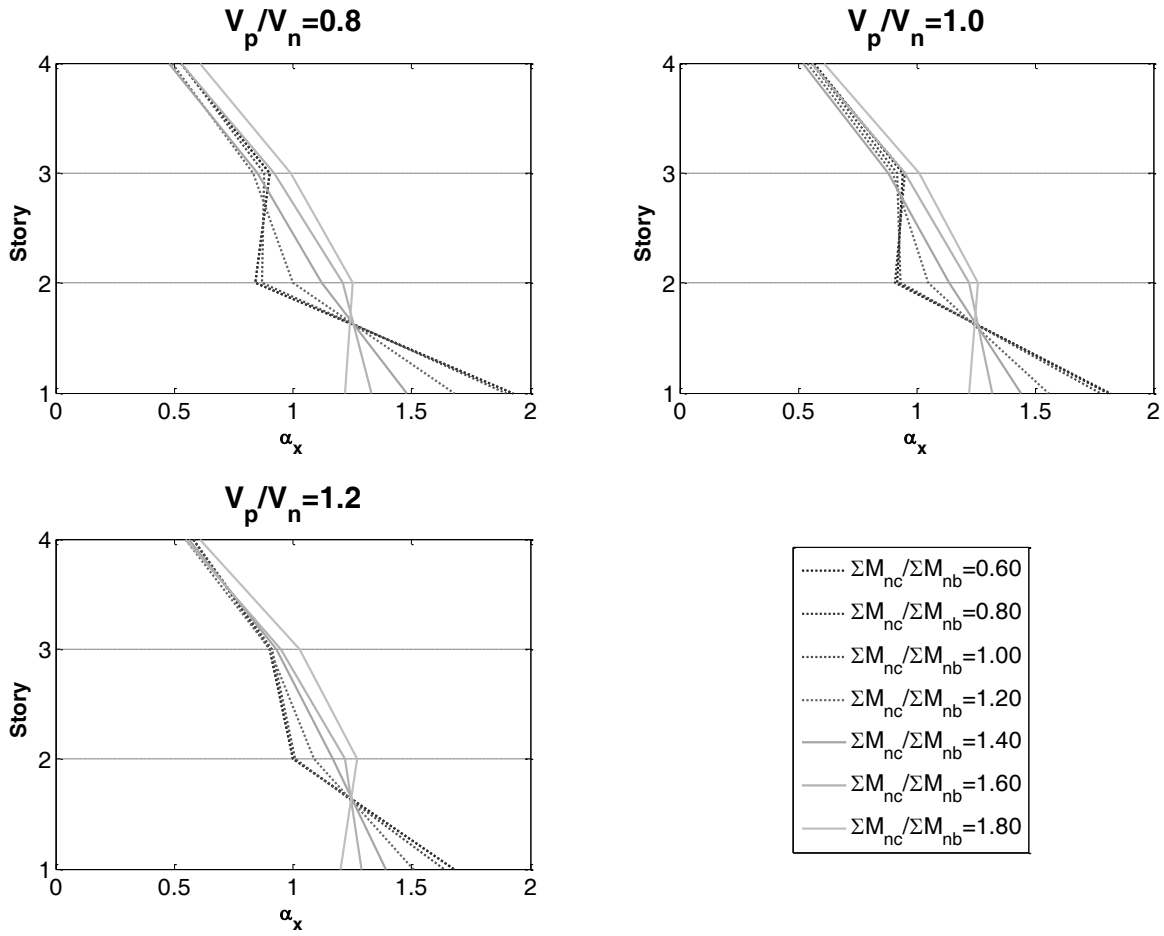


Figure 6.3-a Alpha coefficient story profiles for different variations of the 4-story idealized buildings

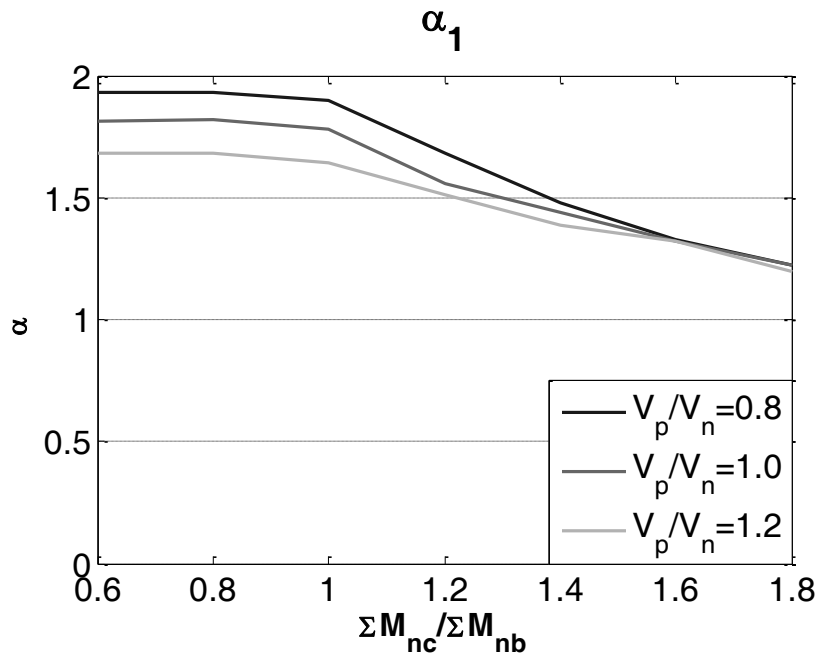


Figure 6.3-b Alpha coefficient value at the 1st story for different variations of the 4-story idealized building

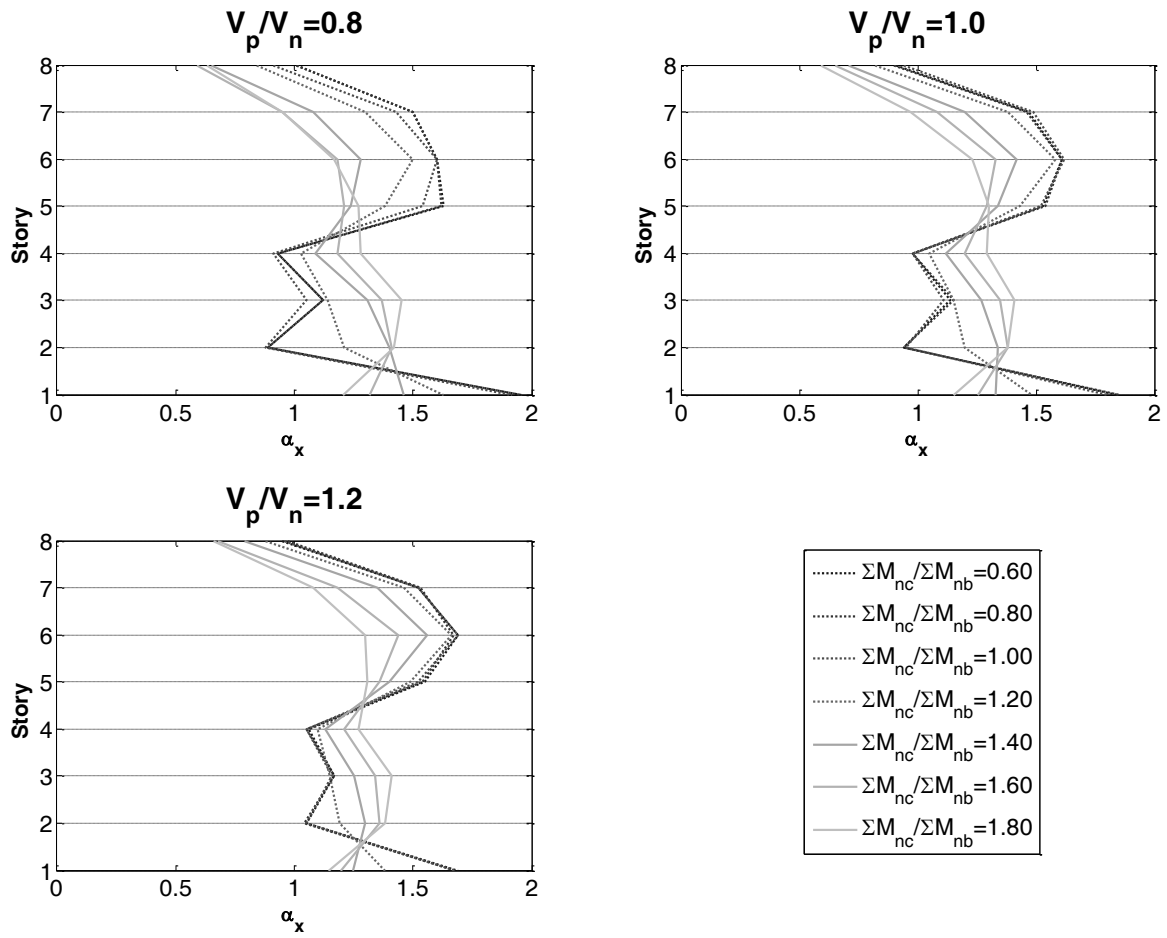


Figure 6.4-a Alpha coefficient story profiles for different variations of the 8-story idealized buildings

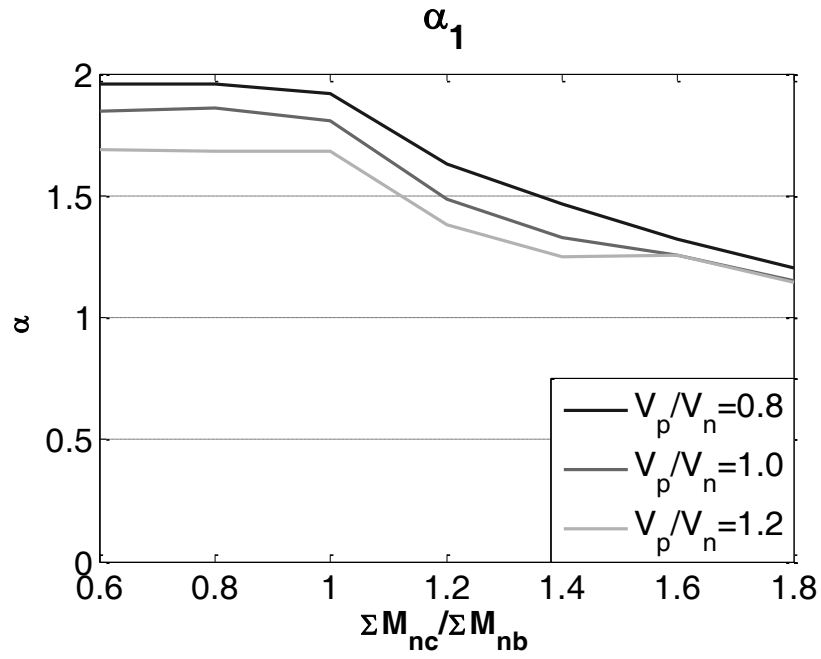


Figure 6.4-b Alpha factor coefficient at the 1st story for different variations of the 8-story idealized building

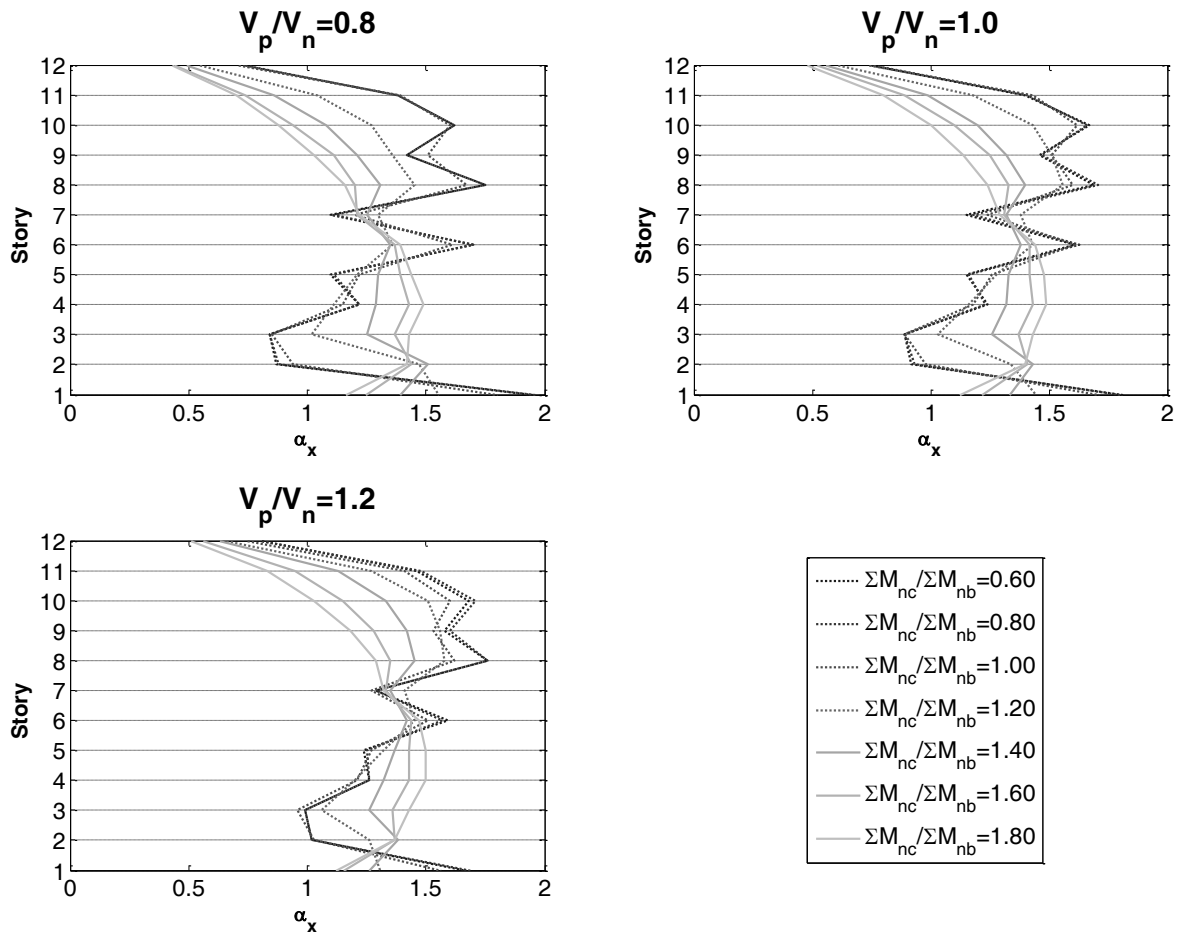


Figure 6.5-a Alpha coefficient story profiles for different variations of the 12-story idealized buildings

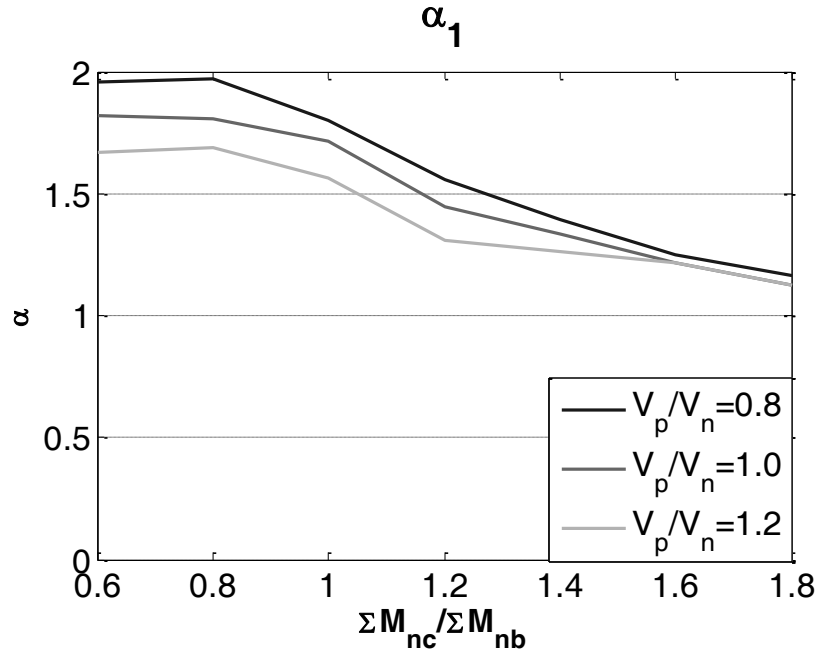


Figure 6.5-b Alpha factor coefficient at the 1st story for different variations of the 12-story idealized building

Figures 6.3 to 6.5 demonstrate that α_x is mainly influenced by the $\Sigma M_{nc}/\Sigma M_{nb}$ ratio, and is less dependent on the V_p/V_n ratio.

A detailed presentation of the α_x values obtained for variations of the idealized buildings is presented in Appendix G.

- **Buildings with Non-Uniform DCRs**

As observed in Figures 6.3 to 6.5 the values of coefficient α_x vary along the height of the building. Intuition suggests that α_x should have higher values at the story x of the building that is the “weakest” (the term weak here corresponds to shear strength capacity of the structural components and is not related with their deformation characteristics). One way to identify the weakest story is by looking at the DCRs of the stories for the considered building. According to this procedure the story that has significantly higher DCR than the rest of the stories can be characterized as the weakest.

In this section, the 8-story building was selected to demonstrate how possessing a weak story at the mid-height could alter the story drift profiles.

Figure 6.6 illustrates the alpha story profile values for variations of the 8-story building with a critical story at the mid-height (critical 4th story).

The critical 4th story building corresponds to a variation of the originally developed idealized 8-story building. For the latter, the columns at the 4th story of the idealized 8-story building were modified such that $DCR_{4th}=1.30*DCR_{1st}$ (critical 4th story). This variation of the 8-story building

is compared with the response of the originally developed idealized building which possesses approximately uniform DCRs along the height.

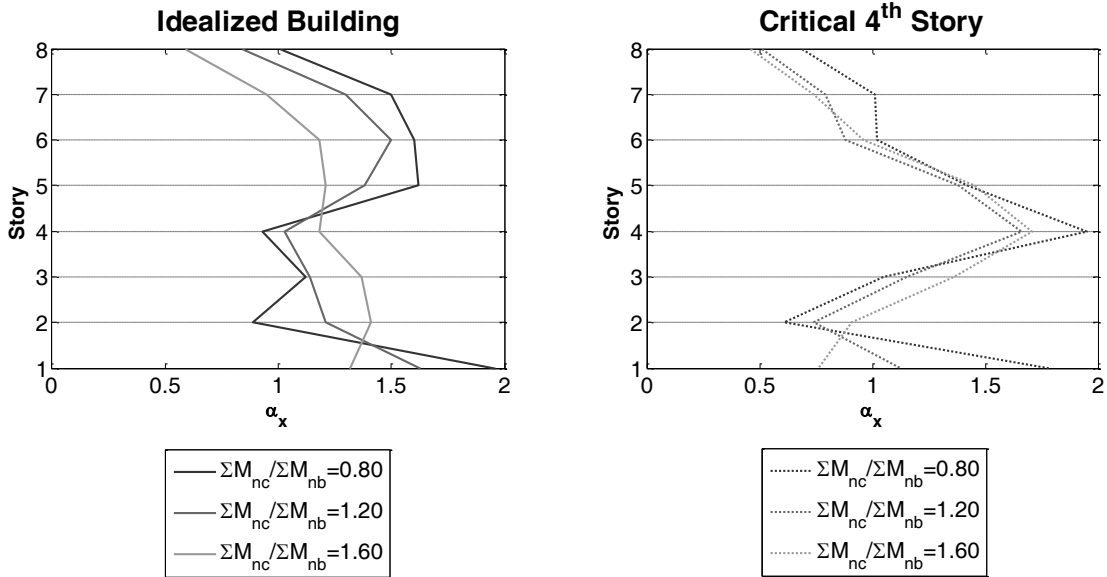


Figure 6.6-a Comparison of the alpha coefficient story profiles for the 8-story with uniform DCRs (idealized building) and with critical story at the mid-height ($V_p/V_n=0.8$ for both cases) (for the critical 4th story case $DCR_{4th}=1.30DCR_{1st}$)

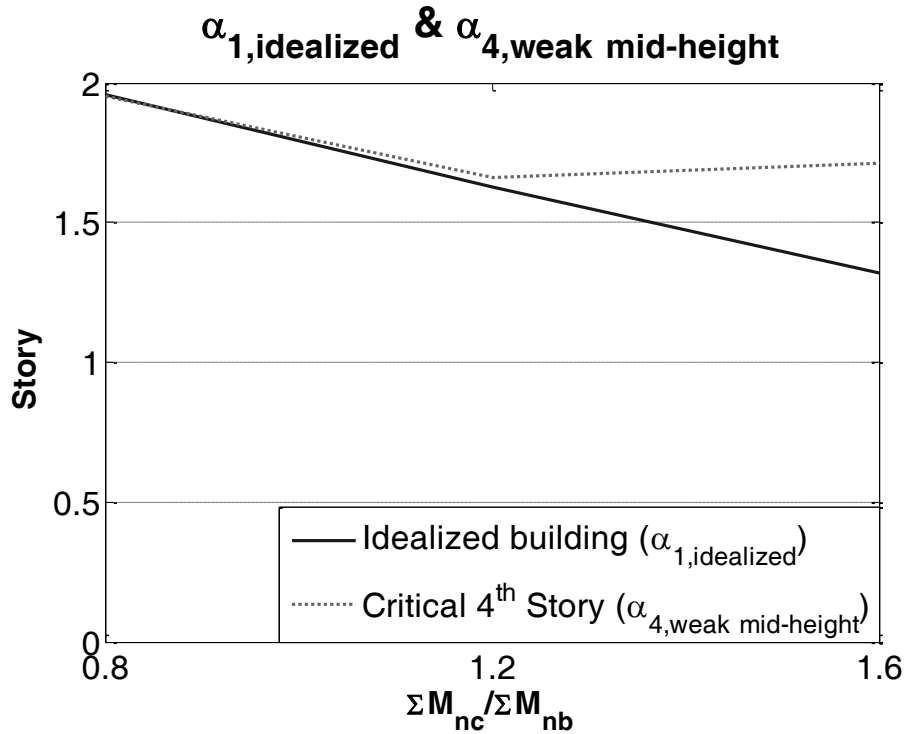


Figure 6.6-b Comparison of the alpha coefficient values at the critical story for the 8-story with uniform DCRs (idealized building) and with critical story at the mid-height ($V_p/V_n=0.8$ for both cases) (for the critical 4th story case $DCR_{4th}=1.30DCR_{1st}$)

When $\Sigma M_{nc} / \Sigma M_{nb} < 1.20$, as demonstrated in Chapter 5, the building has the tendency to form weak stories. A significant strength weakness as shown in Figures 6.6-a,b does not seem to influence particularly the alpha value of the critical story since $\alpha_{4,weak\ mid-height} \approx \alpha_{1,idealized}$. However, for the case of $\Sigma M_{nc} / \Sigma M_{nb} > 1.20$, the building tends to distribute damage along the height of the building more uniformly. The results demonstrate that if the building possesses a significant strength weakness at the mid-height, the building continues to form story mechanisms in that particularly weak story instead of distributing damage to more than one stories as observed in the idealized building with uniform DCRs. Thus we can conclude that for the considered cases increasing the column to beam moment ratio is not that effective in uniform damage distribution and thus $\alpha_{4,weak\ mid-height} > \alpha_{1,idealized}$.

The interested reader can find the tables of the α_x coefficient values corresponding to the idealized buildings with critical stories at the mid-height in Appendix G.

- ***Buildings with column bars having inadequate lap splicing conditions***

For the case of buildings having inadequate lap splice length for column longitudinal reinforcement, with insufficient column confinement, as defined by ACI 318-11 (ACI, 2011), bar slip and eventual failure of the lap splices might occur. Associated damage is likely to result in rapid loss of moment resistance at the location of the lap splice.

To study the effects of this behavior on overall building response, a strength-degrading plastic hinge was introduced at assumed locations of lap splices in the model buildings. The inadequate lap splicing conditions were modeled according to the experimental results provided by Melek and Wallace (2004). The backbone rotational behavior of the plastic hinges to model the inadequate lap splicing conditions is shown in Figure 6.7.

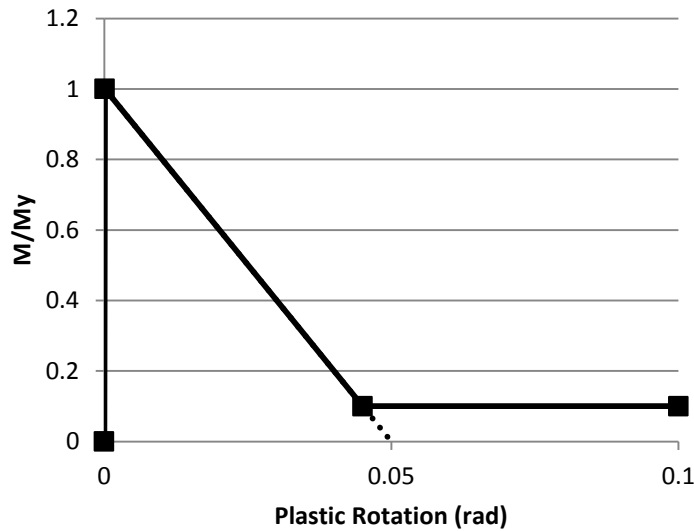


Figure 6.7 Assumed zero-length plastic hinge rotational behavior for inadequate lap-splicing conditions

Nonlinear dynamic analyses were conducted on model frames with flexure-critical columns ($V_p/V_n=0.8$) including lap splices. Frames with different $\Sigma M_{nc}/\Sigma M_{nb}$ ranging from 0.8 to 1.6 were investigated. Figure 6.8 illustrates representative results for the case of lap splices introduced into the base of the column members located in the 1st story of the 8-story frame.

The results demonstrate that, for the case of buildings with a tendency to form weak stories (that is, $\Sigma M_{nc}/\Sigma M_{nb} \leq 1.20$), the lap-splice has minimal effect, while the effect is slightly more pronounced for cases where the building has a tendency to form a more uniform drift profile (that is, $\Sigma M_{nc}/\Sigma M_{nb} > 1.20$). Apparently, the former case corresponds to a case for which a weak story is already formed because of the weak columns, such that further reduction in strength due to splice failure does not significantly exacerbate the story failure. For the latter case, the presence of the lap splice results in reduced moment strength at one end of the column if the column yields, which tends to produce a weak-story condition. However, because the columns

are stronger than the beams, the extent of column yielding is reduced, such that the alpha factor again is not much affected.

Due to the relatively small effect of lap splicing in the α_x values of the considered cases, for the purposes of the current study, the α_x coefficient values can be approximately assumed to be the same for both adequate and inadequate lap splicing conditions.

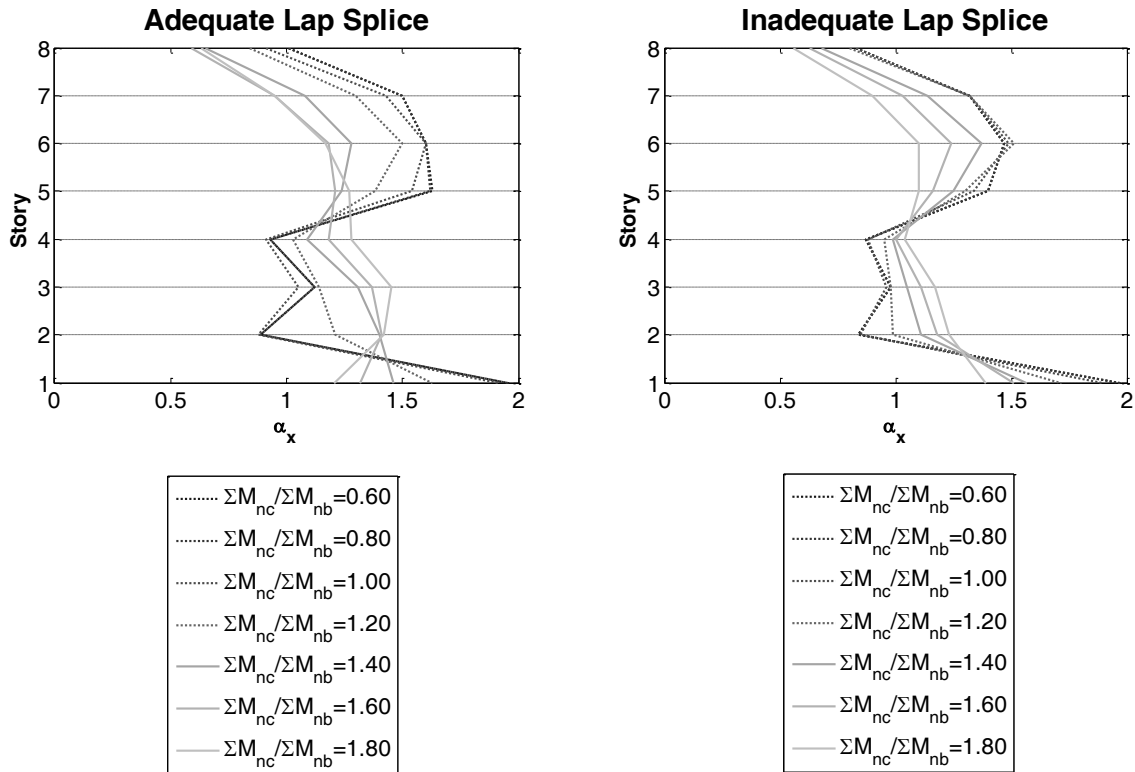


Figure 6.8-a Comparison of the alpha coefficient story profiles for different variation of the 8-story idealized building with adequate and inadequate lap splicing conditions at the base of the 1st story ($V_p/V_n=0.8$ for both cases)

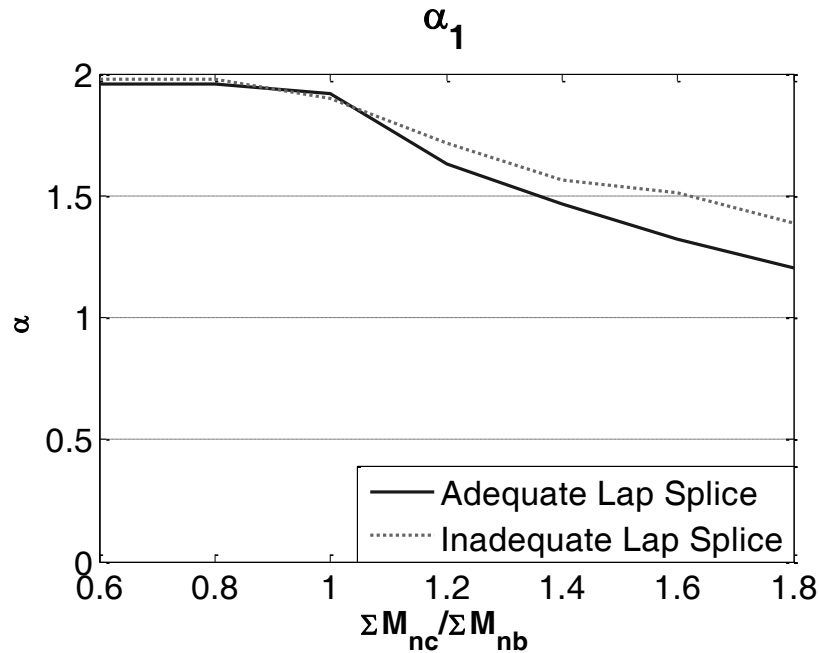


Figure 6.8-b Comparison of the alpha coefficient value at the critical 1st story for different variations of the 8-story idealized building with adequate and inadequate lap splicing conditions at the base of the 1st story ($V_p/V_n=0.8$ for both cases)

The suggestions regarding the lap-splicing conditions were based on limited studies performed on the idealized buildings considered in the current study. Further study needs to be conducted in the future in order to provide more general suggestions regarding the assessment of buildings with such deficiencies.

The interested reader can find the results of the analyses performed to obtain the effect of inadequate column bar lap splicing in Appendix G.

6.2 DETERMINATION OF COLUMN DRIFT CAPACITY

In the previous section a procedure to estimate the story drift ratio demand was presented. In the current section it is attempted to define a similar procedure to estimate the column drift capacity.

- ***Shear Critical Column Members***

For shear critical columns possessing $0.7 \leq V_p/V_n \leq 1.2$ column drift capacity can be determined according to Equation 6.5 as suggested by Elwood (2002).

$$\overline{\Delta_{Cx}} = 0.03 + 4 * \rho'' - (1/500) * \frac{v}{\sqrt{f'_c}} - \left(\frac{1}{40}\right) * \frac{P}{A_g * f'_c} \quad (\text{Eq. 6.5})$$

where ρ'' is the column transverse reinforcement ratio, v is the applied shear stress (provided in psi units), f'_c is the expected concrete stress (provided in psi units), P is the column axial load (provided in lb units), A_g the column gross sectional area (provided in in² units).

- ***Columns having Inadequate Lap Splicing Conditions***

Columns having longitudinal bars with inadequate lap splicing conditions are expected to start degrading at or before they reach their shear yielding capacity (corresponding to flexural yielding at the column ends). Thus, Equation 6.6 corresponds to a relatively conservative estimate of their drift capacity. Further study is required to develop less conservative capacity relationships.

$$\overline{\Delta_{Cx}} = \frac{M_{y, \text{bottom}}}{6 * E * I_{\text{eff}} / h_x} + 0.01 \quad (\text{Eq. 6.6})$$

where $M_{y, \text{bottom}}$ corresponds to the yielding moment at the base of the column, E is the concrete Young's modulus, I_{eff} is the effective stiffness, and h_x is story x height.

The column drift capacity that was assigned for such columns was approximated so that it corresponds to total column rotation where the column has degraded to moment equal to 80% of the maximum observed moment (80% of the yielding moment in that case). The relationship providing the column drift capacity is given in Equation 6.6 and is computed such that it is consistent with the modeling assumptions of inadequate lap splicing for longitudinal column reinforcement followed in the current study.

6.3 A METHODOLOGY TO ESTIMATE THE COLUMN FAILURE POTENTIAL

In sections 6.2 and 6.3 procedures to estimate story drift demand and column drift capacity were defined. Since the same quantity, drift, was used to describe both demand and capacity a direct comparison between the two is possible. This comparison could provide an estimate of whether an individual column member located in story x is likely to fail.

In the current section, a method to evaluate column failure potential is presented. The method is based on the results presented above. Sections 6.1 and 6.2 are revisited and estimation of story drift demand and column drift capacity is presented using a simplified approach that requires only hand-calculations.

6.3.1 Estimating Column Drift Demand using only Hand Calculations

In similar fashion with Chapter 5, basic information that can be easily found after review of the structural drawings or estimated using simple hand calculations are employed as the basic input parameters to estimate column drift demand at story x .

The basic input parameters required correspond to the geometry of the structural system, member dimensions, and reinforcement details.

The structural parameters that were linked with the collapse performance of the considered buildings in this study were the following:

- a) The column-to-beam bending moment strength ratio,
- b) The shear demand over shear capacity ratio
- c) Determination of potential column bar inadequate lap splice conditions

To apply the procedure described in Section 6.1, a certain earthquake intensity level needs to be provided. The earthquake intensity is given as Spectral Acceleration $Sa(T_1)$ at the first fundamental period of the building. To estimate the fundamental period of the building an engineer has two options:

- a) Perform eigenvalue analysis for the considered building
- b) Apply Equation 6.7 to estimate T_1 . The latter equation was derived specifically for the purposes of the current study based on statistical regression of concrete frame buildings. The interested reader can find more details regarding the procedure followed to derive Equation 6.7 in Appendix F.

$$T_{G.F.} = 0.072 * H^{0.39} * \left(\frac{V}{W}\right)^{-0.69} \quad (\text{Eq. 6.7})$$

where W is the weight of the building, V is the estimated base shear capacity (should be estimated according to the procedure presented in Appendix E for $V_{\max, \text{estimated}}$) (V and W should be provided in the same units), and H is the height of the building given in feet.

After all the structural parameters of the building have been calculated, the procedure presented in Section 6.1 can be followed to estimate the average drift ratio $\delta_{\text{eff}}/h_{\text{eff}}$.

Using the results of statistical regression presented in section 6.1, the values of α_x presented in Table 6.5 were selected to, approximately, represent the story drift patterns observed in the previous figure for different building variations. It should be noted that the alpha values in Table 6.5 were selected such that they would systematically provide conservative estimates of story drift ratio demands.

Table 6.5 Values of α_x for buildings with 1st Story Critical

Number of stories	$\Sigma M_{nc}/\Sigma M_{nb}$	α_1	$\alpha_{x \neq 1}$
≤ 6	≤ 1.2	2.0	$1 - 0.5 \frac{i-2}{n-2}$ ⁵
	<i>Interpolate</i>		
	≥ 1.4	1.5	$1.50 - 0.5 \frac{i-1}{n-1}$
7-8	≤ 1.2	2.0	1.50
	<i>Interpolate</i>		
	≥ 1.4	1.5	$1.50 - 0.5 \frac{i-1}{n-1}$
≥ 9	≤ 1.2	2.0	1.5
	<i>Interpolate</i>		
	≥ 1.4	1.5	$1.50 - 0.5 \frac{i-1}{n-1}$

Using the value α_x suggested in Table 6.5 the story drift ratio demand $\overline{\Delta_{Dx}}$ can be estimated for each story according to Equation 6.4.

⁵ i:examined story for which α value is defined n:total number of stories of the studied building , for a building with n=2, $\alpha_2=1.0$, for a building with n=1 $\alpha_1=1.0$

6.3.1.1 Uncertainty in Estimation of Column Drift Demand

As discussed in Section 6.1, statistical regression using the results from a number of non-linear dynamic analyses was performed to estimate story drift ratio demands for the studied buildings. For simplification purposes, α_x values suggested in Table 6.5 are only a function of the column-to-beam moment strength ratio. In reality the relation between the average drift and the story drift demand is influenced by various factors not considered in the simple regression model employed for the purposes of the current study. Among others, these factors include, earthquake characteristics, building geometry, and building dynamic properties. The source of uncertainty that is observed in the column drift demand is both epistemic (use of a simplified regression formula not representing all the influential factors that determine the story drift patterns) and aleatory (record-to-record variability).

The uncertainty in the estimation of story drift ratio demand ranges from 0.10 to 0.70 (see Appendix G). On the basis of these data, the approximate values of standard deviation reported in Table 6.6 are suggested for application in the suggested methodology.

Table 6.6 **Uncertainty in predictions of drift demand**

Number of stories	$\sigma_{ln,\Delta D1}$	$\sigma_{ln,\Delta D_{x \neq 1}}$
≤ 6	0.40	0.40
7-8	<i>interpolate values</i>	
≥ 9	0.50	0.50

6.3.2 Estimating Column Drift Capacity

Information from the building drawings regarding the detailing characteristics of individual column members could be utilized to estimate column drift capacity according to the procedure described in Section 6.2. Two basic terms need to be estimated in order to evaluate Equation 6.7.

- The applied shear stress at the studied column (v) could be estimated as $v = V_{pCx}/A_g$, where V_{pCx} is the column shear force that can be estimated according to the procedure described in Appendix D while A_g is the column gross sectional area.
- The axial load taken by the studied column at story x (P). In the methodology suggested in this chapter, the axial load is calculated using the expected gravity load according to the tributary area that corresponds to each column. The expected gravity load is estimated according to the un-factored dead load plus 25% of the live load as proposed by Ellinwood (1980).

Due to overturning effects, the axial load at corner columns will be different significantly than the one estimated by the procedure described above. Since the exact value of axial load due to seismic overturning is difficult to determine without sophisticated dynamic analyses, this chapter presents a simplified methodology to determine the effect of overturning in the corner columns.

In this study P_{eq} will be denoted as the extra axial load due to seismic overturning. P_{eq} will be assumed to be equal to zero for all interior frame columns. Equation 6.8 will be used to take into account approximately overturning effects in corner columns:

$$P_{eq,x} = \frac{V_{p1} * (h_{eff} - h_{floor,x})}{L_{frame}} \quad (\text{Eq. 6.8})$$

Where, V_{p1} is the 1st story (base) shear capacity, estimated according to the procedure described in Appendix D, h_{eff} is the effective floor height of the building assumed to be equal to $h_{eff}=0.70*h_{building}$ (where $h_{building}$ is the total building height), h_{floor} is the elevation height of the bottom floor of the story of interest, L_{frame} is the total frame length. The calculation of axial load is illustrated in Figure 6.9 below:

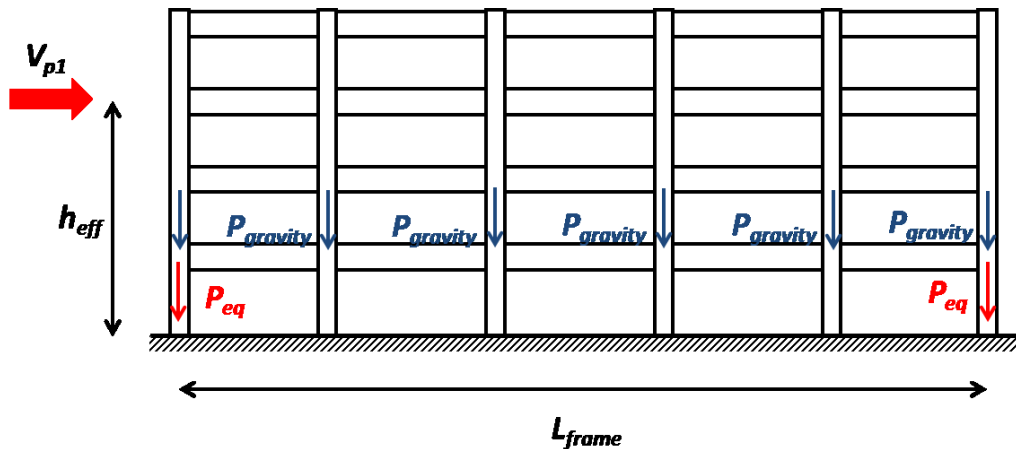


Figure 6.9 Illustration of the calculation of axial load for the critical 1st story of the 4-story idealized building

6.3.2.1 Uncertainty in Estimation of Column Drift Capacity

The proposed methodology used to evaluate the column failure potential does not incorporate column drift capacity (due to uncertainty in modeling or material properties) since it was not included in the analytical models used to calibrate the values presented above.

In case uncertainty in the column drift capacity needs to be incorporated, the method could be adjusted to include it as is shown in Section 6.3.3. Equation 6.5, used to determine the column drift capacity, was derived by Elwood (2002) based on linear statistical regression of an experimental database of 50 concrete columns failing in flexure-shear or direct shear mode. Elwood (2003) reported that the coefficient of variation between the measured drift ratio at shear failure and calculated drift ratio was C.V.=0.34. This value includes uncertainty in both the test data and in the empirical model (equation) predicting the test result. Dr. Liel and her colleagues (2014, ATC-78) suggest an alternative column drift capacity model that incorporates uncertainty in the column drift capacity as well. This alternative approach is discussed further in Chapter 2.

6.3.3 Estimating Column Failure Potential

Structural reliability methods could be utilized to determine the probability that the story drift demand exceeds the column drift capacity. The formulation presented in Equation 6.9 addresses the general case where both story drift demand $\overline{\Delta_{Dx}}$ and column drift capacity $\overline{\Delta_{Cx}}$ are treated as random variables.

$$Z_{Cx} = \frac{\overline{\Delta_{Cx}}}{\overline{\Delta_{Dx}}} \quad (\text{Eq. 6.9})$$

According to Equation 6.10, column “collapse” occurs if $Z_{Cx} \leq 1$.

Assuming that both column drift demand and column drift capacity are log-normally distributed and statistically independent, the reliability index, β_{Cx} , can be obtained from the Equation 6.10 or Equation 6.11 (Melchers, 1999).

$$\beta_{Cx} = \frac{\ln \left\{ \frac{\mu_{\Delta_{Cx}}}{\mu_{\Delta_{Dx}}} * \sqrt{\frac{(1 + \sigma_{\Delta_{Cx}}^2)}{(1 + \sigma_{\Delta_{Dx}}^2)}} \right\}}{\left\{ \ln \left[(1 + \sigma_{\Delta_{Cx}}^2) * (1 + \sigma_{\Delta_{Dx}}^2) \right] \right\}^2} \quad (\text{Eq. 6.10})$$

which is equivalent to,

$$\beta_{Cx} = \frac{\mu_{\ln, \Delta_{Cx}} - \mu_{\ln, \Delta_{Dx}}}{\sqrt{\sigma_{\ln, \Delta_{Cx}}^2 + \sigma_{\ln, \Delta_{Dx}}^2}} \quad (\text{Eq. 6.11})$$

where,

$\mu_{\Delta_{Cx}}$ is the mean column drift capacity for an individual column at story x

$\mu_{\Delta Dx}$ is the mean column drift demands for an individual column at story x

$\sigma_{\Delta Cx}$ is the standard deviation in column drift capacity for an individual column at story x

$\sigma_{\Delta Dx}$ is the standard deviation in column drift demand for an individual column at story x

$\mu_{\ln, \Delta Cx}$ is the mean of the natural logarithm column drift capacity for an individual column at story x

$\mu_{\ln, \Delta Dx}$ is the mean of the natural logarithm column drift demand for an individual column at story x

$\sigma_{\ln, \Delta Cx}$ is the standard deviation in the natural logarithm column drift capacity for an individual column at story x

$\sigma_{\ln, \Delta Dx}$ is the standard deviation in the natural logarithm column drift demand for an individual column at story x

Equation 6.11 can be modified for the purposes of the current study. Since uncertainty in the column drift capacity was not taken into account in the current study, $\sigma_{\ln, \Delta Cx} = 0$.

The probability of failure for an individual column at story x can be computed from the reliability index β_{Cx} according to Equation 6.12.

$$P_{\text{failure}, Cx} = \Phi(-\beta_{Cx}) \quad (\text{Eq. 6.12})$$

, where the operator Φ corresponds to the cumulative standard normal probability distribution.

6.4 EVALUATION OF THE STORY COLLAPSE POTENTIAL

Performing the procedure described in section 6.3 could provide useful information regarding the failure potential of individual column members of the studied building. To make use of these information a procedure to relate column failure potential to story collapse potential needs to be defined.

Buildings with columns having non-uniform structural characteristics would possess different values of $P_{\text{failure}, Cx}$ computed for each column at story x. As suggested by studies in Chapter 5, using the average value of parameters V_p/V_n or $\Sigma M_{nc}/\Sigma M_{nb}$ provides a relatively good approximation for calculation of the building probability of collapse.

Based on these findings the story collapse potential $P_{\text{collapse}, \text{story}, x}$ can be defined as the average $P_{\text{failure}, Cx}$ for all the individual columns located at the same story (Equation 6.13). Studies performed by Liel and her colleagues (ATC-78, 2014) based on Monte Carlo simulations in which random realizations of columns with different characteristics in a story were generated support this definition of story collapse potential if the $P_{\text{collapse}, Cx}$ between the columns of story x do not differ significantly (more than 25%).

$$P_{\text{collapse,story},x} = \frac{\sum_{i=1}^n P_{\text{failure,Cx},j}}{n} \quad (\text{Eq. 6.13})$$

, where n is the total number of columns located at story x.

6.5 EVALUATION OF THE BUILDING COLLAPSE POTENTIAL

Gathering information regarding the collapse potential for all the stories of the considered building could lead to conclusions regarding its overall collapse performance. There are multiple ways to evaluate the collapse performance of a building. According to the modeling approach followed in this study, collapse occurs when at least one of the stories fails (see Chapter 4 for definition of building collapse), thereby Equation 6.14 is employed to relate the story x collapse potential, $P_{\text{collapse,story},x}$, with the building collapse potential, $P_{\text{collapse,bldg}}$.

$$P_{\text{collapse,bldg}} = \max_{x=1}^j P_{\text{collapse,story},x} \quad (\text{Eq. 6.14})$$

, where j is the total number of stories of the studied building.

It becomes obvious that the methodology presented in Sections 6.3 to 6.5 contains numerous simplifications and assumptions. Chapter 7 attempts to verify that application of the suggested method for evaluation of collapse of the idealized buildings (that the method is calibrated from) would lead to accurate results compared to IDA. Further research that would apply the proposed evaluation method to real buildings needs to be performed to verify its validity.

7 Evaluation of the Displacement-Based Method for the Idealized Buildings

In the current chapter the three idealized buildings presented in Chapter 4 are evaluated using the displacement based method proposed in Chapter 6. The results of the simplified evaluation method that require only hand calculations are compared with those obtained from IDA described in Chapter 5. The comparison is performed in terms of probability of collapse of the considered building variations.

The results obtained from IDA are derived through sophisticated collapse modeling, using a large number of ground motion records. Thus, in the current chapter they will be assumed to be the “true” collapse potential values. The results suggest that the displacement-based method proposed is successful for identification of concrete frame buildings with structural characteristics similar to those considered in this study. This is a necessary characteristic of the method. Additional study should verify that the methodology also is successful at identifying high-risk buildings that are different from those from which it was derived.

7.1 EVALUATION OF THE COLLAPSE POTENTIAL FOR THE IDEALIZED BUILDINGS

The idealized 4, 8 and 12 story buildings developed in Chapter 4 are evaluated using the procedure described in Chapter 6. Six variations, for each of the idealized buildings are evaluated. The structural parameter values considered are:

- $\Sigma M_{nc}/\Sigma M_{nb}=1.00, 1.40$
- $V_p/V_n=0.8, 1.0, 1.2$

For the idealized 8-story building the following additional two variations are also evaluated:

- Inadequate column bar lap splicing conditions at the base of the 1st story (for $V_p/V_n=0.80$) with $\Sigma M_{nc}/\Sigma M_{nb}=1.00, 1.40$

The collapse evaluation is performed for three spectral acceleration levels. To determine the spectral acceleration values, the buildings are assumed to be located in Berkeley, California.

Using the Probabilistic Seismic Hazard Analysis suite provided by U.S. Geological Survey (USGS), the following uniform hazard spectra for the site are computed.

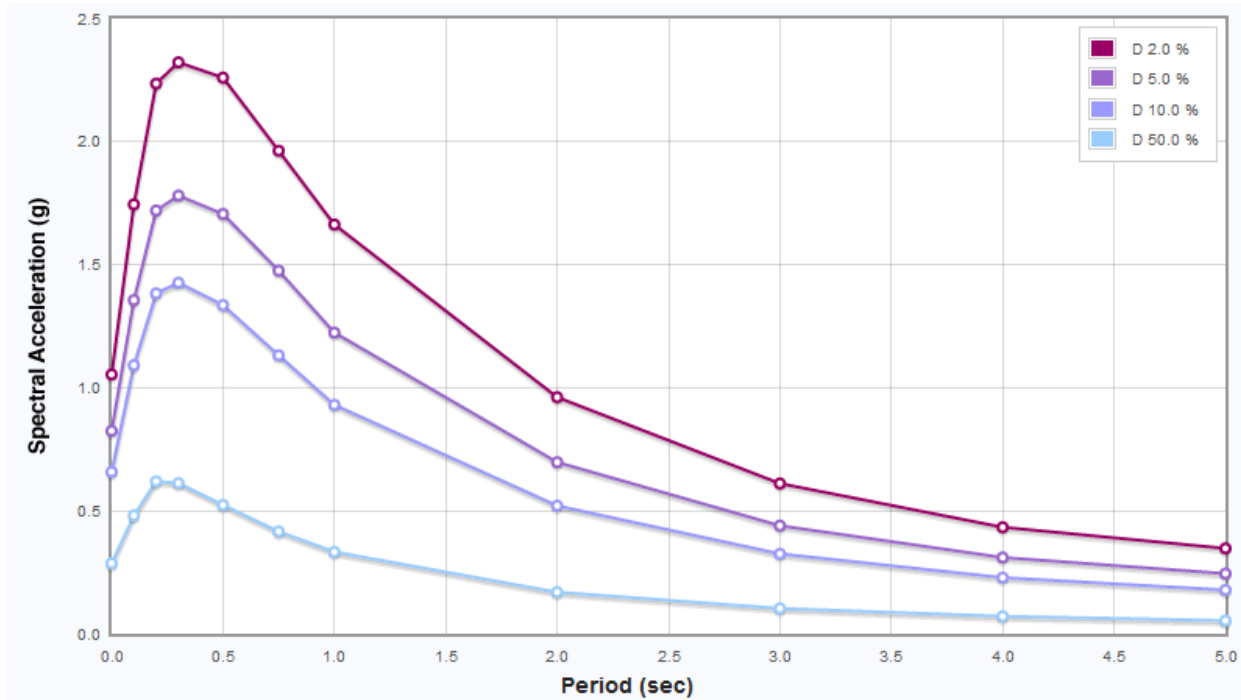


Figure 7.1 Uniform Hazard Spectra (UHS) for the idealized buildings located at Berkeley, CA (Site Class D)

Consistent with the damping ratio values assumed for the analyses performed in the current study, the spectra corresponding to damping ratio $\zeta=2\%$ are selected and the buildings are evaluated at the spectral acceleration level of the estimated fundamental building period for probability of exceedance levels equal to 10% in 50 years, 50% in 50 years and for an intermediate spectral acceleration level between the two latter ones. The selected spectral acceleration values are reported in Table 7.1.

Table 7.1 Spectral acceleration values used for the collapse evaluation

Idealized Building	Actual Building Period (sec)	Estimated Building Period⁶ (sec)	Probability of Exceedance in 50 years	Spectral Acceleration at the Actual Building Period (in g units)
4-Story	1.14	0.96	50%	0.31
			-	0.50
			10%	0.87
8-Story	1.62	1.51	50%	0.23
			-	0.40
			10%	0.68
12-Story	1.95	1.81	50%	0.18
			-	0.30
			10%	0.54

The evaluation results are presented in sections 7.1.1 – 7.1.3

7.1.1 Evaluation of Collapse Potential for the 4-Story Idealized Building

Table 7.2 summarizes the results of the collapse evaluation for the 4-story idealized building. The methodology identifies the 1st of the building as critical for collapse for both $\Sigma M_{nc}/\Sigma M_{nb} = 1.00$ and 1.40. Collapse simulation confirmed the validity of the results of the study since for $\Sigma M_{nc}/\Sigma M_{nb} = 1.00$ and 1.40 approximately 90% of building collapses occur due to shear or axial failure of columns located at the 1st story. For the case of $V_p/V_n = 0.80$ and 1.00 the method consistently provides conservative estimates of collapse potential in accordance with the conservative values that were selected for the alpha values of the critical story. The method gives the higher error for the case of $V_p/V_n = 1.20$. For the case of $\Sigma M_{nc}/\Sigma M_{nb} = 1.00$ the method provides lower probability of collapse. This can be explained since the collapse drift capacity as estimated by Equation 6.5 provides lower drift values than the ones that correspond to the case where shear demand exceeds shear strength triggering shear and axial failure.

⁶ The estimated building period was computed using Equation 6.7

Table 7.2 Comparison of collapse evaluation using the displacement-based methodology and IDA for the 4-story idealized building

$\Sigma M_{nc}/\Sigma M_{nb}$	V_p/V_n	R_e ($S_{a,T1} * W/V_{max}$)	<i>Spectral Acceleration at Actual Building Period (in g units)</i>	<i>Estimated Probability of Collapse</i>	<i>Probability of Collapse IDA</i>
1.00	0.80	1.73	0.31	0.06	0.06
		2.79	0.50	0.36	0.32
		4.85	0.87	0.87	0.81
1.40	0.80	2.14	0.31	0.04	0.03
		3.45	0.50	0.19	0.17
		6.00	0.87	0.64	0.60
1.00	1.00	1.73	0.31	0.16	0.12
		2.79	0.50	0.54	0.48
		4.85	0.87	0.97	0.90
1.40	1.00	2.14	0.31	0.06	0.05
		3.45	0.50	0.28	0.25
		6.00	0.87	0.80	0.75
1.00	1.20	2.07	0.31	0.51	0.69
		3.35	0.50	0.69	0.86
		5.82	0.87	1.00	1.00

$\Sigma M_{nc}/\Sigma M_{nb}$	V_p/V_n	Re ($S_{a,T1} * W/V_{ma}$)	<i>Spectral Acceleration at Estimated Building Period (in g units)</i>	<i>Estimated Probability of Collapse</i>	<i>Probability of Collapse IDA</i>
1.40	1.20	2.38	0.31	0.05	0.12
		3.83	0.50	0.34	0.43
		6.67	0.87	0.93	0.97

7.1.2 Evaluation of Collapse Potential for the 8-Story Idealized Building

Table 7.3 summarizes the results of the collapse evaluation for the 8-story idealized building. Similar observations with the 4-story building can be made comparing the results of the approximate method with the IDA. For the 8-story building for the case of $\Sigma M_{nc}/\Sigma M_{nb}=1.00$ the method identifies the 1st story critical for collapse while for $\Sigma M_{nc}/\Sigma M_{nb}=1.40$ both 1st and 2nd story provide approximately the same story collapse estimates. The results are confirmed by IDA where for $\Sigma M_{nc}/\Sigma M_{nb}=1.00$ approximately 85% of building collapses occur due to failure of the 1st story. For the case of $\Sigma M_{nc}/\Sigma M_{nb}=1.40$ approximately 90% of building collapses occur due to columns failing in the 1st or 2nd story.

Table 7.3 Comparison of collapse evaluation using the displacement-based methodology and IDA for the 8-story idealized building

$\Sigma M_{nc}/\Sigma M_{nb}$	V_p/V_n	R_e ($S_{a,T1} * W/V_{max}$)	<i>Spectral Acceleration at Actual Building Period (in g units)</i>	<i>Estimated Probability of Collapse</i>	<i>Probability of Collapse IDA</i>
1.00	0.80	1.48	0.23	0.24	0.20
		2.57	0.40	0.55	0.49
		4.36	0.68	0.96	0.89
1.40	0.80	1.77	0.23	0.05	0.02
		3.08	0.40	0.22	0.14
		5.24	0.68	0.70	0.59
1.00	1.00	1.48	0.23	0.40	0.33
		2.57	0.40	0.77	0.65
		4.36	0.68	1.00	0.95
1.40	1.00	1.77	0.23	0.06	0.03
		3.08	0.40	0.32	0.22
		5.24	0.68	0.85	0.72
1.00	1.20	1.78	0.23	0.55	0.60
		3.08	0.40	0.87	0.94
		5.23	0.68	1.00	1.00

$\Sigma M_{nc}/\Sigma M_{nb}$	V_p/V_n	R_e ($S_{a,T1} * W/V_{ma}$)	<i>Spectral Acceleration at Estimated Building Period (in g units)</i>	<i>Estimated Probability of Collapse</i>	<i>Probability of Collapse IDA</i>
1.40	1.20	1.96	0.23	0.10	0.10
		3.42	0.40	0.52	0.50
		5.82	0.68	0.89	0.85

Table 7.4 summarizes the results of the collapse evaluation for the 8-story idealized building with inadequate lap splicing conditions of the column longitudinal reinforcement at the base of the 1st story. As expected, 100% of building collapses occur due to failure of the columns at the 1st story. As explained in Chapter 6, a relatively conservative drift capacity estimate was selected in that case. This is the main reason why the approximate method provides more conservative collapse estimates compared to IDA although the alpha values selected were slightly less conservative than the average alpha values observed for the critical story in IDA.

Table 7.4 Comparison of collapse evaluation using the displacement-based methodology and IDA for the 8-story idealized building with inadequate lap splicing conditions at the base of the 1st story

$\Sigma M_{nc}/\Sigma M_{nb}$	V_p/V_n	R_e ($S_{a,T1} * W/V_{max}$)	<i>Spectral Acceleration at Actual Building Period (in g units)</i>	<i>Estimated Probability of Collapse</i>	<i>Probability of Collapse IDA</i>
1.00	0.80	1.48	0.23	0.37	0.26
		2.57	0.40	0.81	0.74
		4.36	0.68	1.00	0.98
1.40	0.80	1.77	0.23	0.10	0.04
		3.08	0.40	0.43	0.33
		5.24	0.68	0.99	0.78

Table 7.5 summarizes the results of the collapse evaluation for the 8-story idealized building with non-uniform DCRs. The latter variation of the 8-story building possesses a weak/critical story at the mid-height (4th story) with $DCR_{4th}=1.30DCR_{1st}$. The method identifies correctly the 4th story as critical for collapse. In that case IDA showed that approximately 70% of building collapses occurred due to failure of the 4th story while the remaining 30% of collapses occurred due to failure of the 1st or 2nd story for the cases of $\Sigma M_{nc}/\Sigma M_{nb}=0.80$ and 1.20. For the case of $\Sigma M_{nc}/\Sigma M_{nb}=1.60$ approximately 85% of building collapses occurred due to failure of the 4th story. The method again provides conservative collapse estimates with the exception of $\Sigma M_{nc}/\Sigma M_{nb}=1.60$ where the method defined the alpha value of the critical story slightly lower than what IDA provided as an average value.

Table 7.5 Comparison of collapse evaluation using the displacement-based methodology and IDA for the 8-story idealized building with weak story at the mid-height

$\Sigma M_{nc}/\Sigma M_{nb}$	V_p/V_n	R_e ($S_{a,T1} * W/V_{max}$)	<i>Spectral Acceleration at Actual Building Period (in g units)</i>	<i>Estimated Probability of Collapse</i>	<i>Probability of Collapse IDA</i>
0.80	0.80	1.65	0.23	0.24	0.21
		2.86	0.40	0.61	0.57
		4.87	0.68	1.00	0.95
1.20	0.80	1.88	0.23	0.06	0.05
		3.26	0.40	0.42	0.39
		5.54	0.68	0.87	0.82
1.60	0.80	2.37	0.23	0.01	0.02
		4.12	0.40	0.20	0.27
		7.01	0.68	0.60	0.71

7.1.3 Evaluation of Collapse Potential for the 12-Story Idealized Building

Table 7.6 summarizes the results of the collapse evaluation for the 12-story idealized building. Similar trends with the previous two buildings were observed for the 12-story building as well. The methodology identifies the 1st story as critical for collapse for $\Sigma M_{nc}/\Sigma M_{nb}=1.00$, while for $\Sigma M_{nc}/\Sigma M_{nb}=1.40$ the first three stories yield similar story collapse potential values. IDA showed that for $\Sigma M_{nc}/\Sigma M_{nb}=1.00$ approximately 75% of the building collapses occurred due to collapse of the 1st story. For $\Sigma M_{nc}/\Sigma M_{nb}=1.40$ approximately 85% of the collapse mechanisms occur due to failure of the first three stories. Application of the approximate method for the 12-story building yields larger errors in the collapse estimates compared to the 4 and 8-story buildings.

This can be explained by the higher mode effects that are not incorporated in the approximate method.

Table 7.6 Comparison of collapse evaluation using the displacement-based methodology and IDA for the 12-story idealized building

$\Sigma M_{nc}/\Sigma M_{nb}$	V_p/V_n	Re ($S_{a,T1} * W/V_{max}$)	<i>Spectral Acceleration at Actual Building Period (in g units)</i>	<i>Estimated Probability of Collapse</i>	<i>Probability of Collapse IDA</i>
1.00	0.80	1.02	0.18	0.03	0.02
		1.70	0.30	0.38	0.29
		3.11	0.55	1.00	0.88
1.40	0.80	1.19	0.18	0.01	0.01
		1.98	0.30	0.02	0.01
		3.62	0.55	0.45	0.35
1.00	1.00	1.02	0.18	0.09	0.06
		1.70	0.30	0.59	0.47
		3.11	0.55	1.00	0.92
1.40	1.00	1.19	0.18	0.01	0.01
		1.98	0.30	0.11	0.04
		3.62	0.55	0.66	0.53
1.00	1.20	1.22	0.18	0.23	0.20
		2.04	0.30	0.70	0.61
		3.73	0.55	1.00	1.00

$\Sigma M_{nc}/\Sigma M_{nb}$	V_p/V_n	Re ($S_{a,T1} * W/V_{ma}$)	<i>Spectral Acceleration at Estimated Building Period (in g units)</i>	<i>Estimated Probability of Collapse</i>	<i>Probability of Collapse IDA</i>
1.40	1.20	1.31	0.18	0.07	0.01
		2.18	0.30	0.36	0.21
		3.99	0.55	0.90	0.79

The tables above demonstrate that application of the approximate method correctly identifies the critical story and provides relatively accurate collapse estimates in comparison with IDA results. Apart from the case of buildings with uniform strength characteristics along the height, the method was also applied for cases where inadequate lap splicing conditions exist at the base of column members located at the 1st story and for cases where the building possessed a particularly weak story at the mid-height. For both of these cases the approximate method was able to identify the weak story and provide collapse estimates with relatively low error compared to IDA. For most cases the method yielded conservative estimates of the probability of collapse which is consistent with the way that the alpha values were selected. The results above indicate that the method shows potential for rapid identification of hazardous concrete frame buildings; though further verification using real older-type buildings is required before more generalized conclusions regarding its applicability can be drawn.

8 Summary and Conclusions

The purpose of this study was to explore methodologies suitable for identification of seismically hazardous reinforced concrete frame buildings. Three idealized concrete buildings were developed for the purposes of the current study. The buildings were sequentially weakened such that the following deficiencies were introduced: a) Weak column mechanism, b) Shear critical columns, and c) Inadequate column bar lap splicing conditions. Consequently the collapse potential of the buildings possessing each of the aforementioned deficiencies or combinations of them was performed using the three evaluation methods described below:

- ***Collapse Simulation using IDA.*** According to this approach Incremental Dynamic Analysis (IDA) was used to evaluate the collapse performance of the considered buildings. This method is considered to provide the most accurate results compared to the other two methods presented in this study since state of the art collapse simulation tools are employed to model the structural response. However, the method requires detailed non-linear modeling of the considered building and multiple non-linear analyses, rendering this approach inefficient for rapid identification of hazardous buildings.
- ***Collapse Indicators – a Strength-Based Approach for Collapse Evaluation.*** This method considered simple engineering parameters (collapse indicators) which could be easily defined based only on hand calculations to estimate the building collapse performance. To avoid comparison bias between buildings of different strength a strength-based normalization parameter was employed. According to this method, an engineer needs to estimate the values of the collapse indicator parameters and the building strength to evaluate the building collapse performance. Although this method seems to provide rational results it should be applied with caution for buildings with strength characteristics different from those considered in the buildings developed in the current study.
- ***A Displacement-Based Approach for Collapse Evaluation.*** The latter method employs a displacement-based approach that estimates drift demand and uses relationships available in the literature to determine the drift capacity for the columns of the studied building. After the procedure is repeated for each story, the building collapse potential can be determined based on a comparison of the estimated demand and capacity values. This method has the advantage that the procedure followed is not based on strength (at least for buildings with $T_1 > 1.0$ sec) and so it can be applied for a range of buildings with different strength properties.

The current chapter discusses all the main conclusions that were drawn from the application of the aforementioned methodologies as well as recommendations for further study in the future.

8.1 COLLAPSE SIMULATION

Two different models to simulate collapse were employed in the study. According to the first model, zero-length plastic hinges were incorporated at the ends of column and beam members to account for non-linear material response. The zero-length plastic hinges were modeled according to Haselton et al. (2008), with some parameter updates to better reflect the characteristics of the columns to which it was applied.

The second model used the limit state model which was developed by Elwood and Moehle (2002). This model is capable of simulating shear and shear-induced axial failure in columns with inadequate amount of transverse reinforcement.

Both models have been calibrated using different column databases and thus result in different column dynamic response for the same column detailing. To evaluate the validity of both modeling approaches, the dynamic response for eleven shaking table test structures incorporating two different types of concrete columns was investigated. The first column type was detailed according to the current seismic code provisions, while the second column type was detailed to mimic older design practices. The test structures were scaled, one-bay frames consisting of two concrete columns at opposite ends of a single bay. In some frames, both columns were ductile columns, in other frames they were both nonductile columns, and in yet other frames a combination of ductile and nonductile columns was used. Each frame was then subjected to one of two different axial load levels and one of two different ground motion records.

The tested structures were analyzed using both the Elwood and Haselton models. The study showed that the limit state material developed by Elwood tracks with sufficient accuracy the onset of shear failure and simulates satisfactorily the dynamic response of columns with inadequate transverse reinforcement ratio, for which it was calibrated. The plastic hinge model calibrated by Haselton, was not as accurate as the Elwood model for columns lacking adequate amount of transverse reinforcement and thus being flexure-shear critical. However, the Haselton plastic hinge model reproduced with sufficient accuracy the dynamic response of columns following modern design practice. A combination of the Haselton and Elwood model was employed successfully for cases where the test frames consisted of columns following both old and current design codes.

Overall, the comparison of experimental results with the two analytical models demonstrated that the plastic hinge model calibrated by Haselton et al. represents accurately the dynamic response of building frames consisting of columns with sufficient transverse reinforcement ratio ($V_p/V_n < 0.7$) and thus being flexure critical, while the limit state material is more appropriate for building frames consisting of columns with inadequate transverse reinforcement ratio ($V_p/V_n > 0.7$) and thus being shear critical.

After exploring the validity of collapse simulation techniques using shaking table tests, the Elwood and Haselton models were used to simulate the collapse response of idealized concrete frame buildings developed for the purposes of this study. The idealized buildings were initially

designed according to current seismic code provisions. Consequently the performance of variations of the idealized buildings was explored including one or more structural deficiencies indicative of older design practice (weak column story mechanisms, columns with inadequate transverse reinforcement, and inadequate column bar lap splicing conditions). As explained above, it was decided to use the Haselton model to simulate the response of code complying column and beam members, while the Elwood model was used to simulate the response of buildings which consisted of column members with inadequate transverse reinforcement.

Collapse evaluation was performed using Incremental Dynamic Analysis. According to this method, a set of far-fault ground motions was scaled until the structure reaches collapse. Using statistical post-processing of the results, curves linking earthquake intensity with probability of collapse were derived.

Evaluation of building performance using results from numerous collapse simulations is considered today to be one of the most accurate methods to estimate building collapse performance. Thereby, the IDA results obtained from collapse simulations were used to calibrate the two approximate methods presented below, which are more efficient for rapid identification of seismically hazardous concrete buildings

8.2 COLLAPSE INDICATORS – A STRENGTH-BASED APPROACH FOR COLLAPSE EVALUATION

In Chapter 5 a study was performed to explore the effect of two simple engineering parameters, termed as collapse indicators, in the collapse potential of concrete frame structures. The collapse indicators selected constitute key concepts of the capacity design principles of modern seismic codes. According to the results of this study, both the column-to-beam bending moment strength ratio and the plastic shear capacity over the required shear demand exhibit strong correlation with the collapse potential.

As expected, the increase of beam-to-column bending moment strength ratio leads to concentration of damage in one story and consequently to lateral instability. Conversely decrease of the value of this ratio allows a better distribution of damage over the height of the building with beams failing first. For regular frames of the type considered in this study, having reasonable values of the variable $\Sigma M_{nc}/\Sigma M_{nb}$, beam yielding mechanisms do not extend full height but instead are concentrated in the lower stories. For the case of $\Sigma M_{nc}/\Sigma M_{nb} = 1.2$ about 25-30% of the building height participates in the collapse mechanism while for the case of $\Sigma M_{nc}/\Sigma M_{nb} = 1.6$ the percentage increases to 30-60%.

The decrease in the amount of transverse reinforcement results in decrease of the column shear strength. This corresponds to an increase in the column flexural demand over capacity ratio, V_p/V_n . For all other variables being the same, the collapse probability increases with increasing values of the variable V_p/V_n , that is, as columns become increasingly shear-critical.

Finally the study demonstrated that all parameters explored, $\Sigma M_{nc}/\Sigma M_{nb}$ and V_p/V_n , interact, such that it is necessary to consider the combination of variables in order to quantify the probability of collapse. To avoid comparison bias for buildings having different strength two normalization factors, R_e and M , based on base shear capacity were employed.

At Appendix E, tables with the input parameters $\Sigma M_{nc}/\Sigma M_{nb}$, V_p/V_n , R_e and M are provided to estimate the building collapse potential.

8.3 A DISPLACEMENT-BASED APPROACH FOR COLLAPSE EVALUATION

A displacement based approach was developed in Chapter 6. This approach requires the engineer to select the level of seismic hazard and then use an equivalent Single Degree of Freedom (SDOF) system to estimate story drift demand. The procedure followed in this chapter is considered more rational than the one presented in Chapter 5, since collapse is mainly occurring due to inability of one or more structural members to accommodate excessive drifts/deformation demands.

One of the main advantages of this procedure is that for buildings with period $T_1 > 1.0$ sec, the application of the method was shown to be independent of the building strength which could vary for different considered buildings. Another advantage is that since both drift demand and drift capacity can be quantified in a probabilistic framework, a simple mathematical formulation that can accommodate both uncertainty in the drift demand and uncertainty in the drift capacity is possible.

Chapter 7 deployed the displacement-based approach of Chapter 6 to estimate the collapse risk of the various buildings studied in the course of this work. The procedure described in Chapter 6 was shown to correctly identify the weakest stories of the considered buildings and estimate with sufficient accuracy the building collapse potential. The accuracy of the results was evaluated using the results obtained from collapse simulation studies presented in Chapters 4 and 5. Taking into account both the accuracy and the efficiency in application, the displacement based method was overall shown to be the most appropriate method for rapid identification of seismically hazardous concrete buildings.

8.4 RECOMMENDATIONS FOR FUTURE STUDY

Although the proposed methodologies were successful in estimating building collapse risk, further work needs to be done in order to explore the effect of some additional deficiencies and structural systems that have not been considered in the current study. Some of the most common cases of systems and deficiencies that need to be investigated in order to be able to use the proposed methodology for a wide range of existing buildings would be:

- **Column-slab frames.** Many older-type concrete building include frames with no beams or girders. Instead, flat slabs act to transfer the lateral forces to the column members. In such cases, excessive drift due to seismic forces can cause punching shear failure. A number of laboratory tests performed for slab-column connections with and without shear reinforcement could be used to derive probabilistic capacity models.
- **Building with structural walls.** A significant number of older concrete buildings include either lightly confined concrete walls or masonry infill walls confined by structural beams and columns. The presence of walls would alter significantly the assumed drift profiles, while failure of a wall would lead to increased drift or even loss of vertical support. Drift pattern profiles need to be developed for buildings with structural systems that consist of a combination of walls and frames. An important issue in that case would be modeling the sudden strength and stiffness degradation of lightly reinforced concrete walls and how this affects the drift demands and eventually the progressive collapse of the building.
- **Plan irregularities.** The current study did not consider the effect of plan irregularity in creating torsional moments and thus, increase in the inter-story drift demands. A magnification factor for drift demand could be calibrated using three dimensional analyses.
- **Unconfined beam column joints.** A structural deficiency very commonly observed in older-type buildings is beam-column connections without joint transverse reinforcement. Several laboratory tests have been conducted for both interior and exterior joints. Although there have not been adequate physical evidence of building collapses triggered by joint failures, severe joint damage has been reported in past earthquakes. The effect of joints on both the demand and capacity estimates should be incorporated using the available experimental data.

This study considered data from a large number of non-linear dynamic analyses to develop profiles of story drift patterns as a function of the spectral acceleration. The input parameter (spectral acceleration) and predicted variable (story drift patterns) were assumed to be related in a linear way. The coefficient linking this two variables, a_x , was estimated through minimizing the sum of squared errors. The large dispersion observed indicates that the assumed model might not be the ideal model to relate the two aforementioned variables. A more in-depth statistical procedure should be followed to reduce the observed dispersion between observed and predicted values in the story drift demands. This would lead to a more accurate approximation of the building collapse potential.

The methodologies presented have been calibrated by using, in most cases, idealized buildings with uniform structural parameters values such that varying the value of each parameter could be directly linked to collapse potential. Although this approach is appealing due to its simplicity, it

may oversimplify response of actual buildings in which structural parameters can be significantly non-uniform within the same story and from story to story. Therefore, the proposed methodologies needs to be further verified using examples of existing older-type concrete buildings.

The presented collapse evaluation methodologies could be incorporated as a part of a holistic risk assessment approach that should be followed in a regional level. Cost-benefit analysis principles towards optimal risk management should be applied when forming seismic policy to classify buildings as particularly hazardous, moderately hazardous, and slightly hazardous. It is suggested that since human loss is difficult to quantify in financial terms, life safety standards for collapse prone buildings could be established using risk metrics and recovery costs that can be directly compared with other routine hazards like car accidents or plane crashes. Unnecessary conservatism in classifying earthquake hazardous buildings introduces increased financial burden to building owners or authorities. Communities that implement plans using such a methodology would become more resilient, enabling them to recover from future disasters.

REFERENCES

- ACI, (2008), “*Guide to Durable Concrete*”, ACI 201R-08, American Concrete Institute, Farmington Hills, Michigan.
- ACI,(2011), “*Building Code Requirements for Structural Concrete and Commentary*”, ACI 318-11, American Concrete Institute, Farmington Hills, Michigan.
- ASCE,(2003), “*Seismic Evaluation of Existing Buildings*”, ASCE/SEI 31-03, American Society of Civil Engineers, Structural Engineering Institute, Reston, Virginia.
- ASCE, (2006), “*Seismic Rehabilitation of Existing Buildings*”, ASCE/SEI 41-06, Including Supplement No. 1, American Society of Civil Engineers, Structural Engineering Institute, Reston, Virginia.
- ASCE, (2010), “*Minimum Design Loads for Buildings and Other Structures*”, ASCE/SEI 7-10, American Society of Civil Engineers, Structural Engineering Institute, Reston, Virginia.
- ASCE, (2013), “*Seismic Evaluation and Retrofit of Existing Buildings*”, ASCE/SEI 41-13, American Society of Civil Engineers, Structural Engineering Institute, Reston, Virginia.
- ATC, (2013), “*Evaluation of the Methodology to Select and Prioritize Collapse Indicators in Older Concrete Buildings*”, ATC-78-1 Report, Applied Technology Council, Redwood City, California.
- ATC, (2014), “*Seismic Evaluation for Collapse Potential of Older Concrete Frame Buildings*”, ATC-78-2, Applied Technology Council, Redwood City, California.
- Baker, J., (2007), “*Probabilistic Structural Response Assessment Using Vector-Valued Intensity Measures*”, Earthquake Engineering and Structural Dynamics, Vol. 36, p. 1861-1883

- Berry, M., Parrish, M., and Eberhard, M., (2004), "*PEER Structural Performance Database User's Manual*", Pacific Earthquake Engineering Research Center, University of California, Berkeley, California, last accessed September 26, 2013, Available at <http://nisee.berkeley.edu/spd/> and <http://maximus.ce.washington.edu/~peera1>.
- Blume, J.A., Newmark, N.M., and Corning, L.M., (1961), "*Design of Multi-story Reinforced Concrete Buildings for Earthquake Motions*", Portland Cement Association, Chicago, Illinois.
- Concrete Coalition, (2013), Online Database, Sponsored by the Earthquake Engineering Research Institute, the Pacific Earthquake Engineering Research Center, and the Applied Technology Council, Oakland, California, <http://www.concretecoalition.org>
- DeBock, D.J., Liel, A.B., Haselton, C.B., Hooper, J.D., and Henige, R.A., (2014), "*Importance of seismic design accidental torsion requirements for building collapse capacity*", Earthquake Engineering and Structural Dynamics, Vol. 43, Issue 6, p. 831-850
- Ellingwood, B., Galambos, T.V., MacGregor, J.G., and Cornell, C.A., (1980), "*Development of a Probability Based Load Criterion for American National Standard A58*", Special Publication No. 577, National Bureau of Standards, Washington, D.C.
- Elwood, K.J., (2002), "*Shake Table Tests and Analytical Studies on the Gravity Load Collapse of Reinforced Concrete Frames*", Ph.D. Dissertation, University of California, Berkeley
- Elwood, K.J., (2004), "*Modelling failures in existing reinforced concrete columns*, *Canadian Journal of Civil Engineering*", Vol. 31, No. 5, pp. 846-859.
- Elwood, K.J., Matamoros, A., Wallace, J.W., Lehman, D.E., Heintz, J.A., Mitchell, A., Moore, M.A., Valley, M.T., Lowes, L. Comartin, C., and Moehle, J.P., (2007), "*Update of ASCE/SEI 41 Concrete Provisions, Earthquake Spectra*", Vol. 23, No. 3, pp. 493-523.
- FEMA, (1998), "*Evaluation of Earthquake Damaged Concrete and Masonry Wall Buildings*", FEMA 306, Federal Emergency Management Agency, Washington, D.C.
- FEMA, (2000), "*Prestandard and Commentary for the Seismic Rehabilitation of Buildings*", FEMA 356 Report, prepared by the Applied Technology Council, under contract to the Building Seismic Safety Council, for the Federal Emergency Management Agency, Washington, D.C.
- FEMA, (2009), "*Quantification of Building Seismic Performance Factors*", FEMA P-695, prepared by the Applied Technology Council for the Federal Emergency Management Agency, Washington, D.C.

- Galanis P., and Moehle, J.P., (2014), “*Development of Collapse Indicators for Older-Type Reinforced Concrete Buildings*”, 15th WCEE, September 24-28 2012, Lisbon, Portugal
- Galanis P., and Moehle, J.P., (2014), “*Development of Collapse Indicators for Seismic Risk Assessment of Older-Type Reinforced Concrete buildings*”, Earthquake Spectra, (in-press), <http://dx.doi.org/10.1193/080613EQS225M>
- Galanis P., and Moehle, J.P., (2014), “*Development of Collapse Indicators for Seismic Risk Assessment of Older-Type Reinforced Concrete buildings*”, UCB/SEMM Report 2014/03, <http://nisee.berkeley.edu/documents/SEMM/SEMM-2014-03.pdf>
- Galanis P., Shin Y.P. and Moehle, J.P., (2014), “*Modeling the Dynamic Structural Behavior of Ductile and Non-Ductile Reinforced Concrete Frames*”, 10th NCEE, July 21-25 2014, Alaska
- Goel, R., and Chopra, A.K., (1997), “*Vibration Properties of Buildings Determined from Recorded Earthquake Motions*”, UCB/EERC-97/14, Earthquake Engineering Research Center, University of California, Berkeley, California.
- Ghannoum, W.M., and Matamoros, A.B., (2013), “*Nonlinear Modeling Parameters and Acceptance Criteria for Concrete Columns*”, Submitted for publication in ACI Special Publications, American Concrete Institute, Farmington Hills, Michigan.
- Haselton, C., Liel, A., Lange, S.T., and Deierlein, G.G.,(2008), “*Beam-Column Element Model Calibrated for Predicting Flexural Response Leading to Global Collapse of RC Frame Buildings*”, PEER Report, 2007/03
- Hassan, W.M. , Moehle, J.P. (2012), “*A Cyclic Nonlinear Macro Model for Numerical simulation of Beam-Column Joints in Existing Concrete Buildings*”, 15th WCEE, September 24-28 2012, Lisbon, Portugal
- Hassan, W.M. , Moehle, J.P. (2013), “*Quantification of Residual Axial Capacity of Beam-Column Joints in Existing Concrete Buildings under Seismic Load Reversals*”, COMPDYN, 4th ECCOMAS Thematic Conference on Computational Methods in Structural Dynamics and Earthquake Engineering, 12-14 June 2013, Kos island, Greece
- Henkhaus, K., (2010), “*Axial Failure of Vulnerable Reinforced Concrete Columns Damaged by Shear Reversals*”, Ph.D. Dissertation, Purdue University, West Lafayette, Indiana.
- Ibarra, L. F., and Krawinkler, H. (2005). “*Global collapse of frame structures under seismic excitations*,” Technical Report 152, The John A. Blume Earthquake Engineering Research Center, Department of Civil Engineering, Stanford University, Stanford, CA.

- Ibarra, L. F., Medina, R. A., and Krawinkler, H. (2005). “*Hysteretic models that incorporate strength and stiffness deterioration*,” *Earthquake Engineering and Structural Dynamics*, Vol. 34, 12, pp. 1489-1511.
- ICBO, (1976), “*Uniform Building Code*”, International Council of Building Officials, Whittier, California.
- Li, Y., Elwood K.J., and Hwang S.-J., (2013), “*Assessment of ASCE/SEI 41 Concrete Column Provisions using Shaking Table Tests*”, Submitted for publication in ACI Special Publications, American Concrete Institute, Farmington Hills, Michigan.
- Luco, N., Mori, Y., Funahashi, Y., Cornell, C.A., and Nakashima, M., (2003), “*Evaluation of Predictors of Non-Linear Seismic Demands using "Fishbone" Models of SMRF Buildings*, *Earthquake Engineering and Structural Dynamics*”, Vol. 32, No. 14, pp. 2267-2288.
- Lynn, A. C., Moehle, J. P., Mahin, S. A., and Holmes, W. T. (1996), “*Seismic Evaluation of Existing Reinforced Concrete Columns*”, *Earthquake Spectra*, Earthquake Engineering Research Institute, Vol. 12, No. 4, November 1996, pp. 715-739
- Melchers, R.E., (1999), “*Structural Reliability Analysis and Prediction*”, Second Edition, John Wiley and Sons Ltd., West Sussex, England.
- Melek, M., and Wallace, J.W., (1999), “*Cyclic Behavior of Columns with Short Lap Splices*”, *ACI Structural Journal*, Vol. 101, pp. 802-811.
- Nakashima, M., Ogawa K. and Inoue, K., (2002), “*Generic Frame Model Simulation of Earthquake Responses of Steel Moment Frames*”, *Earthquake Engineering and Structural Dynamics*, Vol. 31, pp. 671-692.
- NEES, (2010), Grand Challenge Research Project, “*Mitigation of Collapse Risks in Older Reinforced Concrete Buildings*”, George E. Brown Network for Earthquake Engineering Simulation, <http://peer.berkeley.edu/grandchallenge/index.html>,
- NIST, (2010a), “*Concrete Model Building Subtypes Recommended for Use in Collecting Inventory Data*”, NIST GCR 10-917-6, prepared by the Building Seismic Safety Council for the National Institute of Standards and Technology, Gaithersburg, Maryland.
- NIST, (2010b), “*Evaluation of the FEMA P-695 Methodology for Quantification of Building Seismic Performance Factors*”, NIST GCR 10-917-8, prepared by the NEHRP Consultants Joint Venture, a partnership of the Applied Technology Council and Consortium of Universities for Research in Earthquake Engineering, for the National Institute of Standards and Technology, Gaithersburg, Maryland.

- NIST, (2010c), “*Program Plan for the Development of Collapse Assessment and Mitigation Strategies for Existing Reinforced Concrete Buildings*”, NIST GCR 10-917-7, prepared by the NEHRP Consultants Joint Venture, a partnership of the Applied Technology Council and Consortium of Universities for Research in Earthquake Engineering, for the National Institute of Standards and Technology, Gaithersburg, Maryland.
- Park, S. and Mosalam, K. , (2013), “*Simulation of Reinforced Concrete Frames with Nonductile Beam-Column Joints*”, EERI Spectra, Vol. 29, pp. 233-257
- Renouard, F. (2014), “*Evaluation Methodology to Assess the Collapse of Older Reinforced Concrete Buildings*”, Master of Science Thesis (in-press)
- Sattar, S. (2013), “*Influence of Masonry Infill Walls and Other Building Characteristics on Seismic Collapse of Concrete Frame Buildings*”, Ph.D. Dissertation, University of Colorado, Boulder.
- Sezen, H. (2002), “*Seismic Behavior and Modeling of Reinforced Concrete Building Columns*”, Ph.D. Dissertation, University of California, Berkeley.
- Shin, Y. B. (2007), “*Dynamic Response of Ductile and Non-Ductile Reinforced Concrete Columns*”, Ph.D. Dissertation, University of California, Berkeley.
- Shome N. (1999), “*Probabilistic Seismic Demand Analysis of Nonlinear Structures*”, Ph.D. Dissertation, Stanford University
- Smith, W. (2005), “*The Challenge of Earthquake Risk Assessment*”, Seism. Res. Lett., Vol. 76, p. 415-416
- USGS, (2008), “*Earthquake Hazard Maps*”, United States Geological Survey, Reston, Virginia, <http://earthquake.usgs.gov/hazards/products/conterminous/2008/maps/>
- Vamvatsikos, D. and Cornell, C.A., (2004), “*Applied Incremental Dynamic Analysis*”, Earthquake Spectra, Vol. 20, No. 2, p.523-553
- Wang, Z., (2006), “*Understanding Seismic Hazard and Risk Assessment: A Gap between Engineers and Seismologists*”, Proceedings, 14th World Conference on Earthquake Engineering, October 12-17 2008, Beijing, China.
- Woods, C., and Matamoros, A., (2010), “*Effect of Longitudinal Reinforcement Ratio on the Failure Mechanism of R/C Columns Most Vulnerable to Collapse*”, Proceedings, The 9th U.S. National Conference and 10th Canadian Conference on Earthquake Engineering, Toronto, Canada.

Yosimura, M., Nakamura, T. (2002), "*Intermediate-Story Collapse of Concrete Buildings*",
Proceedings of the Third U.S. – Japan Workshop on Performance Based Earthquake
Engineering Methodology for Reinforced Concrete Building Structures, August 16-18,
2001, Seattle, Washington, 107-118

A. Design Parameters of the Idealized Buildings

The current section presents details regarding the design of the three (4, 8, and 12 –story) idealized buildings that were considered in the current study.

As mentioned in Chapter 4, all the considered archetype buildings were designed such that they correspond to regular concrete frame buildings. The archetype buildings have a rectangular plan with five bays in each direction without plan torsion. The structural system consists of reinforced concrete frames without any infill or structural walls. The archetype buildings for each category were designed to have proportions and force-deformation characteristics similar to those of new buildings. More specifically the detailing of archetype buildings satisfies ACI 318-11 code requirements, except $\Sigma M_{nc}/\Sigma M_{nb} = 1.0$ at every joint except the roof level (ΣM_{nc} = sum of nominal moment strengths of columns at a beam-column joint and ΣM_{nb} = sum of nominal moment strengths of beams at the same joint).

Consequently the structural properties of the archetype buildings were varied and structural deficiencies were introduced somewhat typical of those found in older buildings.

The design base-shear of the archetype buildings was set at approximately $0.10 \cdot W$, where W is the effective seismic weight of the building.

A.1. DESIGN PHILOSOPHY OF ARCHETYPE BUILDINGS

Although the prototype buildings vary in height they have similar building geometry, depicted in Figure A.1. The buildings have square plan shape with five bays in each principal direction. All frames were designated as seismic-force-resisting frames and designed to carry appropriate earthquake and gravity loading according to the corresponding tributary area.

Only the interior frames were modeled, using a two dimensional method, because interior frames support larger tributary area and therefore have larger column loads. This causes interior frames to be more vulnerable to shear induced axial load failure that is typical in older-type buildings. Thus, the design parameters and drawings only of the interior frame are presented.

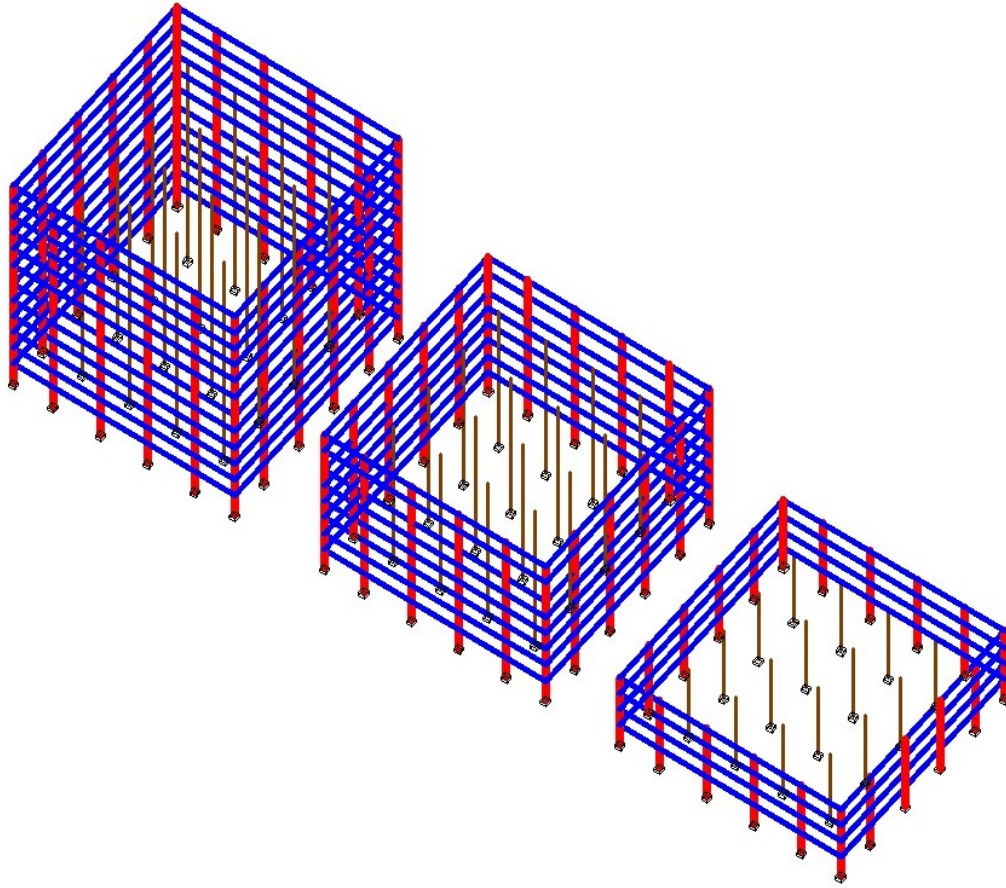


Figure A.1 Three- dimensional view of the studied buildings (for clarity of presentation, only the perimeter frames are shown)

A.2. DESIGN ASSUMPTIONS

A.2.1 Applied Loads

- Dead Load: 150 psf (includes the self-weight)
- Cladding: 15 psf
- Live Load: 60 psf
- The tributary width for the gravity loads is 10 feet
- The lateral load design for inverted triangular load with design base-shear strength of $0.10W$, where W is the effective seismic weight resisted by each frame

A.2.2 Material Properties

- Reinforced Concrete characteristic strength $f'_c=3000\text{psi}=3\text{ ksi}$
- Steel Reinforcement Grade 60 – $f_y=60000\text{ psi} = 60\text{ ksi}$
- Reinforced Concrete modulus of Elasticity $E_c=3122\text{ ksi}$
- Steel Reinforcement modulus of Elasticity $E_s=29000\text{ ksi}$

A.2.3 Calculation of Loads

The tributary width for the interior frame is $(10+12)\text{ ft} = 22\text{ ft}$. The selected frame is shown in Figure A.2 .

- Distributed Dead Load per floor: $w_{\text{dead}}=150\text{ psf} * 22\text{ ft} = 3300\text{ pounds/ft} = \mathbf{3.30\text{ kips/ft}}$
- Distributed Live Load per floor: $w_{\text{live}}=60\text{ psf} * 22\text{ ft} = 1320\text{ pounds/ft} = \mathbf{1.32\text{ kips/ft}}$

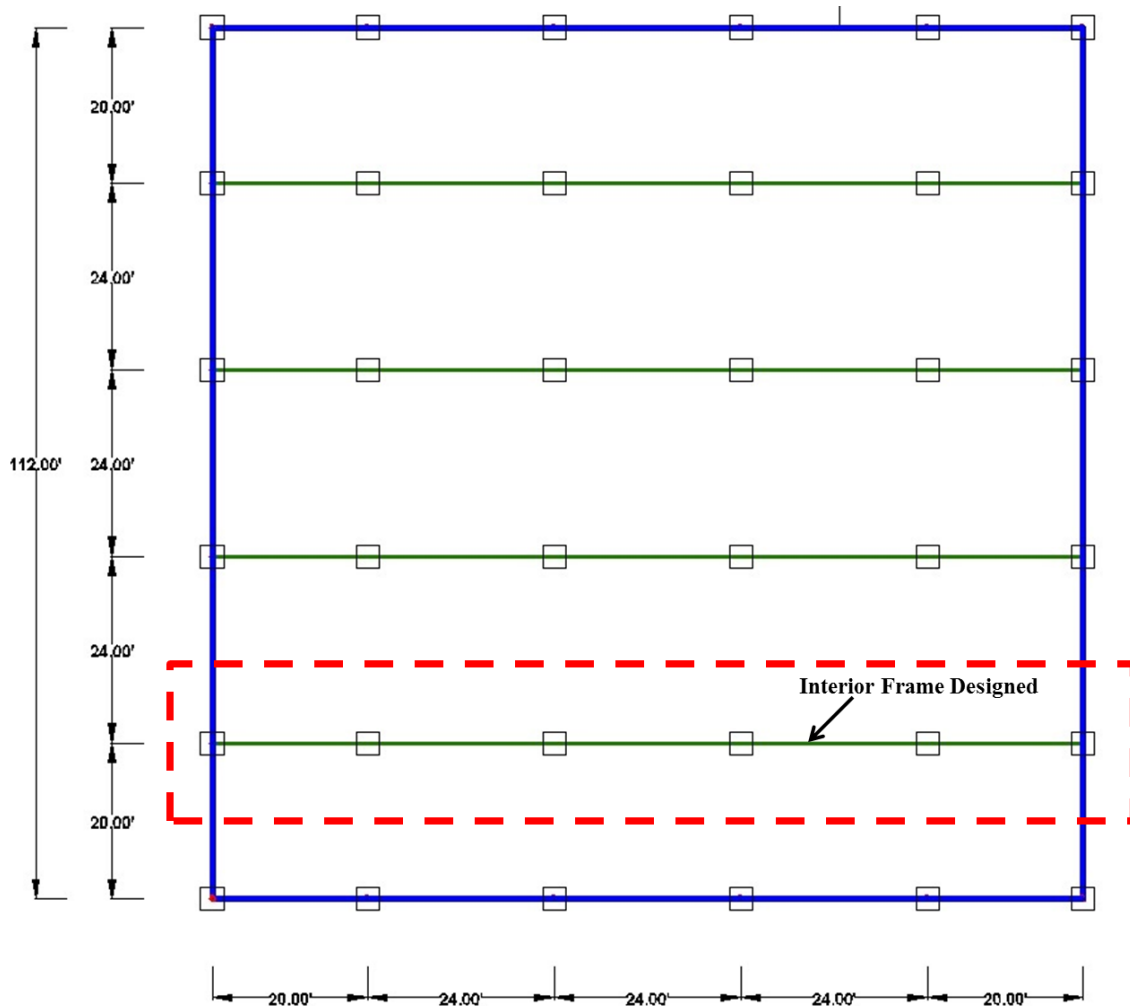


Figure A.2 Plan view of the archetype idealized buildings

A.2.4 Strength Requirements

All designs follow the strength design procedure of ACI 318-11, except the design load combinations, including seismic, were modified. The following specific procedures were used.

- Designs were checked for the following load combinations, with Static_1 and EQ_1 controlling the designs:
 - $1.2*D + 1.6*L$ (Static 1)
 - $1.4*D$ (Static 2)
 - $1.0*D + 0.25*L \pm 1.0*E$ (EQ_1)
 - $0.9*D \pm 1.0*E$ (EQ_2)

, where D = dead load, L = live load, and E = earthquake load.

- The earthquake loading considered for the member design in combinations EQ_1 and EQ_2 was assumed to be equal to 10% of the effective seismic building weight uniformly for all the archetype buildings.
- Member moment design strengths, M_d , were set equal to moment demands obtained from design load combinations including gravity and seismic loads, and then nominal moment strengths, M_n , were defined as $M_n = a_1 M_d / \phi$; ϕ is a resistance factor for tension-controlled members, from ACI 318-11, such that $\phi = 0.90$; a_1 is a modification factor to increase strength due to section oversizing, such that $a_1 = 1.15$. For each value of $M_n = a_1 M_d / \phi$, the required longitudinal reinforcement was determined. If the reinforcement was less than the building code minimum (ACI 318-11), code minimum values were assigned. Finally, effective yield strength for nonlinear analysis was increased to $a_2 M_n$ in which a_2 is a modification factor to increase strength due to material overstrength, such that, $a_2 = 1.15$.
- Transverse reinforcement was selected for every column so that the target value of V_p/V_n was obtained, where V_n corresponds to the shear strength of each column calculated according to ASCE/SEI 41 (ASCE/SEI, 2006) and V_p is the plastic shear demand (controlled by flexure). For the archetype buildings V_p/V_n ratio was selected to be equal to $V_p/V_n = 0.6$. The spacing of transverse reinforcement for the beams in all the buildings was selected to be equal to $d/2$, where d is the beam effective depth.
- Beam-column joints were not considered in the design. It is likely that some of the joint dimensions did not meet current code requirements; however, joint failure was not considered in this study.

A.3. DIMENSIONS AND REINFORCEMENT FOR ARCHETYPE BUILDINGS

To be able to define the moment-rotation behavior for flexural response, the shear failure surface for shear response, and the axial failure surface for axial response, it was considered necessary to select indicative reinforcement that approximated reinforcement that would be required for the design seismic forces.

A.3.1 4-Story Archetype Building

Figure A.3 illustrates an elevation view of the 4-story archetype building.

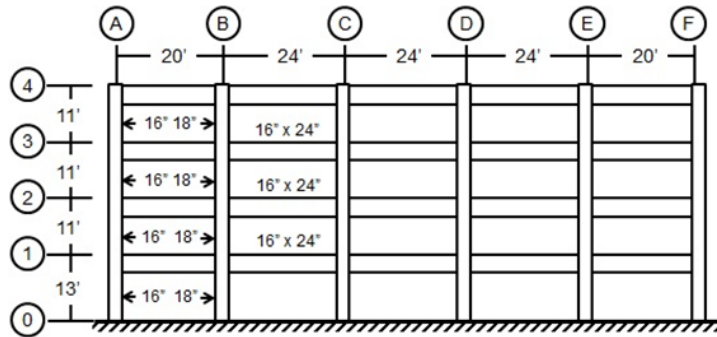


Figure A.3 Schematic elevation view of the 4-story archetype building

The reinforcement schedules of the column and beam members for the 4-story building are provided in Tables A.1-3.

Table A.1 Interior column reinforcement schedule of the 4-story archetype building

Level	Dimensions	Longitudinal Reinforcement	ρ_{long}	Transverse Reinforcement	$\rho_{transverse}$
1	18"x18"	12#8	0.029	#3/3.7" (3-legs)	0.0050
2	18"x18"	10#8	0.024	#3/2.8" (3-legs)	0.0065
3	18"x18"	10#7	0.019	#3/3.4" (3-legs)	0.0054
4	18"x18"	8#7	0.015	#3/4.4" (3-legs)	0.0042

Table A.2 Corner column reinforcement schedule of the 4-story archetype building

Level	Dimensions	Longitudinal Reinforcement	ρ_{long}	Transverse Reinforcement	$\rho_{transverse}$
1	16"x16"	8#7	0.019	#3/6.5" (3-legs)	0.0032
2	16"x16"	8#7	0.019	#3/4.7" (3-legs)	0.0044
3	16"x16"	8#7	0.019	#3/4.6" (3-legs)	0.0045
4	16"x16"	8#7	0.019	#3/4.5" (3-legs)	0.0046

Table A.3 Beam reinforcement schedule of the 4-story archetype building

Level	Dimensions	Longitudinal Reinforcement		ρ_{long}	Transverse Reinforcement	$\rho_{transverse}$
		Top	Bottom			
1	16"x24"	6#7	3#7	0.014	#3/10" (2-legs)	0.0014
2	16"x24"	5#7+1#6	3#7	0.014	#3/10" (2-legs)	0.0014
3	16"x24"	5#7+1#6	2#7+1#6	0.013	#3/10" (2-legs)	0.0014
4	16"x24"	4#7	2#7	0.0095	#3/10" (2-legs)	0.0014

A.3.2 8-Story Archetype Building

Figure A.4 illustrates an elevation view of the 8-story archetype building.

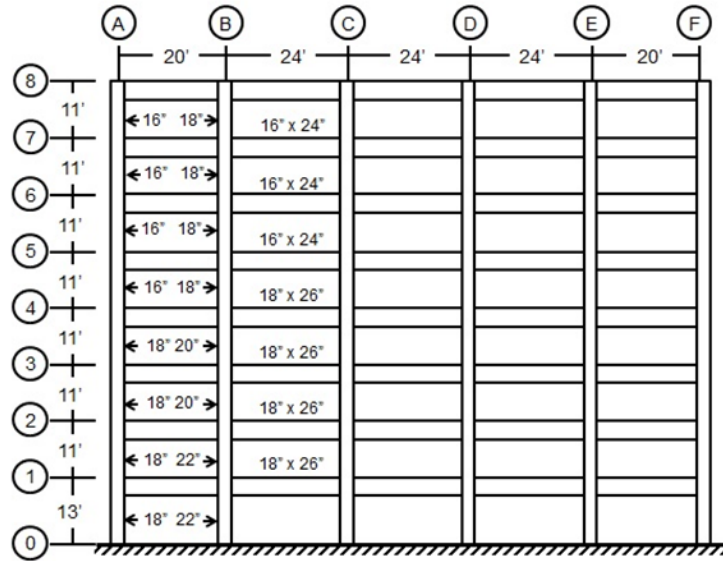


Figure A.4 Schematic elevation view of the 8-story archetype building

The reinforcement schedules of the column and beam members for the 8-story building are provided in Tables A.4-6.

Table A.4 Interior column reinforcement schedule of the 8-story archetype building

Level	Dimensions	Longitudinal Reinforcement	ρ_{long}	Transverse Reinforcement	$\rho_{\text{transverse}}$
1	22"x22"	14#9	0.029	#3/4.0" (4-legs)	0.0050
2	22"x22"	4#9+6#8	0.018	#3/3.1" (4-legs)	0.0065
3	20"x20"	4#9+4#8	0.018	#3/3.4" (4-legs)	0.0065
4	20"x20"	10#9	0.021	#3/2.7" (4-legs)	0.0081
5	18"x18"	4#9+6#8	0.027	#4/4.4" (4-legs)	0.0076
6	18"x18"	4#9+4#8	0.022	#4/4.6" (4-legs)	0.0072
7	18"x18"	4#9+4#8	0.022	#4/5.3" (4-legs)	0.0063
8	18"x18"	4#9	0.012	#4/3.8" (4-legs)	0.0048

Table A.5 Corner column reinforcement schedule of the 8-story archetype building

Level	Dimensions	Longitudinal Reinforcement	ρ_{long}	Transverse Reinforcement	$\rho_{transverse}$
1	18"x18"	4#7+4#6	0.013	#3/5.6" (3-legs)	0.0032
2	18"x18"	4#7+4#6	0.013	#3/3.6" (3-legs)	0.0051
3	18"x18"	8#7	0.015	#3/3.6" (3-legs)	0.0051
4	18"x18"	8#7	0.015	#3/3.9" (3-legs)	0.0047
5	16"x16"	8#7	0.019	#3/4.8" (3-legs)	0.0043
6	16"x16"	8#7	0.019	#3/4.9" (3-legs)	0.0042
7	16"x16"	8#7	0.019	#3/5.7" (3-legs)	0.0036
8	16"x16"	8#6	0.014	#3/6.6" (3-legs)	0.0031

Table A.6 Beam reinforcement schedule of the 8-story archetype building

Level	Dimensions	Longitudinal Reinforcement		ρ_{long}	Transverse Reinforcement	$\rho_{transverse}$
		Top	Bottom			
1	18"x26"	4#8+4#7	3#7+1#6	0.017	#4/11" (2-legs)	0.002
2	18"x26"	4#8+4#7	3#7+1#6	0.017	#4/11" (2-legs)	0.002
3	18"x26"	4#8+4#7	3#7+1#6	0.017	#4/11" (2-legs)	0.002
4	18"x26"	4#8+4#7	3#7+1#6	0.017	#4/11" (2-legs)	0.002
5	16"x24"	3#7+2#6	2#7	0.01	#4/10" (2-legs)	0.0025
6	16"x24"	3#7+2#6	2#7	0.01	#4/10" (2-legs)	0.0025
7	16"x24"	3#7+2#6	2#7	0.01	#4/10" (2-legs)	0.0025
8	16"x24"	3#7+2#6	2#7	0.01	#4/10" (2-legs)	0.0025

A.3.3 12-Story Archetype Building

Figure A.5 illustrates an elevation view of the 12-story archetype building.

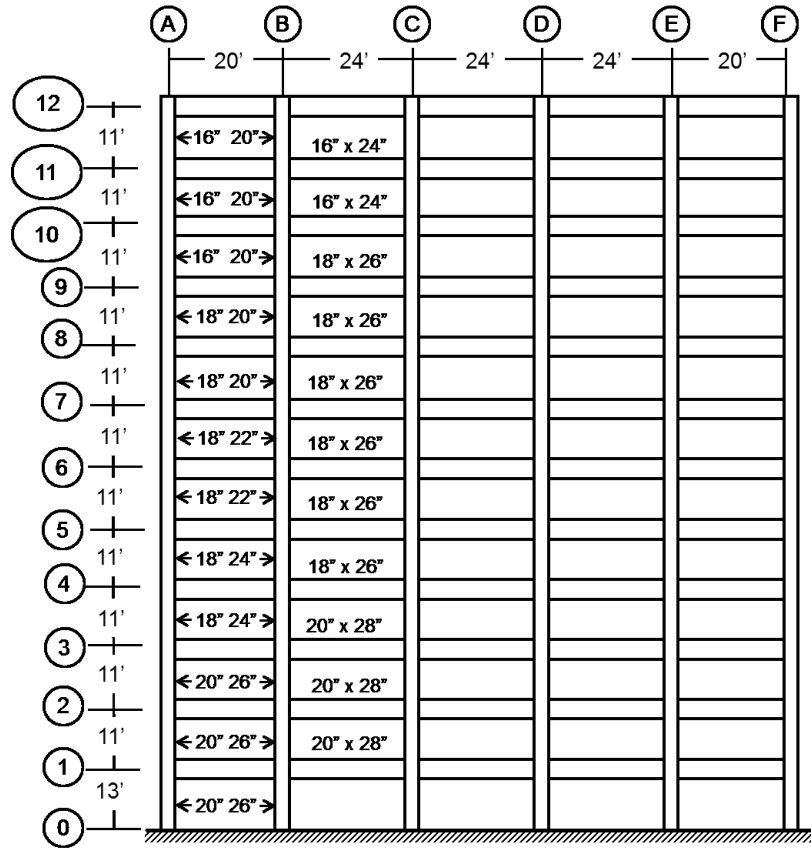


Figure A.5 Schematic elevation view of the 12-story archetype building

The reinforcement schedules of the column and beam members for the 12-story building are provided in Tables A.7-9.

Table A.7 Interior column reinforcement schedule of the 12-story archetype building

Level	Dimensions	Longitudinal Reinforcement	ρ_{long}	Transverse Reinforcement	$\rho_{transverse}$
1	26"x26"	18#9	0.027	#3/3.2" (4-legs)	0.0053
2	26"x26"	12#8	0.014	#3/3.0" (4-legs)	0.0056
3	26"x26"	6#9+6#8	0.016	#3/2.4" (4-legs)	0.0071
4	24"x24"	6#9+6#9	0.019	#3/2.8" (4-legs)	0.0065
5	24"x24"	8#9+4#8	0.019	#3/2.7" (4-legs)	0.0066
6	22"x22"	8#9+4#8	0.023	#3/3.0" (4-legs)	0.0067
7	22"x22"	6#9+6#8	0.022	#3/2.6" (4-legs)	0.0077
8	20"x20"	6#9+6#8	0.027	#3/3.0" (4-legs)	0.0073
9	20"x20"	4#9+6#8	0.022	#3/2.9" (4-legs)	0.0076
10	20"x20"	12#8	0.024	#3/3.2" (4-legs)	0.0069
11	20"x20"	4#8+8#7	0.020	#3/3.6" (4-legs)	0.0061
12	20"x20"	4#8+4#7	0.014	#3/4.1" (4-legs)	0.0054

Table A.8 Corner column reinforcement schedule of the 12-story archetype building

Level	Dimensions	Longitudinal Reinforcement	ρ_{long}	Transverse Reinforcement	$\rho_{transverse}$
1	20"x20"	4#8+4#7	0.014	#3/3.7" (3-legs)	0.0045
2	20"x20"	4#8+4#7	0.014	#3/4.1" (3-legs)	0.0040
3	20"x20"	4#9+4#8	0.018	#3/4.1" (3-legs)	0.0040
4	18"x18"	4#9+4#8	0.022	#3/2.9" (3-legs)	0.0063
5	18"x18"	4#9+4#8	0.022	#3/2.9" (3-legs)	0.0063
6	18"x18"	4#9+4#8	0.022	#3/3.0" (3-legs)	0.0061
7	18"x18"	8#8	0.020	#3/3.3" (3-legs)	0.0056
8	18"x18"	8#8	0.020	#3/3.7" (3-legs)	0.0050
9	18"x18"	4#8+4#7	0.017	#3/4.3" (3-legs)	0.0043
10	16"x16"	4#8+4#7	0.022	#3/5.3" (3-legs)	0.0035
11	16"x16"	8#7	0.019	#3/6.3" (3-legs)	0.0029
12	16"x16"	4#7+4#6	0.016	#3/6.7" (3-legs)	0.0027

Table A.9 Beam reinforcement schedule of the 12-story archetype building

Level	Dimensions	Longitudinal Reinforcement		ρ_{long}	Transverse Reinforcement	$\rho_{transverse}$
		Top	Bottom			
1	20"x28"	8#8	2#8+2#7	0.016	#4/12" (2-legs)	0.0017
2	20"x28"	8#8	2#8+2#7	0.016	#4/12" (2-legs)	0.0017
3	20"x28"	6#8+3#7	2#8+2#7	0.017	#4/12" (2-legs)	0.0017
4	18"x26"	4#8+3#7	2#8+2#7	0.017	#4/11" (2-legs)	0.002
5	18"x26"	8#8	1#8+3#7	0.019	#4/11" (2-legs)	0.002
6	18"x26"	4#8+4#7	4#7	0.017	#4/11" (2-legs)	0.002
7	18"x26"	2#8+6#7	3#7+1#6	0.016	#4/11" (2-legs)	0.002
8	18"x26"	8#7	3#7+1#6	0.015	#4/11" (2-legs)	0.002
9	18"x26"	8#7	3#7	0.015	#4/11" (2-legs)	0.002
10	16"x24"	6#7	3#7	0.014	#4/10" (2-legs)	0.0025
11	16"x24"	5#7	3#7	0.013	#4/10" (2-legs)	0.0025
12	16"x24"	4#7	3#7	0.011	#4/10" (2-legs)	0.0025

A.4. BUILDING MODEL VARIATIONS OF ARCHETYPE BUILDINGS

As mentioned in section A.2.4 for the archetype buildings the transverse reinforcement ratio was selected such that $V_p/V_n=0.6$ uniformly for all column members of the considered buildings. The archetype building models were sequentially weakened by modifying transverse reinforcement and column to beam bending moment strength ratio to test the sensitivity of collapse performance to these parameters.

The modification of beam bending moment strength ratio was performed by decreasing the bending moment strength of the beam members but leaving their member dimensions the same (this change is equivalent to modifying the longitudinal transverse reinforcement ratio).

The modification of transverse reinforcement ratio was performed such that the parameter V_p/V_n equals 0.8, 1.0 and 1.2 uniformly for all the column members (the V_p/V_n ratio of beam members was not modified).

In the section below, the reinforcement and modeling details for variations of the considered archetype buildings for $V_p/V_n=0.6$ (Archetype building), 0.8,1.0 and 1.2 are provided.

A.4.1 4-Story Building Column Transverse Reinforcement Variations

Details regarding the transverse reinforcement and modeling parameters of the column members for the 4-story building are provided in Tables A.10-13.

Table A.10 Reinforcement and modeling parameter details of the 4-story building for the case of $V_p/V_n=0.6$ (Archetype 4-story building)

		Dimensions	spacing (in)	Ast,transv (in ²)	ρsh	Vn(ASCE41)	Vp/Vn	θcap, pl	θpc	λ
1st Story	Interior	18"x18"	3.70	0.33	0.0050	112.47	0.60	0.049	0.083	79.32
	Corner	16"x16"	6.50	0.33	0.0032	59.95	0.60	0.052	0.096	56.33
2nd Story	Interior	18"x18"	2.80	0.33	0.0065	128.68	0.60	0.062	0.100	98.12
	Corner	16"x16"	4.70	0.33	0.0044	71.33	0.60	0.062	0.100	77.94
3rd Story	Interior	18"x18"	3.40	0.33	0.0054	108.82	0.60	0.062	0.100	97.04
	Corner	16"x16"	4.60	0.33	0.0045	70.87	0.60	0.064	0.100	81.12
4th Story	Interior	18"x18"	4.40	0.33	0.0042	87.29	0.60	0.060	0.100	90.51
	Corner	16"x16"	4.50	0.33	0.0046	69.97	0.60	0.067	0.100	84.89

Table A.11 Reinforcement and modeling parameter details of the 4-story building for the case of $V_p/V_n=0.8$

		Dimensions	spacing (in)	Ast,transv (in ²)	ρsh	Vn(ASCE41)	Vp/Vn	Drshear,Elwood
1st Story	Interior	18"x18"	6.70	0.33	0.0027	83.72	0.80	0.029
	Corner	16"x16"	12.00	0.33	0.0017	45.05	0.80	0.031
2nd Story	Interior	18"x18"	4.50	0.33	0.0041	96.62	0.80	0.035
	Corner	16"x16"	7.60	0.33	0.0027	54.18	0.80	0.034
3rd Story	Interior	18"x18"	5.60	0.33	0.0033	81.37	0.80	0.034
	Corner	16"x16"	7.60	0.33	0.0027	52.74	0.80	0.035
4th Story	Interior	18"x18"	7.30	0.33	0.0025	65.83	0.80	0.034
	Corner	16"x16"	7.20	0.33	0.0029	52.37	0.80	0.036

Table A.12 Reinforcement and modeling parameter details of the 4-story building for the case of $V_p/V_n=1.0$

		Dimensions	spacing (in)	Ast,transv (in ²)	ρsh	Vn(ASCE41)	Vp/Vn	Drshear,Elwood
1st Story	Interior	18"x18"	12.50	0.33	0.0015	67.27	1.00	0.024
	Corner	16"x16"	11.00	0.15	0.0008	36.07	1.00	0.027
2nd Story	Interior	18"x18"	7.10	0.33	0.0026	77.29	1.00	0.029
	Corner	16"x16"	12.50	0.33	0.0017	43.29	1.00	0.030
3rd Story	Interior	18"x18"	8.90	0.33	0.0021	65.64	1.00	0.029
	Corner	16"x16"	12.30	0.33	0.0017	42.12	1.01	0.031
4th Story	Interior	18"x18"	12.50	0.33	0.0015	52.29	1.00	0.030
	Corner	16"x16"	11.10	0.33	0.0019	42.07	1.00	0.032

Table A.13 Reinforcement and modeling parameter details of the 4-story building for the case of $V_p/V_n=1.2$

		Dimensions	spacing (in)	Ast,transv (in ²)	ρsh	Vn(ASCE41)	Vp/Vn	Drshear,Elwood
1st Story	Interior	18"x18"	9.20	0.10	0.0006	56.01	1.20	0.021
	Corner	16"x16"	24.00	0.10	0.0003	30.09	1.20	0.025
2nd Story	Interior	18"x18"	7.80	0.22	0.0016	64.13	1.20	0.025
	Corner	16"x16"	14.40	0.22	0.0010	36.17	1.20	0.027
3rd Story	Interior	18"x18"	10.20	0.22	0.0012	54.47	1.20	0.026
	Corner	16"x16"	13.70	0.22	0.0010	35.23	1.20	0.028
4th Story	Interior	18"x18"	10.30	0.15	0.0008	43.63	1.20	0.027
	Corner	16"x16"	11.80	0.22	0.0012	34.97	1.20	0.029

A.4.2 8-Story Building Column Transverse Reinforcement Variations

Details regarding the transverse reinforcement and modeling parameters of the column members for the 8-story building are provided in Tables A.14-17.

Table A.14 Reinforcement and modeling parameter details of the 8-story building for the case of $V_p/V_n=0.6$ (Archetype 8-story building)

		Dimensions	spacing (in)	Ast,transv (in ²)	ρ_{sh}	Vn(ASCE41)	Vp/Vn	$\theta_{cap,pl}$	θ_{pc}	λ
1st Story	Interior	22"x22"	4.00	0.44	0.0050	176.14	0.60	0.044	0.065	77.93
	Corner	18"x18"	5.60	0.33	0.0033	76.79	0.60	0.053	0.100	74.67
2nd Story	Interior	22"x22"	3.10	0.44	0.0065	200.37	0.60	0.053	0.098	91.29
	Corner	18"x18"	3.60	0.33	0.0051	100.30	0.60	0.066	0.100	100.59
3rd Story	Interior	20"x20"	3.40	0.44	0.0065	166.89	0.60	0.052	0.094	82.83
	Corner	18"x18"	3.60	0.33	0.0051	100.10	0.60	0.066	0.100	100.85
4th Story	Interior	20"x20"	2.70	0.44	0.0081	189.88	0.60	0.063	0.100	96.44
	Corner	18"x18"	3.90	0.33	0.0047	94.63	0.60	0.064	0.100	96.96
5th Story	Interior	18"x18"	4.40	0.60	0.0076	146.25	0.60	0.061	0.100	71.74
	Corner	16"x16"	4.80	0.33	0.0043	71.37	0.60	0.060	0.100	75.39
6th Story	Interior	18"x18"	4.60	0.60	0.0072	137.62	0.60	0.066	0.100	75.24
	Corner	16"x16"	4.90	0.33	0.0042	69.50	0.60	0.060	0.100	75.31
7th Story	Interior	18"x18"	5.30	0.60	0.0063	120.39	0.60	0.067	0.100	73.24
	Corner	16"x16"	5.70	0.33	0.0036	62.12	0.60	0.058	0.100	67.12
8th Story	Interior	18"x18"	3.80	0.33	0.0048	95.80	0.60	0.065	0.100	98.96
	Corner	16"x16"	6.60	0.33	0.0031	55.12	0.60	0.056	0.100	59.26

Table A.15 Reinforcement and modeling parameter details of the 8-story building for the case of $V_p/V_n=0.8$

		Dimensions	spacing (in)	Ast,transv (in ²)	ρ_{sh}	Vn(ASCE41)	Vp/Vn	Drshear,Elwood
1st Story	Interior	22"x22"	7.30	0.44	0.0027	132.38	0.80	0.027
	Corner	18"x18"	10.50	0.33	0.0017	56.99	0.80	0.031
2nd Story	Interior	22"x22"	5.10	0.44	0.0039	151.38	0.80	0.032
	Corner	18"x18"	5.90	0.33	0.0031	74.57	0.80	0.035
3rd Story	Interior	20"x20"	5.70	0.44	0.0039	125.12	0.80	0.032
	Corner	18"x18"	5.70	0.33	0.0032	75.79	0.80	0.036
4th Story	Interior	20"x20"	4.30	0.44	0.0051	141.37	0.80	0.037
	Corner	18"x18"	6.40	0.33	0.0029	70.83	0.80	0.035
5th Story	Interior	18"x18"	7.00	0.60	0.0048	109.78	0.80	0.036
	Corner	16"x16"	8.00	0.33	0.0026	53.77	0.80	0.034
6th Story	Interior	18"x18"	7.30	0.60	0.0046	102.89	0.80	0.037
	Corner	16"x16"	8.30	0.33	0.0025	51.85	0.80	0.034
7th Story	Interior	18"x18"	8.30	0.60	0.0040	90.93	0.80	0.037
	Corner	16"x16"	9.80	0.33	0.0021	46.62	0.80	0.033
8th Story	Interior	18"x18"	11.30	0.60	0.0029	71.50	0.80	0.035
	Corner	16"x16"	11.50	0.33	0.0018	41.49	0.80	0.033

Table A.16 Reinforcement and modeling parameter details of the 8-story building for the case of $V_p/V_n=1.0$

		Dimensions	spacing (in)	Ast,transv (in ²)	ρ_{sh}	Vn(ASCE41)	Vp/Vn	Drshear,Elwood
1st Story	Interior	22"x22"	11.00	0.33	0.0014	106.04	1.00	0.022
	Corner	18"x18"	9.50	0.15	0.0009	45.50	1.00	0.028
2nd Story	Interior	22"x22"	8.60	0.44	0.0023	120.49	1.00	0.026
	Corner	18"x18"	9.30	0.33	0.0020	59.85	1.00	0.031
3rd Story	Interior	20"x20"	9.70	0.44	0.0023	99.65	1.00	0.025
	Corner	18"x18"	9.00	0.33	0.0020	60.50	1.00	0.031
4th Story	Interior	20"x20"	6.50	0.44	0.0034	113.66	1.00	0.030
	Corner	18"x18"	10.50	0.33	0.0017	56.33	1.00	0.030
5th Story	Interior	18"x18"	11.00	0.60	0.0030	87.34	1.00	0.029
	Corner	16"x16"	9.00	0.22	0.0015	43.01	1.00	0.029
6th Story	Interior	18"x18"	11.20	0.60	0.0030	82.28	1.00	0.030
	Corner	16"x16"	9.50	0.22	0.0014	41.22	1.00	0.030
7th Story	Interior	18"x18"	13.00	0.60	0.0026	72.12	1.00	0.031
	Corner	16"x16"	11.50	0.22	0.0012	37.31	1.00	0.029
8th Story	Interior	18"x18"	10.00	0.33	0.0018	57.03	1.00	0.031
	Corner	16"x16"	14.00	0.22	0.0010	33.18	1.00	0.029

Table A.17 Reinforcement and modeling parameter details of the 8-story building for the case of $V_p/V_n=1.2$

		Dimensions	spacing (in)	Ast,transv (in ²)	psh	Vn(ASCE41)	Vp/Vn	Drshear,Elwood
1st Story	Interior	22"x22"	14.80	0.15	0.0005	88.08	1.20	0.018
	Corner	18"x18"	19.00	0.10	0.0003	38.11	1.20	0.025
2nd Story	Interior	22"x22"	11.40	0.33	0.0013	100.94	1.20	0.022
	Corner	18"x18"	15.30	0.33	0.0012	49.83	1.20	0.028
3rd Story	Interior	20"x20"	13.00	0.33	0.0013	83.67	1.20	0.021
	Corner	18"x18"	14.60	0.33	0.0013	50.38	1.20	0.028
4th Story	Interior	20"x20"	10.30	0.44	0.0021	93.68	1.20	0.025
	Corner	18"x18"	17.50	0.33	0.0010	47.28	1.20	0.027
5th Story	Interior	18"x18"	9.50	0.33	0.0019	73.08	1.20	0.024
	Corner	16"x16"	16.00	0.22	0.0009	36.17	1.20	0.027
6th Story	Interior	18"x18"	9.50	0.33	0.0019	68.72	1.20	0.026
	Corner	16"x16"	11.50	0.15	0.0008	34.58	1.20	0.027
7th Story	Interior	18"x18"	11.00	0.33	0.0017	60.48	1.20	0.027
	Corner	16"x16"	15.50	0.15	0.0006	31.14	1.20	0.027
8th Story	Interior	18"x18"	16.50	0.33	0.0011	47.67	1.20	0.028
	Corner	16"x16"	14.00	0.10	0.0004	27.65	1.20	0.027

A.4.3 12-Story Building Column Transverse Reinforcement Variations

Details regarding the transverse reinforcement and modeling parameters of the column members for the 12-story building are provided in Tables A.18-21.

Table A.18 Reinforcement and modeling parameter details of the 12-story building for the case of $V_p/V_n=0.6$ (Archetype 12-story building)

		Dimensions	spacing (in)	Ast,transv (in ²)	ρ_{sh}	Vn(ASCE41)	Vp/Vn	$\theta_{cap,pl}$	θ_{pc}	λ
1st Story	Interior	26"x26"	3.20	0.44	0.0053	256.77	0.61	0.043	0.063	88.68
	Corner	20"x20"	3.70	0.33	0.0045	108.83	0.60	0.065	0.100	110.86
2nd Story	Interior	26"x26"	3.00	0.44	0.0056	262.66	0.61	0.047	0.075	93.77
	Corner	20"x20"	4.10	0.33	0.0040	102.89	0.81	0.061	0.100	104.15
3rd Story	Interior	26"x26"	2.40	0.44	0.0071	297.16	0.60	0.055	0.100	102.99
	Corner	20"x20"	4.10	0.33	0.0040	103.76	0.80	0.061	0.100	103.26
4th Story	Interior	24"x24"	2.80	0.44	0.0065	243.69	0.61	0.051	0.090	94.29
	Corner	18"x18"	2.90	0.33	0.0063	115.69	0.60	0.074	0.100	112.41
5th Story	Interior	24"x24"	2.70	0.44	0.0068	245.23	0.60	0.055	0.100	99.69
	Corner	18"x18"	2.90	0.33	0.0063	115.98	0.60	0.073	0.100	111.98
6th Story	Interior	22"x22"	3.00	0.44	0.0067	204.86	0.61	0.054	0.100	91.97
	Corner	18"x18"	3.00	0.33	0.0061	113.45	0.61	0.072	0.100	110.04
7th Story	Interior	22"x22"	2.60	0.44	0.0077	220.69	0.60	0.062	0.100	101.51
	Corner	18"x18"	3.30	0.33	0.0056	106.19	0.60	0.069	0.100	105.33
8th Story	Interior	20"x20"	3.00	0.44	0.0073	176.88	0.61	0.060	0.100	92.65
	Corner	18"x18"	3.70	0.33	0.0050	98.06	0.60	0.065	0.100	99.70
9th Story	Interior	20"x20"	2.90	0.44	0.0076	176.63	0.61	0.066	0.100	99.94
	Corner	18"x18"	4.30	0.33	0.0043	88.44	0.60	0.061	0.100	91.99
10th Story	Interior	20"x20"	3.20	0.44	0.0069	160.69	0.61	0.067	0.100	102.14
	Corner	16"x16"	5.30	0.33	0.0035	77.04	0.60	0.056	0.100	80.26
11th Story	Interior	20"x20"	3.60	0.44	0.0061	143.18	0.61	0.069	0.100	103.35
	Corner	16"x16"	6.30	0.33	0.0029	68.52	0.60	0.053	0.100	70.38
12th Story	Interior	20"x20"	4.10	0.44	0.0054	125.26	0.60	0.070	0.100	103.22
	Corner	16"x16"	6.70	0.33	0.0027	64.18	0.60	0.053	0.100	67.94

Table A.19 Reinforcement and modeling parameter details of the 12-story building for the case of $V_p/V_n=0.8$

		Dimensionns	spacing (in)	Ast,transv (in ²)	psh	Vn(ASCE41)	Vp/Vn	Drshear,Elwood
1st Story	Interior	26"x26"	5.60	0.44	0.0030	195.49	0.80	0.028
	Corner	20"x20"	6.00	0.33	0.0028	81.48	0.80	0.035
2nd Story	Interior	26"x26"	5.20	0.44	0.0033	198.13	0.81	0.029
	Corner	20"x20"	4.00	0.33	0.0041	104.50	0.80	0.039
3rd Story	Interior	26"x26"	4.00	0.44	0.0042	220.89	0.80	0.033
	Corner	20"x20"	4.10	0.33	0.0040	103.76	0.80	0.039
4th Story	Interior	24"x24"	4.70	0.44	0.0039	182.71	0.81	0.031
	Corner	18"x18"	4.50	0.33	0.0041	86.56	0.80	0.038
5th Story	Interior	24"x24"	4.50	0.44	0.0041	182.65	0.80	0.033
	Corner	18"x18"	4.50	0.33	0.0041	86.85	0.81	0.038
6th Story	Interior	22"x22"	4.80	0.44	0.0042	156.46	0.80	0.033
	Corner	18"x18"	4.60	0.33	0.0040	85.90	0.80	0.038
7th Story	Interior	22"x22"	4.20	0.44	0.0048	163.96	0.81	0.036
	Corner	18"x18"	5.30	0.33	0.0035	79.02	0.80	0.036
8th Story	Interior	20"x20"	4.70	0.44	0.0047	134.44	0.80	0.035
	Corner	18"x18"	6.10	0.33	0.0030	72.80	0.80	0.035
9th Story	Interior	20"x20"	4.50	0.44	0.0049	133.48	0.80	0.037
	Corner	18"x18"	7.20	0.33	0.0025	66.18	0.80	0.034
10th Story	Interior	20"x20"	5.00	0.44	0.0044	121.09	0.80	0.037
	Corner	16"x16"	9.40	0.33	0.0020	57.49	0.80	0.032
11th Story	Interior	20"x20"	5.60	0.44	0.0039	108.26	0.81	0.037
	Corner	16"x16"	11.50	0.33	0.0016	51.46	0.80	0.032
12th Story	Interior	20"x20"	6.40	0.44	0.0034	94.41	0.80	0.037
	Corner	16"x16"	12.00	0.33	0.0015	48.51	0.80	0.032

Table A.20 Reinforcement and modeling parameter details of the 12-story building for the case of $V_p/V_n=1.0$

		Dimensionns	spacing (in)	Ast,transv (in ²)	ρsh	Vn(ASCE41)	Vp/Vn	Drshear,Elwood
1st Story	Interior	26"x26"	11.00	0.44	0.0015	155.37	1.00	0.022
	Corner	20"x20"	9.50	0.33	0.0017	65.27	1.00	0.031
2nd Story	Interior	26"x26"	9.20	0.44	0.0018	159.87	1.00	0.023
	Corner	20"x20"	6.00	0.33	0.0028	82.50	1.01	0.034
3rd Story	Interior	26"x26"	6.50	0.44	0.0026	176.89	1.00	0.026
	Corner	20"x20"	6.00	0.33	0.0028	83.37	1.00	0.034
4th Story	Interior	24"x24"	7.80	0.44	0.0024	146.99	1.01	0.025
	Corner	18"x18"	6.60	0.33	0.0028	69.76	1.00	0.033
5th Story	Interior	24"x24"	7.30	0.44	0.0025	146.65	1.00	0.026
	Corner	18"x18"	6.60	0.33	0.0028	70.05	1.00	0.033
6th Story	Interior	22"x22"	7.90	0.44	0.0025	124.81	1.00	0.026
	Corner	18"x18"	6.90	0.33	0.0027	68.68	1.00	0.033
7th Story	Interior	22"x22"	6.40	0.44	0.0031	132.27	1.00	0.029
	Corner	18"x18"	8.20	0.33	0.0022	63.17	1.01	0.031
8th Story	Interior	20"x20"	7.50	0.44	0.0029	106.48	1.01	0.028
	Corner	18"x18"	9.70	0.33	0.0019	58.34	1.00	0.031
9th Story	Interior	20"x20"	6.80	0.44	0.0032	107.02	1.00	0.031
	Corner	18"x18"	11.90	0.33	0.0015	53.15	1.00	0.030
10th Story	Interior	20"x20"	7.70	0.44	0.0029	96.40	1.01	0.031
	Corner	16"x16"	11.50	0.22	0.0011	45.99	1.00	0.029
11th Story	Interior	20"x20"	8.50	0.44	0.0026	86.82	1.01	0.032
	Corner	16"x16"	15.50	0.22	0.0008	41.02	1.00	0.029
12th Story	Interior	20"x20"	9.80	0.44	0.0022	75.32	1.00	0.032
	Corner	16"x16"	16.50	0.22	0.0007	38.31	1.01	0.029

Table A.21 Reinforcement and modeling parameter details of the 12-story building for the case of $V_p/V_n=1.2$

		Dimensionns	spacing (in)	Ast,transv (in ²)	ρsh	Vn(ASCE41)	Vp/Vn	Drshear,Elwood
1st Story	Interior	26"x26"	22.00	0.33	0.0006	129.37	1.21	0.018
	Corner	20"x20"	15.50	0.33	0.0011	54.51	1.20	0.029
2nd Story	Interior	26"x26"	20.00	0.44	0.0008	133.01	1.20	0.019
	Corner	20"x20"	8.70	0.33	0.0019	68.84	1.21	0.030
3rd Story	Interior	26"x26"	11.30	0.44	0.0015	146.98	1.20	0.022
	Corner	20"x20"	8.80	0.33	0.0019	69.37	1.20	0.030
4th Story	Interior	24"x24"	14.00	0.44	0.0013	123.01	1.20	0.021
	Corner	18"x18"	10.00	0.33	0.0018	57.52	1.21	0.029
5th Story	Interior	24"x24"	13.00	0.44	0.0014	121.28	1.21	0.022
	Corner	18"x18"	9.80	0.33	0.0019	58.29	1.20	0.029
6th Story	Interior	22"x22"	14.00	0.44	0.0014	103.45	1.20	0.022
	Corner	18"x18"	10.40	0.33	0.0018	57.10	1.20	0.029
7th Story	Interior	22"x22"	10.10	0.44	0.0020	110.11	1.20	0.024
	Corner	18"x18"	12.60	0.33	0.0015	53.05	1.20	0.028
8th Story	Interior	20"x20"	11.80	0.44	0.0019	89.38	1.20	0.024
	Corner	18"x18"	16.00	0.33	0.0011	48.70	1.20	0.028
9th Story	Interior	20"x20"	10.40	0.44	0.0021	89.10	1.20	0.026
	Corner	18"x18"	14.50	0.22	0.0008	44.10	1.20	0.027
10th Story	Interior	20"x20"	11.60	0.44	0.0019	81.03	1.20	0.027
	Corner	16"x16"	11.70	0.10	0.0005	38.31	1.20	0.026
11th Story	Interior	20"x20"	12.80	0.44	0.0017	72.90	1.20	0.028
	Corner	16"x16"	16.00	0.10	0.0003	34.20	1.20	0.026
12th Story	Interior	20"x20"	11.30	0.33	0.0015	62.77	1.20	0.029
	Corner	16"x16"	16.00	0.10	0.0003	32.28	1.20	0.027

B. Recalibration of Haselton et al. Flexure-Controlled Model Parameters

The current study used the equations provided in Haselton et al. (2008) to define the structural parameters of the flexure-controlled models ($V_p/V_n=0.6$). As such, it was decided to recalibrate the coefficients of the model to exclude data for which $V_p/V_n > 0.7$ and for which flexure-shear failure was reported.

The re-calibration was performed by Dr. A. Liel and her colleagues (ATC-78,2013). The results were provided to the authors as personal communication.

The updated equations used in the current study are cited below:

Equation for Plastic Rotation Capacity

Original

$$\theta_{cap,pl} = (0.13)(1 + 0.55a_{sl})(0.13)^v(0.02 + 40\rho_{sh})^{0.65}(0.99412)^{f'_c}, \quad (\text{Eq. B.1})$$

Revised

$$\theta_{cap,pl} = (0.13)(1 + 0.55a_{sl})(0.16)^v(0.02 + 40\rho_{sh})^{0.55}(0.99412)^{f'_c}, \quad (\text{Eq. B.2})$$

Equation for Post-Capping Rotation Capacity

Original

$$\theta_{pc} = (0.76)(0.031)^v (0.02 + 40\rho_{sh})^{1.02}, \quad (\text{Eq. B.3})$$

Revised

$$\theta_{pc} = (1.13)(0.018)^v (0.02 + 40\rho_{sh})^{1.14}, \quad (\text{Eq. B.4})$$

Equation for Cyclic Deteriotation

Original

$$\lambda = (170.7)(0.27)^v (0.10)^{s/d}, \quad (\text{Eq. B.5})$$

Revised

$$\lambda = (189)(0.23)^v (0.10)^{s/d}, \quad (\text{Eq. B.6})$$

Compared with the original equations, the recalibrated equations are increased in plastic rotation capacity, post-capping rotation capacity, and energy dissipation capacity.

C. Eigenvalue Analysis of the Studied Buildings

In the current section, eigenvalue analysis was performed for the idealized buildings developed for the purpose of the current study. The eigenvalue analyses were performed using OpenSees structural analysis software. The results of the analyses are presented below:

C.1 Eigenvalue Analysis of the 4-Story Building

The results of eigenvalue analysis for the 4-story idealized building are presented below:

- Fundamental Period, $T_1 = 1.14$ sec
- Participation factor, $\Gamma_1 = 1.23$
- Effective Mass (1st mode), $M_{1,eff} / M_{total} = 0.91$
- Effective Mass (2nd mode), $M_{2,eff} / M_{total} = 0.07$
- Effective Height (1st mode), $h_{1,eff} / h_{total} = 0.72$

Figure C.1 presents the eigenvectors of the 1st and 2nd mode for the 4-story idealized building.

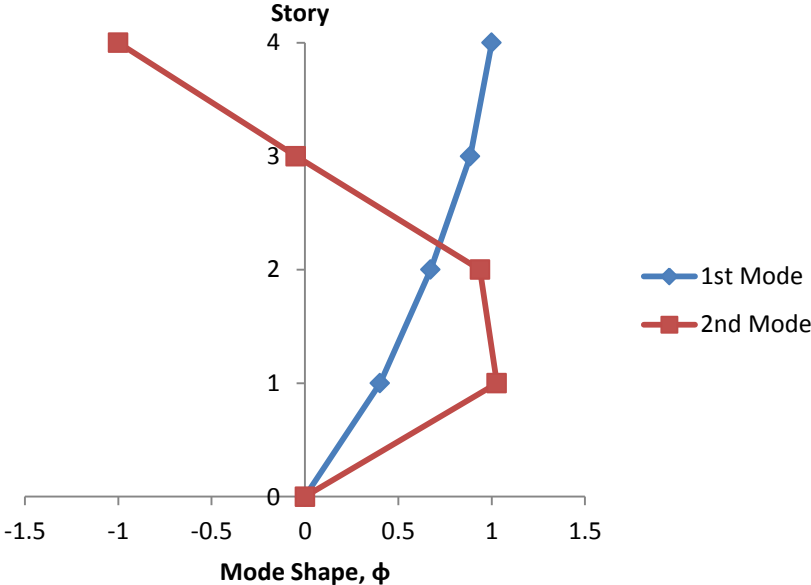


Figure C.1 Eigenvectors of 1st and 2nd modes, 4-story building

C.2 Eigenvalue Analysis of the 8-Story Building

The results of eigenvalue analysis for the 8-story idealized building are presented below:

- Fundamental Period, $T_1 = 1.69$ sec
- Participation factor, $\Gamma_1 = 1.34$
- Effective Mass (1st mode), $M_{1,eff} / M_{total} = 0.81$
- Effective Mass (2nd mode), $M_{2,eff} / M_{total} = 0.13$
- Effective Height (1st mode), $h_{1,eff} / h_{total} = 0.71$

Figure C.1 presents the eigenvectors of the 1st and 2nd mode for the 4-story idealized building.

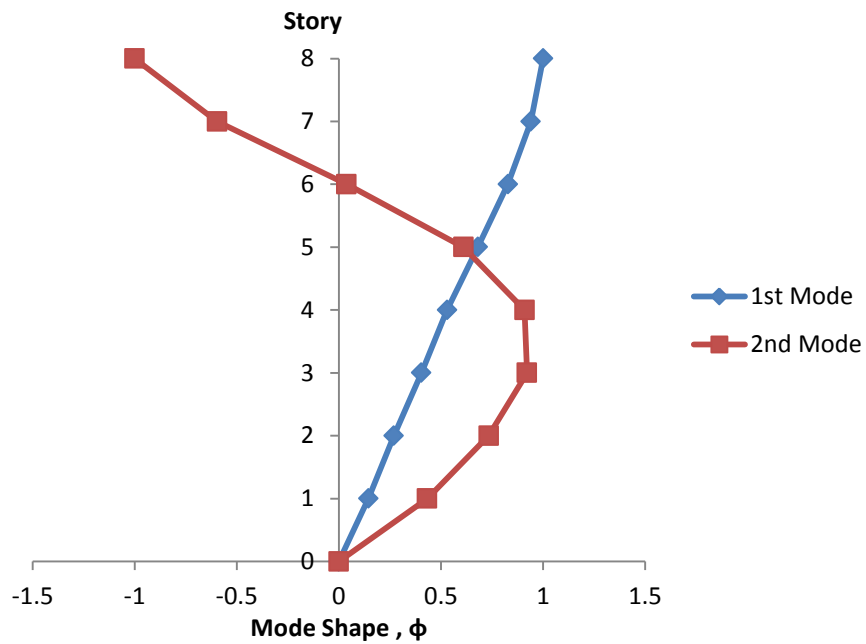


Figure C.2 Eigenvectors of 1st and 2nd modes, 8-story building

C.3 Eigenvalue Analysis of the 12-Story Building

The results of eigenvalue analysis for the 12-story idealized building are presented below:

- Fundamental Period, $T_1 = 1.95$ sec
- Participation factor, $\Gamma_1 = 1.39$
- Effective Mass (1st mode), $M_{1,\text{eff}} / M_{\text{total}} = 0.76$
- Effective Mass (2nd mode), $M_{2,\text{eff}} / M_{\text{total}} = 0.16$
- Effective Height (1st mode), $h_{1,\text{eff}} / h_{\text{total}} = 0.71$

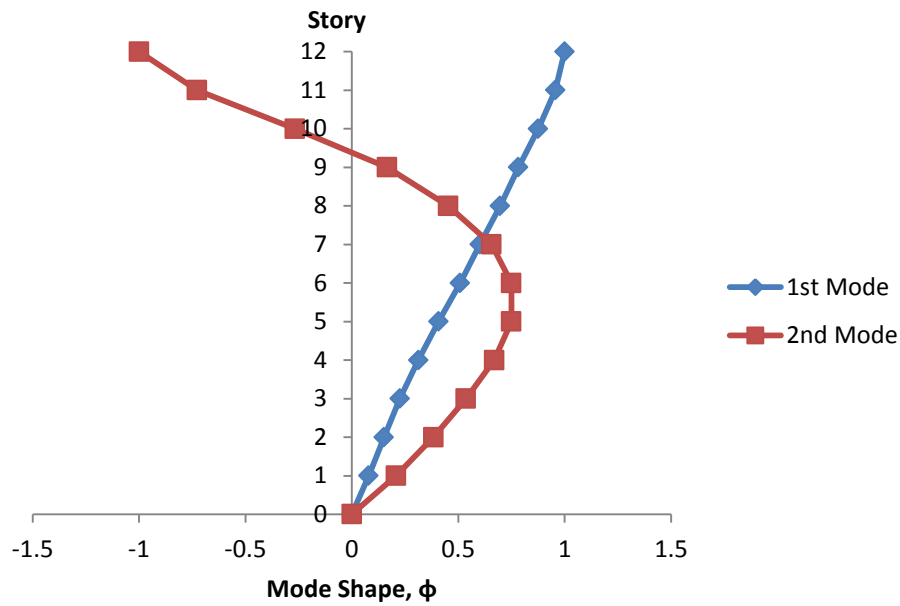


Figure C.3 Eigenvectors of 1st and 2nd modes, 12-story building

D. An Approximate Procedure to Estimate the Base Shear Capacity of Concrete Frame Buildings

The approximate procedure to estimate the base shear capacity of concrete frame buildings was developed by Dr. M. Mehrain as part of the ATC-78 project (2013, 2014). A simplified version of the suggested procedure is presented below.

In this method, the first step corresponds to estimation of the shear capacity of each story of the studied building. Consequently the story capacities are used to estimate the base shear capacity.

The story shear capacity x is estimated as the sum of the individual column plastic capacities, V_{pcx} at story x as shown in Equation D.1.

$$V_{px} = \sum V_{pcx} \quad (\text{Eq. D.1})$$

where:

V_{pcx} is the lower between V_{pMx} and V_{nx} , the column shear capacity controlled by flexure and shear respectively. In the calculation of these strengths the axial load should be assumed equal to the load according to approximate gravity analysis.

V_{nx} is the shear capacity of a column controlled by shear calculated according to Equation 4.1.

V_{pMx} is the plastic capacity of a column at story x calculated according to Equation D.2

$$V_{pMx} = \frac{M_{cTx} + M_{cBx}}{h_x} \quad (\text{Eq. D.2})$$

M_{cTx} is calculated as the minimum of the flexural strength of the top of the column at story x or the flexural strength at the top of the column controlled by the beams as defined in Equation D.3.

$$M_{cTx} = \frac{[M_{bL(x+1)} + M_{bR(x+1)}] * h_x}{h_x + h_{x+1}} \quad (\text{Eq. D.3})$$

Similarly M_{cBx} is calculated as the minimum of the flexural strength of the bottom of the column at story x or the flexural strength at the bottom of the column controlled by the beams as defined in Equation D.4.

$$M_{cBx} = \frac{[M_{bLx} + M_{bRx}] * h_x}{h_x + h_{x-1}} \quad (\text{Eq. D.4})$$

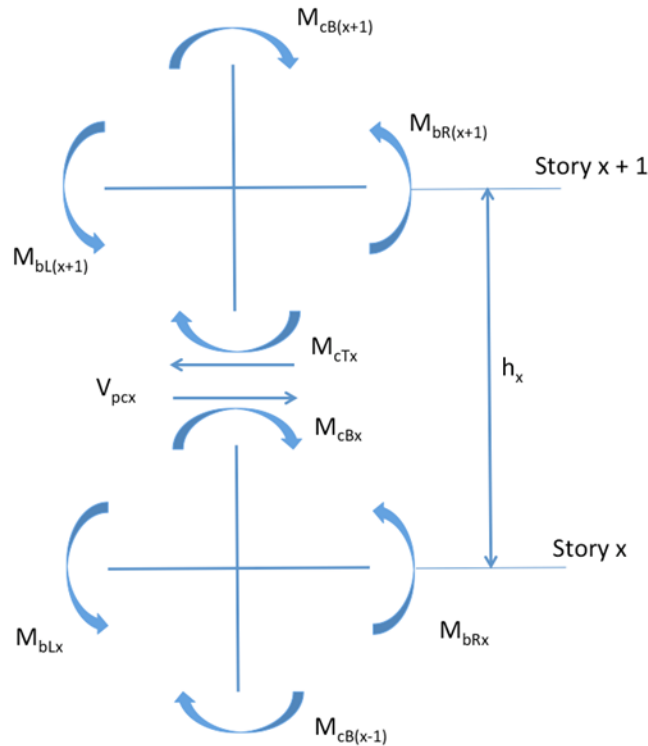


Figure D.1 Schematic Drawing for the calculation of story plastic shear capacity

- Calculation of V_{pMI} (1st Story Shear Capacity)

To account for the effect of boundary conditions located at the first story the method considers two main cases:

- Fixed Columns at Base:** In that case calculation of top and bottom column strength should be done according to the procedure described above, though h_l employed in Equations D.2-4 should be assumed to be equal to 0.8 times the story height ($h_l=0.8h_{\text{story}}$).
- Pinned Columns at Base:** In that case calculation of top and bottom column strength should be done according to the procedure described above, though h_l employed in Equations D.2-4 should be assumed to be equal to 2.0 times the height of the story ($2h$).

Consequently, the shear demand on a structure at each story is computed based on an inverted triangular load pattern. The story Demand over Capacity Ratio (DCR) is defined as the shear demand for a specific story over the story shear capacity, V_{px} , calculated according to Equation D.1.

The load pattern is increased by a constant factor for all stories over the height of the building until the amplified shear demand hits the capacity curve at one or more stories (DCR=1.0) for first time. The base shear of the building corresponding to this shear demand is taken as the estimated maximum base shear capacity of the building $V_{max,estimated}$.

Tables D.1-3 compare the base shear capacity estimated by Pushover Analysis and the approximate method presented in this chapter. The difference in estimation of base shear capacity between the two methods (pushover analysis and approximate method) ranges between 1% to 15%. The main reason for this difference is coming from the numerous assumptions that the approximate method involves as well for the fact that the approximate method does not account for the P-Delta effects.

In conclusion both pushover analysis and the approximate method could be utilized to estimate the base shear capacity of concrete frame buildings. Depending on the method used to estimate the base shear capacity two normalization factors are suggested for collapse risk evaluation:

- Using Pushover Analysis**, the R_e factor as computed in Equation 5.1 should be used to estimate the collapse performance of the studied building.
- Using the Approximate Method** to estimate the base shear capacity, the M factor as computed in Equation 5.2 should be used to estimate the collapse performance of the studied building.

The interested reader can find a more detailed description of the approximate method to estimate the base shear capacity of concrete frame buildings in the ATC 78-1 and ATC 78-2 project reports (2013, 2014).

Table D.1 Comparison of pushover and estimated maximum base shear capacity of the 4-story building

4-Story Building		
$\Sigma M_{nc}/\Sigma M_{nb}$	$V_{max,Pushover}$ (kips)	$V_{max,Estimated}$ (kips)
0.6	269.29	314.12
0.8	269.29	314.12
1	269.02	314.12
1.2	244.01	289.83
1.4	217.44	272.48
1.6	194.73	252.73
1.8	175.12	224.63

Table D.2 Comparison of pushover and estimated maximum base shear capacity of the 8-story Building

8-Story Building		
$\Sigma M_{nc}/\Sigma M_{nb}$	$V_{max,Pushover}$ (kips)	$V_{max,Estimated}$ (kips)
0.6	407.76	468.25
0.8	407.76	468.25
1	407.60	468.25
1.2	381.77	433.51
1.4	339.34	396.87
1.6	303.89	347.36
1.8	273.82	307.88

Table D.3 Comparison of pushover and estimated maximum base shear capacity of the 12-story building

12-Story Building		
$\Sigma M_{nc}/\Sigma M_{nb}$	$V_{max, Pushover}$ (kips)	$V_{max, Estimated}$ (kips)
0.6	591.39	686.79
0.8	591.39	686.79
1	589.67	686.79
1.2	574.00	613.8
1.4	506.31	525.92
1.6	453.41	460.77
1.8	407.77	409.41

E. Collapse Performance Tables for the Idealized Buildings

In the current section, the collapse matrices that could be used to evaluate the collapse risk according to the procedure described in Chapter 5 are presented. The collapse matrices are using both the R_e and M normalization factors to link structural parameters with probability of collapse for the studied buildings.

Linear interpolation is suggested for the case of evaluating a building possessing intermediate values for the studied structural parameters (building height, V_p/V_n , $\Sigma M_{nc}/\Sigma M_{nb}$)

E.1. 4-STORY BUILDING , COLLAPSE MATRICES USING THE R_E FACTOR

Table E.1 Probability of collapse matrix for the 4-story building with $V_p/V_n = 0.6$ (R_e normalization factor)

$R_e \backslash \Sigma M_{nc}/\Sigma M_{nb}$	2	3	4	5	6
0.6	0.02	0.18	0.44	0.68	0.83
0.8	0.02	0.19	0.45	0.68	0.83
1.0	0.02	0.15	0.39	0.62	0.79
1.2	0.00	0.06	0.19	0.36	0.54
1.4	0.00	0.03	0.11	0.24	0.37
1.6	0.00	0.01	0.04	0.12	0.25
1.8	0.00	0.01	0.03	0.10	0.19

Table E.2 Probability of collapse matrix for the 4-story building with $V_p/V_n = 0.8$ (R_e normalization factor)

$\Sigma M_{nc}/\Sigma M_{nb}$ \ R_e	2	3	4	5	6
0.6	0.08	0.40	0.70	0.88	0.95
0.8	0.09	0.40	0.71	0.88	0.95
1.0	0.08	0.40	0.70	0.88	0.95
1.2	0.03	0.21	0.47	0.69	0.83
1.4	0.02	0.10	0.26	0.44	0.60
1.6	0.01	0.05	0.15	0.29	0.44
1.8	0.00	0.02	0.08	0.17	0.29

Table E.3 Probability of collapse matrix for the 4-story building with $V_p/V_n = 1.0$ (R_e normalization factor)

$\Sigma M_{nc}/\Sigma M_{nb}$ \ R_e	2	3	4	5	6
0.6	0.18	0.58	0.84	0.95	0.98
0.8	0.17	0.58	0.84	0.95	0.98
1.0	0.16	0.54	0.81	0.93	0.98
1.2	0.05	0.31	0.61	0.81	0.92
1.4	0.02	0.16	0.38	0.59	0.75
1.6	0.01	0.08	0.22	0.38	0.54
1.8	0.00	0.03	0.11	0.24	0.39

Table E.4 Probability of collapse matrix for the 4-story building with $V_p/V_n = 1.2$ (R_e normalization factor)

$\Sigma M_{nc}/\Sigma M_{nb}$ \ R_e	2	3	4	5	6
0.6	0.68	0.82	0.94	0.98	1.00
0.8	0.68	0.83	0.94	0.98	1.00
1.0	0.67	0.81	0.93	0.97	1.00
1.2	0.23	0.55	0.80	0.90	0.99
1.4	0.03	0.22	0.52	0.75	0.89
1.6	0.01	0.11	0.30	0.51	0.68
1.8	0.01	0.06	0.19	0.35	0.50

E.2. 8-STORY BUILDING , COLLAPSE MATRICES USING THE R_e FACTOR

Table E.5 Probability of collapse matrix for the 8-story building with $V_p/V_n = 0.6$ (R_e normalization factor)

$\Sigma M_{nc}/\Sigma M_{nb}$ \ R_e	2	3	4	5	6
0.6	0.10	0.43	0.73	0.89	0.96
0.8	0.10	0.44	0.74	0.89	0.96
1.0	0.09	0.37	0.65	0.82	0.92
1.2	0.02	0.14	0.35	0.56	0.72
1.4	0.00	0.03	0.14	0.32	0.50
1.6	0.00	0.01	0.08	0.21	0.37
1.8	0.00	0.01	0.06	0.15	0.29

Table E.6 Probability of collapse matrix for the 8-story building with $V_p/V_n = 0.8$ (R_e normalization factor)

$\Sigma M_{nc}/\Sigma M_{nb}$ \ R_e	2	3	4	5	6
0.6	0.31	0.68	0.88	0.95	0.98
0.8	0.33	0.69	0.88	0.96	0.98
1.0	0.31	0.67	0.86	0.95	0.98
1.2	0.08	0.33	0.58	0.76	0.87
1.4	0.02	0.13	0.34	0.55	0.72
1.6	0.00	0.06	0.20	0.38	0.56
1.8	0.00	0.03	0.13	0.28	0.44

Table E.7 Probability of collapse matrix for the 8-story building with $V_p/V_n = 1.0$ (R_e normalization factor)

$\Sigma M_{nc}/\Sigma M_{nb}$ \ R_e	2	3	4	5	6
0.6	0.46	0.83	0.95	0.99	1.00
0.8	0.45	0.82	0.95	0.99	1.00
1.0	0.41	0.78	0.93	0.98	0.99
1.2	0.13	0.44	0.70	0.86	0.93
1.4	0.03	0.21	0.47	0.68	0.82
1.6	0.02	0.12	0.32	0.52	0.69
1.8	0.00	0.06	0.20	0.39	0.57

Table E.8 Probability of collapse matrix for the 8-story building with $V_p/V_n = 1.2$ (R_e normalization factor)

$\Sigma M_{nc}/\Sigma M_{nb}$ \ R_e	2	3	4	5	6
0.6	0.70	0.93	0.99	1.00	1.00
0.8	0.67	0.92	0.98	0.99	1.00
1.0	0.65	0.93	0.99	1.00	1.00
1.2	0.23	0.64	0.87	0.96	0.99
1.4	0.10	0.37	0.62	0.79	0.89
1.6	0.02	0.16	0.40	0.62	0.78
1.8	0.01	0.09	0.27	0.49	0.67

E.3. 12-STORY BUILDING , COLLAPSE MATRICES USING THE R_e FACTOR

Table E.9 Probability of collapse matrix for the 12-story building with $V_p/V_n = 0.6$ (R_e normalization factor)

$\Sigma M_{nc}/\Sigma M_{nb}$ \ R_e	2	3	4	5	6
0.6	0.12	0.55	0.85	0.96	0.99
0.8	0.12	0.54	0.85	0.96	0.99
1.0	0.08	0.45	0.79	0.93	0.98
1.2	0.03	0.24	0.56	0.79	0.91
1.4	0.00	0.08	0.30	0.55	0.75
1.6	0.00	0.04	0.18	0.40	0.62
1.8	0.00	0.03	0.14	0.32	0.52

Table E.10 Probability of collapse matrix for the 12-story building with $V_p/V_n = 0.8$ (R_e normalization factor)

$\Sigma M_{nc}/\Sigma M_{nb}$ \ R_e	2	3	4	5	6
0.6	0.52	0.89	0.98	1.00	1.00
0.8	0.52	0.89	0.98	1.00	1.00
1.0	0.44	0.85	0.97	0.99	1.00
1.2	0.09	0.44	0.75	0.91	0.97
1.4	0.02	0.18	0.48	0.73	0.87
1.6	0.00	0.09	0.32	0.58	0.78
1.8	0.00	0.06	0.23	0.46	0.66

Table E.11 Probability of collapse matrix for the 12-story building with $V_p/V_n = 1.0$ (R_e normalization factor)

$\Sigma M_{nc}/\Sigma M_{nb}$ \ R_e	2	3	4	5	6
0.6	0.65	0.93	0.99	1.00	1.00
0.8	0.65	0.93	0.99	1.00	1.00
1.0	0.56	0.91	0.99	1.00	1.00
1.2	0.16	0.60	0.87	0.96	0.99
1.4	0.05	0.33	0.65	0.85	0.94
1.6	0.01	0.17	0.46	0.72	0.87
1.8	0.01	0.11	0.35	0.61	0.79

Table E.12 Probability of collapse matrix for the 12-story building with $V_p/V_n = 1.2$ (R_e normalization factor)

$\Sigma M_{nc}/\Sigma M_{nb}$ \ R_e	2	3	4	5	6
0.6	0.80	0.98	1.00	1.00	1.00
0.8	0.82	0.98	1.00	1.00	1.00
1.0	0.69	0.96	1.00	1.00	1.00
1.2	0.31	0.74	0.93	0.98	1.00
1.4	0.10	0.48	0.80	0.93	0.98
1.6	0.04	0.29	0.61	0.83	0.93
1.8	0.02	0.16	0.44	0.69	0.85

E.4. 4-STORY BUILDING , COLLAPSE MATRICES USING THE M FACTOR

Table E.13 Probability of collapse matrix for the 4-story building with $V_p/V_n=0.6$ (M normalization factor)

$\Sigma M_{nc}/\Sigma M_{nb}$ \ M	2	3	4	5	6
0.6	0.03	0.20	0.46	0.69	0.84
0.8	0.03	0.20	0.46	0.69	0.84
1.0	0.02	0.16	0.41	0.64	0.80
1.2	0.01	0.07	0.21	0.39	0.57
1.4	0.01	0.05	0.15	0.30	0.45
1.6	0.00	0.02	0.08	0.20	0.35
1.8	0.00	0.01	0.06	0.15	0.27

Table E.14 Probability of collapse matrix for the 4-story building with $V_p/V_n=0.8$ (M normalization factor)

$\Sigma M_{nc}/\Sigma M_{nb}$ \ M	2	3	4	5	6
0.6	0.17	0.58	0.85	0.95	0.99
0.8	0.17	0.57	0.84	0.94	0.98
1.0	0.17	0.57	0.83	0.94	0.98
1.2	0.08	0.36	0.64	0.83	0.92
1.4	0.05	0.22	0.45	0.64	0.78
1.6	0.03	0.14	0.32	0.50	0.65
1.8	0.01	0.06	0.19	0.35	0.50

Table E.15 Probability of collapse matrix for the 4-story building with $V_p/V_n=1.0$ (M normalization factor)

$\Sigma M_{nc}/\Sigma M_{nb}$ \ M	2	3	4	5	6
0.6	0.31	0.74	0.92	0.98	0.99
0.8	0.31	0.74	0.92	0.98	0.99
1.0	0.28	0.70	0.91	0.97	0.99
1.2	0.13	0.49	0.77	0.91	0.97
1.4	0.08	0.32	0.59	0.78	0.89
1.6	0.04	0.20	0.41	0.60	0.73
1.8	0.01	0.10	0.26	0.45	0.57

Table E.16 Probability of collapse matrix for the 4-story building with $V_p/V_n=1.2$ (M normalization factor)

$\Sigma M_{nc}/\Sigma M_{nb}$ \ M	2	3	4	5	6
0.6	0.71	0.97	0.99	1.00	1.00
0.8	0.71	0.97	0.99	1.00	1.00
1.0	0.66	0.90	0.99	1.00	1.00
1.2	0.31	0.68	0.85	0.92	0.97
1.4	0.10	0.40	0.65	0.82	0.90
1.6	0.02	0.18	0.44	0.67	0.80
1.8	0.01	0.10	0.30	0.52	0.69

E.5. 8-STORY BUILDING , COLLAPSE MATRICES USING THE M FACTOR

Table E.17 Probability of collapse matrix for the 8-story building with $V_p/V_n=0.6$ (M normalization factor)

$\Sigma M_{nc}/\Sigma M_{nb}$ \ M	2	3	4	5	6
0.6	0.19	0.59	0.84	0.95	0.98
0.8	0.19	0.59	0.84	0.95	0.98
1.0	0.16	0.51	0.77	0.90	0.96
1.2	0.04	0.22	0.47	0.68	0.81
1.4	0.01	0.08	0.26	0.48	0.66
1.6	0.00	0.03	0.14	0.33	0.52
1.8	0.00	0.02	0.10	0.23	0.40

Table E.18 Probability of collapse matrix for the 8-story building with $V_p/V_n=0.8$ (M normalization factor)

$\Sigma M_{nc}/\Sigma M_{nb}$ \ M	2	3	4	5	6
0.6	0.47	0.81	0.94	0.98	0.99
0.8	0.47	0.81	0.94	0.98	0.99
1.0	0.46	0.80	0.93	0.98	0.99
1.2	0.16	0.47	0.72	0.86	0.94
1.4	0.05	0.26	0.52	0.72	0.85
1.6	0.04	0.17	0.33	0.55	0.72
1.8	0.01	0.07	0.22	0.41	0.58

Table E.19 Probability of collapse matrix for the 8-story building with $V_p/V_n=1.0$ (M normalization factor)

$\Sigma M_{nc}/\Sigma M_{nb}$ \ M	2	3	4	5	6
0.6	0.60	0.90	0.98	1.00	1.00
0.8	0.59	0.90	0.98	0.99	1.00
1.0	0.55	0.87	0.97	0.99	1.00
1.2	0.25	0.56	0.80	0.91	0.96
1.4	0.12	0.38	0.62	0.81	0.91
1.6	0.05	0.24	0.44	0.65	0.80
1.8	0.02	0.14	0.29	0.51	0.68

Table E.20 Probability of collapse matrix for the 8-story building with $V_p/V_n=1.2$ (M normalization factor)

$\Sigma M_{nc}/\Sigma M_{nb}$ \ M	2	3	4	5	6
0.6	0.74	0.94	0.99	1.00	1.00
0.8	0.74	0.94	0.99	1.00	1.00
1.0	0.74	0.94	0.99	1.00	1.00
1.2	0.30	0.71	0.91	0.97	0.99
1.4	0.16	0.46	0.71	0.86	0.93
1.6	0.04	0.22	0.49	0.70	0.84
1.8	0.01	0.12	0.33	0.56	0.73

E.6. 12-STORY BUILDING , COLLAPSE MATRICES USING THE M FACTOR

Table E.21 Probability of collapse matrix for the 12-story building with $V_p/V_n=0.6$ (M normalization factor)

$\Sigma M_{nc}/\Sigma M_{nb}$ \ M	2	3	4	5	6
0.6	0.43	0.87	0.98	1.00	1.00
0.8	0.43	0.86	0.98	1.00	1.00
1.0	0.34	0.81	0.96	0.99	1.00
1.2	0.09	0.38	0.65	0.85	0.92
1.4	0.00	0.15	0.40	0.65	0.80
1.6	0.00	0.10	0.25	0.48	0.65
1.8	0.00	0.08	0.20	0.35	0.55

Table E.22 Probability of collapse matrix for the 12-story building with $V_p/V_n=0.8$ (M normalization factor)

$\Sigma M_{nc}/\Sigma M_{nb}$ \ M	2	3	4	5	6
0.6	0.69	0.95	0.99	1.00	1.00
0.8	0.69	0.95	0.99	1.00	1.00
1.0	0.62	0.93	0.99	1.00	1.00
1.2	0.14	0.53	0.82	0.94	0.98
1.4	0.02	0.21	0.52	0.76	0.89
1.6	0.01	0.10	0.34	0.60	0.79
1.8	0.00	0.06	0.23	0.46	0.66

Table E.23 Probability of collapse matrix for the 12-story building with $V_p/V_n=1.0$ (M normalization factor)

$\Sigma M_{nc}/\Sigma M_{nb}$ \ M	2	3	4	5	6
0.6	0.79	0.97	1.00	1.00	1.00
0.8	0.79	0.97	1.00	1.00	1.00
1.0	0.72	0.96	1.00	1.00	1.00
1.2	0.30	0.69	0.91	0.98	1.00
1.4	0.15	0.42	0.69	0.88	0.95
1.6	0.10	0.28	0.48	0.73	0.88
1.8	0.05	0.17	0.35	0.61	0.79

Table E.24 Probability of collapse matrix for the 12-story building with $V_p/V_n=1.2$ (M normalization factor)

$\Sigma M_{nc}/\Sigma M_{nb}$ \ M	2	3	4	5	6
0.6	0.90	0.99	1.00	1.00	1.00
0.8	0.91	0.99	1.00	1.00	1.00
1.0	0.83	0.99	1.00	1.00	1.00
1.2	0.39	0.81	0.95	0.99	1.00
1.4	0.20	0.53	0.83	0.95	0.99
1.6	0.05	0.31	0.63	0.84	0.94
1.8	0.02	0.17	0.45	0.69	0.85

F. Approximate Relationships to Estimate the Fundamental Building Period⁷

Goel and Chopra (1994) reported measured values of building period, T , for concrete frame buildings as a function of building height only. In ASCE-41 these data have been conservatively approximated (a shortened period results in greater base shear for most cases) by Equation F.1.

$$T_{ASCE-41} = 0.018 * H^{0.9} \quad (\text{Eq. F.1})$$

where, H corresponds to the building height in feet.

Equation F.1 corresponds to a simplified approach that does not consider explicitly other building characteristics that are expected to influence significantly the fundamental building period such as the member sizes, the steel reinforcement and the corresponding building strength.

An alternative procedure was developed by Dr. Mehrain for the purposes of the ATC-78 model (ATC-78, 2014), based on results obtained from pushover analysis. The suggested equation as presented in ATC-78 report is shown below:

$$T_{ATC-78} = 0.078 * \sqrt{\frac{H_{building} * W}{V_y}} \quad (\text{Eq. F.2})$$

where, $H_{building}$ corresponds to the building height in feet, W is the building weight and V_y is the base shear yielding strength (W and V_y should be given in the same units).

F.1. MATHEMATICAL MODEL TO DETERMINE THE FUNDAMENTAL BUILDING PERIOD

Determination of the natural frequencies and modes of a structure, requires solution of the matrix eigenvalue problem presented in Equation F.3

⁷ The contribution of Ms. Francesca Renouard in the development of Appendix G is acknowledged

$$(\mathbf{K}-\omega_n^2*\mathbf{M})*\Phi_n=0 \quad (\text{Eq. F.3})$$

where, \mathbf{K} corresponds to the building stiffness matrix, \mathbf{M} corresponds to the building mass matrix, ω_n^2 corresponds to the eigenvalues and Φ_n to the matrix of eigenvectors. Equation F.4 defines the natural frequency ω_n of the building.

$$\omega_n = \frac{2\pi}{T_n} \quad (\text{Eq. F.4})$$

where, T_n is the n^{th} -mode building period (T_1 is the 1st mode or fundamental building period)

The eigenvalues ω_n^2 are the roots of Equation F.5.

$$\det [\mathbf{K}-\omega_n^2*\mathbf{M}] =0 \quad (\text{Eq. F.5})$$

F.2. USING SIMPLIFIED FISHBONE MODELS TO APPROXIMATE THE FUNAMENTAL BUILDING PERIOD

Nakashima et al. (2002) and Luco et al. (2003) suggested a generic frame model (or otherwise termed as “fishbone” model) as a computationally efficient alternative to predict the dynamic response of moment frames rather than modeling the whole structure.

In the current study the generic frame as suggested by Nakashima was utilized to generate a range of buildings with different structural properties such as flexural strength, reinforcement ratio, column dimensions and building height.

An example of a generic frame model is shown in Figure F.1. The generic frame model lumps column and beam stiffnesses by condensing all the columns of a story into one column and condensing all the beams into two beams with length equal to the length of the mid-span of a typical bay corresponding to the studied frame.

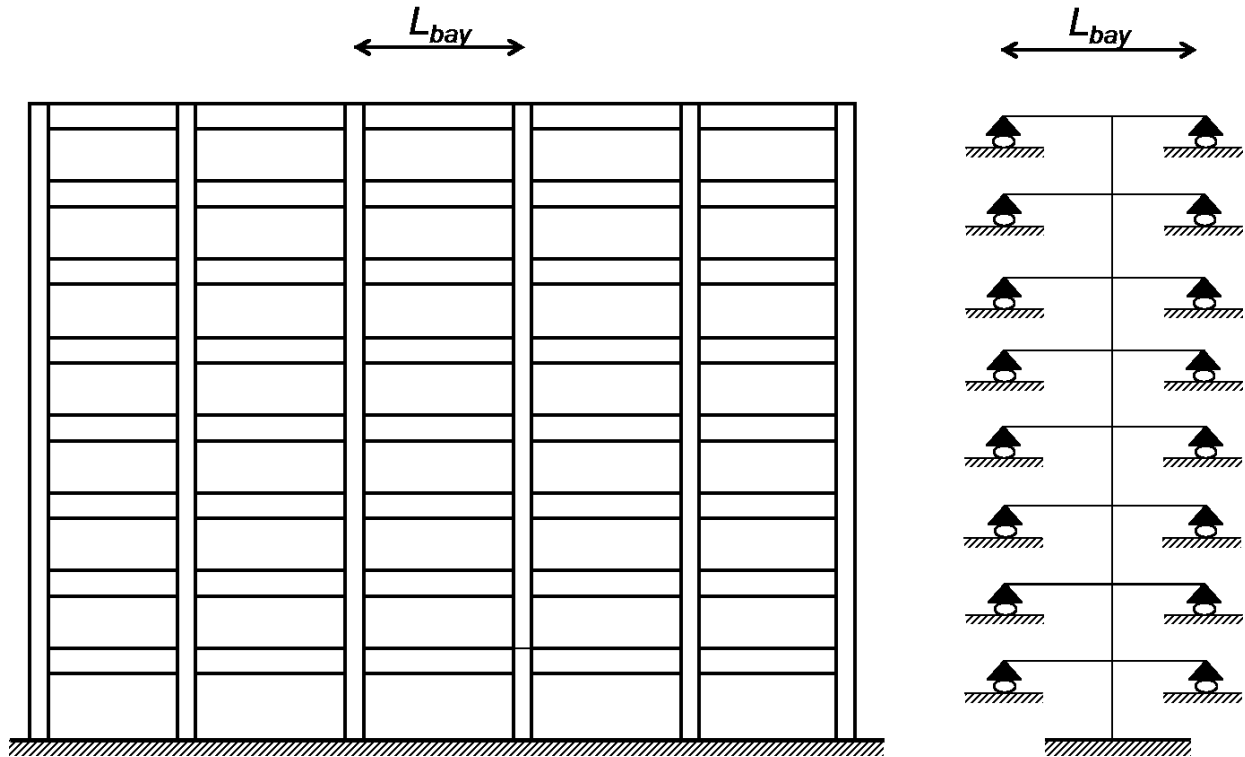


Figure F.1 Schematic illustration of the generic frame model (on the right) used to represent the idealized 8-story building (on the left)

The following structural parameters were used as an input to design generic frame models equivalent to the corresponding concrete moment frames with the assumed building characteristics.

- Building height, H
- Base shear strength normalized by the building weight, V/W
- Average column longitudinal reinforcement ratio, ρ_{long}

For the generic frames designed, it was assumed that the equivalent structural moment frames consist of five bays, with dimensions, material properties and gravity loading per floor equal to the values used for the idealized building presented in Appendix A. All the beam members were assumed to possess longitudinal reinforcement ratio equal to 0.01.

To design the generic frames, an inverted lateral triangular load pattern was considered; the gravity forces were assumed to be the same with those used for the design of the idealized buildings (see Appendix A). The flexural forces determined from the generic frame analytical model were reduced by the factor, Z , provided in Equations F.6-1-3 to estimate the equivalent frame individual member forces.

$$M_{\text{column,frame}} = Z_{\text{column}} * M_{\text{G.F.,column}} \quad (\text{Eq. F.6-1})$$

$$M_{\text{beam,frame}} = Z_{\text{beam}} * M_{\text{G.F.,beam}} \quad (\text{Eq. F.6-2})$$

$$Z = \frac{1}{N_{\text{joints}}} \quad (\text{Eq. F.6-3})$$

where, N_{joints} corresponds to the total number of beam-column joints per story of interest, $M_{\text{G.F.,column}}$ is the bending moment at the top or bottom of the column members of the generic frame model, and $M_{\text{G.F.,beam}}$ is the bending moment at the beam joint of the generic frame.

The column and beam reinforcement ratio were set constant and the member dimensions were estimated such that Equation F.7 (Panagiotakos, 2001), is satisfied:

$$\frac{M_y}{bd^3} = \phi_y \left\{ E_c \frac{k_y^2}{2} \left(0.5(1 + \delta') - \frac{k_y}{3} \right) + \frac{E_s}{2} \left[(1 - k_y)\rho + (k_y - \delta')\rho' + \frac{\rho_v}{6}(1 - \delta') \right] (1 - \delta') \right\} \quad (\text{Eq. F.7})$$

where,

$$\phi_y = \frac{f_y}{E_s(1 - k_y)d} \quad (\text{Eq. F.7-1})$$

M_y = member yield moment (kip-in)

f_y = yield strength of reinforcement steel (ksi)

E_s = modulus of elasticity of reinforcement steel (ksi)

E_c = modulus of elasticity of concrete (ksi)

d = effective depth of cross section (in)

d' = distance of center of compression reinforcement from extreme compression fiber (in)

$$k_y = (n^2 A^2 + 2nB)^{1/2} - nA \quad (\text{Eq. F.7-2})$$

$$A = \rho + \rho' + \rho_v + \frac{N}{bdf_y} \quad (\text{Eq. F.7-3})$$

$$B = \rho + \rho'\delta' + 0.5\rho_v(1 + \delta') \quad (\text{Eq. F.7-4})$$

ρ = tension reinforcement ratio

ρ' = compression reinforcement ratio

ρ_v = reinforcement ratio of transverse steel

N = axial force (kip)

$$\delta' = d'/d \quad (\text{Eq. F.7-5})$$

The following constraints were used to better emulate actual construction and member size selection:

- Column and beam sizes were changed every two stories.
- Column size was limited to no smaller than 12” x 12”.
- Beam depth to width ratio limited to no greater than 1.5.

After the member dimensions have been determined such that they satisfy certain flexural strength demands and reinforcement properties, the effective moment of inertia was calculated according to the procedure suggested by Elwood and Eberhard (2006) as follows:

$$EI_{eff,calc} = \frac{M_y * L^2}{6 * \Delta_y} \quad (\text{Eq. F.8})$$

Where M_y is calculated according to Equation F.7, Δ_y is calculated according to Equation F.8-1 and L is the corresponding column height

$$\Delta_y = \Delta_{flex} + \Delta_{slip}^8 \quad (\text{Eq. F.8-1})$$

where,

Δ_{flex} corresponds to the displacement due to flexural deformations

$$\Delta_{flex} = \frac{L^2}{6} \phi_y \quad (\text{Eq. F.8-2})$$

Δ_{slip} corresponds to the displacement due to bar slip

$$\Delta_{slip} = \frac{L d_b f_s \phi_y}{8u} \quad (\text{Eq. F.8-3})$$

L =column height (in)

ϕ_y =yield curvature

f_s =stress of tensions reinforcement (psi)

d_b =diameter of longitudinal reinforcement (in)

u =average bond stress assumed to be equal $6\sqrt{f'_c}$ (psi)

Using the generic frame geometry and the effective stiffness properties as calculated according to Equation F.8-1-3 eigenvalue analysis was performed using OpenSees structural analysis software.

Applying the geometric and reinforcement properties of the idealized 4, 8 and 12 story buildings used in the current study (Appendix A) eigenvalue analysis was performed to test the accuracy of

⁸ The deformation due to shear was not included, assuming to be negligible for the elastic deformation range

the generic frame model in predicting the dynamic response of frame buildings. Table F.1 compares the results of the fundamental period obtained from eigenvalue analysis of the idealized buildings and the equivalent generic frames.

Table F.1 Comparison of eigenvalue analysis of the idealized building models and the equivalent generic frame model

Period (sec)		
<i>Building</i>	Idealized Building	Generic Frame
4-Story	1.14	1.11
8-Story	1.62	1.52
12-Story	1.95	1.81

The results demonstrate that the generic frame model provides good accuracy in estimation of the actual building period of the idealized buildings.

F.3. EFFECT OF STRUCTURAL PARAMETERS AND BUILDING GEOMETRY IN ESTIMATION OF THE FUNDAMENTAL BUILDING PERIOD

The following structural parameters were used to produce building variations as generic frame models equivalent to concrete moment frames possessing similar structural properties.

- Building height, H (ft): 46 ft (4-story bldg.) , 90 ft (8-story bldg.) , 134 ft (12-story bldg.)
- Base shear strength normalized by the building weight, V^o/W : 0.05 , 0.10, 0.15, 0.25.
- Average column longitudinal reinforcement ratio, ρ_{long} : 0.01, 0.015, 0.018, 0.02, 0.025, and 0.03

Figures F.2 –F.4 show how the structural parameters discussed above influence the fundamental period of the building.

⁹ V can be estimated by ΣV_{PMI} (sum of the flexural column strength of the 1st story) as defined in Appendix E

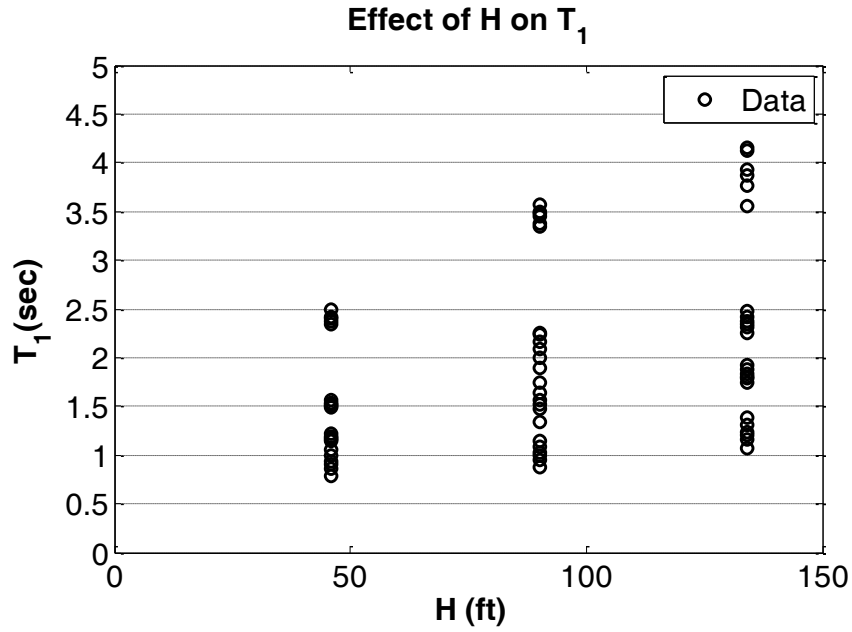


Figure F.2 Effect of building height (H) on the fundamental period T_1 of the building

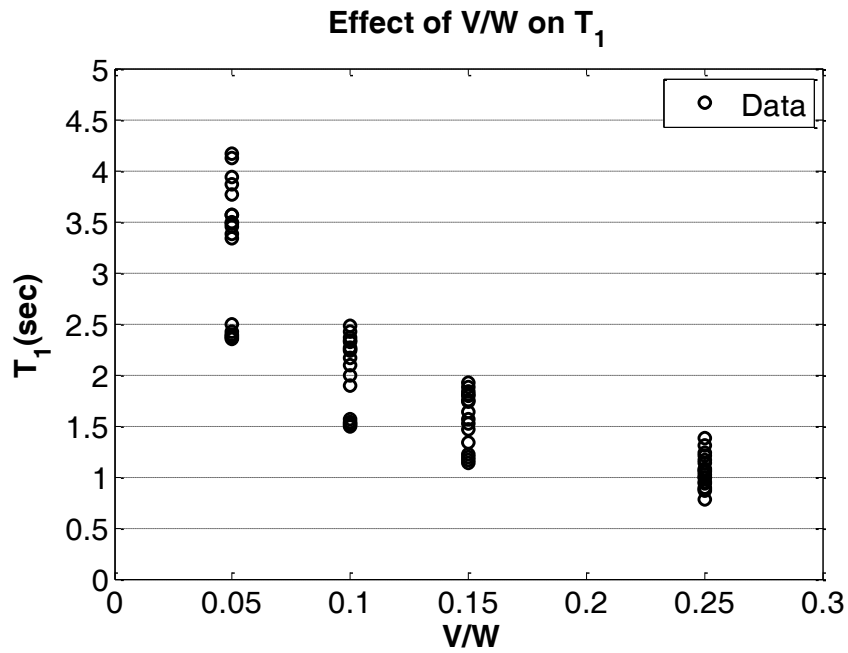


Figure F.3 Effect of normalized base shear strength (V/W) on the fundamental period T_1 of the building

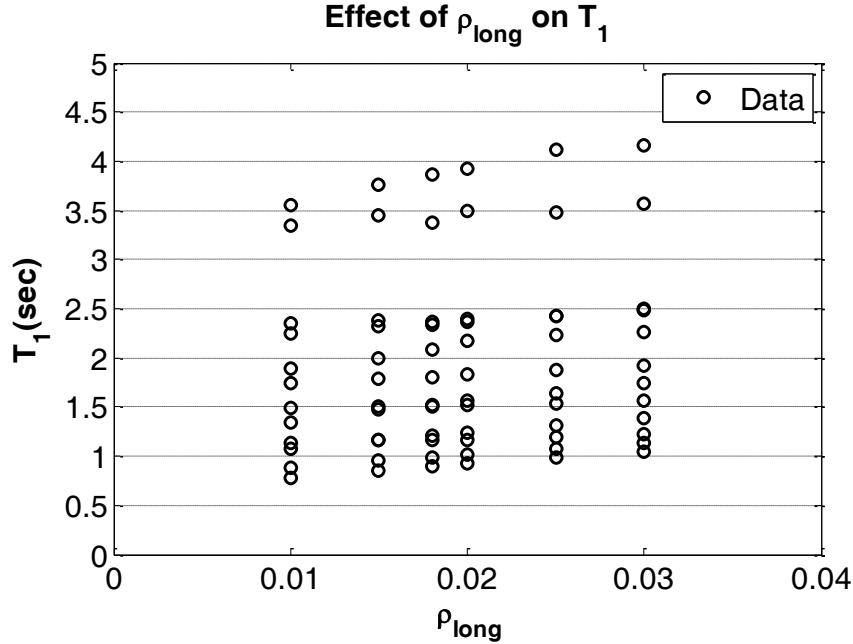


Figure F.4 Effect of longitudinal reinforcement ratio (ρ_{long}) on the fundamental period T_1 of the building

As illustrated in Figure F.2, building height is significantly influencing the fundamental period of the building. Increasing building height results in higher fundamental period values. However in the same Figure we observe large dispersion for all the studied building heights. The main reason for this is the different V/W ratio values that the building is designed for. Contrary to Equation F.1 which suggests that the building height is the only parameter that affects the building fundamental period, the normalized base shear strength (V/W) according to Figure F.3 also influences greatly the fundamental period. On the other hand, the column longitudinal reinforcement ratio does not seem to dramatically influence the fundamental building period. Figure F.4 demonstrates that as ρ_{long} increases, T_1 tends to increase as well, but less pronounced in comparison with the other two considered parameters, H and V/W .

Using the observed data from the building variations discussed above an analytical model to estimate the building period should be defined according to the following form:

$$T_{G.F.,1} = f(H, V/W, \rho_{long}) \quad (\text{Eq. F.8})$$

Based on the aforementioned model, forward stepwise linear regression of the form shown in Equation F.9 was used:

$$\ln(T_{G.F.,1}) = \beta_0 + \beta_1 \ln(H) + \beta_2 \ln(V/W) + \beta_3 * \ln(\rho_{long}) + \varepsilon \quad (\text{Eq. F.9})$$

where, $\beta_0, \beta_1, \beta_2, \beta_3$ are the linear regression parameters, $H, V/W$, and ρ_{long} are the predictor variables and ε is the model error

Forward stepwise regression starts with assuming initially that $\beta_0 \neq 0$ and $\beta_1 = \beta_2 = \beta_3 = 0$. Consequently the most statistically significant term (the one with the highest t-statistic or the lowest p-value) is added at each step until no other significant terms are left (a term is not included in the model if it corresponds to $p\text{-value} > 0.10$). The results of the stepwise regression are presented in Table F.2.

Table F.2 Regression parameters for model $T_{G.F.,1}$

Regression Coefficient	Estimate	Standard Error	p-value	R²	$\sigma_{\ln(T_{\text{effective},1})}$
$\ln(\beta_0)$	-2.074	0.099	<0.01	0.9862	0.054
$\ln(\beta_1)$	0.388	0.014	<0.01		
$\ln(\beta_2)$	-0.69	0.011	<0.01		
$\ln(\beta_3)$	0.140	0.018	<0.01		

As explained above, in the current model, stepwise regression started with the constant model (β_0) and used forward selection to incrementally add terms β_2, β_1 and β_3 cited in declining significance order. Given the small number of the p-values for all the regression coefficients, we deduce that all terms are statistically significant.

Before proceeding further it should be noted that the method used in this chapter to determine the building period, employed simplified models, termed as generic frames (fishbone models) which had a predetermined, constant reinforcement ratio in all the column members. In reality, buildings cannot be characterized by a single value for the reinforcement ratio, so using a term which includes the reinforcement ratio to estimate the building period as appears in Equation F.8 would be difficult to determine. Therefore, although, the longitudinal reinforcement ratio appears to be a statistically significant term in Equation F.9, engineering practice requires a simpler equation that takes into account only terms that can be relatively easily determined such as the building height (H) and the normalized base shear strength (V/W). Therefore a more appealing equation for engineering practice is of the form presented in Equation F.10.

$$\ln(T_{G.F.,2}) = \beta_0 + \beta_1 \ln(H) + \beta_2 \ln(V/W) + \varepsilon \quad (\text{Eq. F.10})$$

Stepwise regression is repeated for Equation F.10. The results are presented in Table F.3.

Table F.3 Regression parameters for model $T_{G.F.,2}$

Regression Coefficient	Estimate	Standard Error	p-value	R²	$\sigma_{\ln(T_{\text{effective},1})}$
$\ln(\beta_0)$	-2.632	0.093	<0.01	0.974	0.074
$\ln(\beta_1)$	0.388	0.020	<0.01		
$\ln(\beta_2)$	-0.694	0.015	<0.01		

As expected, the simplified model of Equation F.10 gives higher value for the standard deviation of the model error compared to Equation F.9 that includes also the ρ_{long} parameter. The increase in the standard deviation though is judged not to be so important for structural engineering purposes taking into account the difficulty that it would entail defining a unique value for ρ_{long} for a real building.

Substituting the regression coefficient values corresponding to linear regression, Equation F.10 can be written as follows:

$$T_{G.F,2} = 0.072 * H^{0.39} * (V / W)^{-0.69} \quad (\text{Eq. F.11})$$

Figure F.5 provides a comparison of the relationships for estimation of the building period.

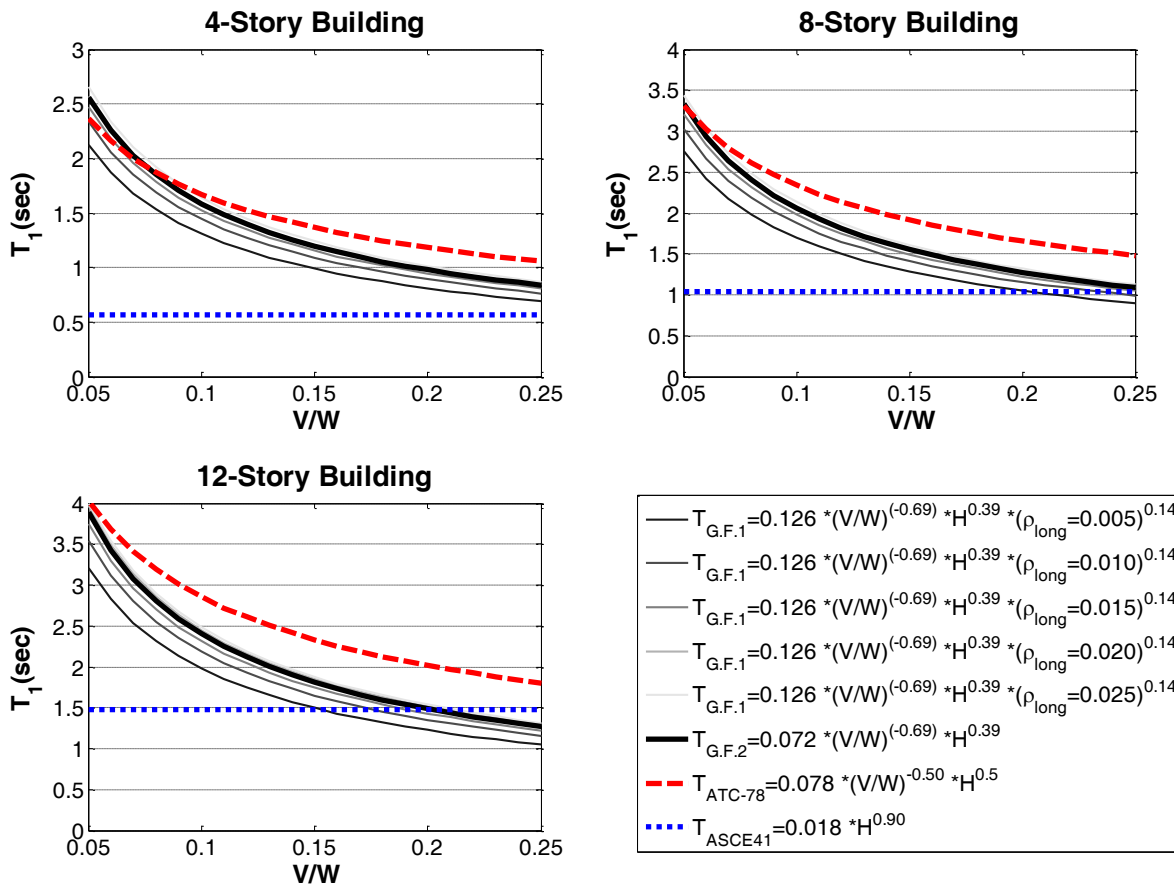


Figure F.5 Comparison of relationships for estimation of the fundamental building period

Looking at the graphs in Figure F.5 the following observations can be made:

- Increasing the building height for the same normalized base shear strength corresponds to higher building period values

- Increasing the normalized base shear strength for the same height corresponds to a decrease in the building period values.
- Increasing the longitudinal reinforcement ratio for the same normalized base shear strength and height results in an increase in the fundamental building period since it corresponds to smaller member sizes.
- Equation F.11 estimates with sufficient accuracy for structural engineering applications the fundamental building period. Given the fact that Equation F.9 involves an additional term (ρ_{long}) that it is hard to be defined with a single value for a real building, Equation F.11 seems to provide an appealing alternative for estimating the building period.

The trends discussed above are in agreement with physical intuition and with physical data provided in the literature.

A comparison of relationships provided by Equations F.1, F.2 and F.11 with the analytical data obtained from eigenvalue analysis using simplified generic frame models are presented in Figures F.6 and F.7. Equations F.2 and F.11 seem to provide relatively accurate estimates of the effective period obtained from analytical results, while the Equation suggested by ASCE-41 provides systematically lower estimates of the fundamental building period for buildings with normalized base shear strength $V/W < 0.20$.

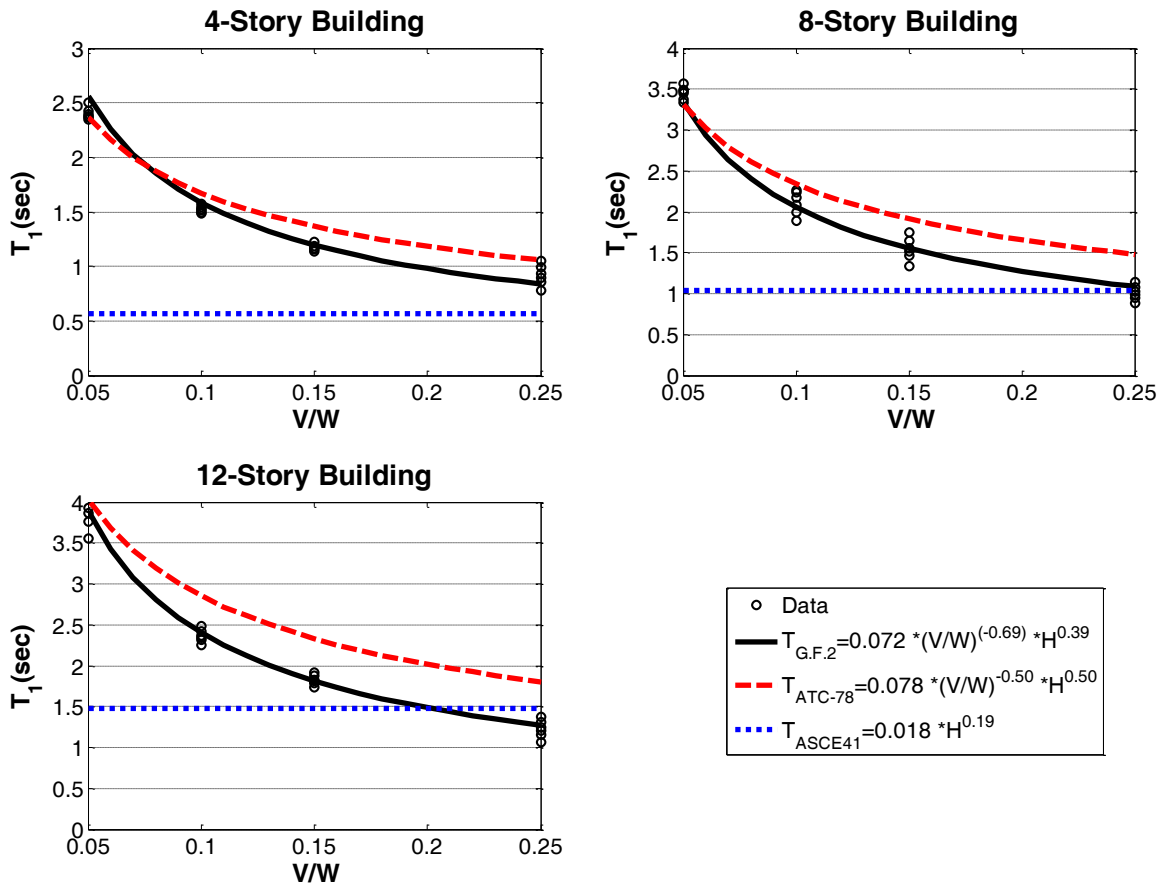


Figure F.6 Comparison of relationships for estimation of the fundamental building period with analytical data (Effect of V/W on T_1)

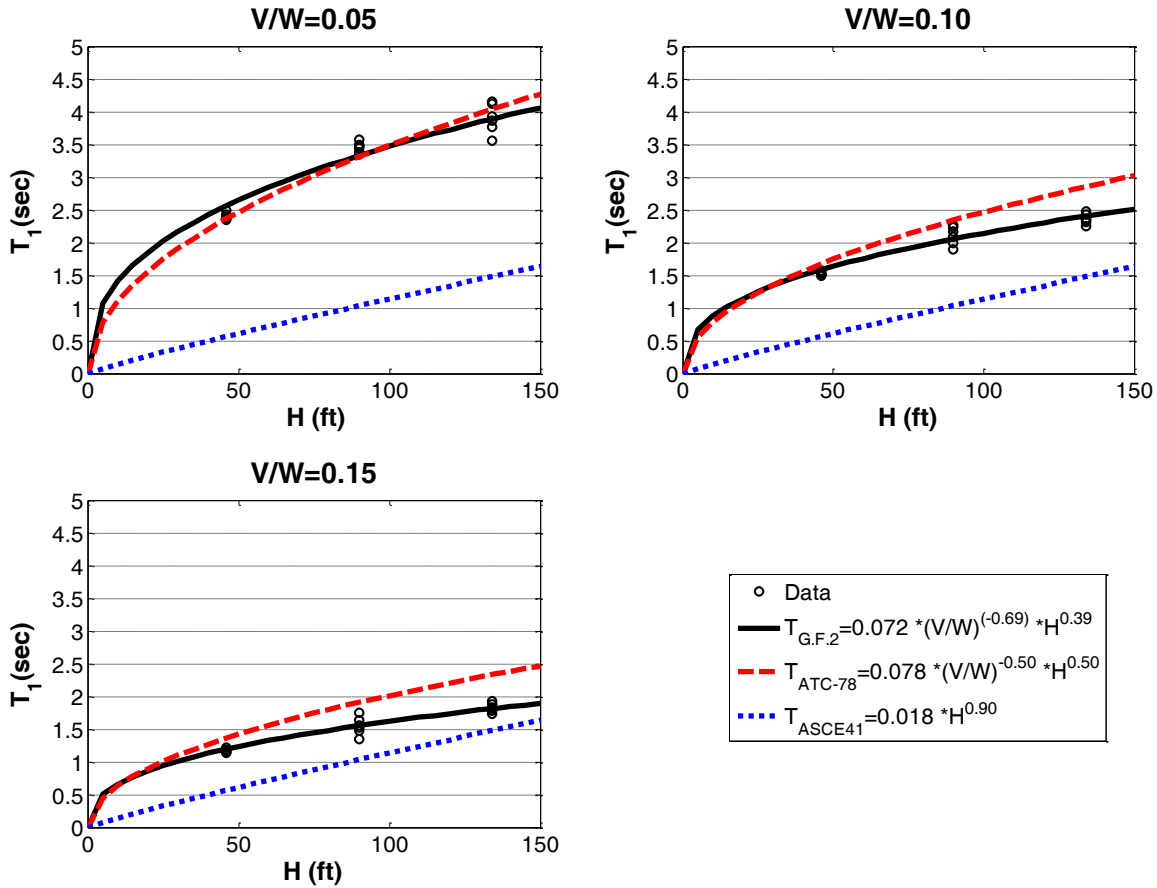


Figure F.7 Comparison of relationships for estimation of the fundamental building period with analytical data (Effect of H on T_1)

As shown in Table F.4 the data from the Equations F.2 and F.11 provide good approximations of the periods of the idealized buildings used in this study obtained from eigenvalue analysis.

Table F.4 Comparison of eigenvalue analysis of the idealized building models and the estimated building period values

Idealized Building	Period (sec)			
	Eigenvalue Analysis	$T_{G.F.,2}$	T_{ATC-78}	$T_{ASCE-41}$
4-Story	1.14	0.96	1.16	0.57
8-Story	1.62	1.51	1.87	1.03
12-Story	1.95	1.81	2.33	1.48

In conclusion, Equation F.11 seems to provide overall the best estimates of the building period for the concrete frame buildings analyzed in the current study. Equation F.2 provides also a good approximation of the analytical results. Therefore, for the purposes of the current study T_1 (fundamental building period) will be approximated with $T_{G.F.}$ as shown in equation F.12:

$$T_{G.F.} = 0.072 * H^{0.39} * (V / W)^{-0.69} \quad (\text{Eq. F.12})$$

G. Story Drift Profiles

Equation 6.4 provided in Chapter 6 relates the maximum¹⁰ story drift ratio demand with the estimated average drift ratio observed in the studied building.

As discussed in Chapter 2, Shome and Cornell (1999), used statistical regression for numerous non-linear dynamic analyses to estimate story drift ratios. Shome and Cornell employed different predictors to estimate the story drift ratio. The predictors included Spectral acceleration at the building 1st mode period ($Sa(T_1)$), Spectral acceleration at the 2nd mode period ($Sa(T_2)$), earthquake magnitude (M), epicentral distance (R), and ground motion duration (D). The statistical processing of the results showed that the spectral acceleration at the 1st mode period constitutes the most statistically significant parameter, while for taller buildings the spectral acceleration at the 2nd mode period influences also the predicted variable. The results of Shome's study indicated that story drift ratio demand is almost a linear function of $Sa(T_1)$.

Using the results of IDA, this study initially related the story drift ratio demand with $Sa(T_1)$ using a similar statistical model with the one suggested by Shome and Cornell, presented in Equation G.1

$$\ln\left(\frac{\delta_x}{h_x}\right) = \beta_0 + \beta_1 * \ln\left(\frac{\delta_{eff} (= f(Sa(T_1)))}{h_{eff}}\right) + \varepsilon \quad (\text{Eq. G.1})$$

where, δ_x is the story drift demand, h_x is the story height, α_x is the coefficient for story x used to estimate the story drift pattern, δ_{eff} is the displacement at the effective floor height calculated according to Equation 6.1 (δ_{eff} is a function of $Sa(T_1)$), h_{eff} is the story height (assumed to be $h_{eff}=0.7*h_{building}$, where $h_{building}$ is the total building height)

The results of statistical regression using Equation G.1 confirmed the findings of Shome's study:

- The estimated values of coefficient β_1 ranged from 0.93 to 1.07. Based on this we could assume that the story drift ratio demand is approximately a linear function of δ_{eff} (δ_{eff} employed in Equation G.1 was calculated according to Equation 6.1, where δ_{eff} is a function of $Sa(T_1)$), and thus of $Sa(T_1)$.

¹⁰ The term maximum corresponds to the maximum value of drift ratio expected over the entire dynamic response of the building for each story. For brevity the word maximum will be omitted when the term story drift ratio demand is used.

- For buildings possessing strong columns –weak beams ($\Sigma M_{nc}/\Sigma M_{nb} \geq 1.20$), β_0 was estimated approximately equal to 1.5, in agreement with the value suggested by Shome and Cornell using 5 and 20-story moment resisting frames (see Chapter 2).

Although a more complicated statistical model could be utilized to relate (δ_x/h_x) with (δ_{eff}/h_{eff}) , a linear model with a single coefficient, $\beta_0 = \ln(\alpha_x)$ (β_1 was set equal to unity based on the findings mentioned above), was employed. This allows an engineer to directly observe and understand the effect of each structural parameter to the drift pattern of the building. To calibrate the coefficient $\beta_0 = \ln(\alpha_x)$ for each story of the studied building, a linear model with the form shown in Equation G.2 was fitted such that the sum of the squares of the errors in the analyzed model is minimized.

$$\ln\left(\frac{\delta_x}{h_x}\right) = \ln(\alpha_x) + \ln\left(\frac{\delta_{eff}}{h_{eff}}\right) + \varepsilon \quad (\text{Eq. G.2})$$

The data used for fitting equation G.2 were taken from numerous non-linear dynamic analysis that were performed as part of IDA employing ground motions with scaling factor values slightly lower than those leading to building collapse.

It should be noted that Equation G.2 was suggested to fit the data by practicing engineers due to its simplicity and engineering appeal. The goodness of fit of the model presented in Equation G.2 was checked visually.

In the current study it was preferred to perform separate statistical regression for different $\Sigma M_{nc}/\Sigma M_{nb}$ and V_p/V_n building variations such that the estimates of $\ln(\alpha_x)$ could be defined according to statistics but also engineering judgment.

However, an alternative approach could also be followed employing both $\Sigma M_{nc}/\Sigma M_{nb}$ ratio and V_p/V_n ratio as predictors. The alternative statistical model is shown in Equation G.3:

$$\ln\left(\frac{\delta_x}{h_x}\right) = \beta_0 + \beta_1 * \ln\left(\frac{\delta_{eff}}{h_{eff}}\right) + \beta_2 * \Sigma M_{nc} / \Sigma M_{nb} + \beta_3 * V_p / V_n + \varepsilon \quad (\text{Eq. G.3})$$

Although Equation G.3 seemed to estimate more accurately the story drift ratio demand, it was recognized that in reality it would be rare to find buildings with column members possessing uniform values of $\Sigma M_{nc}/\Sigma M_{nb}$ and V_p/V_n in a specific story. Thus, Equation G.2 was preferred for the estimation of story drift ratio demand. due to its simplicity.

Due to the lack of sufficient amount of studies, confirming the relationship between story drift ratio demand and average drift ratio, the values of $\ln(\alpha_x)$ in this study were selected such that the estimate of the story drift ratio demand would be more conservative than what statistical regression of the Equation G.2 would provide for the weaker/critical story.

Figure G.1 compares the results obtained from Equation G.2 with analytical data obtained from IDA for the critical 1st story. As we observe in Figure G.1, for a certain value of average drift ratio (δ_{eff}/h_{eff}) there is large variability in the 1st story drift ratio demand (δ_1/h_1) (typical values of the coefficient of determination, R^2 , of the model presented in Equation G.2 range from 0.35 to 0.70 for the critical story regression estimates).

This indicates that further research is required in the future to select a more accurate statistical model to relate story drift ratio demand with estimated building displacements such that an optimal balance of goodness of fit and simplicity can be obtained.

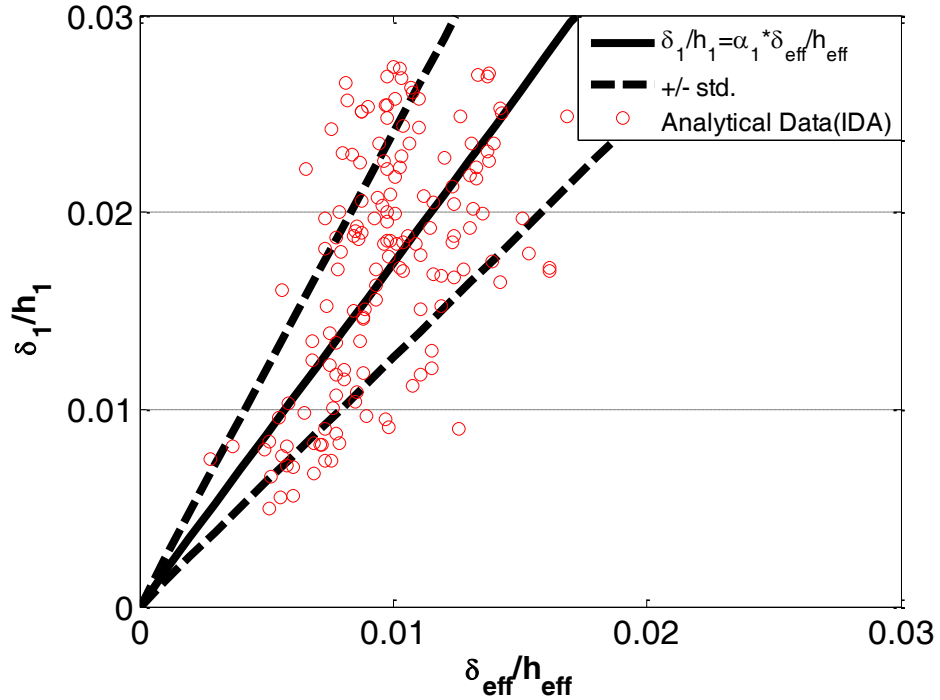


Figure G.1 Observed story drift ratio demand (δ_1/h_1) at the 1st story over estimated average drift (δ_{eff}/h_{eff}) (8-Story building, $V_p/V_n=0.8$, $\Sigma M_{nc}/\Sigma M_{nb}=1.20$)

Tables G.1-G.3 present the estimated values of $\alpha_x = \exp(\hat{\beta}_0)$ and the standard deviation of the natural logarithm of the story drift ratio demand based on statistical regression for different variations of the idealized 4,8 and 12-story buildings.

Table G.1.a Least squares estimation results of $\alpha_x = \exp(\hat{\beta}_0)$ for the idealized 4- story building

$\alpha_x = \exp(\hat{\beta}_0)$							
$V_p/V_n=0.8$							
$\Sigma M_{nc}/\Sigma M_{nb}$							
Story	0.6	0.8	1.0	1.2	1.4	1.6	1.8
4	0.53	0.53	0.53	0.49	0.48	0.53	0.61
3	0.90	0.90	0.88	0.83	0.85	0.92	0.99
2	0.84	0.84	0.87	1.00	1.12	1.21	1.25
1	1.93	1.93	1.90	1.68	1.48	1.33	1.22
$V_p/V_n=1.0$							
$\Sigma M_{nc}/\Sigma M_{nb}$							
Story	0.6	0.8	1.0	1.2	1.4	1.6	1.8
4	0.57	0.56	0.56	0.54	0.52	0.56	0.61
3	0.94	0.95	0.92	0.90	0.88	0.95	1.01
2	0.92	0.91	0.93	1.05	1.14	1.22	1.26
1	1.81	1.82	1.78	1.56	1.44	1.32	1.22
$V_p/V_n=1.2$							
$\Sigma M_{nc}/\Sigma M_{nb}$							
Story	0.6	0.8	1.0	1.2	1.4	1.6	1.8
4	0.58	0.58	0.58	0.55	0.56	0.55	0.61
3	0.90	0.90	0.91	0.90	0.93	0.95	1.03
2	1.00	1.00	1.01	1.09	1.17	1.22	1.27
1	1.68	1.68	1.64	1.51	1.39	1.29	1.20

Table G.1.b Least squares estimation results of $\hat{\sigma}_{\ln, \frac{\delta_x}{h_x}}$ for the idealized 4- story building

$\hat{\sigma}_{\ln, \frac{\delta_x}{h_x}}$							
$V_p/V_n=0.8$							
$\Sigma M_{nc}/\Sigma M_{nb}$							
Story	0.6	0.8	1.0	1.2	1.4	1.6	1.8
4	0.23	0.24	0.27	0.40	0.46	0.51	0.53
3	0.33	0.34	0.31	0.32	0.30	0.28	0.25
2	0.16	0.16	0.15	0.12	0.09	0.05	0.05
1	0.18	0.18	0.17	0.17	0.14	0.13	0.13
$V_p/V_n=1.0$							
$\Sigma M_c/\Sigma M_b$							
Story	0.6	0.8	1.0	1.2	1.4	1.6	1.8
4	0.25	0.24	0.25	0.43	0.47	0.51	0.54
3	0.28	0.30	0.27	0.30	0.30	0.27	0.27
2	0.12	0.12	0.12	0.10	0.07	0.05	0.04
1	0.16	0.16	0.16	0.18	0.14	0.12	0.13
$V_p/V_n=1.2$							
$\Sigma M_c/\Sigma M_b$							
Story	0.6	0.8	1.0	1.2	1.4	1.6	1.8
4	0.24	0.24	0.25	0.33	0.49	0.47	0.50
3	0.19	0.19	0.19	0.22	0.29	0.28	0.27
2	0.10	0.10	0.09	0.08	0.05	0.04	0.04
1	0.16	0.16	0.16	0.14	0.14	0.14	0.13

Table G.2.a Least squares estimation results of $\alpha_x = \exp(\hat{\beta}_0)$ for the idealized 8-story building

$\alpha_x = \exp(\hat{\beta}_0)$							
$V_p/V_n=0.8$							
$\Sigma M_{nc}/\Sigma M_{nb}$							
Story	0.6	0.8	1.0	1.2	1.4	1.6	1.8
8	1.01	1.01	0.91	0.84	0.65	0.59	0.63
7	1.50	1.50	1.43	1.30	1.08	0.95	0.95
6	1.60	1.60	1.60	1.50	1.28	1.18	1.17
5	1.63	1.62	1.54	1.38	1.24	1.21	1.27
4	0.93	0.93	0.91	1.03	1.09	1.18	1.28
3	1.12	1.12	1.05	1.14	1.31	1.37	1.45
2	0.89	0.89	0.88	1.21	1.40	1.41	1.42
1	1.96	1.96	1.92	1.63	1.46	1.32	1.21
$V_p/V_n=1.0$							
$\Sigma M_{nc}/\Sigma M_{nb}$							
Story	0.6	0.8	1.0	1.2	1.4	1.6	1.8
8	0.91	0.90	0.94	0.82	0.71	0.65	0.59
7	1.47	1.46	1.49	1.38	1.20	1.08	0.97
6	1.61	1.61	1.62	1.58	1.42	1.33	1.23
5	1.53	1.54	1.52	1.43	1.34	1.29	1.30
4	0.98	0.98	0.98	1.05	1.12	1.20	1.29
3	1.14	1.15	1.11	1.15	1.27	1.35	1.41
2	0.94	0.94	0.95	1.20	1.34	1.38	1.38
1	1.85	1.86	1.81	1.48	1.33	1.26	1.15
$V_p/V_n=1.2$							
$\Sigma M_{nc}/\Sigma M_{nb}$							
Story	0.6	0.8	1.0	1.2	1.4	1.6	1.8
8	0.95	0.97	0.96	0.88	0.79	0.68	0.66
7	1.52	1.53	1.52	1.46	1.35	1.18	1.08
6	1.69	1.67	1.69	1.66	1.56	1.44	1.30
5	1.55	1.54	1.52	1.49	1.40	1.36	1.31
4	1.06	1.05	1.05	1.10	1.13	1.21	1.27
3	1.17	1.17	1.16	1.15	1.25	1.34	1.41
2	1.05	1.04	1.05	1.19	1.30	1.36	1.38
1	1.69	1.68	1.68	1.38	1.25	1.19	1.14

Table G.2.b Least squares estimation results of $\hat{\sigma}_{\ln, \frac{\delta_x}{h_x}}$ for the idealized 8- story building

$\hat{\sigma}_{\ln, \frac{\delta_x}{h_x}}$							
$V_p/V_n=0.8$							
$\Sigma M_{nc}/\Sigma M_{nb}$							
Story	0.6	0.8	1.0	1.2	1.4	1.6	1.8
8	0.46	0.47	0.46	0.52	0.45	0.48	0.46
7	0.46	0.46	0.45	0.43	0.45	0.47	0.43
6	0.30	0.30	0.32	0.33	0.38	0.40	0.35
5	0.32	0.31	0.28	0.28	0.30	0.28	0.23
4	0.19	0.20	0.18	0.20	0.20	0.15	0.14
3	0.29	0.29	0.27	0.20	0.16	0.14	0.14
2	0.24	0.24	0.24	0.20	0.23	0.22	0.22
1	0.31	0.30	0.32	0.35	0.31	0.30	0.30
$V_p/V_n=1.0$							
$\Sigma M_{nc}/\Sigma M_{nb}$							
Story	0.6	0.8	1.0	1.2	1.4	1.6	1.8
8	0.38	0.39	0.43	0.39	0.27	0.29	0.29
7	0.75	0.75	0.73	0.59	0.43	0.37	0.36
6	0.52	0.52	0.54	0.49	0.42	0.39	0.38
5	0.45	0.44	0.45	0.37	0.35	0.32	0.29
4	0.12	0.12	0.13	0.19	0.20	0.16	0.15
3	0.37	0.37	0.27	0.23	0.19	0.17	0.17
2	0.15	0.14	0.16	0.22	0.28	0.26	0.26
1	0.54	0.54	0.52	0.46	0.39	0.32	0.31
$V_p/V_n=1.2$							
$\Sigma M_{nc}/\Sigma M_{nb}$							
Story	0.6	0.8	1.0	1.2	1.4	1.6	1.8
8	0.41	0.42	0.42	0.45	0.52	0.45	0.46
7	0.42	0.43	0.41	0.41	0.47	0.44	0.41
6	0.31	0.30	0.30	0.32	0.38	0.36	0.33
5	0.23	0.23	0.22	0.23	0.27	0.26	0.25
4	0.12	0.13	0.13	0.18	0.20	0.17	0.15
3	0.22	0.23	0.21	0.19	0.18	0.17	0.16
2	0.19	0.20	0.20	0.19	0.24	0.24	0.23
1	0.30	0.31	0.29	0.25	0.31	0.30	0.30

Table G.3.a Least squares estimation results of $\alpha_x = \exp(\hat{\beta}_0)$ for the idealized 12- story building

$\alpha_x = \exp(\hat{\beta}_0)$							
$V_p/V_n=0.8$							
$\Sigma M_{nc}/\Sigma M_{nb}$							
Story	0.6	0.8	1.0	1.2	1.4	1.6	1.8
12	0.73	0.74	0.71	0.55	0.49	0.44	0.43
11	1.38	1.38	1.39	1.04	0.86	0.74	0.70
10	1.62	1.62	1.60	1.27	1.08	0.94	0.88
9	1.42	1.42	1.51	1.36	1.21	1.11	1.03
8	1.75	1.75	1.67	1.45	1.31	1.20	1.16
7	1.10	1.11	1.20	1.30	1.25	1.21	1.22
6	1.70	1.70	1.61	1.36	1.35	1.37	1.39
5	1.10	1.11	1.22	1.21	1.30	1.39	1.44
4	1.22	1.22	1.15	1.11	1.29	1.43	1.49
3	0.84	0.84	0.85	1.02	1.25	1.37	1.43
2	0.87	0.88	0.94	1.47	1.51	1.44	1.42
1	1.96	1.97	1.80	1.56	1.39	1.25	1.16
$V_p/V_n=1.0$							
$\Sigma M_{nc}/\Sigma M_{nb}$							
Story	0.6	0.8	1.0	1.2	1.4	1.6	1.8
12	0.75	0.76	0.74	0.61	0.56	0.52	0.48
11	1.40	1.41	1.43	1.18	0.99	0.89	0.80
10	1.67	1.66	1.62	1.43	1.20	1.10	1.00
9	1.46	1.47	1.51	1.51	1.32	1.25	1.14
8	1.69	1.71	1.60	1.56	1.40	1.33	1.24
7	1.15	1.18	1.24	1.38	1.32	1.31	1.29
6	1.61	1.63	1.61	1.43	1.38	1.42	1.44
5	1.15	1.16	1.26	1.28	1.33	1.42	1.48
4	1.24	1.23	1.18	1.16	1.32	1.43	1.49
3	0.89	0.89	0.89	1.03	1.26	1.37	1.43
2	0.92	0.93	0.98	1.34	1.43	1.41	1.40
1	1.82	1.81	1.71	1.45	1.33	1.22	1.12

$$\alpha_x = \exp(\hat{\beta}_0)$$

$$V_p/V_n=1.2$$

$$\Sigma M_{nc}/\Sigma M_{nb}$$

Story	0.6	0.8	1.0	1.2	1.4	1.6	1.8
12	0.81	0.81	0.75	0.66	0.63	0.56	0.51
11	1.46	1.48	1.41	1.27	1.13	0.95	0.83
10	1.68	1.71	1.60	1.51	1.33	1.15	1.03
9	1.58	1.60	1.53	1.56	1.42	1.28	1.18
8	1.76	1.76	1.62	1.58	1.45	1.35	1.29
7	1.29	1.29	1.27	1.41	1.35	1.33	1.32
6	1.59	1.57	1.51	1.45	1.42	1.44	1.47
5	1.24	1.25	1.27	1.32	1.37	1.43	1.50
4	1.26	1.26	1.21	1.20	1.32	1.43	1.50
3	0.99	0.99	0.96	1.06	1.26	1.36	1.43
2	1.02	1.02	1.03	1.26	1.38	1.37	1.37
1	1.67	1.69	1.56	1.31	1.26	1.16	1.12

Table G.3.b Least squares estimation results of $\hat{\sigma}_{\ln \frac{\delta_x}{h_x}}$ for the idealized 12- story building

$\hat{\sigma}_{\ln \frac{\delta_x}{h_x}}$							
$V_p/V_n=0.8$							
$\Sigma M_{nc}/\Sigma M_{nb}$							
Story	0.6	0.8	1	1.2	1.4	1.6	1.8
12	0.34	0.35	0.39	0.44	0.48	0.49	0.50
11	0.54	0.54	0.55	0.53	0.50	0.49	0.50
10	0.53	0.53	0.48	0.49	0.48	0.49	0.48
9	0.33	0.33	0.35	0.37	0.39	0.41	0.42
8	0.38	0.39	0.38	0.34	0.33	0.35	0.33
7	0.19	0.19	0.19	0.28	0.25	0.26	0.25
6	0.34	0.34	0.29	0.21	0.17	0.16	0.16
5	0.16	0.16	0.15	0.19	0.18	0.15	0.15
4	0.20	0.20	0.18	0.20	0.19	0.17	0.17
3	0.20	0.20	0.21	0.23	0.20	0.21	0.22
2	0.20	0.20	0.21	0.33	0.30	0.31	0.30
1	0.41	0.40	0.41	0.40	0.36	0.39	0.38
$V_p/V_n=1.0$							
$\Sigma M_{nc}/\Sigma M_{nb}$							
Story	0.6	0.8	1	1.2	1.4	1.6	1.8
12	0.35	0.36	0.38	0.44	0.44	0.48	0.46
11	0.53	0.52	0.53	0.51	0.50	0.48	0.44
10	0.52	0.51	0.48	0.48	0.48	0.48	0.42
9	0.32	0.32	0.34	0.38	0.39	0.40	0.38
8	0.34	0.35	0.34	0.33	0.36	0.35	0.34
7	0.17	0.19	0.19	0.26	0.27	0.25	0.25
6	0.28	0.27	0.27	0.21	0.18	0.16	0.16
5	0.15	0.15	0.13	0.18	0.18	0.16	0.13
4	0.19	0.19	0.16	0.20	0.21	0.19	0.17
3	0.19	0.19	0.18	0.23	0.25	0.24	0.23
2	0.19	0.20	0.18	0.34	0.33	0.31	0.30
1	0.38	0.38	0.36	0.40	0.39	0.39	0.41

$\hat{\sigma}_{\ln, \frac{\delta_x}{h_x}}$							
$V_p/V_n=1.2$							
$\Sigma M_{nc}/\Sigma M_{nb}$							
Story	0.6	0.8	1	1.2	1.4	1.6	1.8
12	0.41	0.40	0.41	0.40	0.36	0.39	0.38
11	0.20	0.20	0.21	0.33	0.30	0.31	0.30
10	0.20	0.20	0.21	0.23	0.20	0.21	0.22
9	0.20	0.20	0.18	0.20	0.19	0.17	0.17
8	0.16	0.16	0.15	0.19	0.18	0.15	0.15
7	0.34	0.34	0.29	0.21	0.17	0.16	0.16
6	0.19	0.19	0.19	0.28	0.25	0.26	0.25
5	0.38	0.39	0.38	0.34	0.33	0.35	0.33
4	0.33	0.33	0.35	0.37	0.39	0.41	0.42
3	0.53	0.53	0.48	0.49	0.48	0.49	0.48
2	0.54	0.54	0.55	0.53	0.50	0.49	0.50
1	0.34	0.35	0.39	0.44	0.48	0.49	0.50

G.1. STORY DRIFT PROFILES FOR BUILDINGS WITH CRITICAL STORIES IN THE MID-HEIGHT

In this section, Table G.4 presents the results of least squares estimation for the case of 8-story building variations where the critical story is located at the mid-height (4th story). For this buildings variations the column strengths are modified such that $DCR_{4th}=1.30*DCR_{1st}$, where DCR_{4th} corresponds to the Demand over Capacity ratio of the 4th story and DCR_{1st} corresponds to the Demand over Capacity ratio of the 1st story.

Table G.4.a Least squares estimation results of $\alpha_x = \exp(\hat{\beta}_0)$ for the idealized 8- story building with critical story at the mid-height ($DCR_{4th}=1.30DCR_{1st}$)

$\alpha_x = \exp(\hat{\beta}_0)$			
Vp/Vn=0.8			
$\Sigma M_{nc}/\Sigma M_{nb}$			
Story	0.8	1.2	1.6
8	0.69	0.51	0.46
7	1.01	0.79	0.74
6	1.02	0.88	0.96
5	1.42	1.38	1.45
4	1.95	1.66	1.71
3	1.05	1.15	1.36
2	0.61	0.74	0.91
1	1.79	1.13	0.76

Table G.4.b Least squares estimation results of $\hat{\sigma}_{\ln, \frac{\delta_x}{h_x}}$ for the idealized 8- story building with critical story at the mid-height ($DCR_{4th}=1.30DCR_{1st}$)

$\hat{\sigma}_{\ln, \frac{\delta_x}{h_x}}$			
Vp/Vn=0.8			
$\Sigma M_{nc}/\Sigma M_{nb}$			
Story	0.8	1.2	1.6
8	0.31	0.22	0.25
7	0.57	0.33	0.35
6	0.40	0.34	0.36
5	0.57	0.35	0.33
4	0.11	0.20	0.25
3	0.35	0.23	0.17
2	0.12	0.20	0.24
1	0.72	0.62	0.36

G.2. STORY DRIFT PROFILES FOR THE 8-STORY BUILDING WITH INADEQUATE LAP SPLICING CONDITIONS AT THE BASE OF THE 1ST STORY

In this section, Table G.5 presents the results of least squares estimation for the case of 8-story building variations where inadequate longitudinal reinforcing bar lap splicing conditions are introduced at the base of the column members located at the 1st story of the idealized 8-story buildings

Table G.5.a Least squares estimation results of $\alpha_x = \exp(\hat{\beta}_0)$ for the idealized 8-story building with inadequate lap splicing conditions at the base of the 1st story

$\alpha_x = \exp(\hat{\beta}_0)$							
Vp/Vn=0.8							
$\Sigma Mc/\Sigma Mb$							
Story	0.6	0.8	1	1.2	1.4	1.6	1.8
8	0.83	0.83	0.83	0.80	0.68	0.63	0.56
7	1.32	1.32	1.32	1.32	1.14	1.03	0.90
6	1.47	1.47	1.49	1.51	1.37	1.24	1.10
5	1.40	1.40	1.34	1.30	1.25	1.16	1.10
4	0.87	0.87	0.88	0.95	0.99	1.00	1.04
3	0.98	0.98	0.96	0.98	1.05	1.11	1.17
2	0.84	0.84	0.85	0.99	1.11	1.18	1.23
1	1.83	1.83	1.76	1.59	1.45	1.40	1.35

Table G.5.b Least squares estimation results of $\hat{\sigma}_{\ln, \frac{\delta_x}{h_x}}$ for the idealized 8- story building inadequate lap splicing conditions at the base of the 1st story

$\hat{\sigma}_{\ln, \frac{\delta_x}{h_x}}$							
Vp/Vn=0.8							
$\Sigma Mc/\Sigma Mb$							
Story	0.6	0.8	1	1.2	1.4	1.6	1.8
8	0.38	0.39	0.43	0.39	0.27	0.29	0.38
7	0.75	0.75	0.73	0.59	0.43	0.37	0.75
6	0.52	0.52	0.54	0.49	0.42	0.39	0.52
5	0.45	0.44	0.45	0.37	0.35	0.32	0.45
4	0.12	0.12	0.13	0.19	0.20	0.16	0.12
3	0.37	0.37	0.27	0.23	0.19	0.17	0.37
2	0.15	0.14	0.16	0.22	0.28	0.26	0.15
1	0.54	0.54	0.52	0.46	0.39	0.32	0.54